GRANULITES FROM ENDERBY LAND, ANTARCTICA.

The Application of Experimentally Determined Cation Partition Data

to Estimation of Pressures and Temperatures of Metamorphism.

by

David John Ellis, B.Sc.(Hons.), M.Sc.

I agree that, this thesis may be
available for loan and copying,
immediately after its acceptance
by the University of Tasmania.

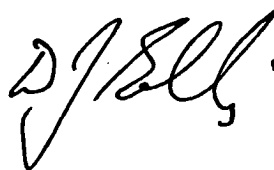(Signed) ....

Date 30/3/1979

Submitted in fulfillment of the requirements
for the degree of Doctor of Philosophy.

University of Tasmania

Hobart

1979

This thesis contains no material which has been accepted for the award of any other degree or diploma in any university, and to the best of my knowledge and belief, contains no copy or paraphrase of material previously published or written by another person, except where due reference is made in the text of this thesis.

D.J. Ellis

University of Tasmania.
March, 1979.

CONTENTS

<u>List of Figures</u>   page

List of Figures cont.

List of Tables

ABSTRACT

The Precambrian granulites of Enderby Land, Antarctica, were metamorphosed at temperatures as high as $900^{\circ}C$ and then underwent slow isobaric cooling at about 10 kb pressure. The mafic and pelitic granulites are characterised by the presence of retrograde reaction coronas, a variety of exsolution assemblages in clinopyroxenes and compositional zoning in minerals. The recognition of staggered closure temperatures of cation exchange for different mineral systems permits the use of geothermometers and geobarometers to evaluate the P-T cooling paths of these granulites.

The pelitic rocks contain coexisting spinel-quartz, sapphirine-quartz, hypersthene-sillimanite-quartz and osumilite on a regional scale. Osumilite is present in a variety of mineral assemblages, most of which have not previously been reported. These assemblages have been used to construct theoretical P-T diagrams for the stability of osumilite in the $K_2O-MgO-Al_2O_3-SiO_2$ and $K_2O-FeO-MgO-Al_2O_3-SiO_2$ chemical systems.

Secondary cordierite has developed by a variety of mineral reactions on cooling of these higher temperature-pressure equivalents of coexisting garnet and cordierite. Available Fe-Mg partition data for garnet-cordierite would imply equilibrium at temperatures of $500-600^{\circ}C$, which is inconsistent with both mineral compatibilities in these rocks and temperature estimates based on other geothermometers. It is suggested that the garnet-cordierite Fe-Mg exchange reaction may be dependent upon P_{H_2O}. An experimental study to test this possibility has proved inconclusive, but theoretical considerations indicate that this exchange reaction cannot be considered applicable as a quantitative geothermometer because of our current lack of understanding.

Study of the mafic granulites from Enderby Land demonstrates the control of differing bulk rock compositions upon the variety of reactions involved in the development of garnet with cooling through the pyroxene granulite-eclogite transition. Data obtained from the staggered closure temperatures of cation exchange in different mineral systems supports the proposal for a curvature to the pyroxene granulite-eclogite transition at low temperatures. The formation of garnet in metamorphosed quartz tholeiite dykes is consistent with previous descriptions of the continuous reaction of plagioclase feldspar with orthopyroxene and opaque oxide to produce garnet and clinopyroxene or quartz. The disappearance of plagioclase feldspar in the more mafic, quartz-free rocks involves a different series of reactions in which garnet and an aluminous clino-pyroxene are formed. At still lower temperatures a second generation of plagioclase feldspar may form through exsolution from aluminous clino-pyroxene. This feldspar would eventually react at still lower temperatures to form a Ca-rich garnet and kyanite.

A marked compositional dependence to the garnet-clinopyroxene Fe-Mg exchange reaction is evident from this study of the Enderby Land granulites, and an experimental investigation of this effect has been carried out. The results of this study reconcile previous inconsistencies in the temperature and pressure dependence of the Fe-Mg distribution coefficient for coexisting garnet-clinopyroxene determined in previous experimental studies of simple systems, complex basalt, garnet peridotite and grospydite compositions. The derived geothermometer yields similar estimates for garnet-clinopyroxene equilibration for neighbouring meta-morphic rocks of different composition and different K_D values. In addition, temperature estimates using this geothermometer are more consistent with independent temperature estimates based on other geo-thermometers than previous estimates which did not correct for the Ca-effect.

Application of this geothermometer to the temperature of equilibration of garnet-peridotite and eclogite xenoliths in kimberlites has revealed inconsistencies in our current concepts of strongly silica-undersaturated basalt magma petrogenesis.

ACKNOWLEDGEMENTS

completed without the unselfish effort of my fellow student Brendon Griffin in automating the electron microprobe at Hobart.

Finally I would like to thank my wife, Chris, for her help and understanding, and her good sense of humour on the subject of science and Ph.D. students.

Chapter 1

<u>INTRODUCTION</u>

Chapter 1

INTRODUCTION

This thesis presents the results of a field, petrologic and experimental study of granulite facies metamorphic rocks, with particular reference to the pressures and temperatures of formation of mineral assemblages on the basis of Fe^{2+}-Mg partitioning between coexisting minerals.

Considerable advance has been made in our understanding of metamorphism since the pioneering works of Barrow (1893, 1912) and Eskola (1920, 1939) on the mineral assemblages in metamorphosed argillaceous sediments and basaltic rocks respectively. The realisation that the phase rule can be applied to mineral assemblages in metamorphic rocks of the Oslo region, Norway (Goldschmidt, 1911) was an important step in the understanding and treatment of mineral equilibria in metamorphic rocks. Since these early works the study of metamorphism has progressed along two avenues - the study of natural rocks and the experimental study of key mineral equilibria. Although Goldschmidt's mineralogical phase rule emphasized the importance of divariant equilibria (two degrees of freedom) in the occurrence of mineral assemblages, most experimental studies have been concerned with univariant reactions in simple end member and multicomponent systems which define the stability limits of individual minerals and mineral assemblages.

Recently, the importance of divariant equilibria for the stability of coexisting garnet and cordierite in pelitic rocks has been emphasized in a series of experimental studies by Hensen and

Green (1971, 72, 73).   Considerable discussion has arisen in recent years about the phase relations and Fe-Mg cation exchange equilibria pertaining to the upper pressure-temperature stability limit of coexisting garnet and cordierite.   Views differ considerably on this topic, and attempts to sort out such differences have been hampered by the extreme rarity in nature of rocks containing the higher pressure and temperature analogues of garnet and cordierite.   In the granulites of Enderby Land, Antarctica, coexisting sapphirine-quartz, hypersthene-sillimanite-quartz and spinel-quartz occur on a regional scale (Figure 1.1).   The phase relations in these assemblages and the mineral compositions of garnet and cordierite in reaction coronas surrounding these minerals provide invaluable data for testing the different views on such equilibria based on the experimental studies.·

The mineral assemblages in the Enderby Land granulites have also necessitated a considerable revision of our understanding of mineral assemblages in pelitic rocks.   In pelitic rocks described by the system $K_2O-FeO-MgO-Al_2O_3-SiO_2$, the mineral reactions occurring at high temperatures above the breakdown of biotite and in the absence of a melt (refractory granulites) it has been assumed that K_2O is present as an excess inert component, as Kfeldspar (e.g. Hess, 1969; Hensen and Green, 1971, 72, 73; Holdaway, 1976).   The occurrence of osumilite on a regional scale in the Enderby Land granulites invalidates this assumption.   Several new mineral assemblages and reactions are reported.

The role of osumilite in granulite facies rocks is discussed in this thesis and a theoretical P-T diagram for its stability is presented.

Fig. 1.1A Spot Height 945, Enderby Land, Antarctica. The rocks
           consist of gently dipping banded metasediments which
           pass upwards into massive, brown weathering ortho-
           pyroxene-quartz-feldspar(-garnet) gneiss. Dark brown
           bands of mafic rocks are of minor abundance.

Fig. 1.1B Spot Height 945, showing blue quartzite bands together
           with a layer of sapphirine (dark blue), quartz and
           other minerals as described in Chapter 4.

The mafic granulites from Enderby Land have also been studied. One locality has been examined in detail. These rocks show a wide range in mineral assemblages and mineral compositions. These features have enabled the testing of the internal consistency of several geothermometers and geobarometers. A compositional dependence to the garnet-clinopyroxene Fe-Mg K_D is indicated, and it is found that different mineral systems have staggered closure temperatures for cation exchange equilibria.

The study of the pelitic and mafic granulites have pointed out many problems in our current understanding of mineral equilibria in granulite facies metamorphic rocks. Two projects have been selected from these problems for experimental study - a study of the effect of Ca upon the garnet-clinopyroxene Fe-Mg exchange reaction, and the effect of water upon the garnet-cordierite Fe-Mg exchange reaction.

In the following thesis the petrology of the mafic granulites from Enderby Land is discussed in chapter 2. The experimental study of garnet-clinopyroxene equilibria is presented in chapter 3. The petrology of the pelitic granulites is given in chapter 4 and the experimental study of garnet-cordierite equilibria in chapter 5. Finally, in chapter 6 some of the broader implications of this work are discussed. Some of the detailed thermodynamic calculations and data tables are given in appendices so as to not interrupt the general train of thought presented in the main part of the thesis.

Chapter 2

GARNET-FORMING REACTIONS IN HIGH PRESSURE CRUSTAL

MAFIC GRANULITES FROM ENDERBY LAND, ANTARCTICA

Contents   page

I. SUMMARY

This study of an outcrop of high pressure mafic granulites from Enderby Land, Antarctica, demonstrates the control of differing bulk rock compositions upon the variety of reactions involved in the development of garnet with cooling through the pyroxene granulite-eclogite transition. The mafic rocks were originally a sequence of cumulates crystallized from the enclosing basalt dyke at about 10 kb pressure. Subsequent regional metamorphism at about 820^OC, 11 kb pressure was followed by isobaric cooling to about 610^OC.

The formation of garnet in the metamorphosed quartz-tholeiite dyke is consistent with previous descriptions of the reaction of plagioclase feldspar with opaque oxide and orthopyroxene to produce garnet and clinopyroxene or quartz with decreasing temperature.

In contrast the disappearance of plagioclase feldspar in the more mafic, quartz-free rocks involves a different series of reactions with decreasing temperature. Spinel and plagioclase initially reacted to form aluminous clinopyroxene (± garnet), but at still lower temperatures a second generation of plagioclase feldspar formed by exsolution from the aluminous clinopyroxene. This feldspar would eventually react at still lower temperatures to form a Ca-rich garnet and kyanite in the eclogite stability field.

A number of exsolution products are observed in the clinopyroxenes. The range of mineral associations in these exsolutions reflects compositional variations in the original aluminous clinopyroxenes. The following exsolution products have been found -

Clinopyroxene-Orthopyroxene

Clinopyroxene-Orthopyroxene-Garnet

Clinopyroxene-Garnet

Clinopyroxene-Garnet-Plagioclase

Plagioclase Feldspar-Quartz-Opaque Oxide.

This range in mineral associations and mineral compositions has been used to evaluate the internal consistency of currently available methods of geothermometry and geobarometry for crustal granulites. There is an increase in K_D $[(Fe/Mg)^{Gt}.(Mg/Fe)^{Cpx}]$ for coexisting garnet and clinopyroxene with increasing Ca-content of the garnet. Nelgect of this effect on K_D results in temperature underestimates for many crustal garnet-clinopyroxene pairs compared to other geothermometers.

II. INTRODUCTION

This chapter describes an ultramafic pod of pyroxenite and garnet clinopyroxenite within a metamorphosed basaltic gneiss from Enderby Land, Antarctica. The rocks were collected by the author and other geologists with the Bureau of Mineral Resources during a regional mapping program with the Australian National Antarctic Research Expedition in the 1976-1977 summer field season.

The petrology of the sheared basaltic gneiss is similar to that described from other high pressure granulite metamorphic terrains in which garnet has developed by reaction between plagioclase, opaque oxides and orthopyroxene. The associated ultramafic rocks and their wide variety of pyroxene exsolution products bear many similarities to the garnet clinopyroxenite xenoliths found in alkali basalts and as lenses in alpine-type peridotites (Lovering and White, 1969; Conquéré, 1977).

Chemical zoning in the pyroxene and garnets, and the variety of minerals exsolved from the pyroxenes can be used to establish the upper temperature and pressure of metamorphism and the subsequent cooling path for part of this Precambrian metamorphic terrain. The presence of garnet, orthopyroxene and clinopyroxene which equilibrated under iso-facial metamorphic conditions, and which display wide ranges in mineral compositions provides an opportunity to evaluate the consistency of many of the currently available methods of geothermometry and geobarometry for such metamorphic terrains.

III. GEOLOGICAL SETTING

Enderby Land is part of the Precambrian East Antarctic Shield, and consists of granulite facies regional metamorphic rocks with local areas of retrogression to the amphibolite facies. The most recent description of the area is that of Sheraton et al. (in prep.), with earlier descriptions being given by McLeod (1964), Kamenev (1972, 1975), and Sheraton and Offe (1977).

The mafic rocks outcrop on the northern island of the western shore of Amundsen Bay (49°50'E, 67°07'S) (Figure 2.1). They occur as a boudin in a sheared basaltic gneiss which is concordant with foliated quartz-feldspar granulites of the surrounding regional metamorphics. The boudin is 4-5 metres in width and the enclosing basaltic gneiss (up to 10 m in width) has a foliation parallel to that of the surrounding granulites.

The boudin consists of coarse grained clinopyroxenite with lesser amounts of finergrained pyroxenite and garnet clinopyroxenite. At the margins of this pod are irregular bands of similar rock types which in addition, contain a minor amount of feldspar. These plagioclase-bearing
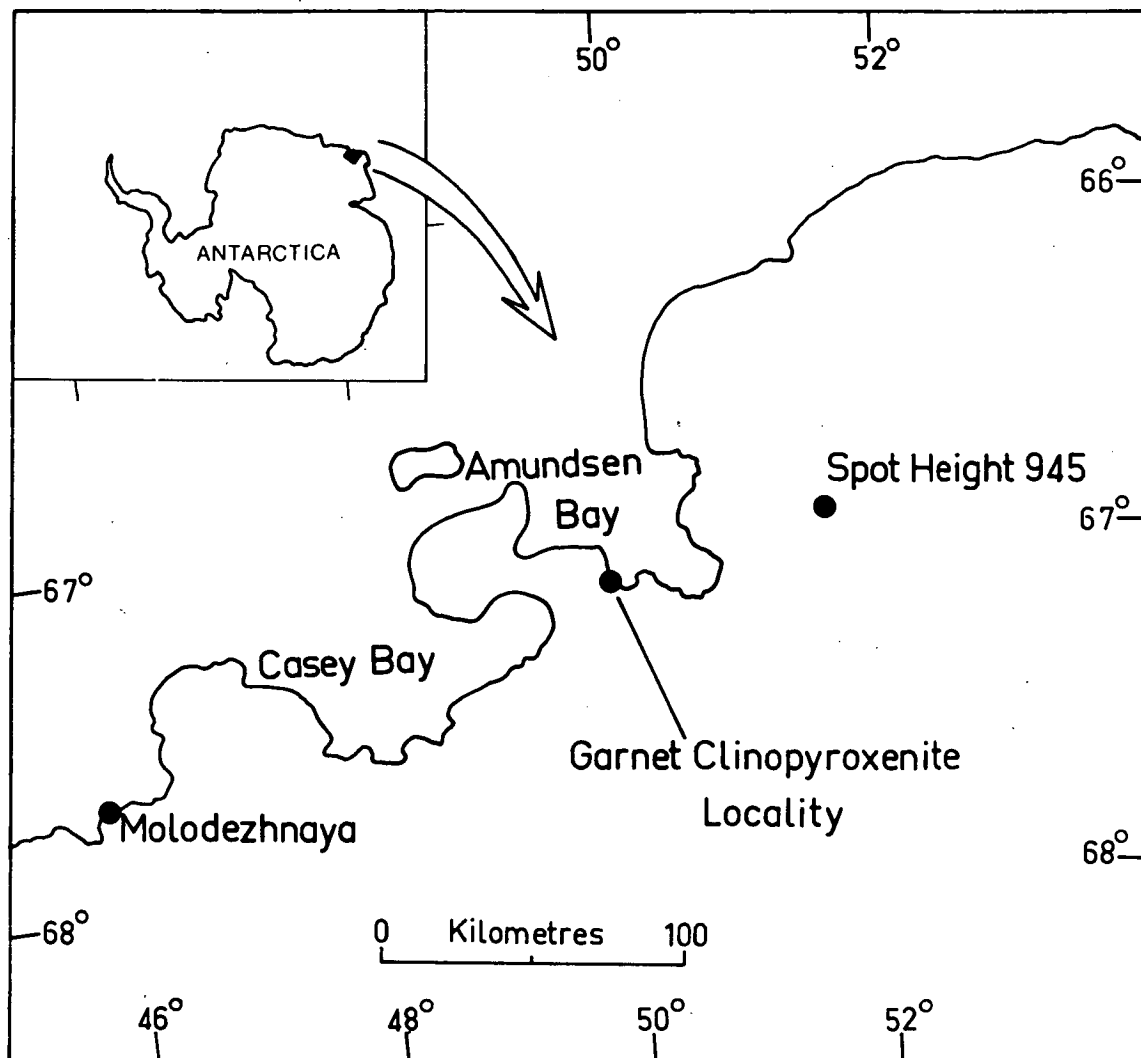
Figure 2.1 Map of the western part of Enderby Land, Antarctica.
showing the location of the garnet clinopyroxenite-
bearing mafic granulites described in this chapter.
The pelitic granulites at Spot Height 945 are described
in Chapter 4.

varieties consist of porphyroblasts of clinopyroxene set in a finer grained pyroxene-feldspar assemblage. The enclosing sheared basaltic gneiss contains folded lenticular layers of garnet orthopyroxenite, which are up to 5 cm thick and about 30 cm in length. A thin layer of sapphirine-bearing granulite occurs along the contact between the basaltic gneiss and the quartz-feldspar granulites, but the sapphirine-bearing assemblage is separated from the quartz-bearing rocks by a thin zone of hypersthene.

IV. PETROLOGY

1. The Sheared Basaltic Gneiss

This rock consists of the assemblage clinopyroxene, orthopyroxene, garnet, plagioclase feldspar, quartz, ilmenite together with a minor amount of biotite and amphibole.

Medium to coarse grained plagioclase and pyroxene have amoebid grain boundaries and undulose extinction. The plagioclase contains rounded inclusions of quartz. The pyroxenes have rare pyroxene exsolution lamellae and recrystallized, strain free margins of fine grained pyroxene. One large clinopyroxene porphyroblast contains exsolution lamellae of plagioclase, quartz, magnetite and ilmenite aligned along the (100) direction of the host clinopyroxene.

Garnet is present as reaction coronas around the ilmenite and orthopyroxene where these were originally in contact with plagioclase. The garnet coronas around orthopyroxene contain fine grained inclusions of clinopyroxene and that around the ilmenite contains vermicular inclusions of quartz (Figure 2.2A). The ilmenite does not have garnet reaction rims where it is in contact with the clinopyroxene.

Fig. 2.2A Thin section photograph of sheared basaltic gneiss
(registered BMR thin section number 77284029)
showing a corona of garnet with quartz inclusions
surrounding ilmenite (black) where originally in
contact with plagioclase feldspar (light grey).
Dark grey colour is pyroxene. Plain polarised
light. x25 magnification.

Fig. 2.2B Thin section photograph of garnet exsolution
lamellae in clinopyroxene. Garnet clino-
pyroxenite (sample 77284022). Cross   polarised
light. x63 magnification.

Fig. 2.2C Thin section photograph of idiomorphic garnet
inclusions in a clinopyroxene, together with second
generation garnet exsolved from the clinopyroxene.
Note the exsolution-free zones in the clinopyroxene
near the idiomorphic garnets. Black areas at the
corners of photograph are marking ink (sample
77284022). Cross polarised light. x25 magnification.
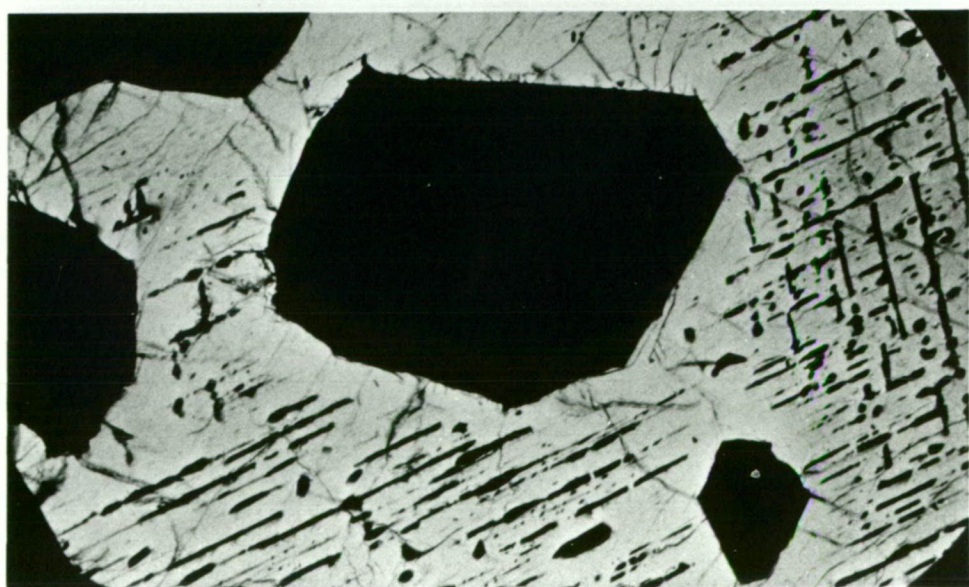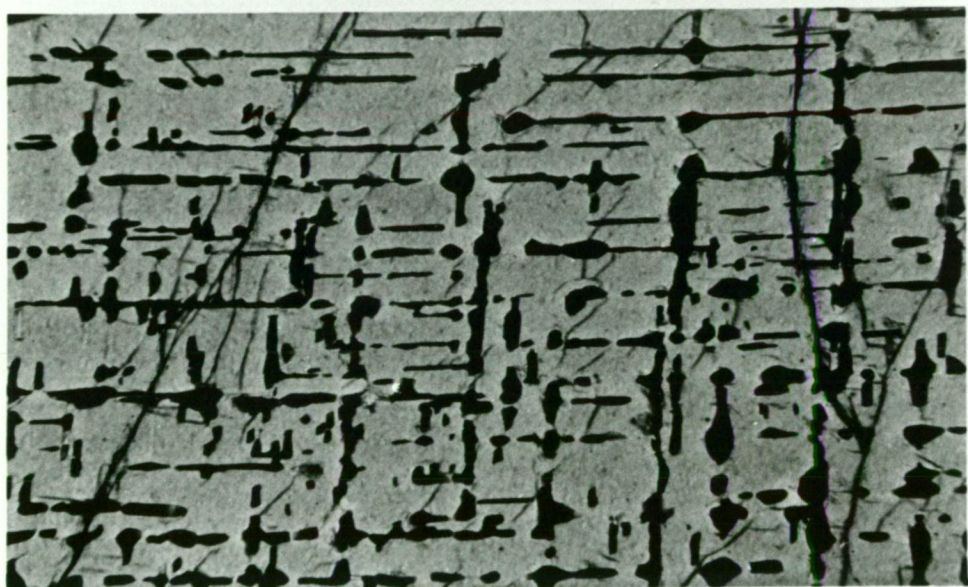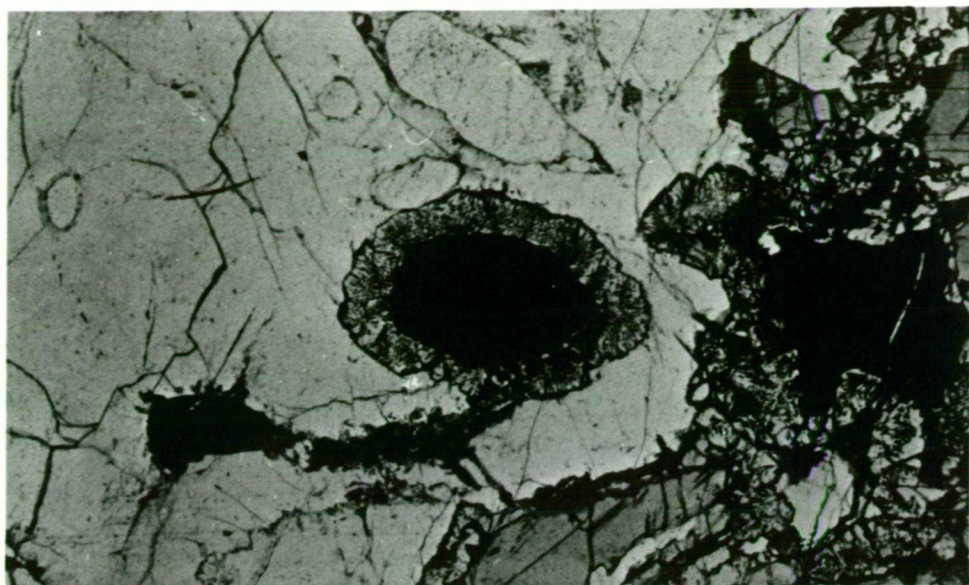
A chemical analysis of this rock is given in Table 2.1 (sample 77284029). The composition is similar to a quartz tholeiite, with 1.15% quartz in the CIPW norm, and a low K_2O content. It is somewhat similar in composition to the quartz tholeiites A and B of Green and Ringwood (1967), though slightly more iron rich (Mg/Mg + Fe^{2+} = 50 compared to 61).

Representative mineral analyses are given in Table 2.2. The plagioclase is more sodic and potassic than that of the more melanocratic rocks and is only slightly zoned ($Or_{1.7}Ab_{48.2}An_{50}-Or_{2.2}Ab_{50.8}An_{47.0}$). The orthopyroxene ($En_{56}$) has higher iron and lower Al_2O_3 contents (1.2-1.9 wt. %) than that of the other rock types (Figure 2.3). The clinopyroxene is richer in FeO, Na_2O and TiO_2, and has less Al_2O_3 than that of the other rock types. Plagioclase (An_{52}) exsolved from the clinopyroxene is similar in composition to that in the rest of the rock. Average electron microprobe beam scan analyses of the clinopyroxene together with the exsolved plagioclase, quartz and opaque oxides (Table 2.6) show that the original pyroxene had higher CaO, Al_2O_3 and Na_2O contents (5.83% jadeite and 8.7% Ca Tschermaks molecule). Garnet present as reaction rims around opaque oxide and orthopyroxene is more iron rich (Mg/Mg + Fe = .25) than that from the garnet clinopyroxenite. The clinopyroxene inclusions in the garnet are more Mg-rich than the larger porphyroblasts in association with orthopyroxene and plagioclase (Table 2.2).

2. The Pyroxenite (Websterite)

The pyroxenite, which is intermixed with the clinopyroxenite and garnet clinopyroxenite in the boudin, is a dense, coarse grained, brown-black coloured rock. It consists of even grained orthopyroxene and clinopyroxene (av. 0.5 cm grain size) with triple point grain boundaries.

TABLE 2.1

Rock Analyses

	1	2	3	4	5	6
SiO_2	49.18	51.94	42.82	36.86	50.42	49.31
TiO_2	0.24	0.00	0.56	1.17	0.23	2.10
Al_2O_3	3.39	2.84	12.58	12.08	8.67	14.42
Cr_2O_3	0.00	0.00	0.12	0.26	0.11	0.00
Fe_2O_3	5.48	2.29	4.63	11.55	1.43	3.84
FeO	15.65	6.59	14.00	12.26	4.85	12.29
MnO	0.74	0.38	0.95	0.34	0.16	0.14
MgO	24.37	16.16	14.32	10.02	12.25	6.96
CaO	1.34	19.88	9.68	14.61	21.04	8.55
Na_2O	0.17	0.16	0.48	0.56	0.91	2.38
K_2O	0.00	0.00	0.33	0.24	0.08	0.38
Total	100.56	100.24	100.47	99.95	100.15	100.37

CIPW NORM

	1	2	3	4	5	6
C	0.67					
Q						1.15
Or			1.94		0.47	2.24
Ab	1.43	1.35	4.04		3.48	20.06
An	6.61	7.01	31.05	29.80	19.31	27.44
Ne				2.57	2.28	
Di		72.90	13.65	28.01	67.62	12.23
Hy	76.55	13.25	14.72			27.35
Ol	6.39	2.18	26.68	16.59	4.17	
Cs				2.52		
Mt	7.90	3.31	6.68	16.78	2.07	5.55
Cm			0.18	0.38	0.16	
Il	0.45		1.06	2.23	0.44	3.97
Lc				1.11		

Cations on the basis of 6 Oxygen Atoms

	1	2	3	4	5	6
Si	1.815	1.914	1.616	1.455	1.843	1.803
Ti	0.007	0.000	0.016	0.035	0.006	0.058
Al	0.148	0.123	0.560	0.562	0.374	0.622
Cr	0.000	0.000	0.004	0.008	0.003	0.000
Fe^{3+}	0.152	0.063	0.131	0.343	0.039	0.106
Fe^{2+}	0.483	0.203	0.442	0.405	0.148	0.376
Mn	0.023	0.012	0.030	0.011	0.005	0.004
Mg	1.341	0.887	0.805	0.589	0.667	0.379
Ca	0.053	0.785	0.391	0.618	0.824	0.335
Na	0.012	0.011	0.035	0.043	0.064	0.169
K	0.000	0.000	0.016	0.012	0.004	0.018
Cation Sum	4.034	3.999	4.046	4.081	3.977	3.869
$\dfrac{100Mg}{(Mg+Fe^{2+})}$	73.5	81	63.3	58.6	81.8	50.2

1. Pyroxenite 77284023*
2. Clinopyroxenite 77284019
3. Garnet clinopyroxenite 77284020
4. Garnet clinopyroxenite 77284028
5. Plagioclase pyroxenite 77284025
6. Sheared basaltic gneiss 77284029
* Registered Bureau of Mineral Resources sample number.

TABLE 2.2

Compositions of minerals in the sheared basaltic gneiss

	1 Cpx	2 Opx	3 Ilm	4 Cpx	5 Plag	6 Mt	7 Ilm	8 Gt	9 Cpx	10 Opx	11 Opx
SiO_2	49.55	50.48	0.00	51.29	55.13			37.77	52.26	50.88	51.19
TiO_2	0.26	0.00	47.28	0.15	0.00	0.85	48.69	0.00	0.00	0.29	0.00
Al_2O_3	3.76	1.96	0.17	2.91	28.41			21.58	2.23	1.40	1.26
Cr_2O_3	0.22	0.00		0.11		0.97	0.61	0.00	0.18	0.00	0.00
Fe_2O_3	3.56	1.88		2.63					0.77	2.17	2.00
FeO	9.66	25.06	49.11	9.50		92.92	48.66	27.40	8.40	24.12	25.10
MnO	0.00	0.33	0.14			0.29	0.77	0.84	0.00	0.19	0.20
MgO	11.96	19.07	1.26	12.53			0.53	5.25	14.23	19.42	19.98
CaO	20.58	1.17	0.00	20.72	10.02			6.86	21.74	1.45	0.26
Na_2O	0.81	0.25		0.42	5.91				0.27	0.27	0.19
K_2O	0.00	0.00		0.00	0.24						
Si	1.868	1.920	0.000	1.920	2.490	0.000	0.000	2.972	1.944	1.930	1.941
Ti	0.007	0.000	0.932	0.004	0.000	0.032	0.946	0.000	0.000	0.008	0.000
Al	0.167	0.088	0.005	0.128	1.513	0.000	0.000	2.002	0.098	0.063	0.056
Cr	0.006	0.000	0.000	0.003	0.000	0.038	0.012	0.000	0.005	0.000	0.000
Fe^{3+}	0.101	0.054	0.000	0.074	0.000	0.000	0.000	0.000	0.022	0.062	0.057
Fe^{2+}	0.304	0.797	1.076	0.297	0.000	3.867	1.052	1.803	0.261	0.765	0.796
Mn	0.000	0.007	0.003	0.000	0.000	0.012	0.017	0.056	0.000	0.006	0.006
Mg	0.672	1.081	0.049	0.699	0.000	0.000	0.020	0.616	0.789	1.098	1.129
Ca	0.831	0.048	0.000	0.831	0.485	0.000	0.000	0.578	0.866	0.059	0.011
Na	0.059	0.018	0.000	0.030	0.518	0.000	0.000	0.000	0.019	0.020	0.014
K	0.000	0.000	0.000	0.000	0.014	0.000	0.000	0.000	0.000	0.000	0.000
Cations	4.016	4.014	2.066	3.988	5.019	3.949	2.048	8.027	4.004	4.010	4.010
Oxygens	6	6	3	6	8	4	3	12	6	6	6
Original FeO	12.87	26.75	49.11	11.87		92.92	48.66				

1. Cpx core sheared basaltic gneiss 77284029 (core of coexisting Plag - An48)
2. Opx core sheared basaltic gneiss 77284029
3. Ilmenite sheared basaltic gneiss 77284029
4. Cpx which has exsolved Plag and opaque oxides + quartz 77284029
5. Plag exsolved out of above Cpx 77284029

6. Magnetite exsolved out of above Cpx 77284029
7. Ilmenite exsolved out of above Cpx 77284029
8. Gt reaction rim between Plag (An48) and Opx 77284029
9. Cpx inclusion in above Gt 77284029
10. Core of Opx rimmed by above Gt-Cpx corona 77284029
11. Rim of Opx next to above Gt 77284029
Fe^{3+} in pyroxenes determined from probe analyses using the formula $Fe^{3+} = 4 - 2Si - 2Ti - Al - Cr + Na$

Fig. 2.3 Ca-Mg-Fe plot of analyzed pyroxenes and garnets, from the websterites, garnet clinopyroxenite, garnet-orthopyroxenite and sheared basaltic gneiss. Tie lines connect compositions of coexisting phases. Coexisting Opx=Cpx in sheared basaltic gneiss indicated by dots; garnet and clinopyroxene reaction coronas around orthopyroxene and zoned rim composition of orthopyroxene at corona indicated by triangles.

Orthopyroxene is pleochroic (pink-pale green) and contains very fine grained exsolution lamellae of assumed clinopyroxene. Rare kink bands and a minor amount of recrystallization along grain boundaries are also developed. Magnetite and green spinel are present as both medium and fine grained crystals along the recrystallized grain boundaries.

A chemical analysis of one pyroxenite sample is presented in Table 2.1 (sample 77284023). It has low Na_2O, TiO_2 and Al_2O_3 and a high MgO content (Mg/Mg + Fe^{2+} = 0.73), consistent with its orthopyroxene rich nature.

Representative mineral analyses for two pyroxenite samples are given in Table 2.3. They differ slightly in Mg/(Mg + Fe) ratio. The clinopyroxene has low Al_2O_3, Na_2O and TiO_2 contents and is essentially a diopside-enstatite-hedenbergite solid solution with only a minor amount of Ca Tschermaks component (3-7 mol. % $CaAl_2SiO_6$, using the method of Kushiro, 1962). The orthopyroxene is a bronzite (En_{75-76}) with low CaO and Al_2O_3 contents.

3. The Clinopyroxenite

The clinopyroxenite is a coarse grained, very dark green rock composed mainly of large clinopyroxenes with well developed cleavage traces (av. 1-2 cm grain size). In thin section it is seen to consist of clinopyroxene and very rare orthopyroxene with amoebid grain boundaries and finer grained (av. 0.1 mm) recrystallized margins of clinopyroxene, orthopyroxene and amphibole. The large clinopyroxenes contain broad exsolution lamellae of orthopyroxene (0.05 mm wide) which usually do not extend to the recrystallized rims of the clinopyroxenes. The lamellae have numerous transverse cracks in them, a feature which has been noted in exsolutions from clinopyroxene inclusions from the Delegate basalt pipe (Irving, 1974). A minor amount of fine grained

TABLE 2.3

Analyses of minerals within the pyroxenites (websterites).

	1 Cpx	2 Opx	3 Cpx	4 Opx	5 Cpx	6 Opx	7 Cpx	8 Opx	9 Amph
SiO_2	51.45	52.56	53.31	54.40	52.22	52.29	51.79	52.03	44.26
TiO_2	0.00	0.00	0.15	0.00	0.00	0.00	0.00	0.00	0.28
Al_2O_3	3.76	3.06	2.08	1.25	2.64	2.29	3.00	2.66	13.18
Cr_2O_3	0.13	0.00	0.28	0.00	0.13	0.00	0.16	0.00	0.00
Fe_2O_3	0.94	1.87	0.18	1.52	0.68	2.43	0.86	2.06	
FeO	5.61	14.76	4.77	13.43	5.83	16.05	6.29	16.98	12.04
MnO	0.28	0.72	0.00	0.36	0.33	0.96	0.33	1.07	0.21
MgO	14.89	26.67	16.02	28.94	15.11	25.91	14.98	25.01	14.98
CaO	23.03	0.55	22.97	0.25	23.12	0.32	22.66	0.40	12.44
Na_2O	0.00	0.00	0.26	0.00	0.00	0.00	0.00	0.00	2.31
K_2O	0.00	0.00	0.00	0.00	0.00	0.00	0.00	0.00	0.30
Si	1.899	1.900	1.953	1.947	1.928	1.906	1.916	1.904	6.339
Ti	0.000	0.000	0.004	0.000	0.000	0.000	0.000	0.000	0.030
Al	0.164	0.130	0.090	0.053	0.115	0.098	0.131	0.115	2.225
Cr	0.004	0.000	0.008	0.000	0.004	0.000	0.004	0.000	0.000
Fe^{3+}	0.026	0.051	0.005	0.041	0.018	0.066	0.024	0.057	
Fe^{2+}	0.173	0.446	0.146	0.402	0.180	0.489	0.194	0.519	1.442
Mn	0.006	0.014	0.000	0.007	0.007	0.019	0.006	0.022	0.017
Mg	0.819	1.437	0.875	1.543	0.831	1.407	0.826	1.364	3.917
Ca	0.910	0.021	0.902	0.009	0.914	0.012	0.898	0.016	1.909
Na	0.000	0.000	0.018	0.000	0.000	0.000	0.000	0.000	0.641
K									0.055
Cations	4.001	4.001	4.000	4.002	3.999	4.001	4.001	3.998	15.857
Oxygens	6	6	6	6	6	6	6	6	23
Original FeO	6.45	16.44	4.93	14.80	6.45	18.24	7.07	18.83	12.04
Ca	47.84	1.1	46.9	0.46	47.48	0.63	46.8	0.8	10.7
Mg	43.06	75.47	45.5	78.97	43.17	73.7	43.1	71.8	65.3
Fe	9.1	23.42	7.6	20.6	9.35	25.6	10.1	27.3	24.0

1. Cpx Pyroxenite 77284023
2. Opx Pyroxenite 77284023
3. Cpx Pyroxenite 77284024
4. Opx Pyroxenite 77284024
5. Cpx Clinopyroxenite 77284019
6. Opx exsolved out of above Cpx Clinopyroxenite 77284019
7. Recrystallized Cpx Clinopyroxenite 77284019
8. Recrystallized Opx Clinopyroxenite 77284019
9. Amphibole Clinopyroxenite 77284019

magnetite is present, but mainly along grain boundaries.

The analyzed sample of clinopyroxenite (Table 2.1) has low alkalis (0.16 wt. % Na_2O), TiO_2, Al_2O_3 and high CaO and Fe_2O_3 contents. This is reflected in its CIPW norm which has high Di and Hy and only 7% An and 1% Ab.

Mineral analyses for the clinopyroxenite are given in Table 2.3. The host clinopyroxene between the exsolved lamellae of orthopyroxene is very similar in composition to that of the pyroxenite, and contains only 5 mol. % Ca Tschermaks molecule. However the exsolved ortho-pyroxene lamellae (En_{70-72}) are more iron rich than the orthopyroxene from the pyroxenites (Figure 2.3). The original clinopyroxene, prior to exsolution would have been more subcalcic and iron-rich and with less Al_2O_3 (Table 2.6).

The amphibole which is present in trace amounts contains 2.31 wt. % Na_2O. Thus where sodium is present in these ultramafic rocks it is concentrated in amphibole rather than clinopyroxene.

4. The Garnet Clinopyroxenite

This rock consists of garnet and clinopyroxene with minor amounts of magnetite, spinel and occasionally orthopyroxene, biotite and hornblende. The nomenclature for these rocks follows that adopted by Irving (1974). Lovering and White (1969) used the term fossaite eclogite for somewhat similar rocks characterized by Na_2O-poor clinopyroxenes which are found as xenoliths within the Delegate nephelinite pipe.

The term eclogite usually has the connotation of a jadeite-rich (omphacitic) pyroxene whereas the Antarctic clinopyroxenes are sodium-poor diopsides, salites, aluminous augites and fassaites (using the terminology of Clarke and Papike, 1968). Also, as these rocks did not equilibrate in the "eclogite facies" as defined by Green and Ringwood (1967) but at lower pressures, the non-genetic term garnet-clinopyroxenite is preferred.

In hand specimen the garnet clinopyroxenite is a modally inhomogeneous, medium grained (1-2 mm) equigranular rock with pink-red garnet and black clinopyroxene. The simplest mineralogy consists of granular pyroxene and garnet, mainly with triple point grain boundaries. Garnet is sometimes present as idiomorphic inclusions in the clinopyroxene. Areas free of garnet tend to have coarser grained clinopyroxene. A minor amount of orthopyroxene is occasionally present. Granular, green spinel and magnetite have reaction coronas of garnet separating them from the clinopyroxene. The pale pink-green clinopyroxenes contain a variety of exsolution products. Fine grained clinopyroxene and that at contacts with the garnet tend to be devoid of exsolution lamellae.

The simplest type of exsolution product consists of lamellae and blebs of garnet aligned along the (110) and less commonly the (1$\bar{1}$0) directions of the host clinopyroxene (Figure 2.2B). The exsolution assemblages observed are garnet; garnet-plagioclase-opaque oxide; garnet-orthopyroxene-opaque oxide. The exsolved garnet and plagioclase often alternate along the length of an individual lamella. Where coarser grained clinopyroxenes contain idiomorphic inclusions of garnet there is an exsolution-free zone around the inclusion (Figure 2.2C). There is often a thin zone of fine grained garnet along the grain boundaries of clinopyroxenes which have exsolved garnet, possibly due to migration of the exsolved phase to grain boundaries.

Chemical analyses of two samples of garnet clinopyroxenite are given in Table 2.1. They have lower SiO_2 and higher TiO_2, Al_2O_3, FeO and Na_2O contents than the pyroxenite and clinopyroxenite. One sample is olivine-hypersthene normative, while the other has olivine, nepheline (2.57 %) and leucite (1.11 %) in its norm, reflecting the presence of modal biotite. They do not correspond in chemical composition to basaltic rocks because of the low alkalis (0.5 wt. % Na_2O) and high

magnesium and iron contents. Furthermore their compositions do not recast as stoichiometric clinopyroxenes, suggesting that they were spinel-bearing prior to cooling and garnet formation. The moderate Fe_2O_3 content reflects the presence of modal magnetite in this rock.

Representative probe analyses of the minerals from the garnet clinopyroxenite are shown in Table 2.4. Compared to the pyroxenite and clinopyroxenite there is a considerable range in clinopyroxene composition in this rock type. The clinopyroxene contains less SiO_2 and MgO and more TiO_2, Al_2O_3, FeO and Na_2O (Figure 2.3), corresponding to a higher Ca Tschermaks content (10-16 mol. %).

Clinopyroxenes devoid of exsolutions are zoned towards the contacts with the garnet grains. There is an increase in Mg/(Mg + Fe) and decrease in Al_2O_3 content from core to rim near the garnet. The garnet is also zoned, but in an opposite sense, becoming more iron rich towards the clinopyroxenes [Mg/(Mg + Fe) = 49-56 from core to rim]. The garnets are mainly a pyrope-almandine solid solution, with around 20 mol. % grossular and 3 mol. % spessartine. This is a higher Mn content than the garnets from the petrographically similar garnet clinopyroxenite xenoliths in basalt pipes described by Lovering and White (1969).

The clinopyroxene near the exsolutions is of similar composition to the rims of exsolution-free clinopyroxene next to the large garnets. Microprobe beam scan analyses of areas of exsolution and clinopyroxene (Table 2.6) indicate that there was an initial range in composition of these clinopyroxenes, as evidenced by the different types of exsolution assemblages. The original clinopyroxenes were fassaites, with high Al_2O_3 and low Na_2O and TiO_2 contents (up to 17.9 Mol. % Ca Tschermaks' and less than 5.8 mol. % jadeite).

The orthopyroxene which has exsolved from the clinopyroxene together with garnet is more iron-rich (Mg/Mg + Fe $\approx$ 71) than that of the

TABLE 2.4

Composition of minerals in the garnet clinopyroxenites

	1 Gt	2 Cpx	3 Gt	4 Cpx	5 Gt	6 Cpx	7 Opx	8 Mt	9 Gt	10 Cpx	11 Gt	12 Cpx	13 Plag
SiO_2	39.08	46.83	38.69	49.12	38.98	48.89	51.94		38.51	49.16	38.82	48.77	44.01
TiO_2	0.00	0.52	0.00	0.47	0.00	0.33	0.00	1.37	0.00	0.68	0.00	0.30	0.00
Al_2O_3	22.10	8.98	21.85	6.25	22.03	6.54	4.59	2.17	22.99	6.19	22.17	6.46	35.91
Cr_2O_3	0.15	0.30	0.14	0.18	0.00	0.13	0.00	0.13	0.00	0.17	0.00	0.20	0.00
Fe_2O_3		2.62		1.46		1.61	0.14			1.96		2.84	
FeO	19.69	6.05	21.31	5.82	20.85	6.22	18.25		22.02	5.74	20.49	5.28	0.14
MnO	1.63	0.15	1.76	0.00	2.00	0.00	0.34	0.13	1.38	0.00	1.57	0.00	0.00
MgO	9.61	11.59	8.62	13.52	9.49	13.05	23.92	1.49	8.54	12.93	8.39	12.64	0.00
CaO	7.74	22.88	7.63	23.31	6.65	23.40	0.49		7.21	22.87	8.57	23.34	19.11
Na_2O	0.00	0.33	0.00	0.00	0.00	0.00	0.00		0.00	0.47	0.00	0.46	0.75
K_2O													0.07
Si	2.971	1.746	2.966	1.821	2.973	1.816	1.902	0.000	2.953	1.824	2.967	1.811	2.037
Ti	0.000	0.014	0.000	0.013	0.000	0.009	0.000	0.049	0.000	0.019	0.000	0.008	0.000
Al	1.979	0.395	1.974	0.273	1.981	0.286	0.198	0.121	2.014	0.271	1.998	0.283	1.959
Cr	0.009	0.008	0.009	0.005	0.000	0.004	0.000	0.005	0.000	0.005	0.000	0.006	0.000
Fe^3		0.073		0.041		0.045	0.004	0.000		0.055		0.079	
Fe^2	1.252	0.189	1.366	0.180	1.330	0.193	0.559	3.602	1.412	0.178	1.310	0.164	0.005
Mn	0.105	0.003	0.114	0.000	0.129	0.000	0.011	0.005	0.089	0.000	0.102	0.000	0.000
Mg	1.089	0.644	0.985	0.747	1.079	0.722	1.305	0.105	0.976	0.715	0.956	0.699	0.000
Ca	0.631	0.914	0.626	0.926	0.544	0.931	0.019	0.000	0.592	0.909	0.702	0.929	0.948
Na	0.000	0.023	0.000	0.000	0.000	0.000	0.000	0.000	0.000	0.034	0.000	0.033	0.068
K													0.004
Cations	8.035	4.011	8.042	4.006	8.036	4.007	3.997	3.888	8.037	4.010	8.034	4.013	5.020
Oxygens	12	6	12	6	12	6	6	4	12	6	12	6	8
Original FeO	19.69	8.41	21.31	7.14	20.85	7.67	18.39	90.80	22.02	7.54	20.49	7.84	5.020
Ca	21.2	52.3	21.0	50.0	18.4	50.4	1.0	0	19.9	50.4	23.6	51.8	
Mg	36.6	36.9	33.1	40.3	36.5	39.1	69.3	2.83	32.7	39.7	32.2	39.0	
Fe	42.1	10.8	45.9	9.7	45.0	10.5	29.7	97.2	47.4	9.9	44.1	9.1	

1. Garnet core Garnet Clinopyroxenite 77284028
2. Cpx core   Garnet Clinopyroxenite 77284028
3. Garnet rim   Garnet Clinopyroxenite 77284028
4. Cpx rim   Garnet Clinopyroxenite 77284028
5. Garnet exsolution lamellae Garnet Clinopyroxenite 77284021
6. Cpx host which has exsolved Ga+Opx+Mt. Garnet Clinopyroxenite 77284021
7. Opx exsolution lamellae. Garnet Clinopyroxenite 77284021
8. Mt exsolution lamellae. Garnet Clinopyroxenite 77284021
9. Garnet exsolution lamellae. Garnet Clinopyroxenite 77284022
10. Cpx host to above exsolution lamellae. Garnet Clinopyroxenite 77284022
11. Garnet exsolution lamellae. Garnet Clinopyroxenite 77284027
12. Cpx host which has exsolved garnet and plagioclase. Garnet Clinopyroxenite 77284027
13. Plagioclase exsolution lamellae. Garnet clinopyroxenite 77284027.

pyroxenite and clinopyroxenite (Tables 2.3, 2.4). It has a high Al_2O_3 content (4.59 wt. %) and a low CaO content (1 mol. % $CaSiO_3$). Garnet present as reaction rims around spinel is more grossular and spessartine-rich ($Py_{32.4}Alm_{40.6}Gr_{22.3}Sp_{4.6}$) than the other garnets. The green spinel is essentially a spinel-hercynite (Mg/Mg + Fe $\approx$ 50) with less than 2 wt. % Cr_2O_3.

5. The Plagioclase Clinopyroxenite

This rock consists of medium-coarse grained clinopyroxene porphyroblasts (up to 1 cm) set in a medium grained equigranular clinopyroxene and plagioclase feldspar assemblage. The plagioclase shows slight optical zoning.

A chemical analysis of this rock is given in Table 2.1. The clino-pyroxene porphyroblasts are of similar composition to those in the matrix (Table 2.5). They are richer in sodium than the other pyroxenes. The plagioclase is zoned from cores of $Or_{0.8}Ab_{27.7}An_{71}$ to rims of $Or_{0.5}Ab_{21}An_{78}$.

6. The Garnet Plagioclase Clinopyroxenite

This rock consists of the assemblage clinopyroxene, garnet, plagioclase, orthoclase, spinel and biotite. Large porphyroblasts of clinopyroxene, together with finer grained garnet and orthoclase are set in fine grained plagioclase, garnet and spinel. The orthoclase has triple point grain boundaries. Spinel is mainly present as rounded inclusions in garnet and less commonly in plagioclase. The garnet is often present as thin rims around plagioclase. The larger clinopyroxenes have exsolved garnet and plagioclase. A minor amount of biotite is also present.

TABLE 2.5

Compositions of minerals in the garnet orthopyroxenite
and plagioclase clinopyroxenite

	1 Cpx	2 Plag	3 Gt	4 Opx	5 Gt	6 Opx
SiO_2	51.57	49.17	39.37	51.59	39.06	52.55
TiO_2	0.13	0.00	0.00	0.00	0.00	0.00
Al_2O_3	4.52	32.74	22.67	4.68	22.47	3.67
Cr_2O_3	0.11	0.00	0.00	0.00	0.00	0.00
Fe_2O_3	1.19	0.00		4.14		1.84
FeO	5.15	0.00	21.84	13.66	22.77	14.51
MnO	0.19	0.00	0.26	0.00	0.21	0.00
MgO	14.10	0.00	12.50	26.14	12.17	27.53
CaO	22.76	14.57	3.36	0.19	3.32	0.08
Na_2O	0.38	3.02	0.00	0.00	0.00	0.00
K_2O	0.00	0.14	0.00	0.00	0.00	0.00
Si	1.898	2.249	2.961	1.857	2.952	1.889
Ti	0.004	0.000	0.000	0.000	0.000	0.000
Al	0.196	1.766	2.009	0.199	2.002	0.155
Cr	0.003	0.000	0.000	0.000	0.000	0.000
Fe^{3+}	0.033	0.000		0.112		0.050
Fe^{2+}	0.159	0.000	1.374	0.411	1.439	0.436
Mn	0.006	0.000	0.017	0.000	0.013	0.000
Mg	0.773	0.000	1.402	1.402	1.371	1.475
Ca	0.897	0.714	0.271	0.007	0.269	0.003
Na	0.027	0.268	0.000	0.000	0.000	0.000
K		0.008	0.000	0.000	0.000	0.000
Cations	3.996	5.006	8.034	3.988	8.047	4.008
Oxygens	6	8	12	6	12	6
Original FeO	6.23			17.40		16.17

1. Cpx   Plagioclase pyroxenite 77284025
2. Plagioclase Plagioclase pyroxenite 77284025
3. Gt core   Garnet Orthopyroxenite 77284030
4. Opx core   Garnet Orthopyroxenite 77284030
5. Gt rim   Garnet Orthopyroxenite 77284030
6. Opx rim   Garnet Orthopyroxenite 77284030

TABLE 2.6

Pre-exsolution high temperature pyroxene compositions

	1	2	3	4	5
SiO_2	52.11	48.11	47.92	47.54	50.71
TiO_2	0.00	0.28	0.27	0.29	0.26
Al_2O_3	2.47	7.80	8.19	9.04	5.34
Cr_2O_3	0.17	0.29	0.15	0.18	0.26
Fe_2O_3	1.11	1.42	2.02	1.81	0.00
FeO	7.43	8.07	7.46	7.58	12.26
MnO	0.35	0.52	0.36	0.19	0.00
MgO	16.64	13.48	13.16	11.71	10.92
CaO	19.84	20.18	20.46	21.48	19.46
Na_2O	0.00	0.00	0.21	0.37	0.79

Cations on the basis of 6 oxygens

	1	2	3	4	5
Si	1.923	1.790	1.781	1.771	1.905
Ti	0.000	0.008	0.008	0.008	0.007
Al	0.107	0.342	0.359	0.397	0.237
Cr	0.005	0.009	0.004	0.005	0.008
Fe^{3+}	0.031	0.040	0.056	0.051	0.000
Fe^{2+}	0.229	0.251	0.232	0.236	0.385
Mn	0.011	0.016	0.011	0.006	0.000
Mg	0.915	0.747	0.729	0.650	0.611
Ca	0.784	0.804	0.815	0.857	0.783
Na	0.000	0.000	0.015	0.027	0.058
Cations	4.006	4.007	4.010	4.008	3.994
Original FeO	8.44	9.35	9.28	9.21	12.26
Ca	40.7	44.6	45.9	49.2	44.0
Mg	47.5	41.5	41.0	37.3	34.4
Fe	11.9	13.9	13.1	13.5	21.6
A	2.7	8.7	9.2	10.2	6.25
C	39.6	40.7	41.7	44.1	41.26
F	57.7	50.6	49.1	45.6	52.49

1. Clinopyroxene (Cpx+Opx) Clinopyroxenite 77284019
2. Clinopyroxene (Cpx+Opx+Ga+Opaque) Garnet Clinopyroxenite 77284021
3. Clinopyroxene (Cpx+Ga) Garnet Clinopyroxenite 77284020
4. Clinopyroxene (Cpx+Ga+Plag) Garnet-Plagioclase Pyroxenite 77284027
5. Clinopyroxene (Cpx+Plag+Qtz+Opaque) Sheared basaltic gneiss 77284029.

7. The Garnet Orthopyroxenite

This rock occurs as discontinuous folded lenses in the sheared basaltic gneiss, separate from the boudin. It consists of equigranular hypersthene, garnet and opaque oxide, together with very rare biotite, plagioclase and accessory zircon. It appears to be an equilibrium assemblage, with well developed triple point grain boundaries. The hypersthene contains minute needles of rutile and very rarely has sparse exsolution lamellae of garnet.

Mineral analyses are given in Table 2.5. The orthopyroxene has a similar Mg/(Mg + Fe) ratio to that of the clinopyroxenites, but with a lower Ca content. It is zoned, becoming more magnesium-rich (En_{72} to En_{75}) and Al_2O_3 poor (4.7 to 3.7 wt. %) from core to rim where in contact with garnet. The garnet is also zoned, becoming more iron-rich from core to rim [Mg/(Mg+Fe) 50.5-40.8]. This opposite trend of Mg/(Mg + Fe) zoning in orthopyroxene and garnet grains is similar to that observed in the clinopyroxene garnet pairs from the garnet clino-pyroxenite. The garnets differ in composition from that in the other rock types, with lower grossular and spessartine contents ($Py_{45.7}$, $Alm_{44.8}$, $Gr_{8.8}$, $Sp_{0.5}$), which reflects the much lower Ca content of this rock, as indicated by the absence of clinopyroxene.

8. The Sapphirine-Phlogopite Granulite

A thin layer of sapphirine-bearing rocks occurs at the boundary between the sheared basaltic gneiss and the surrounding quartz-feldspar granulites. The sapphirine-bearing rocks are separated from the quartz-bearing granulites by a thin layer of hypersthene. The assemblages found in this zone are -

    Sapphirine-hypersthene-biotite-sphene±plagioclase±spinel

    Hypersthene-quartz-plagioclase-alkali feldspar

    Garnet-biotite-sapphirine.

The green spinel is present as rounded inclusions in the sapphirine.

V. DISCUSSION

It can be shown from the petrography and mineral chemistry that these rocks represent cumulates in a basaltic dyke which after solidification were deformed and metamorphosed at approximately constant pressure. The peak temperature of metamorphism (T_1) was about 820°C and the rocks then cooled at constant pressure to around 610°C. Different reactions occurred at different temperatures over this cooling interval. Below this temperature intracrystalline cation exchange was too sluggish to provide any further information on the physical evolution of these rocks. Temperature estimates based on the compositions of coexisting minerals as well as experimental studies of the effect of different rock compositions upon the temperature of formation of garnet indicate that garnet formed at higher temperatures in the metamorphosed cumulates than in the metamorphosed quartz tholeiite dyke.

1. Development of the Mineral Assemblages

A. Magmatic origin of mafic rock compositions

There is a progressive decrease in the Mg/(Mg + Fe) ratio and increase in Al_2O_3, TiO_2, Na_2O and K_2O in the sequence pyroxenite-clinopyroxenite-garnet clinopyroxenite and sheared basaltic gneiss. The field relations and transitional nature of the chemistries indicate that the more melanocratic rocks may have originally been pyroxene, pyroxene + spinel and pyroxene + feldspar cumulates crystallized from the enclosing sheared basaltic gneiss.

The experimental data of Green and Ringwood (1967, Table 3) for quartz tholeiite basalts shows that above the solidus plagioclase feldspar crystallizes as a major phase up to approximately 20 kb pressure. The analyzed samples of garnet clinopyroxenite (Table 2.1) contain 30-35% normative feldspar, together with normative pyroxene and olivine. The more Mg-rich pyroxenites and clinopyroxenites contain less normative feldspar (7 and 20 %). As it is known that the solubility of Ca Tschermaks' component in clinopyroxene decreases with decreasing temperature (Kushiro, 1969) these variations are consistent with these rocks having originally been a sequence of Opx, Opx + Cpx, Opx + Cpx + Sp, Cpx + Sp ± Opx, Cpx + Sp + Plag (±Opx) cumulates in the sheared basaltic sill or dyke. The crystallization of an anorthite-rich feldspar above the solidus of a tholeiitic magma indicates that the basalt dyke must have crystallized below approximately 14 kb pressure using the data of Green and Ringwood (1967)and Hariya and Kennedy (1968).

B. <u>Mineral reactions during granulite facies metamorphism</u>

(i) The quartz-tholeiite dyke.

Reaction coronas of garnet around olivine, opaque oxide and orthopyroxene in metamorphosed basaltic rocks have been described from many other metamorphic terrains (e.g. Gjelsvik, 1952; de Waard, 1965; Griffin, 1971; Wood, 1975; McLelland and Whitney, 1977). Coronas of garnet around spinel in silica-undersaturated mafic rocks have also been described from metamorphic terrains and also from granulite xenoliths present in basalt pipes (e.g. Green, 1966; Lovering and White, 1969; Griffin, 1971; Irving, 1974; Wilkinson, 1974). Reaction rims of ortho-pyroxene around olivine, and garnet around opaque oxide are more common than is the development of reaction coronas of garnet around orthopyroxene in granulite terrains because of the higher pressures required for the formation of the latter (see Green and Ringwood, 1967).

The chemistry and petrography of the metamorphosed quartz-tholeiite dyke lends for comparison with both simple system and natural rock experimental studies on the basalt-eclogite transition (Yoder and Tilley, 1962; Yoder and Kushiro, 1966; Green and Ringwood, 1967; Irving, 1974; Herzberg, 1978).

The development of an eclogite from a silica oversaturated gabbroic mineral assemblage proceeds via an intermediate stage in which the olivine, ilmenite and orthopyroxene are consumed by continuous reactions with plagioclase to produce garnet (Green and Ringwood, 1967), such as -

$$Opx + An \rightleftharpoons Alm-Py~Gt + Cpx + Qtz \qquad (1)$$

$$Opx + An \rightleftharpoons Alm-Gr-Py~Gt + Qtz \qquad (2)$$

$$Ilmenite + An + Qtz \rightleftharpoons Alm-Gr~Gt + Rutile \qquad (3)$$
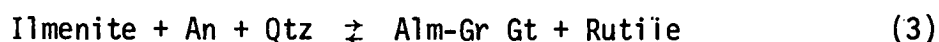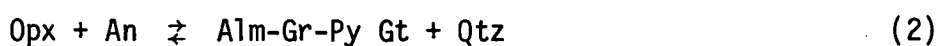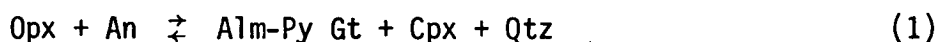
The plagioclase becomes increasingly sodium-rich because of these reactions. The presence of garnet coronas with vermicular inclusions of clinopyroxene in the sheared basaltic gneiss is evidence that reaction (1) has occurred.

The development of garnet-quartz coronas around the opaque oxides where originally in contact with plagioclase (Figure 2.2A) can be explained by reaction such as (3).

This reaction proceeds from the left hand side (L.H.S.) to the right hand side (R.H.S.) with decreasing temperature (Green and Ringwood, 1967). The opaque oxide and clinopyroxene did not react with each other, which suggests that reactions did not proceed to sufficiently low temperatures such that the following reaction (Banno and Green, 1968) could occur -

$$2Ab + Mt + Qtz \rightleftharpoons 2Ac + Gt + Qtz \qquad (4)$$
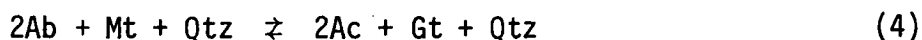
The development of an appreciable acmite content in eclogite clino-pyroxenes is restricted to temperatures below that of this reaction as in

glaucophane schist terrains (e.g. Church, 1967; Black, 1974). Clino-
pyroxenes from granulite facies terrains such as Enderby Land are
characterized by high Ca Tschermak and low jadeite contents (see
White, 1964; Kushiro, 1969).

(ii) The metamorphosed cumulates.

The metamorphosed cumulates provide an excellent example of
the importance of slight differences in bulk rock compositions upon the
mineral reactions and development of different mineral assemblages
under granulite facies metamorphism. The reactions differ from those
in the quartz-tholeiite dyke in that quartz is not a reaction product
together with garnet at the highest temperature (T_1) of metamorphism
(see reactions 1-4).

At the peak of metamorphism (T_1) the igneous cumulate assemblages
(Opx + Cpx ± Sp ± Plag ± Mt) reacted to form garnet-bearing assemblages.
Coexisting pyroxenes in the Mg-rich websterites readjusted at T_1 by
recrystallization and decrease in mutual solid solution due to expansion
of the pyroxene miscibility gap with decreasing temperature. The
reactions which occurred in the more Fe, Na and Al-rich spinel and
plagioclase bearing cumulates are due to the instability of coexisting
orthopyroxene and clinopyroxene with each of the minerals plagioclase,
spinel and magnetite -

$$Plag + Cpx + Opx \rightarrow Gt + Cpx \tag{5}$$

$$Plag + Cpx + Opx + Sp \rightarrow Gt + Cpx \tag{6}$$

$$Cpx + Opx + Sp \rightarrow Gt + Cpx \tag{7}$$

$$Plag + Subcalcic\ Cpx + Sp \rightarrow Gt + Cpx \tag{8}$$

$$Plag + Opx + Cpx + Mt \rightarrow Gt + Cpx + O_2(?) \tag{9}$$
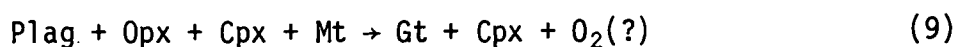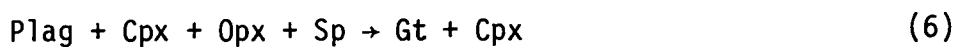
The resultant mineral assemblages at T_1 are shown in Table 2.7.
The clinopyroxenes are characterized by a high Ca Tschermak $(CaAl_2SiO_6)$
content. Garnet and clinopyroxene coexist with either orthopyroxene or
plagioclase feldspar, but not both.

With further cooling to the lower temperature (T_2) of metamorphism, the pyroxenites readjusted in mineral composition by exsolution due to further expansion of the pyroxene miscibility gap. The garnet-clino-pyroxenites readjusted by Fe-Mg cation exchange between the rims of adjacent garnets and clinopyroxenes, becoming more Fe- and Mg-rich respectively towards the grain contacts. This resulted in the Gt-Cpx K_D increasing from core to rim.

The aluminous fassaitic clinopyroxenes formed at T_1 readjusted in composition at T_2 by a wide variety of unmixing processes. This is due to the decreased solubility of aluminium in clinopyroxene in quartz deficient assemblages with decreasing temperature (See Herzberg, 1978a, b and references therein). The exsolution products are shown in Table 2.7.

Of particular interest is the development of a second generation of plagioclase feldspar in the exsolution products. This is due to the fact that at high temperatures (metamorphic T_1) igneous plagioclase is consumed to form an aluminous clinopyroxene and garnet (reactions 5-9). At lower temperatures (T_1 to T_2) there is a marked decrease in the solubility of Al_2O_3 in clinopyroxene and as a result the clinopyroxenes readjust to a less aluminous composition. Slight differences in the original pyroxene compositions have caused subtle but important differences in the exsolution product assemblages (Figure 2.4). In the simple system C-M-A-S reactions involving plagioclase would occur at a unique temperature at any given pressure. In multicomponent systems reactions occur over a broad temperature interval, and changes in temperature are reflected by changes in mineral solid solutions while still being con-sistent with reactions 5-9. Note the range in Ca-content of the garnets from the different assemblages.

TABLE 2.7

Inferred and Observed Mineral Assemblages at the Magmatic and Metamorphic
stages of evolution of the mafic granulites at 10-11 kb pressure.

MAGMATIC	METAMORPHIC			ROCK CHEMISTRY TRENDS
$T\approx1150°C$	$T\approx820°C$	$T\approx720°C$	$T\approx610°C$	
CUMULATES				
Opx	Opx±Cpx			Increasing Fe/Mg
				Na/Ca
Opx+Cpx	Opx+Cpx			Al,Fe^{3+}
Opx+Cpx+Sp-Mt	Cpx+Gt (±Sp±Opx)	Opx Gt exsolved from Cpx		
Opx+Cpx+Plag+Sp-Mt	Cpx+Gt (±Sp±Plag)	Gt-Plag exsolved from Cpx		
Opx+Cpx+Plag+Mt	Cpx+Gt+Plag	Plag exsolved from Cpx		
BASALT				
Opx Cpx Plag Qtz Mt		Cpx Gt Qtz Plag (Opx,Mt)		
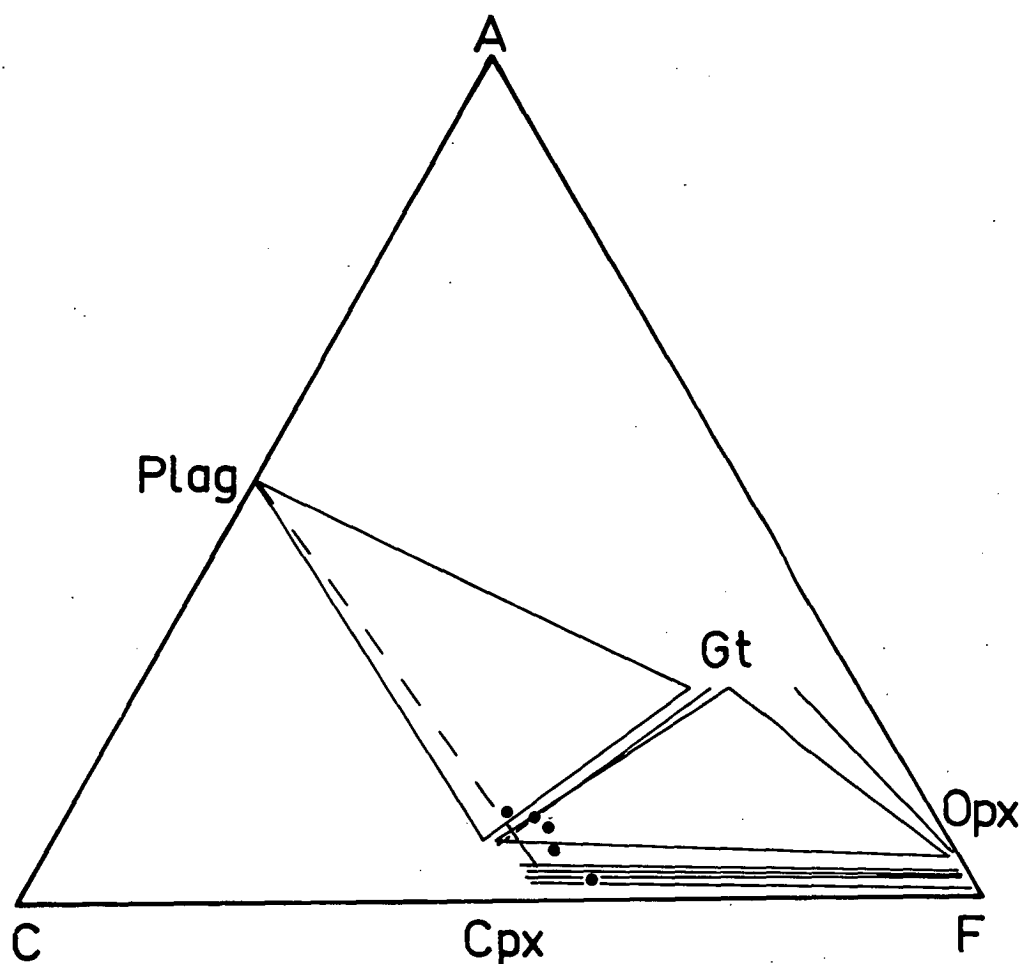
Fig. 2.4 ACF plot showing stable tie lines connecting
compositions of coexisting phases in the garnet
orthopyroxenite and exsolution assemblages in the
websterites, clinopyroxenites and garnet clino-
pyroxenites. Filled circles represent compositions
of aluminous clinopyroxenes before unmixing.
Dashed line connects coexisting clinopyroxene and
plagioclase from the exsolution assemblage Cpx-Plag-
Mt-Ilm-Qtz from the more Fe- and Na-rich sheared
basaltic gneiss.

The stability of the garnet-plagioclase tie line shown in Figure 2.4 is consistent with granulite facies conditions of metamorphism rather than the eclogite stability field where the garnet-plagioclase tie line (grossular poor garnet) is broken because of the stability of coexisting clinopyroxene-kyanite (O'Hara, 1960; Green and Ringwood, 1967). High temperature (T_1) clinopyroxene which exsolved only orthopyroxene at lower temperature had relatively low Al_2O_3 content compared to those which exsolved either garnet or plagioclase (Table 2.6). Those which exsolved both garnet and orthopyroxene were more Mg-rich than those which exsolved only garnet. Similarly, those which exsolved both garnet and plagioclase were more Ca- and Al-rich.

Subsolidus unmixing of an aluminous clinopyroxene can also explain the development of the plagioclase clinopyroxenite. A chemical analysis of this rock (Table 2.1) recalculates on the basis of six oxygen atoms per formula unit to a stoichiometric clinopyroxene, somewhat similar in composition to the clinopyroxene in the garnet clinopyroxenites (with 9 mol. % Ca Tschermak and 1.5 jadeite content).

Green (1966) ascribed garnet lamellae in clinopyroxene ejecta from Salt Lake Crater, Hawaii, as being due to unmixing from an originally high temperature aluminous clinopyroxene precipitated at high pressure from a basaltic magma. Since then, direct and inferred evidence for such unmixing processes in clinopyroxenes has been presented for xenoliths in basaltic pipes (e.g. Lovering and White, 1969; Wilkinson, 1974), and more rarely from other granulite terrains (e.g. Griffin, 1971; Battey and Davidson, 1977). The Antarctic granulite samples are more Fe-rich and contain less Na and Al than the xenolith samples however.

Lovering and White (1969) described samples in which garnet, orthopyroxene and spinel were exsolved from clinopyroxene. They inferred

that other granulite xenoliths in the basalt had developed by unmixing

from originally aluminous clinopyroxenes -

$$Cpx_1 \rightarrow Cpx_2 + Spinel + Opx \qquad (10)$$

which at lower temperatures exsolved further -

$$Cpx_2 \rightarrow Py\text{-}Gr\ Gt + An \qquad (11)$$

Also -

$$Cpx \rightarrow Cpx + Opx + Sp + An \qquad (12)$$

$$Cpx \rightarrow Cpx + Gt \qquad (13)$$

They state (p.41) that quartz or anorthite should be a byproduct of

spinel exsolution from an aluminous clinopyroxene, but observed neither.

The Antarctic clinopyroxenes provide an example of such a reaction. Also,

the variety of exsolutions and mineral assemblage present in the xenoliths

of the Delegate basalt pipe and elsewhere have been inferred to have all

equilibrated under similar P,T conditions (see Lovering and White, 1969;

Irving, 1974).   The Antarctic granulites provide direct evidence that

with small compositional differences in original mineral compositions, a

wide range of mineral assemblages can develop through subsolidus unmixing

under isofacial conditions.

Garnet is believed to have developed at the highest temperatures of

metamorphism (T_1) in the metamorphosed cumulates, but only at lower

temperature in the quartz-tholeiite dyke.   This is consistent with

experimental studies in the simple system Fo-An (Yoder and Kushiro, 1966)

and in complex systems (Green and Ringwood, 1967).   In rocks of a

basaltic composition, Na-rich feldspar is stable to higher pressures

than a Na-poor feldspar.   In such Na-rich rocks, feldspar-free pyroxenites

do not develop as the transitional assemblage between a basalt and eclogite

mineralogy in typical saturated and undersaturated basaltic compositions

at temperatures below 1100°C.   More Na-poor, silica undersaturated

compositions such as the Antarctic cumulates, in which anorthite-rich plagioclase and spinel may be present can develop a pyroxenite assemblage. Green and Ringwood (1967) also note that in magnesian compositions the reaction products are aluminous pyroxenes-spinel, whereas increasing iron content in basalt suppresses this intermediate assemblage in favour of garnet-pyroxene-plagioclase (such as the metamorphosed quartz-tholeiite dyke). The most favourable compositions for producing transitional assemblages of pyroxenes and minor spinel have a very high Mg/(Mg+Fe) ratio, normative olivine and a very low albite content, such as the Loch Duich "eclogite" described by Mercy and O'Hara (1968) or the metamorphosed Antarctic cumulates. Similarly the reaction of aluminous orthopyroxene and clinopyroxene with spinel to form garnet is consistent with experimental studies on the simple system 1:1 Anorthite: Forsterite and on a xenolith from the Delegate pipe (Yoder and Kushiro, 1966; Irving, 1974).

The development of extensive unmixing in the clinopyroxenes of the metamorphosed cumulates, and their higher Al_2O_3 contents compared to the clinopyroxenes from the metamorphosed quartz-tholeiite dyke can be explained in terms of the differing effect of temperature on the solubility of Al_2O_3 in clinopyroxene from the different assemblages. At temperatures above that of the development of garnet in the quartz tholeiite dyke, the solubility of aluminium (as $CaAl_2SiO_6$-Ca Tschermak molecule) in clinopyroxene coexisting with plagioclase and quartz (and not garnet) can be described by the reaction -

$$CaAl_2Si_2O_8 \rightleftharpoons CaAl_2SiO_6 + SiO_2 \qquad (14)$$
Anorthite   CaTs   Qtz
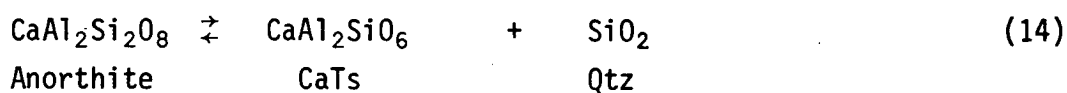
In quartz deficient assemblages such as the garnet clinopyroxenites, which contain a more fassaitic clinopyroxene, the equilibrium between

garnet and clinopyroxene can be described by -

$$Ca_2MgAl_2Si_3O_{12} \rightleftharpoons CaMgSi_2O_6 + CaAl_2SiO_6 \qquad (15)$$
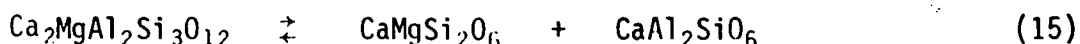
Reaction (14) is considered in Appendix 1 and reaction (15) has been studied by Herzberg (1978 a, b). At $\approx$ 10kb pressure, the solubility of CaTs defined by reaction (14) is largely independent of temperature whereas that defined by reaction (15) is much more temperature dependent, decreasing with decreasing temperature (see Herzberg, 1978a, Fig.7). This explains the higher Al_2O_3 contents and widespread development of exsolutions in the clinopyroxenes from the metamorphosed cumulates compared to the metamorphosed quartz tholeiite dyke.

2. Temperatures and Pressures of Metamorphism

It can be shown that the Antarctic granulites have reequilibrated under decreasing temperature and approximately constant pressure of metamorphism. The experimental data of Irving (1974) on the P,T conditions of equilibration of the various mineral assemblages in the Delegate garnet clinopyroxenite suite of rocks cannot be directly applied to the Antarctic granulites because of the more iron-rich nature of the latter. The Antarctic granulites equilibrated to similar mineral assemblages as inclusions present in basaltic pipes but at considerably lower pressures.

Initial magmatic temperatures of crystallization of the mafic cumulates and solidification of the basaltic dyke are inferred to be $\approx$ 1100°C (at 10kb pressure) by comparison with the experimental data of Green and Ringwood (1967). The subsequent range in temperature and pressures of metamorphism can be estimated by several independent methods. The coincidence in P-T estimates provides an excellent check on the reliability of available methods for granulite terrains.

A. Temperatures of metamorphism

The mutual solubility of enstatite and diopside in coexisting orthopyroxene and clinopyroxene is temperature dependent.   At less than 15kb the effect of pressure on the pyroxene miscibility gap is minimal for both the iron-free systems (Boyd and Schairer, 1964; Davis and Boyd, 1966; Mori and Green, 1975) and iron-bearing systems (Lindsley et al., 1974 a, b; Simmons et al., 1974). Wood and Banno (1974) and Wood (1975) devised a geothermometer which overestimates temperatures of crustal granulites by about 50°C when compared to the 15kb experimental data of Lindsley et al., (1974 a, b) and compared to other geothermometers (e.g. Hewins, 1975). Estimated initial temperature of metamorphism (T_1) is ≈860°C and the temperature of pyroxene exsolution (T_2) is ≈800°C (Table 2.8), after taking account of the above temperature adjustment.

A second method of temperature estimate can be obtained by considering the distribution of MgO and FeO between coexisting garnet and clinopyroxene, due to the following exchange reaction -

$$\frac{1}{3} Mg_3Al_2Si_3O_{12} \quad + \quad CaFeSi_2O_6 \quad \rightleftarrows \quad \frac{1}{3} Fe_3Al_2Si_3O_{12} \quad + CaMgSi_2O_6 \quad (16)$$
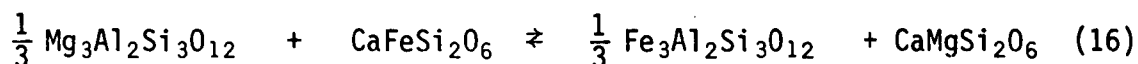
for which $K_D = \left(\frac{Fe}{Mg}\right)^{Gt} \Big/ \left(\frac{Fe}{Mg}\right)^{Cpx}$.   The garnet-clinopyroxene K_D is mainly temperature dependent, with eclogites from different metamorphic terrains and as inclusions in basalts and kimberlites having different distribution coefficients (Banno and Matsui, 1965; Lovering and White, 1969; Banno, 1970; Raheim and Green, 1974).   Temperature estimates using the method of Raheim and Green (1974) are given in Table 2.8.

Study of the garnet-clinopyroxene K_D data reveals a definite increase in K_D with increasing Ca-content of the garnet (Figures 2.4 and 2.5). An experimental study of the effect of Ca upon K_D is presented in the next chapter. Temperature estimates based on garnet-clinopyroxene K_D which take

TABLE 2.8

Temperature estimates for mafic granulites based on
Gt-Cpx and Opx-Cpx geothermometers.

Garnet Clinopyroxene Pairs

Sample No.	K_D	X_{Ca}^{Gt}	Mg/(Mg+Fe)Gt x 100	Description	T°C A	B
77284020	5.1	.166	46.96	Discrete Gt with Cpx Inclusion	725	729
77284020	5.53	.179	43.19	Gt exsolved from Cpx	714	709
77284021	6.04	.223	41.79	Reaction rim around spinel	727	688
77284021	4.61	.176	42.5	Gt-Opx-Mt exsolved from Cpx	763	756
77284022	5.21	.175	45.36	Zoned rim	727	724
77284022	5.81	.193	39.4	Gt exsolved from Cpx	712	697
77284027	3.96	.180	43.1	Core	816	798
77284027	5.57	.183	40.2	Zoned rim to above mineral pair	715	708
77284027	5.84	.229	40.37	Gt exsolved from Cpx	741	696
77284027	3.95	.178	41.51	Gt reaction rim between Cpx-Plag.	814	799
77284028	3.92	.205	44.5	Core	842	801
77284028	5.75	.202	39.9	Zoned rim to above mineral pair	723	700
77284029	8.84	.193	25.5	Gt-Cpx reaction between Opx-Plag.	611	607

Clinopyroxene-Orthopyroxene Pairs

Sample No.	Description	T°C
77284019	Cpx with Opx exsolution lamellae	850
77284019	Recrystallized grains	870
77284021	Cpx with Gt, Opx and Mt exsolution lamellae	800
77284023	Separate grains	870
77284029	Separate grains	860
77284029	Cpx in Gt-Cpx corona around Opx and rim of composition of Opx next to corona	820

A - Temperature estimate based on experimental study presented in next chapter.
B - Temperature estimate using geothermometer of Raheim and Green 1974. Note lower
   temperatures for samples with high grossular garnets compared to A.
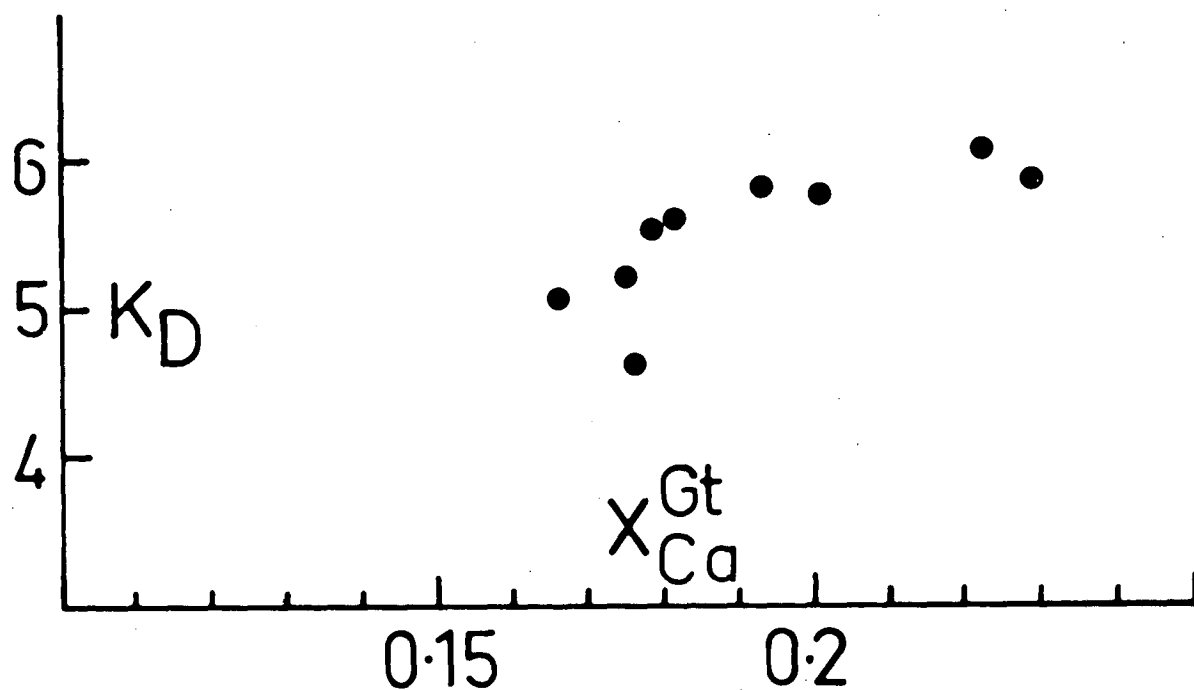
Fig. 2.5   Variation in garnet-clinopyroxene K_D $(Fe/Mg^{Gt}.Mg/Fe^{Cpx})$ with Ca content of the garnet (X_{Ca}^{Gt}) for the exsolution pairs and rim compositions in the garnet clino-pyroxenites.

account of this Ca-effect, and assuming P = 10kb, are given in Table 2.8.

The zoned garnet-clinopyroxene pairs in the garnet clinopyroxenites indicate temperatures of ≈820°C (T_1) for the cores of crystals and ≈720°C for the rims. The garnet exsolution lamellae indicate temperatures of ≈720°C as well. The reaction coronas of garnet with inclusions of clinopyroxene around orthopyroxene in the metamorphosed quartz tholeiite indicate even lower temperatures (610°C). This indicates that the two methods of geothermometry (Opx-Cpx; Gt-Cpx) give similar initial temperatures of equilibration (T_1≈860 and 820°C respectively) but differ at lower temperatures. This discrepancy at lower temperatures is believed to be due to the fact that the pyroxene solvus geothermometer is less sensitive to temperature changes below ≈800°C, whereas the Gt-Cpx K_D increases rapidly with decreasing temperature.

Temperature estimates based on coexisting plagioclase and alkali feldspar are too inaccurate for feldspars with low Ca-contents (see Powell and Powell, 1977).

B. Pressures of metamorphism

Pressures can be estimated by several independent methods. The sheared basaltic gneiss is somewhat similar in composition to the quartz tholeiites A and B of Green and Ringwood (1967), though slightly more iron rich. Comparison with their data indicates that the Antarctic rocks equilibrated at about 9-10kb pressure (at ≈800°C).

An independent method of pressure estimation can be obtained from garnet-orthopyroxene pairs, for which the solubility of Al_2O_3 in the orthopyroxene as given by the following exchange reaction is sensitive to pressure -

$$(MgFe)_2Si_2O_6 + (MgFe)Al_2SiO_6 \rightleftharpoons (MgFe)_3Al_2Si_3O_{12} \qquad (17)$$
$$\text{Opx Solid Solution} \qquad\qquad \text{Garnet}$$
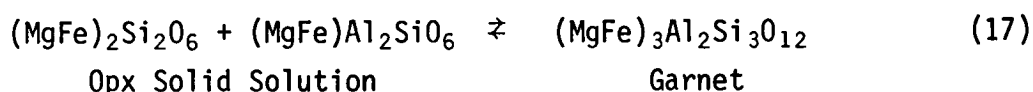
The garnet orthopyroxenite shows zoning from core to rim in the garnet and orthopyroxene. Pressure estimates for the cores (at $T_1 = 840°C$) are ≈6kb pressure whereas the rims (at $T_2 = 720°C$) yield ≈8kb pressure using the method of Wood (1974). The higher pressure estimate is in quite good agreement with that based on the phase boundary marking the incoming of garnet in basaltic rocks (Green and Ringwood, 1967). In contrast, coexisting garnet-orthopyroxene exsolution lamellae in garnet clinopyroxenite (sample 77284021) give an unrealistic equilibration pressure (-0.3kb) at T_2, which suggests that current understanding of this method of pressure estimation is not yet adequate for all P-T conditions.

A similar reaction to (17) can be written for garnet-clinopyroxene assemblages -

$$Ca_2MgAl_2Si_3O_{12} = CaMgSi_2O_6 + CaAl_2SiO_6 \qquad (18)$$

Garnet   Diopside   Ca-Tschermak

Herzberg (1978, a, b) developed a thermodynamic model for this reaction and suggested that it makes a reasonable geobarometer. Application of Herzberg's equation (1978, b, p.376) to the garnet clinopyroxenites (Table 2.3, No. 3-4) would indicate pressures of -13kb at 720°C. Examination of Herzberg's equation indicates that pressure estimates change greatly with small changes in temperature, suggesting that it cannot be used accurately as a geobarometer for crustal rocks.

A fourth method of pressure estimation can be obtained from a study of the concentration of Ca-Tschermak's molecule in clinopyroxene coexisting with plagioclase and quartz (not garnet), as given by the reaction -

$$CaAl_2Si_2O_8 \rightleftarrows CaAl_2SiO_6 + SiO_2 \qquad (19)$$

Anorthite   Ca-Tschermak   Quartz
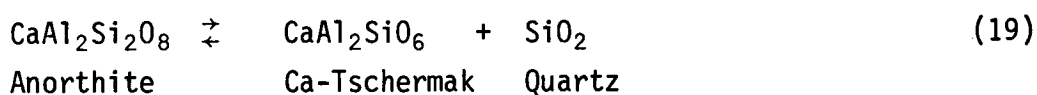
Details of this equilibria are given in Appendix 1. It provides

an excellent geobarometer, as it is very pressure sensitive and insensitive to temperature at about 10kb pressure. Pressure estimates based on the cores of pyroxene and plagioclase in the sheared basaltic gneiss are $\approx$11kb (at T_1) whereas the pressure (at T_2) based on the composition of feldspar coexisting with quartz as exsolution lamellae in the clinopyroxenes is also $\approx$11kb (Table 2.8).

The internal consistency of these various methods of geother-mometry and geobarometry are shown in Figure 2.6. Pressure-temperature curves for equilibration of each of the assemblages using the different methods shows that the garnet-clinopyroxene K_D provides an excellent geothermometer, and is relatively insensitive to pressure. The solubility of Ca Tschermak's molecule in clinopyroxene coexisting with plagioclase and quartz provides an excellent geobarometer, largely independent of temperature. In contrast, the solubility of Al_2O_3 in orthopyroxene coexisting with garnet is much less pressure sensitive under these conditions and provides widely varying pressure estimates. Possible causes for this inconsistency in garnet-orthopyroxene geobarometry lie in the fact that iron-rich orthopyroxenes show significant ordering in the M_1-M_2 site partitioning of Mg and Fe^{2+} as shown by Virgo and Hafner (1969) and Saxena and Ghose (1971). These non-ideal contributions to garnet-orthopyroxene equilibria need to be understood before this potential geobarometer-geothermometer can be quantitatively applied to the low pressure-temperature regimes in crustal metamorphism.

The garnet-clinopyroxene and orthopyroxene-clinopyroxene geo-thermometers give reasonably good agreement for the highest temperatures (T_1) of metamorphism (up to 840°C and down to 860°C respectively, Table 2.8). Similarly, the temperature estimates where both garnet and orthopyroxene have exsolved from the one clinopyroxene grain also give
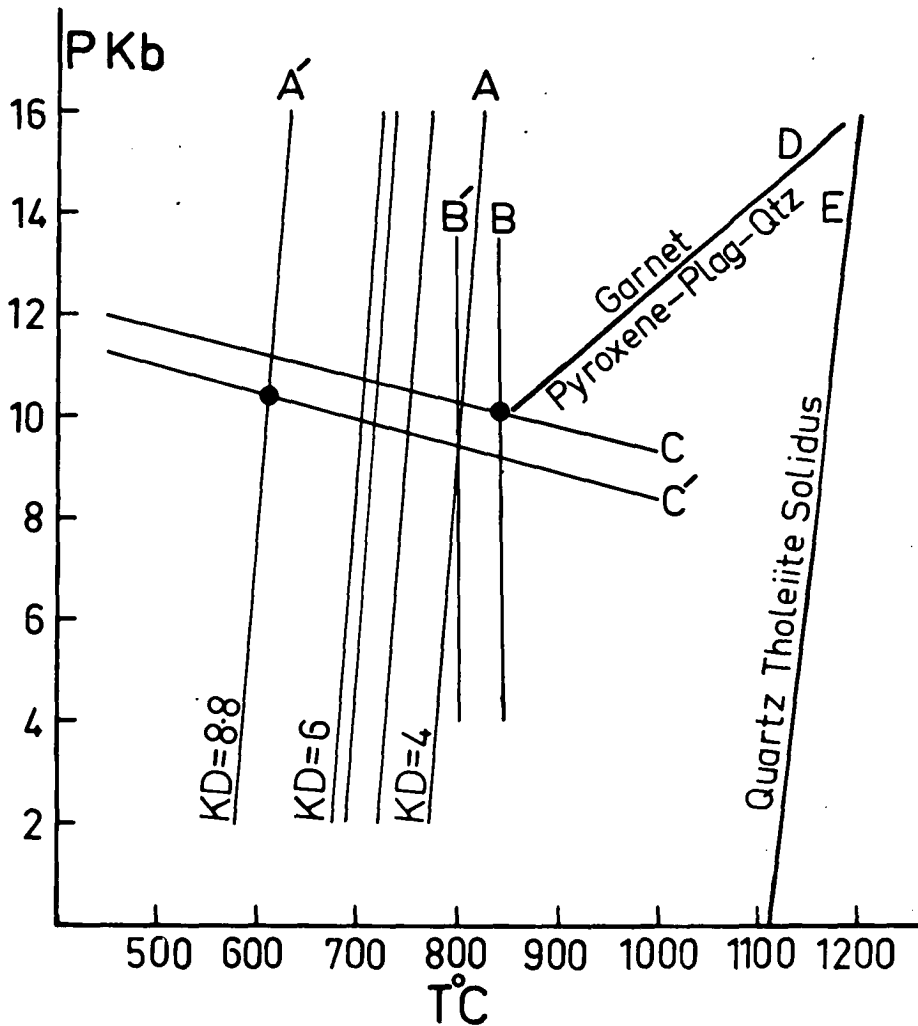
Fig. 2.6 Summary of the estimated P-T conditions of formation of mafic granulites as defined by points of intersection of the geothermometers and geobarometers. Circles show maximum and minimum P-T conditions of metamorphism.
A,A' temperature estimates from Gt-Cpx K_D equilibria.
B,B' temperature estimates from Opx-Cpx solvus.
C,C' pressure estimate from Plag-Cpx-Qtz equilibria.
      Unprimed letter - highest temperature assemblages.
      Primed letter - lowest temperature assemblages.
Note the limited range in temperature estimates based on Opx-Cpx compared to Gt-Cpx geothermometer.
D   First appearance of garnet in quartz tholeiite composition (Mg_{61}) from experimental study of Green and Ringwood (1967).
E   Approximate solidus for a quartz tholeiite magma (Green and Ringwood, 1967).

reasonable coincidence in lower temperature estimates (763 and 800°C respectively, Table 2.8, sample 77284021). In contrast, the garnet-clinopyroxene K_D data indicates that garnet formed in the sheared basaltic gneiss at a considerably lower temperature (611°C) whereas co-existing orthopyroxene and clinopyroxene in this rock (Table 2.8, sample 77284029) indicate temperatures of 860°C. Mineral compositions in the sheared basaltic gneiss indicate that equilibrium may only have existed in adjoining grains. Thus the clinopyroxene present in garnet coronas is more Mg-rich than that associated with plagioclase. Temperature estimates using garnet together with the clinopyroxene which is not in contact with the garnet in this rock would indicate an erroneously higher temperature of garnet formation.

The calculated lower temperature of formation of garnet in the sheared basaltic gneiss compared to that in the quartz-free metamorphosed cumulates, is consistent with experimental studies on the effect of bulk rock composition on the appearance of garnet in mafic rocks. The temperature of garnet equilibration in the sheared basaltic gneiss is somewhat lower than would be predicted by a simple linear extrapolation to lower temperatures of the experimental data of Green and Ringwood (1967) on the basalt-eclogite transition (Figure 2.6). The Antarctic granulites may thus provide supporting evidence for a curvature with decreasing temperature for the reaction $An + Opx \rightleftharpoons Gt + Cpx + Qtz$ which the currently available thermodynamic data suggests should occur (see Herzberg, 1978 a). Such considerations call for a reinvestigation of the basalt-eclogite transition which currently rests upon linear extrapolations of a limited number of higher temperature experimental points (Green and Ringwood, 1967; Herzberg, 1978).

Thus it can be concluded that the basaltic dyke crystallized at

approximately 10kb pressure, 1150°C. Subsequent regional metamorphism at 9-13kb pressure, 800-850°C was followed by cooling at constant pressure. The garnet clinopyroxenites formed at the peak of metamorphism, and extensive unmixing of the fassaitic clinopyroxenes occurred at about 720°C. The more strongly sheared basaltic gneiss developed garnet at still lower temperatures ($\approx$610°C). Except for the mineral zoning in the garnet clinopyroxenites (T_1-T_2 $\approx$800-720°C) the geothermometers apparently reflect temperatures of formation of each specific mineral assemblage rather than responding to low temperature changes by intercrystalline diffusion and zoning.

This style of deep crustal metamorphism is essentially one of slow cooling from a metamorphic thermal peak at constant pressure. Uplift to the surface most probably occurred at temperatures well below 600°C, as suggested by the lack of further low temperature reaction. In contrast, Griffin (1971) has shown that Norwegian mafic granulites from the Indre Sogn area underwent a rapid drop in pressure at relatively high temperatures, as evidenced by the breakdown of garnet to a symplectite of orthopyroxene, plagioclase, spinel ($\pm$ clinopyroxene). This decompression is probably related to the formation of the Jotun Nappes (Griffin, 1971) in contrast to the more tectonically stable nature of this part of the East Antarctic Shield during the Precambrian.

Chapter 3

AN EXPERIMENTAL STUDY OF THE EFFECT OF Ca UPON

GARNET-CLINOPYROXENE Fe-Mg EXCHANGE EQUILIBRIA

Contents   page

I. SUMMARY

A series of basaltic compositions and compositions within the simple system $CaO-MgO-FeO-Al_2O_3-SiO_2$ have been crystallized to garnet-clinopyroxene bearing mineral assemblages in the range 24-30 kb pressure, 750-1300°C temperature. Microprobe analyses of coexisting garnet and clinopyroxene show that K_D ($Fe/Mg^{Gt}/Fe/Mg^{Cpx}$) for the Fe-Mg exchange reaction between coexisting garnet and clinopyroxene is obviously dependent upon the Ca-content and apparently independent of the Mg/(Mg+Fe) content of the clinopyroxene and garnet. The Ca-effect is due to non-ideal Ca-Mg substitutions in the garnet and clinopyroxene M2 site.

Our data and interpretation reconciles previous inconsistencies in the temperature dependence of K_D-values determined in experimental studies of simple systems, complex basalt, grospydite and garnet peridotite compositions. Previous differences between the effect of pressure upon K_D as predicted from simple system theory (Banno, 1970) and that observed in experiments on multicomponent natural rock compositions (Raheim and Green, 1974a) can now be resolved.

We have determined K_D as a function of P,T and X_{Ca}^{Gt} (grossular) and derived the empirical relation -

$$T\ (°K) = \frac{3104\ X_{Ca}^{Gt} + 2837 + 17.08\ P(kb)}{\ln K_D + 1.9034}$$

This empirical relationship has been applied to garnet-clinopyroxene bearing rocks from a wide range of geological environments. The geothermometer yields similar estimates for garnet-clinopyroxene equilibration for neighbouring rocks of different composition and different K_D values. In addition, temperature estimates using the above relationship are more consistent with

independent temperature estimates based on other geothermometers than previous estimates which did not correct for the Ca-effect.

An alternative approach to the above empirical geothermometer is presented using regular solution models to derive Margules parameters for various solid solutions in garnets and clinopyroxenes. Derived parameters are broadly consistent with those determined from binary solid solution studies. The non-ideality of the Ca substitution, documented by the new experiments, decreases with increasing iron contents in both phases. It is proposed that the observed independence of the Ca-effect with Mg/(Mg+Fe) can be explained (within experimental error) in terms of the net excess Gibbs free energy of mixing remaining approximately constant with increasing iron contents for the Fe-Mg exchange reaction. Caution must be excercised in interpreting the derived interaction parameters in terms of actual thermodynamic properties of the relevant crystalline solid solutions because of the assumptions which necessarily have to be made in this approach.

II. INTRODUCTION

Eclogites occur in a wide variety of geological environments (e.g. Coleman et al., 1965) and the stability fields of various eclogites have been experimentally determined in several laboratories (e.g. Yoder and Tilley, 1962; Green and Ringwood, 1967; Ito and Kennedy, 1968). It is well known that eclogites from different geological environments have different K_D values (Banno, 1970; Coleman et al., 1965; Lovering and White, 1969; Mysen and Heier, 1972) and these differences have been interpreted in terms of different P,T conditions of formation. Raheim and Green (1974a) experimentally

calibrated $K_D^{Gt.Cpx} = \left(\frac{Fe^{Gt}}{Mg} \cdot \frac{Mg^{Cpx}}{Fe}\right)$ as a function of P and T for a series of natural basaltic rocks crystallized to eclogite at 20-40 kb, 600-1400°C. They stressed that their results could only be used as a practical geothermometer for rocks of basaltic composition, as the effects of large variations in concentration of other components upon K_D was largely unknown. Empirically Raheim and Green (1974a) observed that the bulk chemical composition did not perceptibly affect the K_D for basaltic rocks in the range Mg/(Mg+Fe) = 0.062 - 0.85. Furthermore they concluded that the effect of pressure°upon K_D for multicomponent equilibria was greater than that estimated on thermodynamic grounds for simple system equilibria (Banno, 1970). Considerable discussion has arisen concerning the magnitude of this pressure effect (e.g. Wood, 1975, 1977). Also, experimental studies for simple systems, garnet peridotite, and highly aluminous compositions have yielded empirical K_D values differing from those for basaltic systems (Kushiro et al., 1972; Raheim and Green, 1974a, b; Hensen, 1973; Akella, 1976; Mori and Green, 1978).

The present experiments were designed to test the effect of varying the Ca-content of clinopyroxene and garnet upon K_D. The possibility that garnet solid solutions are non-ideal (see Thompson, 1967) has previously been suggested from natural rock data on garnet-biotite and garnet-clinopyroxene equilibria (e.g. the last chapter; Saxena, 1973, p.33; Ganguly and Kennedy, 1974) and from simple system experiments and solution calorimetry on pyrope-grossular relations (Hensen et al., 1975; Newton et al., 1977; Wood, 1977).

III. GENERAL THERMODYNAMIC CONSIDERATIONS

The thermodynamic basis for the elucidation of the effects of pressure, temperature and varying mineral compositions upon garnet-clinopyroxene Fe-Mg exchange equilibria has been succinctly presented elsewhere (Thompson, 1967; Banno, 1970) and only brief reference need be given here. The distribution of Fe^{2+} and Mg^{2+} between coexisting garnet and clinopyroxene for the simple system end member exchange reaction -

$$CaFeSi_2O_6 + \frac{1}{3} Mg_3Al_2Si_3O_{12} = CaMgSi_2O_6 + \frac{1}{3} Fe_3Al_2Si_3O_{12} \tag{1}$$

is given by the relationship

$$\Delta G^o_{P,T} = \Delta H - T\Delta S + (P-1)\Delta V = - RT\ln K$$

where

$$K^{Gt.Cpx}_{FeMg} = \left(a^{Gt}_{Fe} \right)^{1/3} \Big/ \left(a^{Cpx}_{Fe} \right) \Big/ \left(a^{Gt}_{Mg} \right)^{1/3} \Big/ \left(a^{Cpx}_{Mg} \right)$$

$$= \left(\frac{X^{Gt}_{Fe}}{X^{Gt}_{Mg}} \cdot \frac{X^{Cpx}_{Mg}}{X^{Cpx}_{Fe}} \right) \cdot \left(\frac{\gamma^{Gt}_{Fe}}{\gamma^{Gt}_{Mg}} \cdot \frac{\gamma^{Cpx}_{Mg}}{\gamma^{Cpx}_{Fe}} \right) \tag{2}$$

where a^{Gt}_{Fe} is the activity of Fe garnet in the garnet solid solution, X^{Gt}_{Fe} is the molecular proportion of Fe to the sum of the divalent cations and γ^{Gt}_{Fe} is the activity coefficient of Fe garnet in the garnet solid solution etc.

In the limiting case where both minerals behave as ideal solid solutions ($a = x\gamma$, $\gamma = 1$) then

$$K^{Gt.Cpx}_{Fe.Mg} = K_D = \left(\frac{Fe}{Mg} \right)^{Ga} \Big/ \left(\frac{Fe}{Mg} \right)^{Cpx} \tag{3}$$

The distribution coefficient (K_D) can be obtained from the mineral compositions, and in the case of ideal solid solutions is a function of P,T only.

However when deviations from ideality exist, this model is inadequate to explain the variations in the measured K_D with P,T and compositional changes, and the application of a rigorous thermodynamic treatment to such Fe-Mg exchange equilibria requires a knowledge of the activity coefficients ($a = x\gamma$, $\gamma \neq 1$) of the various solid solutions. There is as yet little data available on the activity-composition relationships for many binary solid solutions (see Wood, 1975; Hensen et al., 1975; Newton et al., 1977).

In theory at least it is possible to derive activity-composition relationships for different solid solutions from multicomponent experimental data by linear regression analysis of the non-ideal contributions in terms of regular solution model margules or interaction parameters. This approach to the analysis of the data is presented in Appendix 2. Unfortunately our knowledge of the mixing properties of many binary solid solutions is insufficient at this stage to justify such a rigorous treatment. In particular the assumptions which are necessary at this stage for the derivation of activity-composition relations of binary solid solutions from multi-component equilibira render such thermodynamic parameters little more than mathematical expressions for the variations in K_D with mineral composition (Appendix 2).

It is often found that small departures from ideality in solid solutions can be neglected for practical purposes, and tend to have cancelling effect for some equilibria. This is justified for jadeite substitutions from our own data, at least above 1000°C (see discussion).

A limitation of our approach is that the effects of non ideality in the garnet and clinopyroxene solid solutions are cumulative in their effects on K_D, and it is not possible to readily isolate non-ideality

in garnet from that in clinopyroxene since the equilibrium under investigation involves solid solutions in both phases (see Appendix 2). Thus the approach adopted in the following pages is the derivation of a general equation for the P,T and compositional dependence to K_D as a *practical* geothermometer in terms of the variation in K_D with P,T and X_{Ca}^{Gt}. This allocation of all the non-ideal contributions to K_D to the Ca-substitution in garnet is justified for this approach as the variation in Ca-content of clinopyroxene is in the same sense as that in the coexisting garnet with variations in P, T and rock composition.

IV. EXPERIMENTAL STARTING COMPOSITIONS

A series of simple system synthetic glasses with varying Mg/(Mg+Fe) were prepared using AR grade chemicals (Table 3.1). To these were added various amounts of either $CaAl_2SiO_6$ glass, $NaAl_2SiO_6$ glass or natural orthopyroxene (Green, 1969, Opx 2539). The ortho-pyroxene seeds were ground to less than 2 micron grain size. Experiments were also performed on several multicomponent lunar glass mixes (Table 3.1).

The simple system glasses and seeds were prepared in appropriate proportions so as to produce under the P, T conditions of the eclogite facies as defined by Green and Ringwood (1967) the following mineral assemblages with increasing Ca-contents of the garnets (Figure 3.1) -

Ga - Cpx - Opx ± Qtz

Ga - Cpx - Qtz

Ga - Cpx - Qtz - Kyanite

TABLE 3.1

Simple system and natural rock compositions used in experimental study

	1	2	3	4	5	6	7
SiO_2	53.78	52.23	50.81	49.46	56.39	45.03	47.6
TiO_2						2.90	1.2
Al_2O_3	10.11	9.85	9.59	9.33	0.90	8.59	20.7
Cr_2O_3						0.55	0.1
FeO	9.83	15.96	21.73	27.19	9.39	21.03	8.2
MnO						0.28	0.1
MgO	12.90	8.96	5.23	1.70	32.64	11.55	7.6
CaO	13.38	13.00	12.64	12.32	0.55	9.42	12.5
Na_2O						0.23	0.7
K_2O						0.06	0.5
P_2O_5						0.07	0.4
Total	100.00	100.00	100.00	100.00	99.87	99.71	99.6

1. Synthetic glass Mg_{70}

2. Synthetic glass Mg_{50}

3. Synthetic glass Mg_{30}

4. Synthetic glass Mg_{10}

5. Orthopyroxene used for addition to glasses 1-4. Opx 2539, (Green, 1969).

6. Synthetic Lunar Glass 12009 (Green et al., 1971).

7. Synthetic Lunar Glass 14310 (Green et al., 1972).
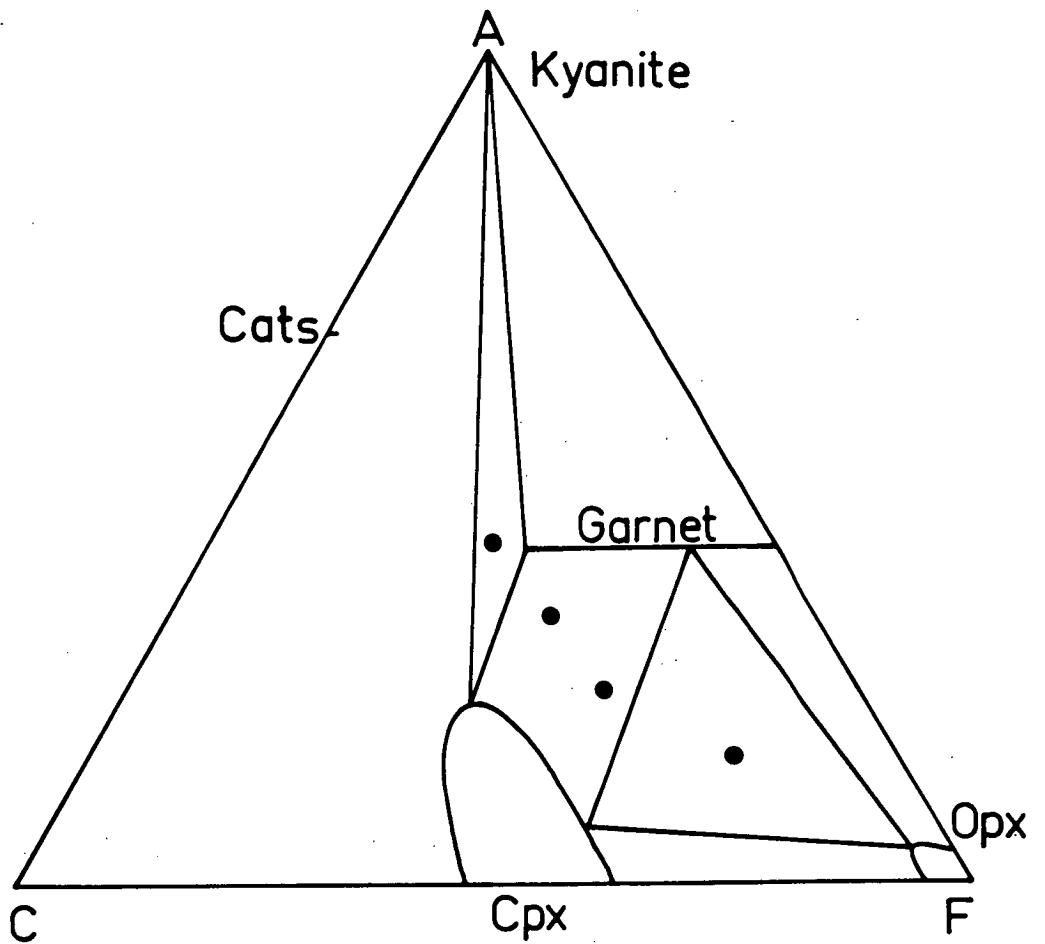
Fig. 3.1 Al-Ca-(Fe+Mg) plot of starting mix compositions showing variation in Ca-content of garnet in the different mineral assemblages. Tie lines are diagrammatic.

V. <u>EXPERIMENTAL TECHNIQUES</u>

High pressure experiments were carried out using piston cylinder apparatuses at the Geology Department, University of Tasmania. Experimental techniques are similar to those described by Green and Ringwood (1967). Temperature was measured using a $Pt/Pt_{90}Rh_{10}$ thermocouple. The recorded temperature was controlled to within ±5°C of the set point, and the precision of temperature measurement when allowance is made for temperature gradients in the samples is ±15°C (calibration experiments by W. Hibberson).

A variety of capsule materials were used, depending upon the run conditions and starting mixes. In order to ensure that there was no iron loss nor oxidation, experiments were initially carried out in Spec Pure Fe capsules. However it was found that reduction of FeO occurred in the more iron-rich glasses, with blebs of metallic iron being produced. When this occurred the pyroxene would selectively reequilibrate to more Mg-rich compositions whereas the garnets were slower to reequilibrate. This resulted in an erroneously high K_D value. Similar problems were previously encountered in attainment of equilibrium using mineral mixes rather than glasses as starting materials (Raheim and Green, 1974a). These experiments were repeated in graphite capsules, which at 30 kb pressure maintain a higher oxygen fugacity than that of metallic iron, whereas at very low pressures graphite is more reducing than metallic iron (Ryabchikov <u>et al</u>., in prep.) At low temperatures (750°C) the presence of an H_2O-rich fluid phase was necessary to speed reactions and experiments were carried out with water in sealed $Ag_{75}Pd_{25}$ capsules.

In order to be certain that variations in K_D values between

samples were due to differing Ca-contents and not to variations
in run conditions, large diameter metallic iron and graphite
capsules were prepared with up to four separate sample holes in
each.   Thus for each run up to four different starting mixes could
be studied under identical experimental conditions.   Such capsules
were sealed inside large diameter $Ag_{75}Pd_{25}$ capsules together with
a minor amount of water.

All mineral analyses have been obtained using a Si(Li)
detector attached to a JEOL scanning electron microscope-microprobe
at the University of Tasmania, following the methods outlined by
Reed and Ware (1975).

VI. RESULTS

1. Presentation of Data

Experimental run conditions are given in Table 3.2 and
representative mineral analyses are presented in Appendix 3.
Results of these experiments are summarized in Figures 3.2-3.7.
It has been found that variations of up to 30 mol. percent jadeite
in the clinopyroxene do not, within experimental error affect the
K_D (Table 3.2).   This is consistent with ideal jadeite-diopside
solid solutions at high temperatures as suggested by Ganguly (1973).
In contrast there is a marked dependence of K_D upon the Ca content
of the garnet and clinopyroxene.   For practical purposes a suitable
method for displaying this variation is to plot the variation of K_D
with X_{Ca}^{Gt} (Ca/Ca+Mg+Fe of garnet).   This does not imply that the
observed variation of K_D with changing rock composition is solely due

Table 3.2

Run Details

Run	P (kb)	T (°C)	Starting Mix	Time (hrs)	Capsule	K_D	Garnet Ca	Mg	Fe	Comments
T-26	30	1200	.7 Ec Mg70+.3 CaTs	48	Fe	3.64	43.7	34.4	21.8	Gt Cpx Qtz Ky
"	"	"	.88 Ec Mg70+.12 CaTs	"	"	3.03	30.8	43.7	25.4	Gt Cpx
"	"	"	1.0 Ec Mg70	"	"	2.31	18.9	49.2	31.9	
"	"	"	.63 Ec Mg70+.37 Opx 2539	"	"	1.96	15.8	57.4	26.8	Gt Cpx Opx
T-27	30	1300	.7 Ec Mg70+.3 CaTs	5½	Fe	3.29	45.9	32.4	21.7	
"	"	"	.88 Ec Mg70+.12 CaTs	"	"	2.45	31.1	42.3	26.6	
"	"	"	1.0 Ec Mg70	"	"	2.32	22.8	45.0	32.2	
"	"	"	.63 Ec Mg70+.37 Opx 2539	"	"	1.91	17.0	58.6	24.3	Fe reduction
T-28	24	1200	.7 Ec Mg70+.3 CaTs	40	Fe	3.00	41.0	37.4	21.6	
"	"	"	.88 Ec Mg70+.12 CaTs	"	"	2.22	26.1	49.9	24.0	
"	"	"	1.0 Ec Mg70	"	"	1.84	18.2	59.2	22.6	
"	"	"	0.63 Ec Mg70+.37 Opx 2539	"	"	1.47	13.1	65.0	21.9	
T-36	24	1300	0.7 Ec Mg70+0.3 CaTs	5½	Fe	2.33- 2.13	33.5- 34.1	42.1- 46.3	24.4- 19.7	
"	"	"	.88 Ec Mg70+0.12 CaTs	"	"	1.62- 2.10	18.5- 21.6	62.0- 53.8	19.5- 24.5	
T-43A	30	1100	0.7 Ec Mg30+0.3 CaTs	26	Fe	4.09- 4.52	47.2	10.3	42.5	
T-47	30	1200	1.0 Ec Mg70			2.21	20.7	47.9	31.3	
"	"	"	.945 Ec Mg70+.055 Jd			2.3	22.7	44.0	33.2	
"	"	"	.833 Ec Mg70+.167 Jd			2.09	20.7	45.2	34.1	
T-52	30	1200	.7 Ec Mg70+.3 Jd	6	Graphite	1.73	11.3	61.6	27.0	
"	"	"	1.0 Ec Mg30	"	"	2.59	24.5	19.5	56.0	
"	"	"	.88 Ec Mg30+.12 CaTs	"	"	3.43	38.5	14.9	46.9	
"	"	"	.7 Ec Mg30+.3CaTs	"	"	3.7	45.4	17.6	37.0	
T-53	30	1200	1.0 Ec Mg70	26	Graphite	2.38- 2.43	17.5- 21.2	48.6- 46.8	33.8- 32.0	
"	"	"	1.0 Ec Mg50	"	"	2.67	38.1	39.3	22.6	

Table 3.2 cont.

Run	P (kb)	T (^{o}C)	Starting Mix	Time (hrs)	Capsule	K_D	Garnet Ca	Garnet Mg	Garnet Fe	Comments
T-53	30	1200	.88 Ec Mg50+.12 CaTs	26	Graphite	2.01	20.8	41.5	37.7	
"	"	"	.7 Ec Mg50+.3 CaTs	"	"	3.0–2.85	30.1–27.5	35.0–36.5	34.9–36.0	
T-72	30	900	1.0 Ec Mg30+H_2O	119½	Graphite in $Ag_{75}Pd_{25}$	4.63–5.07	26.3–19.6	13.2–13.4	60.5–67.0	
"	"	"	.88 Ec Mg30+.12 CaTs + H_2O	"	"	4.48–5.30	29.3–25.2	15.0–13.9	55.7–60.9	
"	"	"	.7 Ec Mg30+.3 CaTs+H_2O	"	"	5.38	29.7	12.4	57.9	
T-77	15	900	.88 Ec Mg30+.12 CaTs+H_2O	132½	"	4.16	30.6	15.4	54.0	
"	"	"	1.0 Ec Mg30+H_2O	"	"	4.62	23.1	12.2	64.8	
"	"	"	.7 Ec Mg30+.3 CaTs+H_2O	"	"	5.4–7.55	37.6–36.5	15.7–12.3	46.7–51.2	
T-81	30	750	.7 Ec Mg30+.3 CaTs+ H_2O	169½	"	9.54–14.15	32.4–34.2	11.4–9.50	56.2–56.4	
T-88	30	900	Lunar 12009 + H_2O		"	4.03–4.51	18.7–19.6	24.8–23.7	56.5–56.7	Gt Cpx Opx Rutile
T-96	30	900	Lunar 14310 + H_2O	168½	"	5.69	32.8	34.2	33.0	Gt Cpx Ky Zos Qtz
"	"	"	Ec Mg50 + H_2O	"	"	4.29	23.5	23.2	53.3	Gt Cpx Qtz
T-110	30	750	Lunar 12009 + H_2O	264	$Ag_{75}Pd_{25}$	6.93	22.0	18.3	59.7	Gt Cpx Opx Ilm
T-126	30	750	Lunar 14310 + H_2O	161	$Ag_{75}Pd_{25}$	8.32–14.67	33.2–29.3	29.9–22.3	36.9–48.4	Gt Cpx Zoisite Ky Rutile

to variations in X_{Ca}^{Gt} (see discussion).

The variation of K_D with X_{Ca}^{Gt} at 30 kb, 1200°C is shown in Figure 3.2. It has been found that *within experimental error* the K_D - X_{Ca}^{Gt} variations are independent of the Mg/(Mg+Fe) content of the run products, in agreement with the earlier work of Raheim and Green (1974a). This feature will be further discussed in a later section.

The K_D - X_{Ca}^{Gt} variation for the temperature range 750° - 1300°C is shown in Figure 3.3. The 1100°C experimental data of Raheim and Green (1974a, b) for terrestrial and high alumina lunar basaltic compositions is also shown. This displays the same relationship as our own data.

At lower temperatures the variation in K_D with X_{Ca}^{Gt} should be more pronounced than at higher temperatures. Our low temperature data does not cover as large a range of X_{Ca}^{Gt} as at higher temperatures, and hence the magnitude of this K_D -Ca dependence is not as clearly demonstrated at low temperatures, even though reproducible results have been obtained. This difficulty is due to shifts in the tie lines for coexisting mineral assemblages with temperature (Figure 3.4). The Ca-content of garnet and clinopyroxene coexisting with ortho-pyroxene increases with decreasing temperature and the Ca-content of garnet coexisting with kyanite and clinopyroxene decreases with decreasing temperature. This contraction in the possible range of Ca-contents of garnet and clinopyroxene with decreasing temperature limits the possible compositional range over which we can obtain data to investigate K_D - X_{Ca}^{Gt} relationships.

In contrast, our data shows that with increase in pressure the range in X_{Ca}^{Gt} expands for the above assemblages. It has previously been shown that the X_{Ca}^{Gt} content decreases with increasing pressure
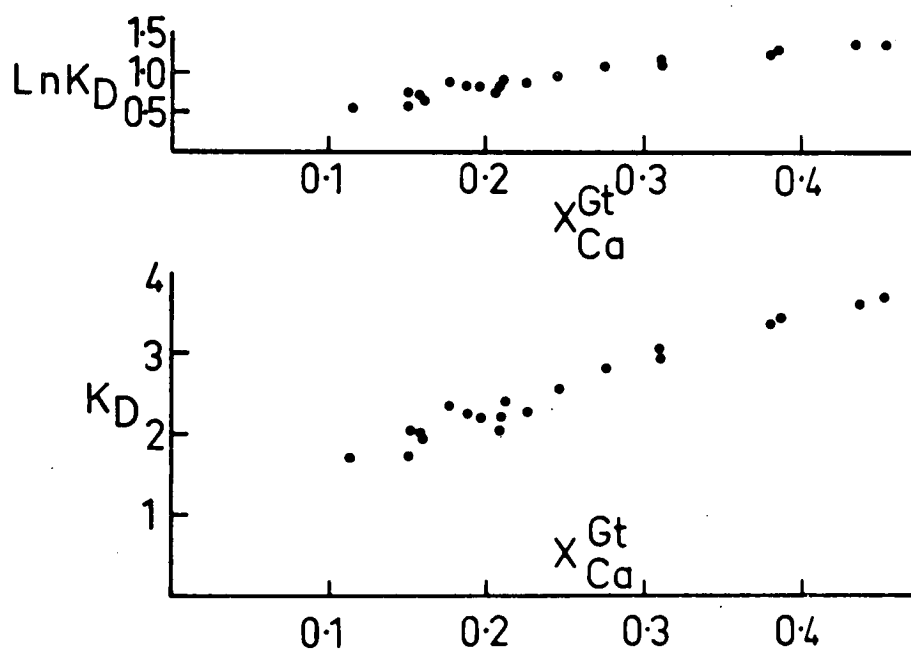
Fig. 3.2   Variation in K_D and ln K_D with X_{Ca}^{Gt} at 30 kb, 1200°C.
Data sources - this thesis; Rahelm and Green, 1974a,
b; Mori and Green, 1978.

Fig. 3.3 Variation in ln K_D with X_{Ca}^{Gt} at 30 kb pressure for the range 800-1500°C. Data sources - this thesis; Raheim and Green, 1974a, b; Mori and Green, 1978; Wood, 1976; Hensen, 1973. Symbols: filled square - 800°C; open square - 900°C; filled triangle - 1000°C; open circle - 1100°C; filled circle - 1200°C; open triangle - 1300°C; open star - 1400°C; filled star - 1500°C. The straight lines show the predicted effect of X_{Ca}^{Gt} upon ln K_D for the temperature range 800-1500°C at 30 kb, using equation (8) - see text.
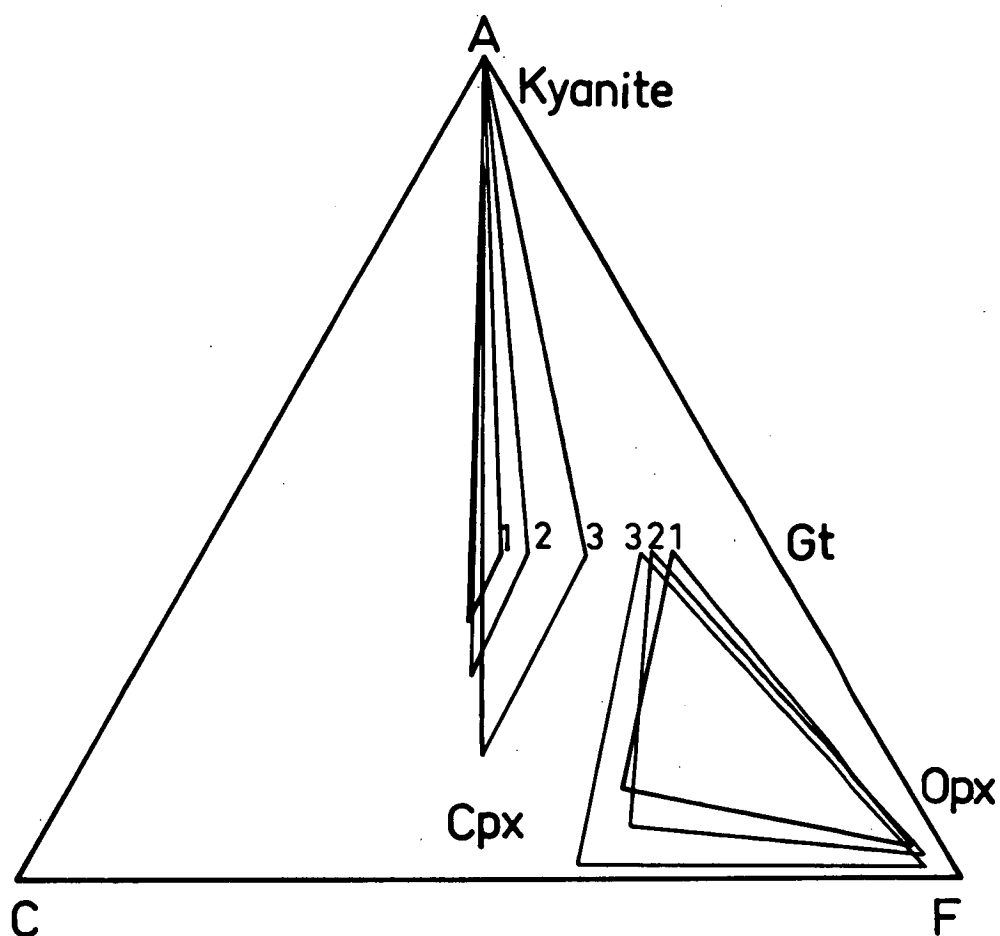
Fig. 3.4 ACF diagram showing the contraction in the width of the two phase field Gt-Cpx with decreasing temperature at 30 kb pressure. 1 = 1300°C data. 2 = 1200°C data. 3 = 900°C data. The two limiting three phase triangles (Gt-Cpx-Ky; Gt-Cpx-Opx) define the limits of Ca-substitution in garnet and CaTs and pyroxene miscibility in clinopyroxene for each temperature.

for the assemblage garnet-clinopyroxene-orthopyroxene (Kushiro et al., 1967; Mori and Green, 1978).

It is possible to select from our own data together with that of Raheim and Green (1974a, b) and Mori and Green (1978) sufficient garnet-clinopyroxene pairs with constant X_{Ca}^{Gt} to show that there is an approximately linear relationship for the variation of K_D with temperature (P, X_{Ca}^{Gt} constant) (Figure 3.5). Garnet peridotites with a low X_{Ca}^{Gt} fall on $\ln K_D - \frac{1}{T}$ lines at lower K_D values for a given T than do basaltic eclogites with higher X_{Ca}^{Gt} contents. The demonstration of K_D variation with X_{Ca}^{Gt} reconciles most of the previous discrepancies in experimental data between garnet peridotites and basaltic eclogites (Hensen, 1973; Raheim and Green, 1974a, b; Akella, 1976; Wood, 1977; Mori and Green, 1978).

2. The Variation of K_D with X_{Ca}^{Gt} and T as a Practical Geothermometer

Experimental data on the variation of K_D over a wide range of pressure, temperature and rock compositions indicate that within experimental error, K_D variations under any given, P,T conditions can be satisfactorily accounted for by the associated change in X_{Ca}^{Gt}.

This variation in K_D can be quantified by assuming that at $X_{Ca}^{Gt} = 0$ the exchange reaction (1) may be considered ideal. Thus at $X_{Ca}^{Gt} = 0$

$$\Delta G_{P,T}^{\circ} (X_{Ca}^{Gt} = 0) = \Delta H - T\Delta S + (P-1)\Delta V = -RT\ln K = -RT\ln K_D \qquad (4)$$

In this manner all non ideal effects on K_D at the one pressure can be accounted for by the following relationship -

$$\ln K_D = a \ X_{Ca}^{Gt} + b \qquad (5)$$

The above constants in (4) and (5) can be determined from the experimental data.
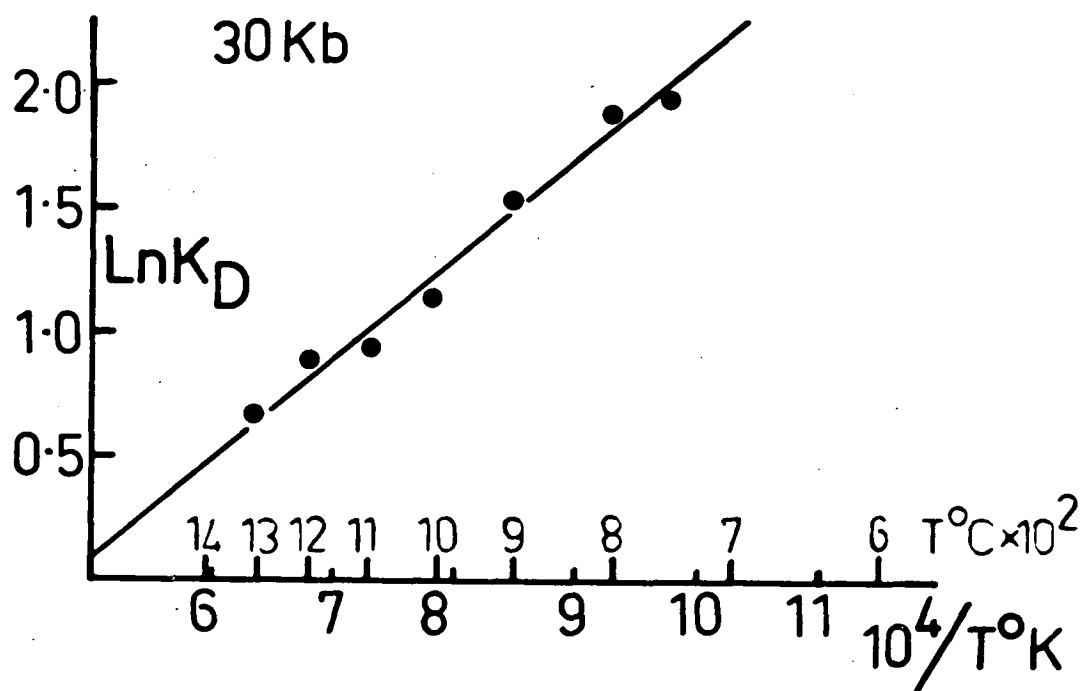
Fig. 3.5 Ln K_D - 1/T plot of the 30 kb, X_{Ca}^{Gt} = 0.2 experimental data. Linear least squares fit ln K_D = (3983/T°K)- 1.9034 r^2 = 0.99.

Reliable data is only available for the variation of K_D with X_{Ca}^{Gt} at high temperatures (1100-1300°C) because of the previously mentioned contraction in the range of X_{Ca}^{Gt} for garnet-clinopyroxene pairs with decreasing temperature. Data for $X_{Ca}^{Gt} = 0.2$ covers the widest range in temperature (Figure 3.5). A least squares fit to this data (P = 30 kb, $X_{Ca}^{Gt} = 0.2$) gives

$$\ln K_D = \frac{3983}{T(°K)} - 1.9034 \qquad r^2 = 0.99 \qquad (6)$$

There is also reliable data for a range in X_{Ca}^{Gt} at 30 kb, 1100 - 1300°C. Least squares fits to this data of the form $\ln K_D = a\, X_{Ca}^{Gt} + b$ is given in Table 3.3 The least squares fits can be used to extrapolate the variation in $\ln K_D$ with X_{Ca}^{Gt} to lower temperatures (Figure 3.6). These extrapolations would indicate that for a constant X_{Ca}^{Gt} the variation in K_D with temperature shows a change in gradient and a slight change in intercept for a wide range in X_{Ca}^{Gt} (up to 0.5 X_{Ca}^{Gt}). This would correspond to a change in both the enthalpy and entropy of mixing with grossular substitution ($\Delta H^{ex} \neq 0$, $\Delta S^{ex} \neq 0$).

However such a proposed variation in intercept ($\Delta S^{ex} \neq 0$) with X_{Ca}^{Gt} is not proven in view of the large extrapolations from data covering only a 200°C temperature interval. In fact the value of ΔS derived from the 1100 - 1300°C least squares fit to the $X_{Ca}^{Gt} = 0.2$ data of Table 3.3 differs considerably from that derived from the more reliable temperature range 750 - 1300°C (Table 3.3). Furthermore calculations based on the above extrapolations ($\Delta H^{ex} \neq 0$, $\Delta S^{ex} \neq 0$) give too low equilibration temperatures for many eclogites compared to calculations based on the assumption of no excess entropy of mixing (that is lines of constant X_{Ca}^{Gt} have the same intercept on a $\ln K_D - \frac{1}{T}$ plot).

TABLE 3.3

Least Squares Fits to the various data sets

Variation in K_D with X_{Ca}^{Gt} at 30 kb pressure. Data sources -
this study and Raheim and Green 1974a, b (and Mori and Green 1978,
1200°C data)

(i)   1300°C $K_D = 5.415 \, X_{Ca}^{Gt} + 0.8208$ $r^2 = 0.93$ (1)

(ii)   1200°C $K_D = 5.466 \, X_{Ca}^{Gt} + 1.1697$ $r^2 = 0.876$ (2)

(iii)   1200°C $\ln K_D = 2.1066 \, X_{Ca}^{Gt} + 0.3753$ $r^2 = 0.868$ (3)

(iv)   1100°C $K_D = 6.034 \, X_{Ca}^{Gt} + 1.4078$ $r^2 = 0.953$ (4)

$\ln K_D - \frac{1}{T}$ variations at 30 kb, $X_{Ca}^{Gt} = 0.2$ for the temperature

range 1300 - 750°C -

(v) $\ln K_D = 3983/T(°K) - 1.9034$ $r^2 = 0.99$

for which the following data were used -

1300°C $K_D = 1.9038$ K_D obtained from least squares fit (i)
                                  above at $X_{Ca}^{Gt} = 0.2$

1200°C $K_D = 2.2629$ K_D obtained from (ii) above

1100°C $K_D = 2.6146$ K_D obtained from (iv) above

1000°C $K_D = 3.3$ Raheim and Green (1974a) Run 4233.

 900°C $K_D = 4.5$ Average value taken from $X_{Ca}^{Gt} \approx 0.2$
                                data of this study and Raheim & Green
                                                          (1974a)

 800°C $K_D = 6.6$ Raheim and Green (1974a) Run 4462.

 750°C $K_D = 6.93$ This study.   Run T-110.

$\ln K_D - \frac{1}{T}$ least squares fits for various X_{Ca}^{Gt} values using equations

(i) - (iv) to obtain K_D points at 1100 - 1300°C for each value of

X_{Ca}^{Gt} at 30 kb pressure -

(vi) $X_{Ca}^{Gt} = 0$ $\ln K_D = 5776/T - 3.833$

(vii) $X_{Ca}^{Gt} = 0.1$ $\ln K_D = 4182/T - 2.332$

(viii) $X_{Ca}^{Gt} = 0.2$ $\ln K_D = 3413/T - 1.5175$ (compare with (v) above)

(ix) $X_{Ca}^{Gt} = 0.3$ $\ln K_D = 2960/T - 0.9837$

(x) $X_{Ca}^{Gt} = 0.4$ $\ln K_D = 2622/T - 0.5976$

(xi) $X_{Ca}^{Gt} = 0.5$ $\ln K_D = 2447/T - 0.2965$
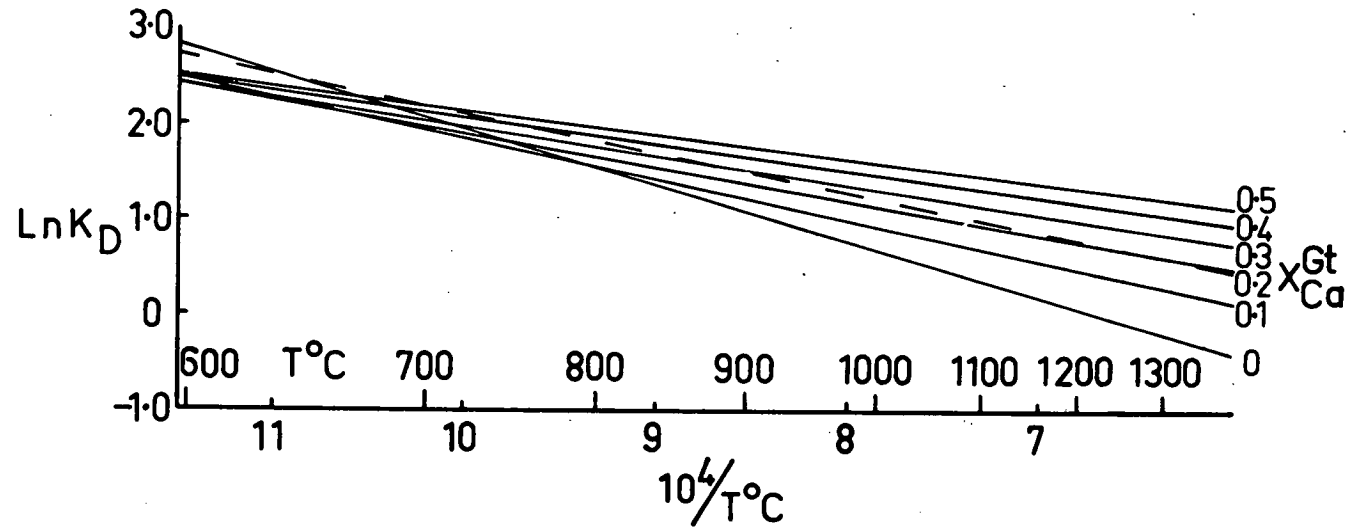
Fig. 3.6 Extrapolated ln K_D-1/T plot of least squares fits to 1100-1300°C data at
30 kb at various values of X_{Ca}^{Gt}. The 1100-1300°C, X_{Ca}^{Gt} = 0-0.5 data points
were obtained by least squares fits of the form ln K_D = aX_{Ca}^{Gt} + b. Dashed
line is least squares fit at X_{Ca}^{Gt} = 0.2 for data of the broader temperature
range 750-1300°C (Fig. 3.5). Note the difference in slope compared to
1100-1300°C data extrapolation only.

In a thermodynamic sense, $\Delta S^{ex} = 0$ and $\Delta H^{ex} = f\, X_{Ca}^{Gt} \neq 0$ is consistent with a symmetric regular solution model of non-ideal substitution of Ca in Mg-Fe garnets (see Thompson, 1967; Wood and Fraser, 1976). This would be expected on crystal-chemical considerations as there is no ordering of atoms in this substitution. All of the eight coordinated sites in the garnet structure are symmetrically equivalent and the distribution of the divalent cations over these sites is expected to be random, or nearly so (Novak and Gibbs, 1972; Ganguly and Kennedy, 1974; Ganguly, 1976), hence $\Delta S^{ex} \approx 0$.

For these reasons it is preferable to use only our best data for deriving a general equation relating the variation in K_D with temperature and X_{Ca}^{Gt}. The least squares fit to the 30 kb, $X_{Ca}^{Gt} = 0.2$ data (Table 3.3) for the temperature range 750 - 1300°C can be combined with that for the variation of K_D with X_{Ca}^{Gt} at 30 kb, 1200°C (6) to derive the following equation, applicable at 30 kb, and assuming $\Delta S^{ex} = 0$ -

$$\ln K_D = \frac{3104\ X_{Ca}^{Gt} + 3356}{T°K} - 1.9034 \tag{7}$$

3. The Effect of Pressure on K_D

The above relationship (7) is only of limited application without a knowledge of the effect of pressure on K_D. Published data on the molar volumes of pyrope (37.71 cm³), almandine (38.48 cm³) (Takahashi and Liu, 1970), diopside (66.20 cm³) and hedenbergite (67.88 cm³) (Rustein and Young, 1969) indicate that for the simple system exchange reaction (1) $\Delta V = -1.42$ cm³ (-0.034 cal/bar). This value, when combined with the above relationships (4, 5 in 6) and

having no excess molar volume ($\Delta V^{ex} = 0$) enables the derivation of a general relationship for the variation of K_D with P, T and X_{Ca}^{Gt} -

$$T^\circ K = \frac{3104 \ Ca + 2837 + 17.08 \ P}{\ln K_D + 1.9034} \tag{8}$$

The assumption that there is no excess volume of mixing in garnet is justified in view of the fact that the unit cell edge of silicate garnets varies linearly with the mean radius of the divalent and trivalent ions (Novak and Gibbs, 1971) and thus $\Delta V^{ex} = 0$.

There has been considerable discussion recently about the magnitude of the effect of pressure upon K_D (Banno, 1970; Raheim and Green, 1974a; Wood, 1975, 1977). The effect of pressure upon K_D, assuming ideal substitutions can be derived from the relationship -

$$\frac{\partial \ln K}{\partial P} = \frac{\partial}{\partial P}\left(\frac{\Delta G}{RT}\right) = \frac{\Delta V}{RT} \tag{9}$$

Thus $\quad \ln K_{D_1} = \ln K_{D_2} + \frac{(P_1 - P_2)\Delta V}{RT} \tag{10}$

On this basis Raheim and Green (1974a) calculated the effect of pressure upon K_D using their experimental data to be considerably larger than that predicted by Banno (1970) from x-ray molar volume data ($\Delta V = 2.357$ and $1.33 \ cm^3$ respectively). This overestimate of the pressure effect by Raheim and Green (1974a) is due to the comparison of K_D data at different pressures for garnets with differing X_{Ca}^{Gt}, which thus also incorporates the increase in K_D due to non ideality of the Ca substitution; a feature also commented on recently by Wood (1977). Calculations using the 30 and 20 kb, 1100°C data of Raheim and Green (1974a, b) as well as our own data, show that the effect of pressure upon K_D, extrapolated back to $X_{Ca}^{Gt} = 0^*$ is $1.41 \ cm^3$,

---

* In fact the simple system end member reaction with a Ca-free garnet would never be found in nature, as the minimum grossular content of garnet coexisting with clinopyroxene is about 11 mol. percent. Lower grossular garnets coexist with orthopyroxene only (see Figure 3.4).

in excellent agreement with the above prediction of Banno and our own calculated value. In fact this data shows a slight excess molar volume with increasing X_{Ca}^{Gt}, but in view of the previous discussion and the very large uncertainties involved in deductions derived from a pressure difference of only 10 kb, together with the small number of lower pressure data points, little credence is placed on this variation. Furthermore, taking account of the excess molar volume results in differences of about 30°C in temperature estimates for crustal rocks in comparison with having $\Delta V^{ex} = 0$. Such a difference is within the error limits for such extrapolations.

VII. DISCUSSION

Although the above equation (8) is applicable as a practical geothermometer for garnet-clinopyroxene assemblages from a wide range in P, T, X conditions, it must be remembered that the included constants cannot be interpreted solely in terms of the thermodynamic mixing properties of the garnet solid solutions. In particular the variation in the measured K_D as a function of X_{Ca}^{Gt} is simply a convenient method of representing the net effect of the different solid solutions upon K_D. There is an increase in Ca content of the clinopyroxene (as Di and CaTs) with increasing Ca content of the coexisting garnet.

High pressure experimental and solution calorimetry studies (Hensen et al., 1975; Newton, 1977) have shown that there is a positive excess enthalpy of mixing in Ca-Mg garnet solid solutions, even though these two studies derived very different ΔH^{ex} values. Up to about $X_{Ca}^{Gt} = 0.5$ this variation can be adequately described by

a regular solution model, though at higher X_{Ca}^{Gt} values a subregular solution model is more appropriate (Newton, 1977).

In contrast, Wood (1977) quotes Schmitt and Cressey (in prep.) that the Ca-Fe substitution in garnet behaves almost ideally up to about $X_{Ca}^{Gt} = 0.3$ ($\gamma_{Ca}^{Gt} \approx 1$). Wood (1977) suggests that Ca-Mg garnet non ideality may be the sole factor affecting the Gt-Cpx K_D with changing rock compositions. As noted by Wood (1977), Ca-Mg garnet non-ideality at any given P and T implies that an increase in X_{Ca}^{Gt} results in an increase in γ_{Mg}^{Gt}, which in order to keep the equilibrium constant K the same must result in a decrease in Mg and hence the measured K_D decreases. If this were the only non ideal substitution affecting K_D, then the effect of X_{Ca}^{Gt} upon K_D would diminish with increasing iron content.

This would be in apparent contradiction to the experimentally determined variation of K_D with X_{Ca}^{Gt} and Mg/(Mg+Fe). This data has shown that the effect of Ca upon K_D, as reflected by increasing X_{Ca}^{Gt} does not decrease with increasing iron contents. The 30 kb, 1200°C data shows that *within experimental error* there is no measurable difference in K_D for a given X_{Ca}^{Gt} for garnets in the range Mg/(Mg+Fe) = 0.79 - 0.24 (see also Raheim and Green, 1974a). This is confirmed in Appendix 2 where it is shown that analysis of the experimental data in terms of ternary and quaternary regular solution models indicates that the effect of Ca upon K_D is due to a combination of non ideal substitutions - Ca substitution in garnet and Ca substitution (as Di or CaTs) in the clinopyroxene. These two effects act in an opposite sense to change K_D with increasing Ca content of a rock, and it is suggested that the net effect of these two factors, as shown by the measured variation in K_D with X_{Ca}^{Gt} is

independent of the Mg/(Mg+Fe) content of the rock (within the experimental error). The reader is referred to Appendix 2 for a complete discussion of the various interaction parameters.

As an independent check, the solution calorimetry data presented by Newton (1977) can be combined with the previous equation for the variation of K_D with P, T at $X_{Ca}^{Gt} = 0$ (see Appendix 2). In this equation the effect of Ca upon K_D decreases with increasing iron contents. This equation overestimates the temperatures of very Mg-rich eclogites and underestimates the temperatures of very Fe-rich eclogites (experimental syntheses) compared to our practical geothermometer (8). As an independent check, Raheim and Green (1974a) have presented experimental K_D data for iron-rich garnets (Mg/(Mg+Fe) = 0.18 - 0.035, 20 kb pressure) which were not used in the derivation of either of these equations. Our preferred equation (8) in which the effect of Ca upon K_D is independent of Mg/(Mg+Fe) gives deviations from the stated temperature of 5 - 85°C, whereas that assuming Ca-Mg garnet substitutions as the non-ideal factor affecting K_D give temperature underestimates from 145-185°C.

As a further test, data on isofacial eclogites from Norway described by Green (1969) (see application section) (Mg/(Mg+Fe)Gt = 0.657 and 0.252) have coincident temperatures of equilibration (602, 610°C) using equation (8), but lower, and differing temperatures using the equation given in the appendix (T = 598, 493°C).

VIII. APPLICATION

The test for any calibrated geothermometer of course is to see whether it gives reliable results when applied to experimental data which lie outside the P,T range for which the thermometer was calibrated and when applied to natural garnet-clinopyroxene assemblages for which either an independent method of temperature estimate can be given or where there is a suite of undoubted iso-facial eclogites which show a wide range in mineral compositions (such as Enderby Land, Antarctica - Chapter 2).

We have applied equation (8) to experimental data not used in the derivation of this equation (Hensen, 1973; Akella, 1976; Wood, 1976; Raheim and Green, 1974a, b; Mori and Green, 1978). These data cover the range P = 45 - 15 kb, T = 1450 - 1100°C, X_{Ca}^{Gt} = 0.12-0.44. The majority of our temperature estimates lie within ±5% of the stated temperature, which is the uncertainty associated with our data. Furthermore, our estimates do not show any bias towards overestimating or underestimating equilibration temperatures for any particular rock type using equation (8).

Several examples may be cited where application of our experimentally calibrated geothermometer results in a refinement of temperature estimates compared to earlier methods. Recent compilations of K_D data for eclogites (e.g. Irving, 1974) shows that Ca-rich garnet varieties (grospydites) generally have much higher K_D values that other kimberlite eclogites and garnet peridotites. Smyth and Hatton (1977) have described a coesite-sanidine grospydite which they deduced from the structural state of the feldspar and the presence of coesite to have equilibrated above 29 kb pressure, 900°C.

Application of previous geothermometers to this rock (Raheim and Green, 1974a) indicated too low an equilibration temperature (825°C at 30 kb). Our data indicates a temperature of 1055°C, which is more consistent with thermal regimes in the mantle.

Diamond-bearing eclogites from both South Africa and Siberia have been extensively studied in recent years (e.g. Reid et al., 1976; Ponomorenko et al., 1977; Sobolev et al., 1966). Estimated temperatures and pressures of equilibration of these nodules (assuming minimum pressures coincident with the graphite-diamond transition) are shown in Figure 3.7. It would appear that they have equilibrated at minimum pressures and temperatures of 42 - 59 kb and 1040 - 1630°C. It is of interest to note that the nodules described by Ponomorenko et al. (1977) define two distinct, tightly clustering groups (45 kb, 1130°C and 59 kb, 1620°C). This would imply kimberlite diapirism from ≈ 60 kb pressure in certain cases.

It has recently been suggested that with increasing pressure garnets may become non-stoichiometric, displaying a slight solid solution towards clinopyroxene (Mori and Green, 1978). We note no observable deviation from stoichiometry in the above garnets, even up to 60 kb inferred pressure.

Garnet lherzolite nodules in kimberlite from South Africa (Boyd, 1973; Nixon and Boyd, 1973) and Montana (Hearn and Boyd, 1973) have been classified on the basis of texture into granular and sheared varieties, with the sheared types having equilibrated at higher temperatures and pressures than the granular types. Estimated P-T conditions of equilibration of these nodules are shown in Figure 3.8. Deduced P-T conditions for each nodule correspond
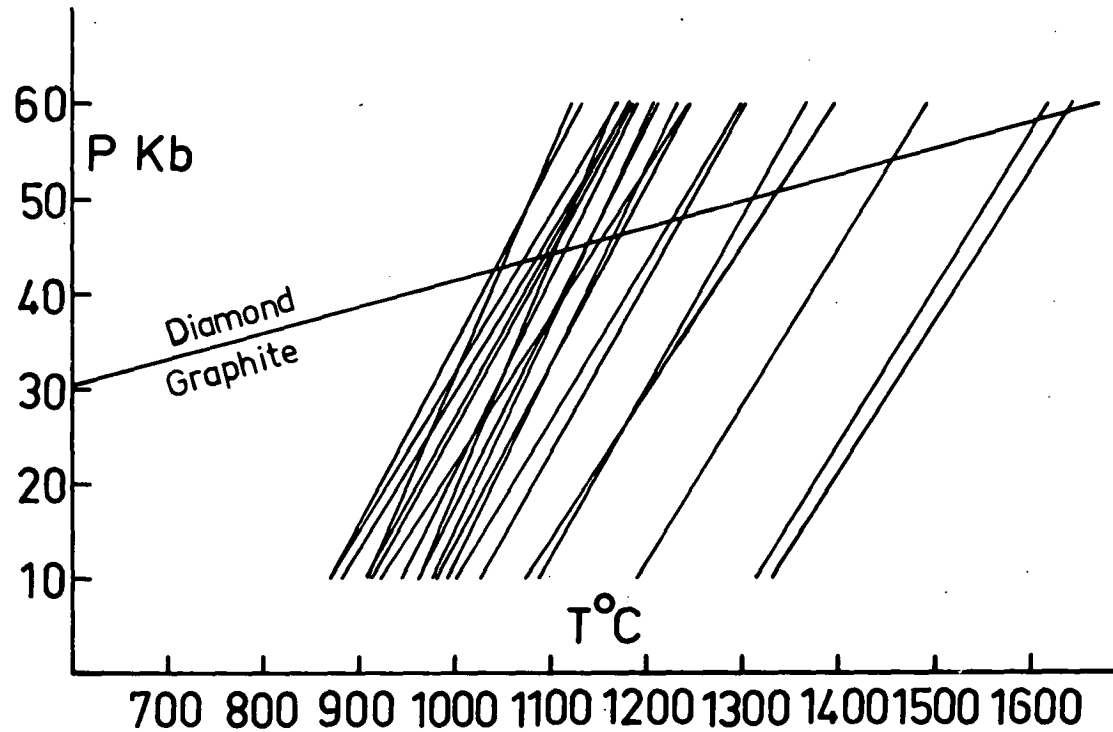
Fig. 3.7   P-T plot of inferred conditions of equilibration of diamond-
bearing xenoliths in kimberlites. Possible P-T conditions of
equilibration given by the intersection of lines showing P-T
variation for constant Gt-Cpx K_D (equation 8) and the graphite
diamond transition. Data sources: Myer and Boyd (1972);
Sobelov et al. (1966); Reid et al. (1976); Ponomorenko et al.
(1977); Smyth and Hatton (1977).

to the P-T point of intersection of temperature estimate with increasing pressure (our data) and pressure estimate for a given temperature using garnet-orthopyroxene equilibria (Wood and Banno, 1973).

Temperature estimates based on the present study define a smooth gradient of increasing temperature with depth for the Montana inclusions. The South African examples are seen to define two groups, with the sheared nodules being a higher temperature and pressure association. We believe that in view of the error associated with any geothermometer or barometer, these sheared nodules cannot be considered to define an inflection in the geotherm (Boyd, 1973, Nixon and Boyd, 1973).

Also shown in Figure 3.8 are temperature estimates for the Montana inclusions given by Hearn and Boyd (1973) which are based on the pyroxene solvus (Boyd, 1973; Wood and Banno, 1973). It can be seen that the Wood-Banno geothermometer gives temperature over-estimates for rocks equilibrated below $\approx$ 1000°C and temperature underestimates above $\approx$ 1000°C [temperatures from Gt-Cpx K_D determined at same pressure as given by Boyd (1973)]. Mori and Green (1978) reached a similar conclusion through comparison with their calibration of the effect of temperature upon the pyroxene solvus. Temperature estimates based on the pyroxene solvus calibration of Mori and Green (1978) (Figure 3.8) do not define as smooth a curve for the Montana nodules as that of the Gt-Cpx thermometer. This is not unexpected considering that the effect of pressure and variation in Mg/(Mg+Fe) content was not considered by them (see discussion of Mori and Green, 1978). In view of the fact that the error associated with temperature estimates based on the pyroxene solvus data is about 100°C (Mori and
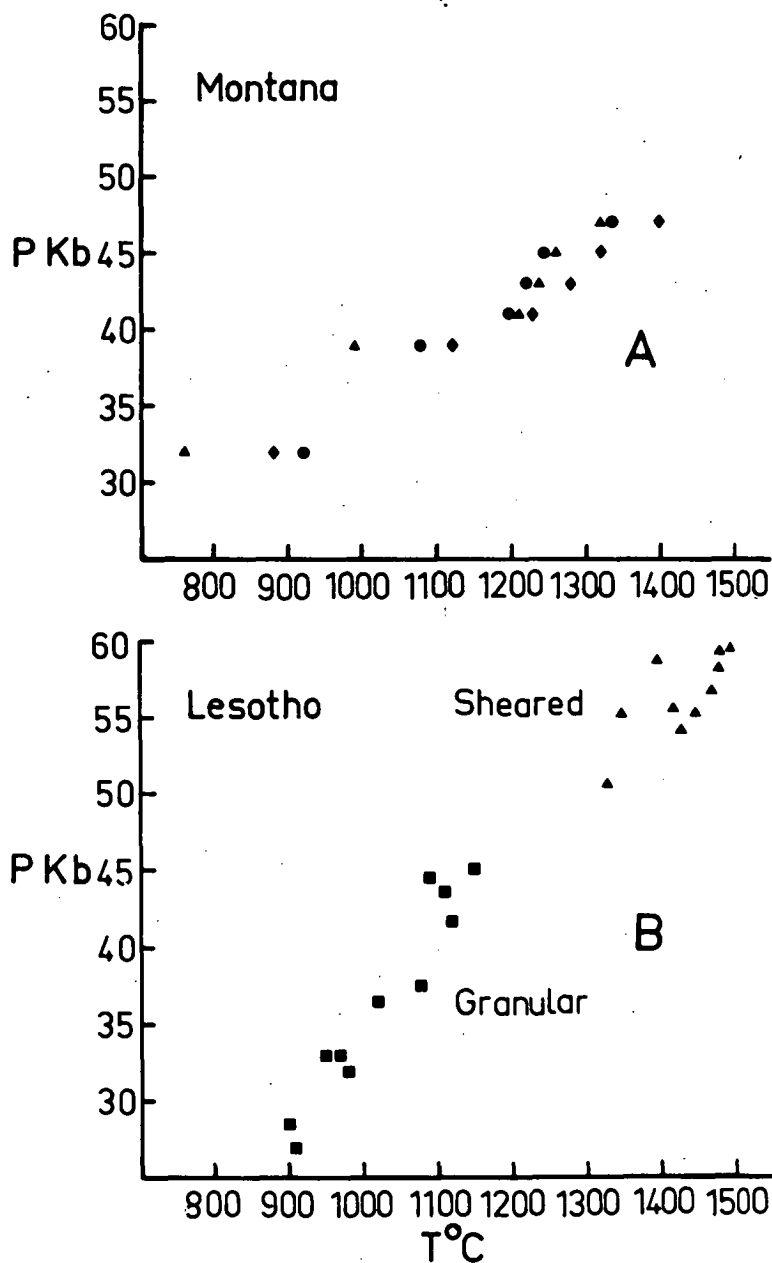
Fig. 3.8   A.   P-T conditions of equilibration of Montana Kimberlite
xenoliths (Hearn and Boyd, 1973) based on Gt-Cpx geothermometry
of this chapter (diamond symbol); Opx-Cpx miscibility gap data
of Mori and Green, 1978 (triangle symbol) and temperature
estimates of Hearn and Boyd, 1973 (circle symbol).

B.   P-T conditions of equilibration of garnet peridotite
xenoliths in Lesotho kimberlite, South Africa (Boyd, 1973;
Boyd and Nixon, 1973), based on Gt-Cpx geothermometry. See text
for the method of estimating pressures. Triangles - sheared
xenoliths. Squares - granular xenoliths.

Green, 1978), the coincidence in temperature estimates between the two methods is satisfactory. Further refinement of the effect of pressure and Mg/(Mg+Fe) content on the pyroxene solvus, may result in temperature estimates based on this method also defining a curve of smooth P-T gradient for the Montana nodules.

Wood (1975) has described some garnet-clinopyroxene orthogneisses from South Harris, Scotland, for which previous Gt-Cpx K_D temperature estimates gave too low an equilibration temperature ($\approx$ 730°C) compared to other methods of temperature and pressure estimation (see Wood, 1975). Application of equation (8) gives higher temperatures of equilibration (838 - 770°C) which are more consistent with these other methods.

Green (1969) has described a series of isofacial eclogites from Norway which show a wide range in K_D, X_{Ca}^{Gt} and Mg/(Mg+Fe) of the garnet (7.016, .116, .657 and 11.16, .259, .252 respectively). Previous temperature estimates (Raheim and Green, 1974a) range from 654 - 564°C (at 10 kb) whereas our data gives almost coincident temperatures (602 and 611°C) for these two rock samples.

The variation in K_D with X_{Ca}^{Gt} for exsolution and rim compositions in the garnet clinopyroxenites described in the last chapter are shown in Figure 3.9. The predicted variation in K_D with X_{Ca}^{Gt} at 10 kb, 720°C using equation (8) fits very well the observed variation in K_D. This indicates that these assemblages could well have equilibrated at the one P-T condition, even though K_D varies with the Ca-content of the garnet.

The coincidence in temperature estimates for these examples of isofacial eclogites with such widely differing chemistries and K_D values provides good evidence for the useful application of equation (8)
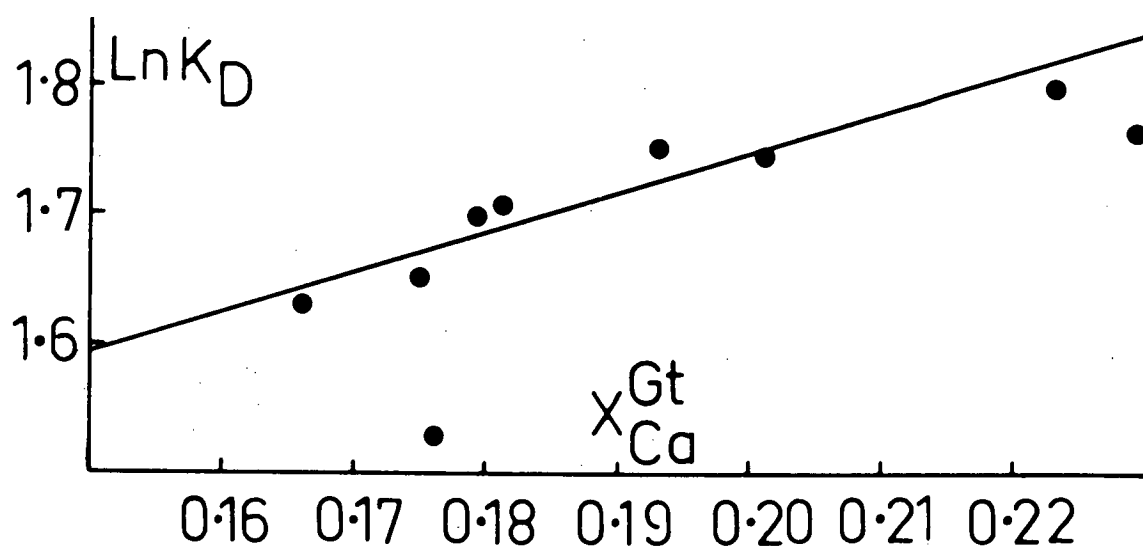
Fig. 3.9   Variation in ln K_D with X_{Ca}^{Gt} for the exsolutions and
mineral rim compositions in the garnet clinopyroxenites
described in Chapter 2. The predicted increase in
ln K_D with X_{Ca}^{Gt} at 10 kb, 720^oC (equation 8)of this
chapter) is shown by the line.

and is an apriori justification for the assumptions made in the derivation of this relationship as a practical geothermometer. It must be remembered that in a thermodynamic sense the observed variation of K_D with X_{Ca}^{Gt} represents the net effect of all competing factors (non-ideal substitutions) in both the garnet and clino-pyroxene solid solutions. In this regard, further data on binary solid solutions derived from high pressure experimental, solution calorimetry and x-ray studies are awaited.

Chapter 4

GRANULITES WITH OSUMILITE AND SAPPHIRINE-QUARTZ

FROM ENDERBY LAND, ANTARCTICA

Contents   page

I. SUMMARY

The pre-Cambrian granulites of Enderby Land Antarctica, contain coexisting spinel-quartz, sapphirine-quartz, hypersthene-sillimanite-quartz and osumilite on a regional extent. Osumilite is present in a variety of mineral assemblages, most of which have not previously been reported. Secondary cordierite has developed by a variety of reactions.

The granulites reached a peak of metamorphism at 8-10 kbar pressure, 900-920°C, under conditions of $P_{H_2O} < P_{Total}$. Mineral reactions record the subsequent cooling at constant pressure. Temperatures of metamorphism deduced from various experimentally calibrated geothermometers vary widely, and in some cases are inconsistent with the stability fields of the actual mineral assemblages. Available Fe-Mg partition data for garnet-cordierite pairs indicates equilibrium at temperatures of 500-600°C, well within the kyanite stability field. The possible effects of $P_{H_2O}-P_{CO_2}$ and Al-Si ordering in cordierite upon garnet-cordierite equilibria, and the problem of applicability of currently available experimental data to such high grade metamorphic rocks are discussed.

A theoretical analysis of the phase relations involving osumilite in the chemical systems $K_2O-MgO-Al_2O_3-SiO_2$ and $K_2O-FeO-MgO-Al_2O_3-SiO_2$ is presented. In the pure Mg-system the lower temperature stability limit of Mg-osumilite is inferred to be defined with increasing pressure by the reactions -

$$Os \rightarrow Cd + En + Kfeld + Qtz$$
$$Os \rightarrow Sa + En + Kfeld + Qtz$$
$$Os \rightarrow Sill + En + Kfeld + Qtz$$
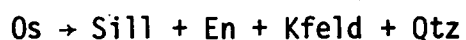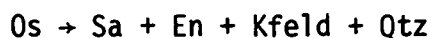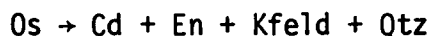
In iron-bearing systems the most important reaction limiting the stability field of osumilite is -

$$Os + Gt \rightarrow Cd + Hy + Kfeld + Qtz$$
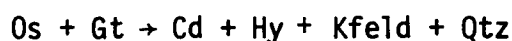
At moderate temperatures and pressures, osumilite is limited to rocks which lie on the Mg-rich side of the Cd-Hy stable tie line on an AFM diagram. At higher pressures and temperatures osumilite occurs in a wide range of rock compositions because of the stability of co-existing garnet and osumilite. Petrographic data, as well as chemographic relations indicate that for many common rock compositions, garnet, cordierite, hypersthene, sapphirine and sillimanite cannot coexist with both osumilite and K-feldspar.

II. <u>INTRODUCTION</u>

Within the last ten years considerable advance has been made in understanding of the mineral reactions and cation exchange equilibria in pelitic rocks at high temperatures and pressures. In particular the terminal and non-terminal univariant reactions (Hess, 1969) defining the stability limits of cordierite have been experimentally studied in several laboratories (e.g. Schreyer and Yoder, 1960, 1964; Schreyer and Seifert, 1969; Seifert and Schreyer, 1970; Seifert, 1970, 1976; Hensen and Green, 1971, 1972, 1973; Chatterjee and Schreyer, 1972; Newton, 1972). The results of these studies differ from each other, as do several recent experimental calibrations of the temperature dependence of Fe-Mg exchange reactions between garnet and cordierite (Hensen and Green, 1971, 1972, 1973; Currie, 1971).

It is particularly important therefore that studies be undertaken of natural examples of rocks containing assemblages which limit the stability field of cordierite, such as sapphirine-quartz, hypersthene-sillimanite (or kyanite). Such examples provide an invaluable link between the experimental studies and those of natural rocks. Occurrences of these assemblages are rare in nature, and are restricted to isolated

outcrops in otherwise typical medium and high pressure granulite terrains (Marakushev, 1965; Morse and Talley, 1971; Bondarenko, 1972; Hermans et al., 1976). In these occurrences the presence of high Fe_2O_3 contents stabilizes sapphirine-quartz and hypersthene-sillimanite to much lower pressures and temperatures than those deduced from the experimental data, because Fe_2O_3 selectively enters hypersthene and sapphirine rather than cordierite and garnet. Under oxidizing conditions orthopyroxene can also incorporate greater amounts of Al_2O_3 due to the coupled substitution $R^{2+}Si \rightleftharpoons Fe^{3+}Al$ (Arima, 1978). The hypersthene from the Annabar Massif (Bondarenko, 1972) contains 9.2 wt. % Al_2O_3 and 6.29 wt. % Fe_2O_3. In contrast the Enderby Land hypersthenes described here (Mg_{70-78}) contain very low Fe_2O_3 ($FeO:Fe_2O_3$ > 9:1), and the Al_2O_3 (up to 11.7 wt. %) is present as $R^{2+}Al_2SiO_6$ rather than $R^{2+}Fe^{3+}AlSiO_6$.

The first recorded occurrence of coexisting sapphirine and quartz was from Spot Height 945, a nunatak in Enderby Land, Antarctica (Dallwitz, 1968). Further work in Enderby Land by the Bureau of Mineral Resources has shown that the granulites in this area contain this and other rare mineral assemblages on a regional scale (Sheraton and Offe, 1977; Sheraton et al., in prep.). Also, the potassic mineral osumilite is found throughout an area of several thousand square kilometres.

This chapter considers the petrology of the granulites from one locality in Enderby Land, and describes several mineral associations and reactions which have not been observed in metamorphic rocks nor predicted to occur on the basis of previous experimental and theoretical discussions on high grade metamorphic rocks. The validity of using currently available experimentally calibrated Fe-Mg cation exchange equilibria to define the maximum pressures and temperatures of granulite facies metamorphism is discussed.

III. REGIONAL GEOLOGIC SETTING

The rocks of Enderby Land form part of the Precambrian East Antarctic Shield and consist almost entirely of medium-high pressure granulite facies metamorphics, with local areas of retrograde amphibolite facies rocks. Two metamorphic complexes have been recognized - the Napier Complex and the younger Rayner Complex (Kamenev, 1972, 1975). Extensive mapping of this terrain has been undertaken by both Australian and Russian geologists (Crohn, 1959; McLeod, 1959, 1964; McLeod et al., 1964; Ruker, 1963; Kamenev, 1972, 1975; Pieters and Wyborn, 1977; Sheraton and Offe, 1977; Grew, 1978; Sheraton et al., in prep.). Geochronological data are few and require further substantiation - dates of 4000 ± 200 m.y. using Pb-Pb and U-Pb techniques have been obtained (Sobotovich et al., 1976). The highest grade rocks belong to the older complex which consists predominantly of two major rock groups - massive pyroxene-quartz-feldspar granulite with minor mafic to ultramafic intercalations and lenses; and layered garnet-quartz-feldspar gneiss with subordinate siliceous, aluminous and ferruginous metasediments. The two types are commonly interlayered. Granite and pegmatite intrusion, mostly confined to the area west of the Rayner Glacier, occurred about 500 m.y. ago.

Coexisting sapphirine-quartz has been found within the Napier Complex at localities over an area of about 2500 sq. km in the northern Scott and Tula Mountains (Figure 4.1). Osumilite is found in metapelites from four localities up to 40 km apart in the Tula Mountains, and its characteristic breakdown products (see later description) are even more widespread. The association sillimanite-orthopyroxene occurs at several localities in the northern Scott Mountains, but is rare in the Tula Mountains and gives way to cordierite in the Napier Mountains (Figure 4.1).
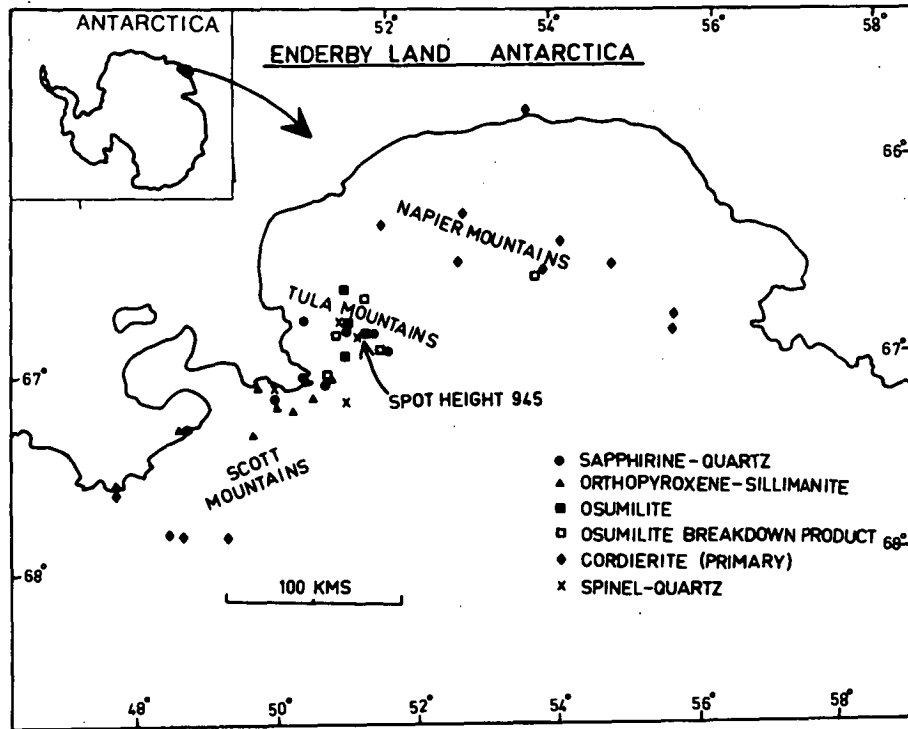
Fig. 4.1   Distribution of various mineral assemblages
in Enderby Land, Antarctica. The eastern
portion of the map also includes part of
Kemp Land.

The granulites from Spot Height 945, which include the assemblages sapphirine-quartz, spinel-quartz, hypersthene-sillimanite and osumilite are discussed in detail. This locality, which is that described by Dallwitz (1968), is a small nunatak in the Tula Mountains, about 65 km east of Amundsen Bay, Enderby Land (66°57'S, 51°31'E), and consists largely of gently dipping, banded metasediments of varied composition, which pass upwards into massive, brown weathering orthopyroxene-quartz-feldspar (-garnet) gneiss. The well layered rocks include quartzite, garnet-rich pelitic granulites, leucocratic garnet-quartz-feldspar gneiss and minor mafic pyroxene granulite. The garnet-quartz-feldspar gneiss locally has discordant contacts with the quartzites, which are generally cream or pale blue in colour, and contain discontinuous and commonly folded layers, mostly 1-5 cm in thickness, with abundant dark blue grains of sapphirine up to 1 cm long (Figure 1.1).

IV. PETROGRAPHIC INTRODUCTION

Mineral assemblages found in the different rocks are listed in Table 4.1. There are four broad groups of rocks - quartzites, quartz feldspar gneisses, aluminous gneisses and mafic granulites.

The quartzites contain variable amounts of quartz, garnet, orthopyroxene, cordierite, sillimanite, perthite, greenish-brown spinel, rutile, and very fine grained symplectites of cordierite with K-feldspar, quartz and usually minor orthopyroxene.

Massive felsic gneisses are the most common rocks throughout Enderby Land, and consist of feldspar and quartz together with minor garnet, orthopyroxene or both. Mesoperthite is widespread in rocks of the Napier Complex, but perthite or antiperthite predominate in the more K-rich and K-poor gneisses respectively (Sheraton et al., in prep.).

Table 4.1

Critical Mineral Assemblages at Spot Height 945.

Sa Opx Qtz	Os Gt Qtz	Cd Gt Opx Qtz
Sa Opx Os Qtz	Os Gt Sill Qtz	Cd Gt Sill Qtz
Sa Os Qtz	Os Opx Qtz	Cd Opx Sill Qtz
Sa Gt Qtz	Os Opx Gt Qtz	
Sa Gt Os Qtz	Os Opx Gt Sill Qtz	
Sa Gt Sill Qtz	Os Sp	
Sa Sill Os Qtz	Os Qtz	
Sa Sill Gt Os Qtz	Os Sill Qtz	
Sa Opx Sill Qtz	Os Cd Opx Kf Qtz	
Sa Qtz		
Sa Cd		
Sp Qtz		
Sp Gt Sill Kf		

Abbreviations: Osumilite (Os), Sapphirine (Sa), Cordierite (Cd), Garnet (Gt), Orthopyroxene (Opx), Spinel (Sp), Sillimanite (Sill), Quartz (Qtz), K feldspar (Kf).

The interlayered mafic granulites are medium-coarse grained rocks consisting of orthopyroxene-clinopyroxene-plagioclase-magnetite (-rare apatite, occasional quartz). Equigranular, idiomorphic-subidiomorphic, medium grained (2-4 mm) pyroxene is abundant. There is no textural evidence of mineral reactions apart from the development of extremely thin pyroxene exsolution lamellae in the pyroxenes and the sporadic development of secondary biotite around opaque oxides.

In contrast, the highest grade mineral assemblages in the aluminous metapelites are marked by the presence of a wide variety of mineral assemblages and spectacular reaction coronas. Although up to 99% of their chemical composition can be explained in terms of the five components K_2O, FeO, MgO, Al_2O_3, SiO_2, they contain a great number of minerals - garnet (Gt), cordierite (Cd), sapphirine (Sa), spinel (Sp), hypersthene (Hy), osumilite (Os), biotite (Bi), sillimanite (Sill), K-feldspar (Kf), quartz (Qtz), accessory rutile, traces of zircon, magnetite (Mt) and very rare corundum (Co). Not all of these phases occur in the one rock (Table 4.1), and the complexity of mineral assemblages and ranges in mineral compositions (see following section) reflect local equilibrium and partial readjustment to new equilibrium P, T conditions implied by the corona textures.

Detailed discussion of the mineralogy follows in a later section, but the Enderby Land granulites are distinctive and noteworthy for the presence of the associations spinel-quartz, sapphirine-quartz and osumilite.

Green and brown spinel (< 0.5 mm) is occasionally in direct contact with quartz. It usually occurs as rounded inclusions in sapphirine, garnet, sillimanite, osumilite and osumilite intergrowth.* The mantling of spinel by these minerals and the less common thin coronas of garnet-sapphirine-sillimanite between spinel and quartz, result from the instability of

---

* The term osumilite intergrowth refers to the distinctive fine grained intergrowths of cordierite-quartz-K feldspar-hypersthene formed by the breakdown of osumilite.

coexisting spinel-quartz except at the highest temperature conditions of metamorphism (see reaction 14, discussion section).

Sapphirine usually occurs within layers 1-10 cm thick in several mineral associations (Table 4.1). Such layers typically consist of angular grains of blue sapphirine (up to 1 cm, commonly 1-2 mm long), garnet (1-2 mm), quartz, and osumilite intergrowth. It occurs with each of the minerals garnet, hypersthene, sillimanite, osumilite, spinel, K-feldspar, quartz, and rutile (and is typical of the highest grade of metamorphism).

Sapphirine and quartz (often together with garnet) were stable at the highest grades of metamorphism. Although there are examples where sapphirine and quartz are in contact, the sapphirine usually has thin (0.1 mm) coronas of cordierite-garnet-sillimanite, cordierite-sillimanite, cordierite, and garnet-sillimanite, as well as rare coronas of hypersthene-sillimanite (Figure 4.2)-see later section for reactions.

The less common assemblage hypersthene-sapphirine-quartz (± sillimanite) is present in thin bands (0.5 cm thick) in some rock specimens. These consist of equigranular, polygonal grains of sillimanite (1 mm) laths of sapphirine (up to 3 mm), hypersthene and quartz. The sapphirine and hypersthene are often separated by a thin corona of secondary cordierite occasionally accompanied by sillimanite (see reaction 13, mineral assemblages and reactions section).

In the less aluminous rocks the assemblages garnet-hypersthene-quartz and hypersthene-quartz are common. They consist of equigranular, polygonal grains with triple point grain boundaries. Garnet has idiomorphic outline in places. Garnet-hypersthene-K feldspar-quartz is present in one sample.

Fig. 4.2A Thin section photograph of pelitic granulite (sample
          76283351) from Spot Height 945. Sapphirine (blue
          colour) has a corona of garnet (black), cordierite
          (grey-black twinning) and sillimanite (pink-blue and
          yellow) separating it from quartz (grey-pale yellow).
          Primary garnet (black), idiomorphic sillimanite,
          osumilite intergrowth and rutile (orange) are also
          present. Cross polarised light.   x25 magnification.

Fig. 4.2B Thin section photograph of osumilite with weak
           cleavage (centre of picture). The osumilite is
           surrounded by fine grained osumilite inter-
           growth (Cd-Kf-Qtz-Ky). Minor garnet and spinel
           (black) and quartz (grey-white, top left hand side
           of picture) are also present. Sample 77284348.
           Cross polarised light.   x25 magnification.

Fig. 4.2C Typical texture of osumilite intergrowth (Cd-Kf-
           Qtz-Hy) after osumilite. The Cd-Kf-Qtz form a
           fingerprint-like intergrowth with the Hy present
           as a dendritic intergrowth and trails (black
           colour) through the other three minerals. Even,
           grey areas are primary hypersthenes. Sample
           77283449. Cross polarised light. x 50 magni-
           fication.

Fig. 4.2D Detail of osumilite intergrowth from 4.2C, showing
           fingerprint-like intergrowth of Cd-Kf-Qtz. Black
           trails are associated hypersthene. Sample
           77283449. Cross polarised light. x100 magni-
           fication.
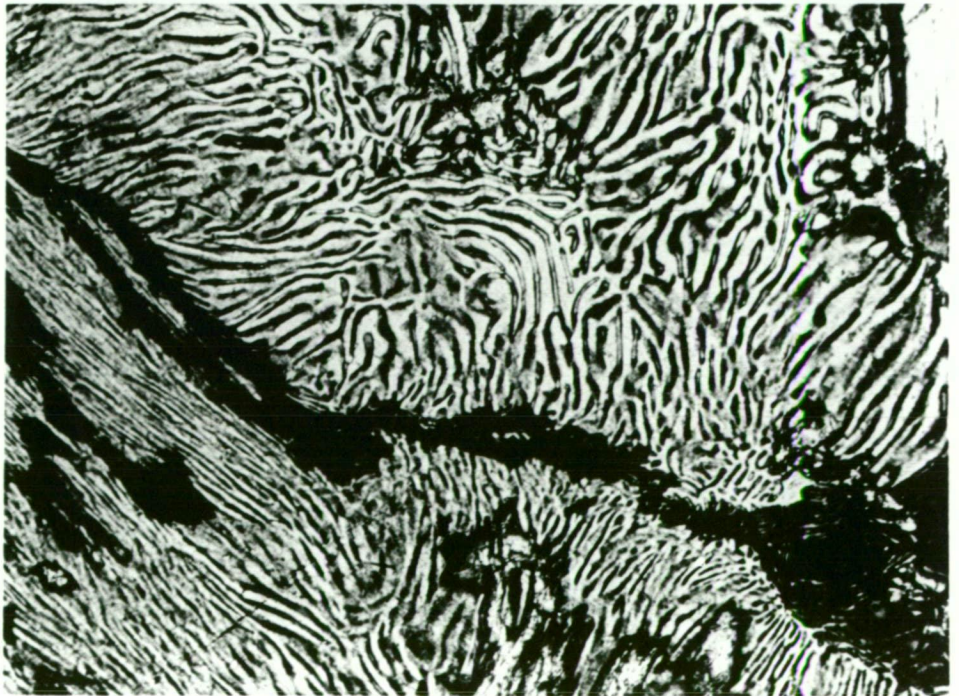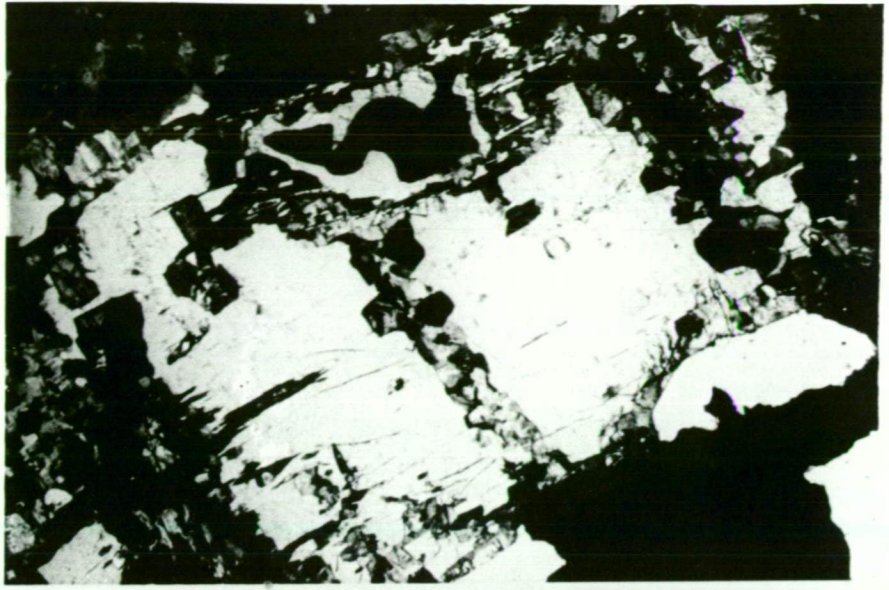
The assemblages garnet-cordierite-hypersthene-quartz and garnet-cordierite-sillimanite-quartz both developed at lower temperatures than the peak of metamorphism. Cordierite is mostly of retrograde origin in these rocks, but it is possible that some may be primary, such as the rare quartz-free sapphirine-cordierite intergrowths.

Osumilite occurs in several mineral associations in the metapelites. It is tabular with a weak basal cleavage, a faint yellow pleochroism, and is length fast with first order yellow-grey interference colours. The most common occurrence of osumilite is as relict grains (up to 5 mm long) in a fine grained symplectite or fingerprint-like intergrowth (termed osumilite intergrowth) of cordierite-quartz-K feldspar-minor hypersthene (Figure 4.2). The intergrowths range in grain size from almost submicroscopic to examples with 0.05 mm individual thickness. Cordierite-quartz-K feldspar form a continuous intergrowth whereas hypersthene forms irregular dendritic patches and trails. In the finer grained intergrowths, hypersthene is distinguished as a "dusting" amongst the other minerals, whereas the coarser grained samples are modally inhomogeneous, with cordierite-quartz and cordierite-K feldspar intergrowths being common. In some intergrowths the parallel alignment of rutile needles defines the cleavage trace of the original osumilite. The development of this association by the breakdown of osumilite is described later (reaction 27) and has previously been described from a contact aureole of the Nain Anorthosite in Labrador (Berg and Wheeler, 1976).

Spinel, sapphirine, sillimanite, garnet, hypersthene, quartz and rutile were each originally in association with osumilite in various rocks (Table 4.1). In osumilite-quartz layers the quartz typically has embayed grain boundaries which is probably due to prograde reaction of quartz and other phases to produce osumilite. Primary K-feldspar is absent from the highest grade rocks in which osumilite is present.

Spinel in contact with osumilite (or osumilite intergrowth) always occurs as rounded inclusions, and coexisting spinel-osumilite probably only co-existed in a quartz deficient environment. The spinel in the osumilite intergrowths is surrounded by thin reaction coronas of cordierite (-K feldspar).

A variety of reactions have occurred in the quartz-bearing osumilite rocks. Sapphirine and sillimanite are now usually separated from the osumilite by thin reaction coronas of cordierite (-K feldspar-quartz) (reactions 29, 30). Garnet is commonly separated from osumilite by thin coronas of cordierite-K feldspar-hypersthene (reaction 28). This secondary hypersthene is present as fine grained blebs against the garnet, and where in association with primary hypersthene forms an irregular fine grained overgrowth. Primary osumilite-hypersthene associations remain stable in these assemblages, and have not developed reaction coronas apart from the osumilite breakdown reaction. In some cases the osumilite intergrowth next to sapphirine is depleted in quartz, which may indicate that sapphirine reacted to form cordierite coronas after the breakdown of osumilite.

More aluminous layers contain the assemblage garnet-sapphirine-sillimanite-quartz together with K-feldspar rather than osumilite. The assemblage hypersthene-sapphirine-osumilite is stable in quartz-free rocks.

Minor biotite developed in the assemblage garnet-biotite-sillimanite-quartz (±K-feldspar), most probably due to lower temperature hydration of these rocks. Idiomorphic prisms of sillimanite and subidiomorphic garnet are set in a matrix of red-brown biotite and quartz. The development of biotite was due to a variety of reactions (see below). Fine grained intergrowths of biotite-quartz have partly replaced the cordierite-K-feldspar-hypersthene of the osumilite intergrowths. Similarly, thin

zones of garnet-biotite-quartz have developed at the expense of hypersthene-K feldspar-rutile.

Where osumilite is absent from the pelitic rocks K-feldspar is often present instead. Such rocks consist of the assemblage garnet-sillimanite-perthite-quartz, and rare spinel and sapphirine are present as inclusions in garnet and sillimanite.

More iron-rich rock types consist of the assemblage garnet-magnetite-quartz-K feldspar (microcline). The minerals typically have amoeboid grain boundaries and a grain size of 1-2 mm. Quartz-free rocks consist of fine grained equigranular garnet, deep green spinel, sillimanite, perthite and minor microcline. The spinel is sometimes intergrown with a small amount of magnetite, which occasionally contains rare inclusions of lath shaped corundum lamellae and has probably developed due to changing f_{O_2} with decreasing temperature (reaction 15).

V. ROCK CHEMISTRY[*]

Representative analyses of sapphirine- and osumilite-bearing metapelites are given in Table 4.2. Sapphirine-rich layers, of which analysis 1 is typical, have high Cr and low Cu, Sr, La, Ce, Pb, Th and U; high Rb/Sr ratios and low Ca/Y and Ba/Rb ratios. Na_2O and CaO are very low, except where plagioclase is present (analysis 3).

Sapphirine is confined to aluminous rocks with Mg values greater than about 0.65 (Fig. 4.3) although the sapphirine itself is considerably more magnesian. More Fe-rich compositions contain abundant garnet, with or without spinel. Many of the more aluminous layers consist essentially

Table 4.2

Chemical analyses of sapphirine and osumilite-
bearing metapelites.

	1.	2.	3.	4.
SiO_2	47.5	68.2	73.4	71.4
TiO_2	1.26	0.94	0.72	0.35
Al_2O_3	31.7	13.09	11.42	15.10
FeO*	7.94	6.52	1.86	5.86
MnO	0.06	0.03	0.01	0.08
MgO	9.21	10.57	4.55	3.86
CaO	0.02	0.06	0.70	0.11
Na_2O	0.12	0.07	2.34	0.22
K_2O	1.10	0.01	2.20	1.68
P_2O_5	0.01	0.02	0.02	0.04
H_2O^+	0.65	0.63	0.62	0.26
H_2O^-	0.03	0.12	0.13	0.14
CO_2	0.05	0.03	0.03	0.02
Total	99.65	100.40	98.01	99.17
V	243			
Cr	1020	4	10	171
Ni	183	3	36	81
Cu	6	3	2	27
Zn	25	14	22	24
Ga	47			
Rb	52	<1	51	43
Sr	10	1	37	19
Y	52	21	1	35
Zr	435	171	355	299
Nb	85	19	7	6
Ba	84	8	1880	291
La	4	23	4	6
Ce	7	38	4	7
Pb	<1	<1	1	3
Th	2	13	<1	<1
U	0.5	1.0	0.5	1.0
K/Rb	176	-	358	324
Rb/Sr	5.2	-	1.4	2.3
Ca/Y	2.8	20	5000	22
Ba/Rb	1.6	-	37	6.8
100Mg/Mg+Fe	67	74	81	54

1. Sapphirine-osumilite-garnet-quartz (-sillimanite) granulite from
    Spot Height 945, Tula Mountains (76283350 A).[1]

2. Quartz-orthopyroxene-sapphirine (-cordierite) granulite from
    Mount Hardy, Tula Mountains (77284633).

3. Osumilite-quartz-plagioclase-orthopyroxene-phlogopite(-sapphirine)
    gneiss from Mt. Dungey, Tula Mountains (77284249).

4. Quartz-garnet-osumilite-sillimanite(-spinel) granulite from Gage Ridge,
    Tula Mountains (77284348).

* Total iron as FeO
[1] B.M.R. registered thin section number.
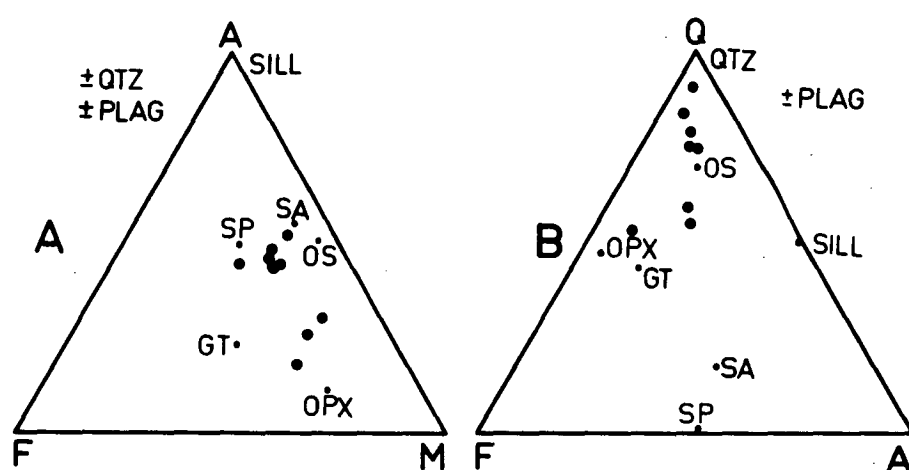
Fig. 4.3   A.   AFM diagram showing compositions of sapphirine
            and osumilite-bearing metapelites (large circles).
            Garnet, orthopyroxene, sillimanite and minor spinel
            and rutile are additional phases (small dots).

            B. SiO_2-(FeO+MgO)-Al_2O_3 diagram showing
            compositions of sapphirine and osumilite-bearing
            metapelites.

of sapphirine (up to 50%), osumilite (or cordierite-rich intergrowth),
and quartz, with variable amounts of garnet. Sillimanite, orthopyroxene
and spinel are present in only minor quantities. This results in most
of the analyses plotting in a roughly linear trend just to the garnet
side of the join quartz-osumilite-sapphirine on the SiO_2-(FeO + MgO)-
Al_2O_3 diagram (Figure 4.3). The sample which plots well of this trend
contains abundant orthopyroxene. Figure 4.3 is an AFM diagram for which
the rock analyses have been corrected for osumilite and feldspar
contents.

The chemical features of the most aluminous layers - low CaO
and Na_2O, high MgO - are consistent with their derivation from
argillaceous sediments. The composition of analysis 1 (Table 4.2)
could be represented fairly closely (ignoring volatiles) by a mixture of
50 percent kaolinite, 34 percent chlorite (e.g. ripidolite or clinochlore
of appropriate composition), 8 percent muscovite (or sericite) and
8 percent quartz. If all of the Cr was originally present in muscovite,
it would have contained about 1.75 percent Cr_2O_3, well within the range
of chromian muscovite (fuchsite) (Deer et al., 1962). Green quartzites
with fuchsite mica are common amongst possibly Archaean metasediments
in the southern Prince Charles Mountains to the southeast of Enderby
Land (Tingey, in press). Although there is a general lack of anatectic
features at this locality it is possible that some degree of melting
and consequent loss of a granitic component occurred during the prograde
metamorphism or a previous metamorphism, which would have been accom-
panied by dehydration of hydrous minerals. Associated quartzo-feldspathic
gneiss locally shows cross cutting relationships with the quartzite and
aluminous layers.

VI. MINERAL CHEMISTRY

Representative mineral compositions from the various assemblages are given in Tables 4.3-4.10. Analyses were obtained using a Si(Li) detector attachment on a TPD electron probe at the Research School of Earth Sciences, Australian National University. Analytical technique and correction procedures are given in Reed and Ware (1975).

1. OSUMILITE

Osumilite is a rare mineral which until recently had only been found in the groundmass or cavities of volcanic rocks and in a buchite from a contact aureole (Miyashiro, 1956; Rossi, 1963; Olsen and Bunch, 1970; Chinner and Dixon, 1973). It has now been reported from two anorthositic contact aureoles in granulite (Berg and Wheeler, 1970; Maijer et al., 1977) and on a regional scale in the granulites of Enderby Land.

The Antarctic osumilite is homogeneous in composition, both within individual crystals and between different grains (Table 4.3). It is more Mg-rich than that from the two other granulite occurrences (Mg_{90-91} compared to Mg_{76-77} respectively - Mg = Mg/(Mg + Fe) x 100). In common with other examples, the Antarctic osumilite has an excess of MgO and FeO compared to the synthetic osumilite investigated experimentally by Schreyer and Seifert (1967) (Figure 4.4). Its composition can be described by the general formula

$$(Na,K)^{xii}_1 \ (Mg,Fe^{2+})^{vi}_2 \ (Al)^{iv}_3 \ (SiAl)^{iv}_{12} \ O_{30}$$
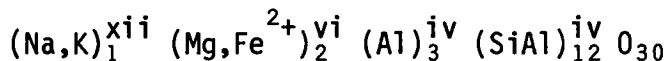
though with a slight excess cation total, which could in part be due to the presence of a small amount of Fe^{3+}. Oxide totals are consistent with there being little or no structural water present, which is consistent with the work of Goldman and Rossman (1978) who have shown that osumilite should be formulated as an anhydrous mineral.

Table 4.3

Chemical Analyses of Osumilite

	1	2	3	4	5	6	7
SiO_2	61.82	61.73	60.94 - 61.85	62.18	60.37	59.50	61.94
TiO_2				0.12	0.22		
Al_2O_3	23.64	23.75	23.36 - 23.92	21.58	22.95	24.77	21.77
FeO*	1.42	1.25	1.25 - 1.63	3.97	3.95	0.52	0.13
MnO				0.07	0.13		
MgO	8.40	8.50	8.30 - 8.78	7.46	7.02	4.68	2.42
CaO				0.06			0.14
Na_2O	0.24	0.32	0.24 - 0.53	0.22	0.59	0.72	1.00
K_2O	4.48	4.45	4.40 - 4.55	4.12	4.14	9.80	12.59
Total	100.0	100.0		100.06	99.37		
		Cations on the basis of 30 oxygens					
Si	10.177	10.157		10.357	10.132	2.687	2.828
Ti				0.015	0.028		
Al	4.588	4.607		4.238	4.541	1.318	1.171
Fe^{2+}	0.195	0.172		0.553	0.554	0.020	0.005
Mn				0.010	0.018		
Mg	2.061	2.084		1.852	1.756	0.315	0.164
Ca				0.011			0.007
Na	0.077	0.102		0.071	0.192	0.063	0.089
K	0.941	0.934		0.876	0.886	0.565	0.733
Cation Sum	18.038	18.057		17.982	18.109	4.968	4.998
Mg	91.3	92.4	90.2 - 92.4	76.8	76		

1,2. Osumilite. Spot Height 945. Sample 76283358 (B.M.R. registered thin section number).

3. Range in compositions of analyzed osumilites, Spot Height 945.
4. Osumilite from Nain Anorthositic Complex, Labrador. Also present 0.03 wt % Cr_2O_3, 0.25 wt % BaO (Berg and Wheeler, 1976).

5. Norwegian osumilite (Maijer et al. 1977).
6,7 "Osumilite intergrowths". Spot Height 945. Sample 76283358. Cations on the basis of 8 oxygens.
* Total iron as FeO in all mineral analyses unless otherwise indicated.
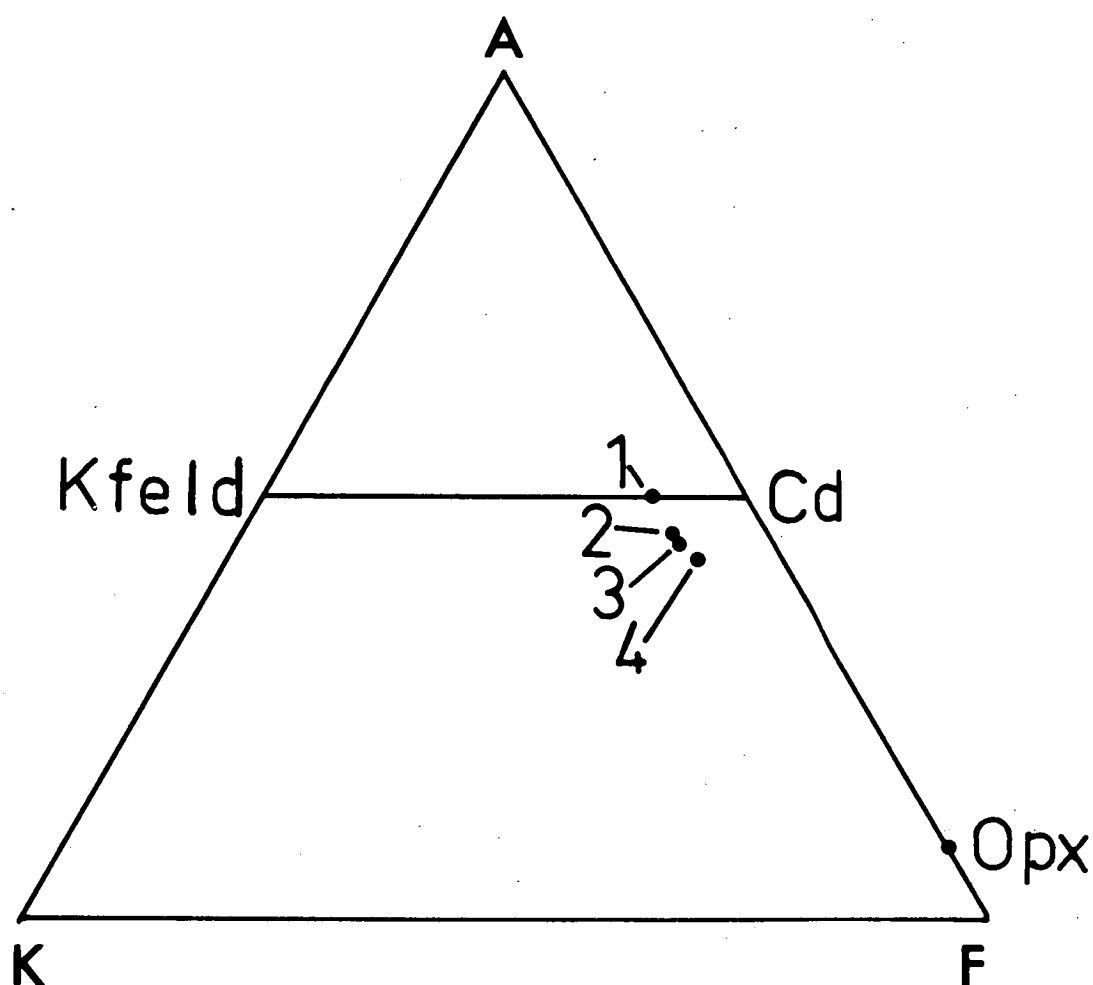
Fig. 4.4   AKF diagram showing compositions of osumilite from
different metamorphic terrains, together with the
synthetic osumilite composition of Schreyer and
Seifert (1967).   1.   Synthetic osumilite composition.
2.   Enderby Land.   3.   Norwegian osumilite (Maijer
et al., 1978).   4.   Nain osumilite (Berg and Wheeler,
1976).

There is an excess of Na + K, Mg + Fe^{2+} and Si and a deficiency in Al relative to the ideal allocations to the twelve-fold coordination, octahedral and the two tetrahedral sites, respectively. In terms of Miyashiro's milarite type structure (Brown and Gibbs, 1969) occupancy of the twelve-fold coordination site slightly exceeds unity, which may be due to the presence of alkalis in the cavities in the structure (Berg and Wheeler, 1976).

Berg and Wheeler (1976) proposed that by combining two coupled substitutions in a 1:1 ratio, a hybrid substitution $[(Mg,Fe)^{2+} + (Na,K)^{+} \rightleftharpoons (Al,Fe)^{3+} + \square]$ is created. However the Antarctic osumilite has a slightly higher K_2O and lower SiO_2 content than the Canadian (Nain) osumilite, whereas the Norwegian sample has a similar K_2O content to that from Antarctica, but with a higher SiO_2 content similar to the Canadian osumilite (Table 4.3, Figure 4.5). Thus the data does not support the concept of the hybrid substitution and the differences can be simply explained in terms of an $(MgFe^{2+})Si \rightleftharpoons 2$ Al substitution, with constant Na, K. Goldman and Rossman (1978) have shown that Fe^{2+} in the Nain osumilite, as well as being present in the octahedral site, does not also substitute in the Al tetrahedral site, but instead in the channels of the structure. In view of the fact that an $(MgFe)Si \rightleftharpoons 2$ Al substitution can explain some of the compositional differences in the three granulite osumilites, it seems probable that this is a charge balance substitution only, without Fe^{2+} substitution in the Al tetrahedral site. The problems of site occupancy and stoichiometry of osumilite are still unresolved.

Most of the finer grained intergrowths of Cd-Kf-Qtz-Hy surrounding osumilite are identical in bulk composition to osumilite, whereas the coarser grained intergrowths differ in composition because of modal inhomogeneities. Some of the fine grained intergrowths also differ in
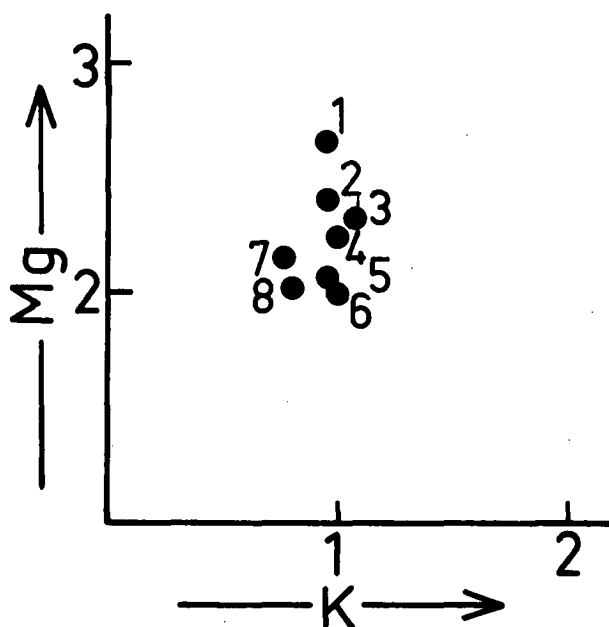
Fig. 4.5 Compositional variations in osumilite. K = (Na,K) and Mg = (Mg,Fe) atoms on the basis of 30 oxygens. 1. Tieveragh osumilite. 2. Nain osumilite. 3. Norwegian osumilite. 4. Enderby Land osumilite. 5. Sakkabira osumilite. 6. Synthetic osumilite. 7. Obsidian Cliffs osumilite. 8. Monte Arci osumilite.

composition from osumilite and have much higher K_2O contents and a wide range in K_2O/MgO ratio (Table 4.3). These differences can best be explained in terms of variable mixtures of cordierite and K-feldspar (Figure 4.6). Their compositions (Table 4.3) can also be recast to a feldspar stoichiometry on the basis of 8 oxygens, with a $KAlSi_3O_8 \rightleftarrows MgAl_2Si_2O_8$ type substitution, similar to that between the feldspar end members Or-An. The possibility that these fine grained intergrowths were originally a distinct but unknown mineral species cannot be dismissed.

2. CORDIERITE

Cordierite has a restricted range in composition from the various mineral assemblages (Table 4.4). Oxide totals from probe analyses usually exceed 99 wt. percent, suggesting the absence or the presence of only a very minor amount of H_2O or CO_2 as a channel filling molecular species in the structure. Alkalis are not detected in nearly all samples, though several grains have up to 0.2 wt. % Na_2O. The structural formula of the cordierites approximates quite well to the ideal formula $R_2^{2+} Al_4Si_5O_{18}$ (where R^{2+} = Mg,Fe) though in many samples there is a slight excess of R^{2+} and Al and deficiency in Si^{4+}.

A notable feature of nearly all of the cordierites is the scarcity of compositional zoning. With rare exceptions, the variation in composition of core-rim pairs between coexisting cordierite and garnet is less than 1 mol. percent and 2 mol. percent Mg/(Mg + Fe), respectively. One cordierite-garnet pair (Cd-Gt-Qtz only) displays opposite trends of regular zoning from core to rim ($Mg_{86.7}$ to $_{90.8}$ and $Mg_{49.5}$ to $_{44.1}$ respectively). The overall variation in composition of the cordierite from the different assemblages is very restricted (Mg_{88-92}, with only three examples of Mg_{86}). Within a single thin section small differences in cordierite composition exist between grains in contact with different
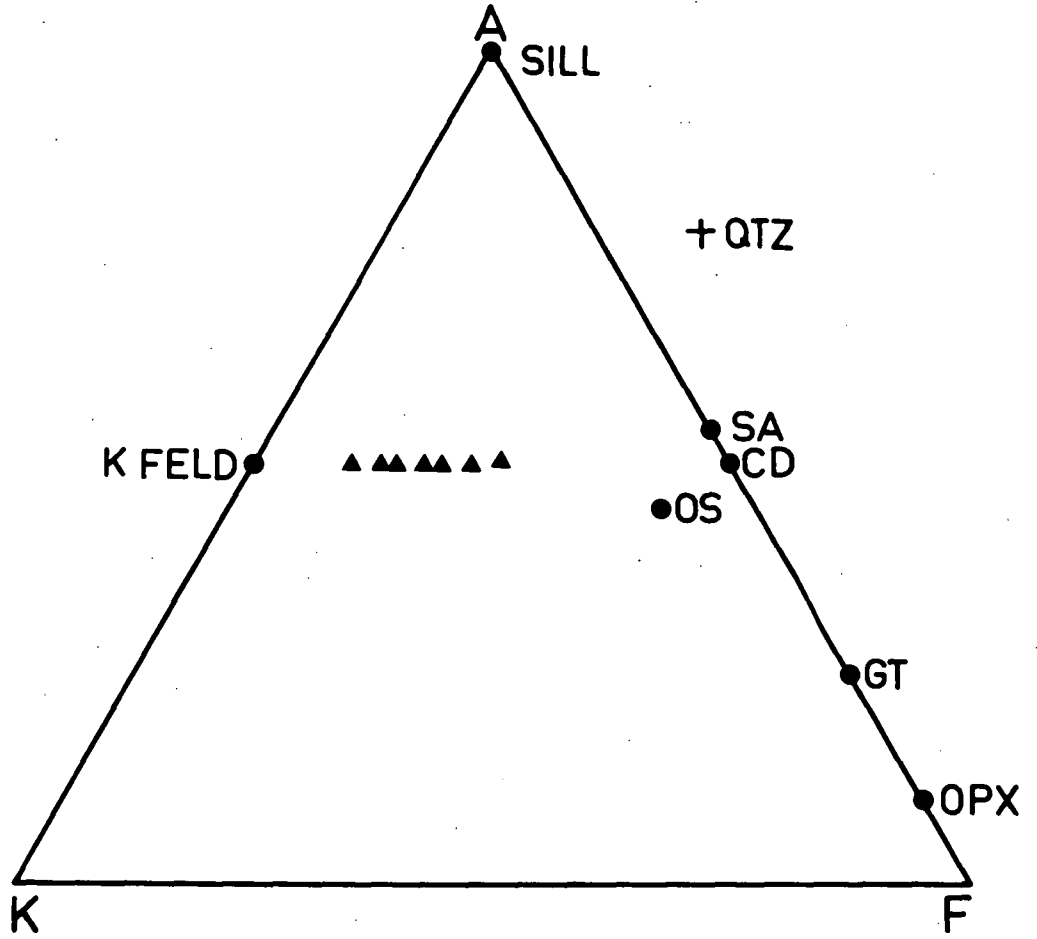
Fig. 4.6 AKF diagram (atomic proportions) showing the range
in compositions of the K_2O-rich variety of intergrowths.

Table 4.4

Chemical Analyses of Cordierite

	1	2
SiO_2	50.24	50.11
Al_2O_3	34.89	34.78
FeO	2.07	2.62
MgO	12.80	12.49
Cations on 18 (0)		
Si	4.943	4.942
Al	4.045	4.043
Fe^{2+}	0.170	0.216
Mg	1.877	1.836
Cation Sum	11.035	11.037
Mg	91.7	89.5

1. Cd in Cd-Gt-Sill reaction rim (Gt Mg 54.3) between sapphirine and quartz (Sample 76283350).

2. Cd from Cd-Kfeld-Qtz-Hy intergrowth formed by breakdown of osumilite (Sample 76280351).

mineral assemblages. For example, cordierite in the osumilite inter-growths is slightly more iron-rich (Mg_{88-91}) than that from other assemblages.

3. SAPPHIRINE

The analyzed sapphirines are all Mg-rich ($Mg_{74.6-85.5}$, Table 4.5) and the main compositional variations are illustrated in Figure 4.7. Structural formulae recalculations on the basis of 20 oxygens show good agreement with the general formula $M_7(M)O_2(T_6O_{18})$ derived by Moore (1969). All of the analyzed sapphirines depart from the theoretical end member sapphirine (R^{2+} : Al : Si $\Rightarrow$ 2:2:1) because of $R^{2+}Si \not{\not{\gtrless}} 2$ Al substitutions. The extent of this substitution is similar to that in sapphirines formed during the breakdown of kornerupine from the Limpopo Belt, Southern Africa (Schreyer and Abraham, 1969), but it not as large as in the "peraluminous" sapphirines of the quartz-free assemblages from Sar e Sang, Afghanistan (Schreyer and Abraham, 1975) as shown in Figure 4.7. The sapphirines plotted on this diagram all lie along the tie line between the ideal sapphirine composition and the trend for the $R^{2+}Si \not{\gtrless} 2$ Al substitution; in which a small amount of ferric iron has also been taken into consideration. Plots with all iron in the ferrous state lie slightly below, but parallel to this line. The slight excess in cation totals over the ideal 7.00 per 10 oxygens (Table 4.5) reflects the presence of a small amount of ferric iron in the sapphirine (1-2% of total Fe as Fe_2O_3). Structural formulae recalculations on the basis of 7 cations per 10 oxygens, and balancing the ratio of trivalent ions to the divalent and silicon changes the compositions only slightly.

Another notable feature is the presence of a small amount of Cr_2O_3 (0.18 - 2.52 wt. % Cr_2O_3) which substitutes for Al_2O_3 in the sapphirine. Other minor components are present in only trace amounts (TiO_2 < 0.05%,

Table 4.5

Chemical Analyses of Sapphirine

	1	2.	3
SiO_2	12.06	13.49	15.08
Al_2O_3	62.72	61.09	58.53
Cr_2O_3	2.52	0.36	1.13
FeO	5.95	8.33	9.52
MgO	16.76	16.47	15.73
	Cations on the basis of 10 (O)		
Si	0.718	0.808	0.906
Al	4.402	4.314	4.146
Cr	0.119	0.016	0.054
Fe^{2+}	0.296	0.417	0.479
Mg	1.487	1.470	1.409
Cation Sum	7.022	7.025	6.99
Mg*	86.4	81.1	74.6

1. Sapphirine reaction rim between spinel and osumilite (Sample 76283355).

2. Sapphirine with reaction rim of Cd-Gt-Sill next to quartz (Sample 76283350).

3. Sapphirine inclusion in sillimanite (Sample 76283235).

* $100Mg/Mg+Fe^{2+}$ recalculated from probe data after adjusting of Fe^{3+} to balance stoichiometry.
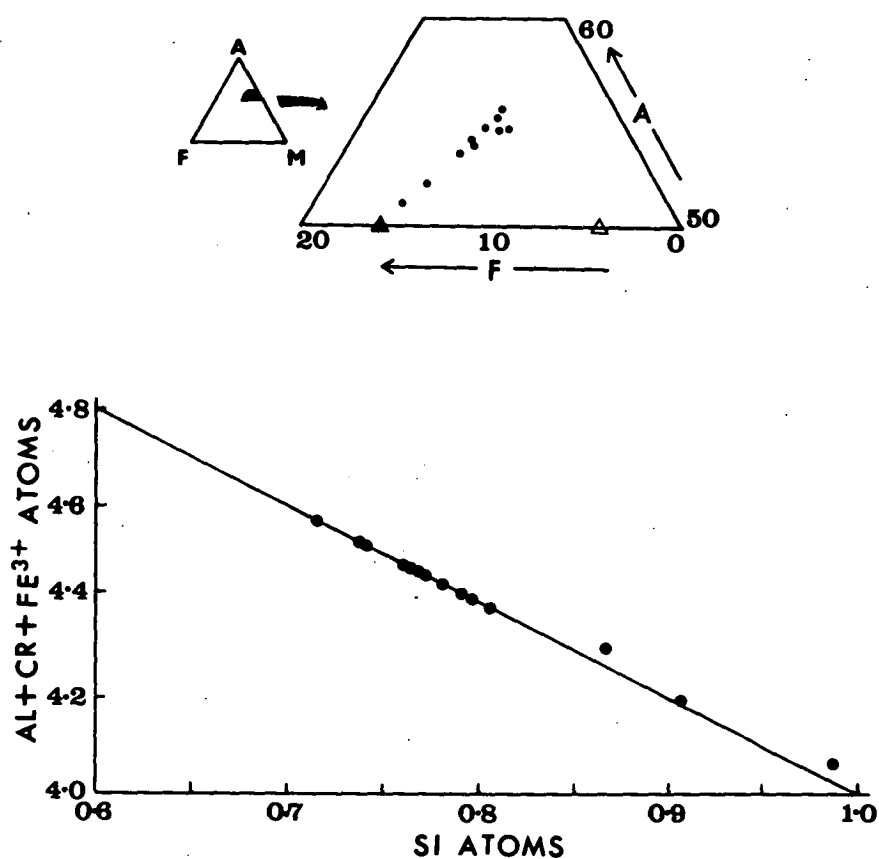
Fig. 4.7   AFM and Al-Si compositional variations in sapphirines.
Fe^{3+} calculated from probe data to maintain valency
charge and stoichiometry requirements. Open and
solid triangles show composition of Cd and ideal
sapphirine ($R_2^{2+}Al_4SiO_{10}$) respectively.

$MnO < 0.1$ wt. %). The substitution $R^{2+} Si \rightleftarrows 2(Al,Cr,Fe^{3+})$ varies systematically for many samples with decrease in Mg/(Mg + Fe). Generally the more iron-rich sapphirines approach more closely the ideal $(R_2^{2+} Al_4SiO_{10})$ sapphirine composition. However, when examined in detail it is found that the extent of Al substitution is determined by the reactions with other minerals. Thus for coexisting sapphirine-hypersthene, there is an increase in Al content from core to rim, without appreciable change in Mg/(Mg + Fe) of the sapphirine. This can be explained in terms of the exchange reaction between the following hypersthene and sapphirine solid solution components -

$$MgAl_2SiO_6 + Mg_2Al_4SiO_{10} \rightleftarrows Mg_2Si_2O_6 + MgAl_6O_{10} \qquad (1)$$
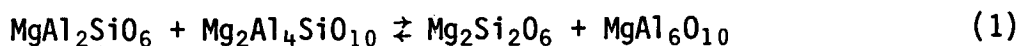
The hypersthene has a corresponding decrease in Al_2O_3 towards the rim (7.86 to 6.52 wt. % Al_2O_3).

There is no clear correlation between Cr_2O_3 contents and the above substitutions. This is most likely due to its relative concentration in the different minerals and to the limited volumes over which equilibrium is attained during corona development and mineral reactions in a cooling terrain. The partitioning of Cr_2O_3 increases in the following minerals in the order - Cr_2O_3 content of garnet < sapphirine < spinel. Thus sapphirine adjacent to and in equilibrium with spinel has a lower Cr_2O_3 content than sapphirine in equilibrium with garnet in any particular rock.

4. HYPERSTHENE

The most distinctive feature of orthopyroxene in the metapelites is the high Al_2O_3 content (up to 11.6 wt. % Al_2O_3 - Table 4.6), accompanied by little in the way of minor components, and usually less than 0.1 wt. % CaO. Cation totals show a slight excess over the ideal 4 per 6 oxygen atoms, suggesting the presence of very small ferric iron content, in

Table 4.6

Chemical Analyses of Pyroxenes

	1	2	3	4	5	6	7	8.	9.	10.	11.
SiO_2	48.28	50.82	52.38	47.98	48.85	49.16	53.79	48.77	50.23	51.4	52.58
TiO_2	0.30			0.14		0.12		0.78		0.77	
Al_2O_3	11.33	8.72	5.47	10.59	9.22	8.74	2.75	5.59	2.01	3.19	2.12
Cr_2O_3	0.40	0.40						0.45	0.18	0.95	0.54
FeO	14.77	13.28	15.05	17.67	18.14	17.09	15.51	12.43	25.83	7.44	18.8
MnO					0.15	0.11		0.28	0.49		0.34
MgO	24.67	26.78	27.09	23.62	23.64	24.78	27.95	12.15	18.93	14.81	25.01
CaO								19.52	2.02	21.45	0.63

Cations on the basis of 6(O)

	1	2	3	4	5	6	7	8.	9.	10.	11.
Si	1.738	1.809	1.877	1.746	1.781	1.785	1.932	1.842	1.924	1.903	1.929
Ti	0.008			0.004		0.003		0.022	0.000	0.021	0.000
Al	0.481	0.366	0.231	0.454	0.396	0.374	0.116	0.248	0.091	0.139	0.092
Cr	0.011	0.112						0.013	0.005	0.027	0.016
Fe^{2+}	0.445	0.395	0.451	0.538	0.553	0.519	0.466	0.392	0.828	0.230	0.577
Mn					0.004	0.003		0.009	0.016	0.000	0.011
Mg	1.324	1.421	1.447	1.281	1.285	1.341	1.496	0.648	1.081	0.817	1.368
Ca								0.790	0.083	0.851	0.025
Cation Sum	4.007	4.103	4.007	4.023	4.020	4.025	4.010	4.003	4.028	3.992	4.017
Mg*	74.8	78.2	76.2	70.4	69.9	72.1	76.2	62.3	56.6	78.0	70.3

1.   Opx-core Gt-Opx pair (Gt Mg 50.9) (Sample 76283355).
2.   Above Opx-rim Gt-Cd-Opx Gt(Mg 52.9) Cd (Mg 92.8) (Sample 76283355)
3.   Opx in Cd-Kfeld-Qtz-Hy intergrowth after osumilite (Cd Mg 90) (Sample 76283350).
4.   Opx-core coexisting with sapphirine (Sample 76283352).
5.   Above Opx-rim at contact with sillimanite between Sa and Hy (Sample 76283352).
6.   Opx in contact with Cd (Mg 88.7) (Sample 76283353)
7.   Opx rim with Cd (Mg 90.7) between Gt (Mg 48.2) and Qtz (Sample 76283368).
8.   Cpx in mafic granulite. Coexisting Plag (An 51) (Sample 76283261).
9.   Opx in mafic granulite (Sample 76283261).
10.   Cpx in mafic granulite. Coexisting Plag An 89 (Sample 76283260).
11.   Opx in mafic granulite (Sample 76283260).

contrast to the hypersthenes reported from similar assemblages elsewhere (Morse and Talley, 1971; Bondarenko, 1972). Hypersthenes in the meta-pelites are all Mg-rich (Mg_{72-78}) while those in the mafic rocks are more Fe-rich (Mg_{60-66}).

Unlike the osumilite and cordierite, the hypersthenes display different trends of compositional variation depending upon the mineral assemblage. In all cases the Al_2O_3 content decreases from core to rim. For a given Al_2O_3 content, hypersthene coexisting with sapphirine-sillimanite-(quartz) is more iron-rich than that coexisting with garnet-cordierite-(quartz) (Figure 4.8A). Hypersthene in the cordierite-quartz-K feldspar-hypersthene intergrowths (after osumilite) has a consistently lower Al_2O_3 content than that from the other assemblages.

Garnet-hypersthene pairs display opposite trends of Mg-Fe zoning with the hypersthene becoming more Mg-rich (Mg_{74-79}) and the garnet more Fe-rich (Mg_{56-50}) from core to rim respectively (Figure 4.8B). This reverse zoning can be explained in terms of an isochemical inter-crystalline exchange reaction, which proceeds from left to right with decreasing temperature -

$$\frac{1}{3} Mg_3Al_2Si_3O_{12} + \frac{1}{2} Fe_2Si_2O_6 \rightleftharpoons \frac{1}{3} Fe_3Al_2Si_3O_{12} + \frac{1}{2} Mg_2Si_2O_6 \qquad (2)$$

K_D ($\frac{Fe^{Gt}}{Mg}$ / $\frac{Fe^{Opx}}{Mg}$) increases from 2.28 for the cores to 3.06 at the rims (one sample from the assemblage Gt-Cd-Hy has K_D = 3.68).

The Al_2O_3 content of the hypersthenes decreases with increasing MgO from core to rim. This decrease is due to the following reaction which proceeds from left to right with decreasing temperature or increasing pressure -

$$\begin{array}{ccc} R^{2+}Al_2SiO_6 \cdot R_2^{2+}Si_2O_6 & \rightleftharpoons & R_3^{2+}Al_2Si_3O_{12} \\ \text{Orthopyroxene solid solution} & & \text{Garnet} \end{array} \qquad (3)$$
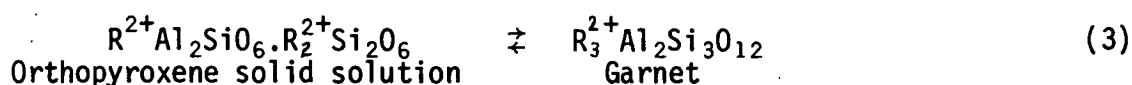
where R^{2+} = Mg,Fe.
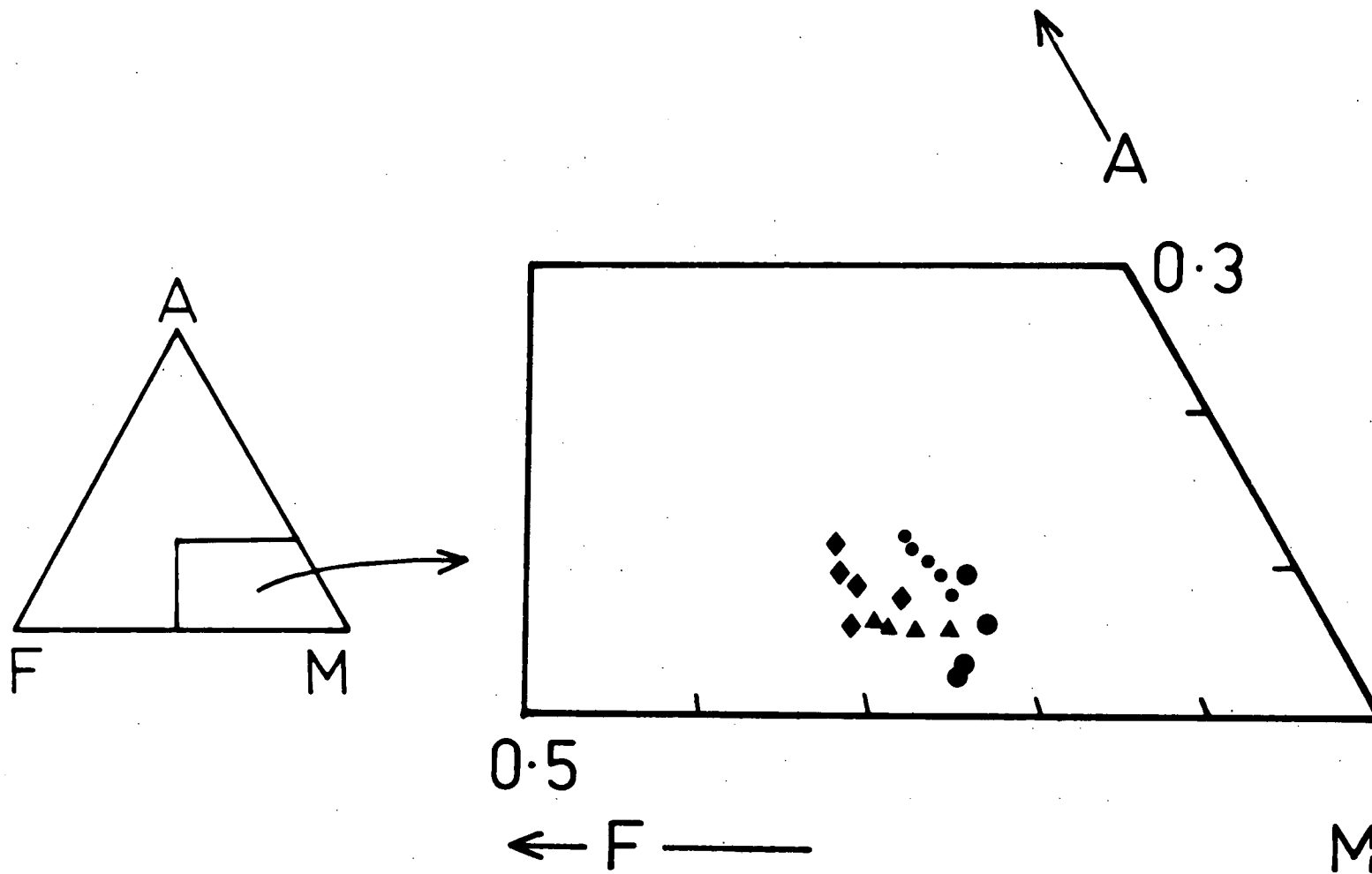
Fig. 4.8A AFM plot of orthopyroxenes from the different mineral
assemblages. Small dots: garnet-hypersthene pairs;
large dots: garnet-cordierite-hypersthene-quartz
assemblage; triangles: osumilite intergrowths
(cordierite-K feldspar-quartz-hypersthene);
diamonds: hypersthene-sapphirine-sillimanite-
quartz.
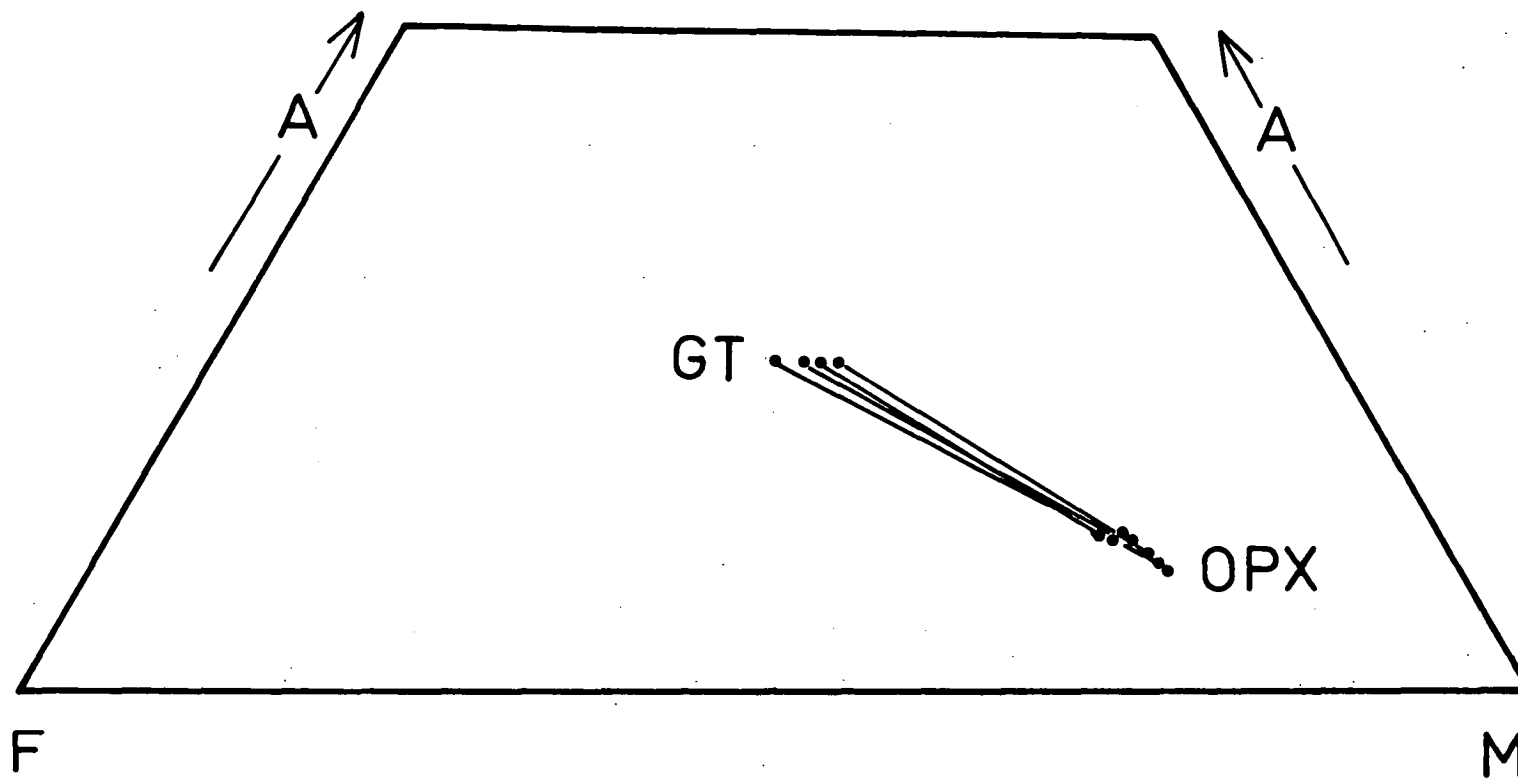
Fig. 4.8B AFM plot showing variation in compositions of coexisting
garnet-hypersthene pairs, including zoned core-rim trends.

Although it is commonly assumed that Al_2O_3 is present as Mg Tschermaks molecule ($MgAl_2SiO_6$) in orthopyroxene, the compositional variation in these orthopyroxenes lies along a trend directly away from an Fe Tschermaks component - $FeAl_2SiO_6$ (Figure 4.8B). It is not possible to decide from this data alone whether R^{2+} = Mg or Fe or both in the Tschermaks molecule, as the net effect of reactions (2) and (3) for the garnet orthopyroxene pairs is similar for both an Mg- and Fe-Tschermaks molecule. This point will be considered again later.

In the assemblage Gt-Cd-Hy-Qtz, the following reaction proceeds from left to right with decreasing temperature (Hensen and Green, 1971) -

$$2(MgFe)_3Al_2Si_3O_{12} + 3SiO_2 \rightleftharpoons (MgFe)_2Al_4Si_5O_{18} + 2(MgFe)_2Si_2O_6 \qquad (4)$$

Garnet   Quartz Cordierite   Hypersthene
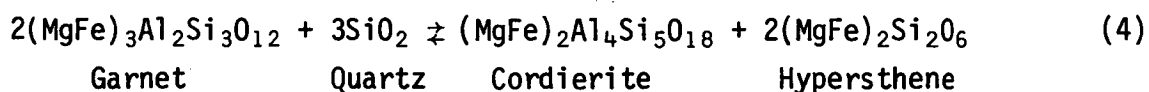
In view of the fact that X_{Mg} Cd > Hy > Gt one would expect all three minerals to become iron-rich with decreasing temperature (the three phase triangle Gt-Cd-Hy moves to more Fe-rich compositions on an AFM diagram with decreasing temperature). The garnet and cordierite do show trends of iron enrichment (especially the garnet), but instead the hypersthene shows a pronounced decrease in Al_2O_3 and only a slight decrease in Mg/(Mg + Fe) (Figure 4.8C).

The decrease in Al_2O_3 can be explained by the two reactions -

$$2R^{2+}Al_2SiO_6 . R_2^{2+}Si_2O_6 + 3SiO_2 \rightleftharpoons R_2^{2+}Al_4Si_5O_{18} + R_2^{2+}Si_2O_6 \qquad (5)$$

Complex Opx solid Quartz Cordierite Hypersthene
 solution

and

$$R^{2+}Al_2SiO_6 . 2R_2^{2+}Si_2O_6 \rightleftharpoons R_3^{2+}Al_2Si_3O_{12} + R_2^{2+}Si_2O_6 \qquad (6)$$

Complex Opx solid   Garnet   Hypersthene
 solution
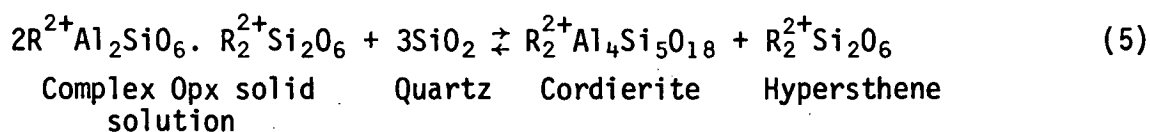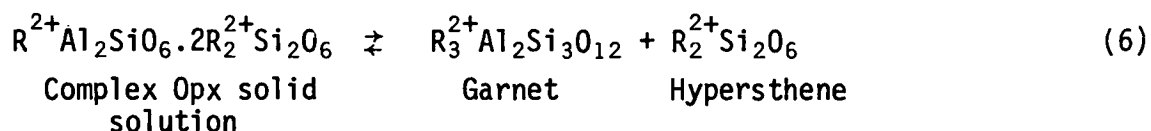
where R^{2+} = Mg,Fe.
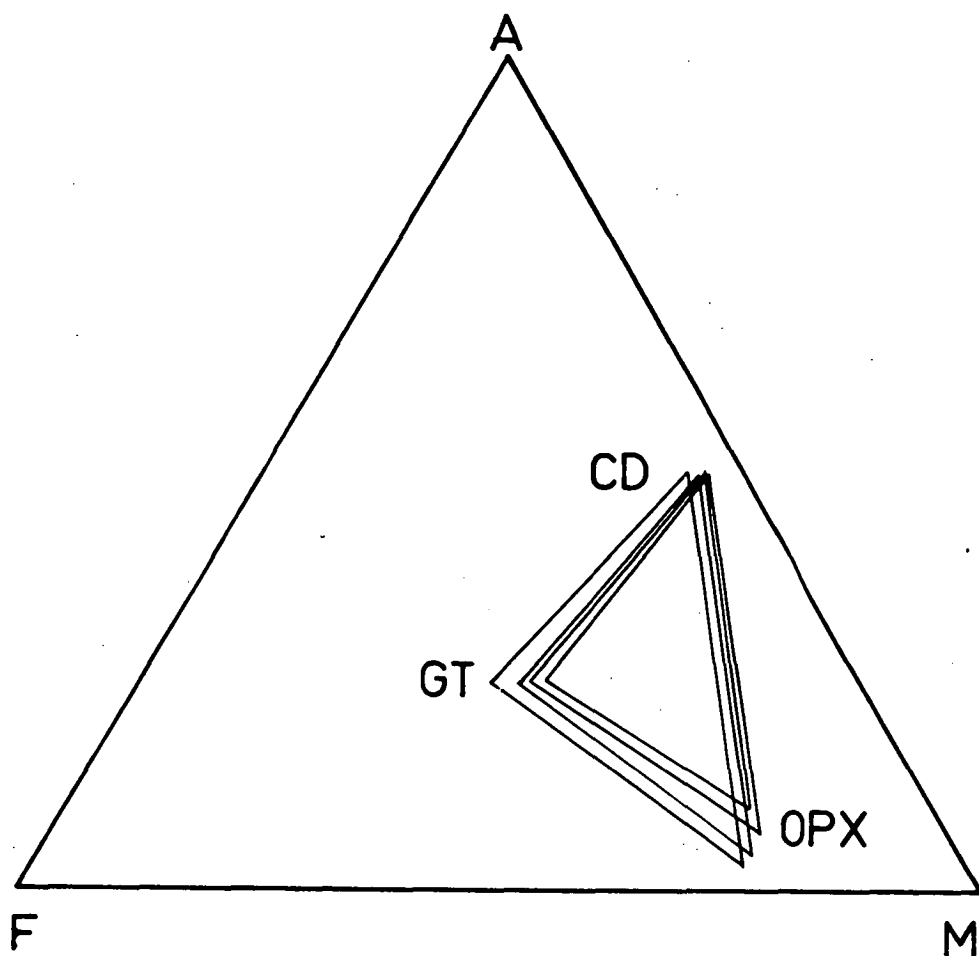
Fig. 4.8C   AFM plot showing variation in compositions of coexisting
garnet-cordierite-hypersthene(-quartz).

Hypersthene from the assemblage Hy-Sa-Sill-(Qtz) differs in composition from that of the above assemblages. It is more Fe-rich (Mg_{70-76} compared to Mg_{74-79}) for a given Al_2O_3 content (Figure 4.8A,D, Table 4.6). Different grains show similar trends of Fe-enrichment of coexisting sapphirine and hypersthene on an AFM diagram. This is consistent with the following reaction, which proceeds from left to right with decreasing temperature -

$$(MgFe)_2Si_2O_6 + 2Al_2SiO_5 \rightleftarrows (MgFe)_2Al_4SiO_{10} + 3SiO_2 \tag{7}$$
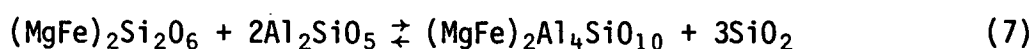
On an AFM diagram the three phase triangle Hy-Sa-Sill shifts towards more iron-rich compositions with decreasing temperature because $X_{Mg}(Sa) > X_{Mg}(Hy)$ (Figure 4.8D).

In areas free of sillimanite and quartz, the zoning observed in coexisting sapphirine-hypersthene differs from that in the above examples. Probe traverses from core to rim of adjoining grains show reverse trends of Al_2O_3 zonation with only slight change in Mg value. There is a slight decrease in Al_2O_3 content from core to rim of the orthopyroxene and increase in Al_2O_3 in the sapphirine (Figure 4.8, Table 4.6). These variations can be explained by the following intercrystalline exchange reactions which proceed from left to right with decreasing temperature -

$$(MgFe)Al_2SiO_6 + (MgFe)_2Al_4SiO_{10} \rightleftarrows (MgFe)_2Si_2O_6 + (MgFe)Al_6O_{10} \tag{8}$$

(in Opx solid solution)   (in sapphirine solid solution)

and

$$Mg_2Si_2O_6 + Fe_2Al_4SiO_{10} \rightleftarrows Fe_2Si_2O_6 + Mg_2Al_4SiO_{10} \tag{9}$$
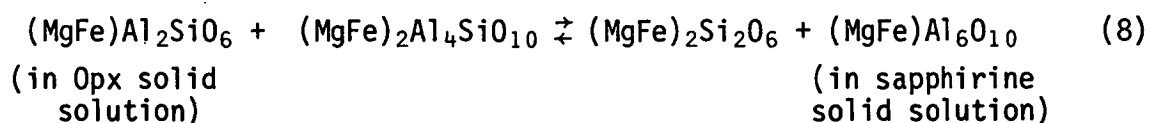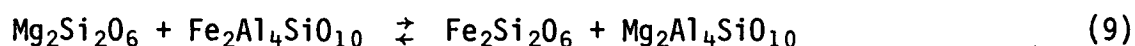
The orthopyroxene present in the Cd-Qtz-Kfeld-Hy osumilite inter-growths has lower Al_2O_3 contents (5.5-7.5 wt. % Al_2O_3, typically 5.5 wt. % Al_2O_3, Table 4.6, Figure 4.8 A,E) than that from the previous assemblages.
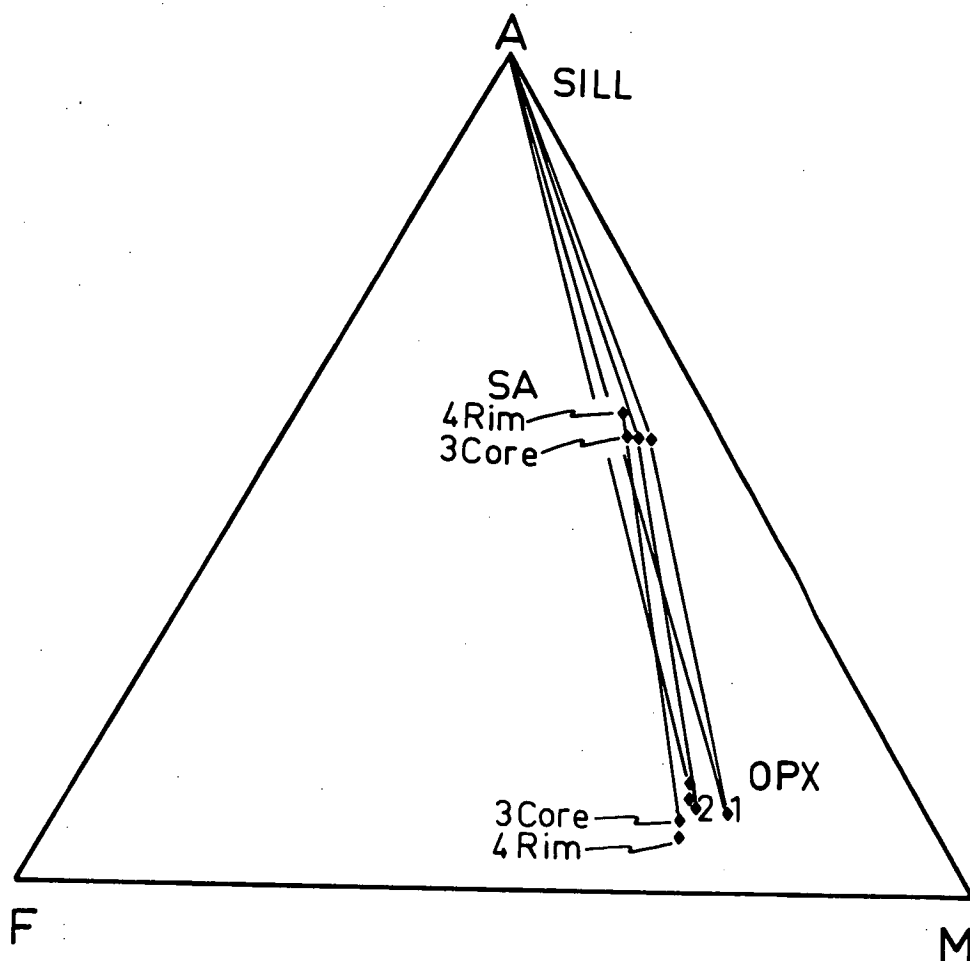
Fig. 4.8D Variation in composition of coexisting Sa-Hy and
Sa-Hy-Sill. 1,2 denote compositional trend of Fe
enrichment in Sa and Hy for the Sa-Hy-Sill assemblage.
3,4 represents reverse zoning, essentially in Al from
core to rim of a Hy-Sa pair with no Sill.
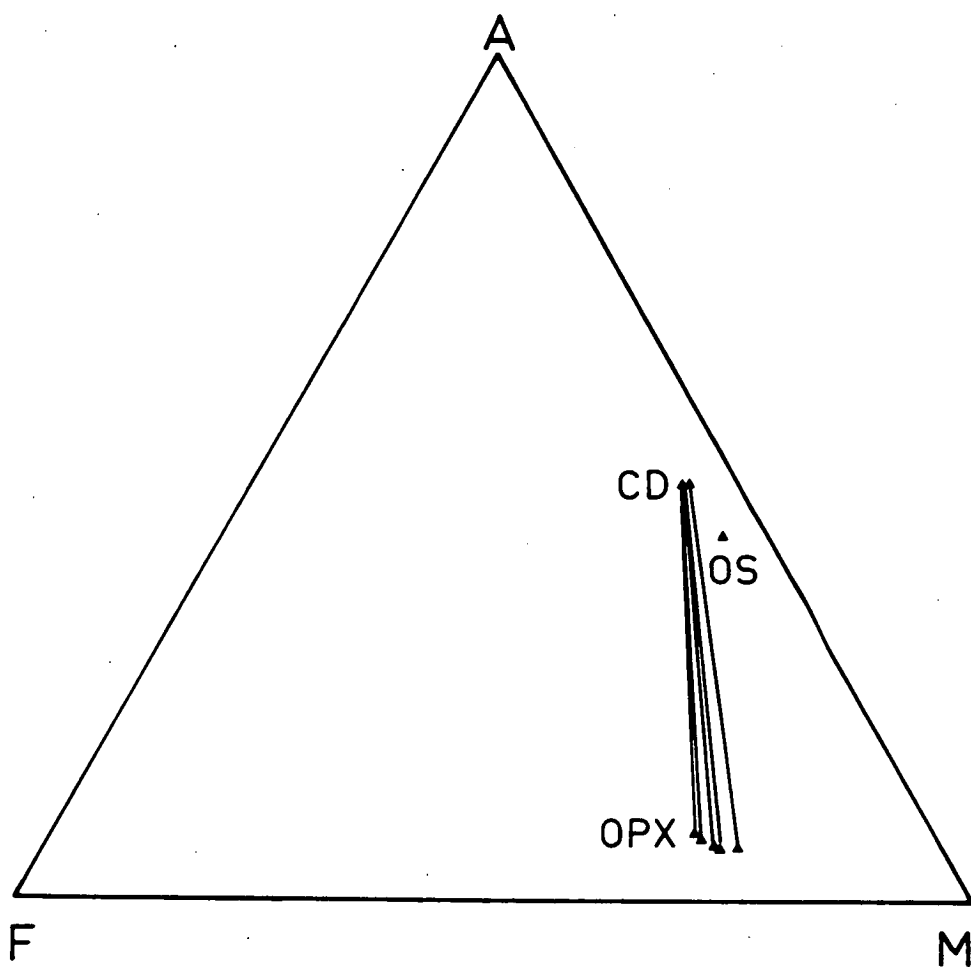
Fig. 4.8E AFM plot showing compositions of coexisting cordierite
and hypersthene from the cordierite-K feldspar-quartz-
hypersthene intergrowths (after osumilite). The composition
of analyzed osumilite is also shown.

Different grains range in composition from Mg_{73-77}, although they are too fine grained to detect compositional zoning. Tie lines connecting coexisting hypersthene and cordierite (Figure 4.8E) show similar trends of iron enrichment in the different samples, with orthopyroxene showing the larger range (Mg_{73-77} compared to Mg_{88-90}). The Al_2O_3 variations are less pronounced than, although similar to, those from the earlier assemblages - there is a slight increase of Al_2O_3 content in the ortho-pyroxene with increasing iron content.

Analyses of the coexisting pyroxenes from the mafic granulites are given in Table 4.6. The orthopyroxene is more Fe- and Ca-rich and contains less Al_2O_3 than that of the metapelites (1.6-2.0 wt. % Al_2O_3 and 1.0-2.0 wt. % CaO).

5. GARNET

Garnets show wide but systematic variations in composition in the various mineral assemblages, and are characterized by very low CaO contents (Table 4.7); their compositions can be almost entirely expressed by pyrope-almandine solid solutions. Cation summations on the basis of 12 oxygens indicate the presence of negligible ferric iron.

The Gt-Cd-Sill reaction rims between sapphirine and quartz show a small range in composition of both the garnet and cordierite. The most Mg-rich sample has Gt $Mg_{54.3}$, Cd $Mg_{91.7}$ and the least Mg-rich has Gt $Mg_{48.2}$, Cd $Mg_{90.7}$. The tie lines between coexisting garnet-cordierite show a systematic shift on the AFM diagram with increasing iron contents (Figure 4.9).

Little zoning exists within individual minerals. Probe traverses across idiomorphic garnets next to twinned cordierite reveals the cordierite to be homogeneous in composition while the garnet only varied from $Mg_{56.7}$ in the core to $Mg_{56.3}$ at the rim.

Table 4.7

Chemical Analyses of Garnets

	1.	2.	3.	4.	5.
SiO$_2$	39.56	39.40	39.31	39.15	39.24
TiO$_2$					
Al$_2$O$_3$	23.24	23.26	23.27	22.91	22.91
Cr$_2$O$_3$				0.18	0.26
FeO	22.11	22.06	22.74	22.10	21.21
MnO	0.18	0.38	0.51	0.76	0.70
MgO	14.76	14.75	13.93	13.94	14.51
CaO	0.16	0.15	0.23	0.71	1.17
Cations on the basis of 12 (O).					
Si	2.948	2.940	2.944	2.942	2.934
Ti					
Al	2.041	2.045	2.054	2.030	2.019
Cr				0.011	0.016
Fe^{2+}	1.378	1.376	1.424	1.389	1.326
Mn	0.011	0.024	0.032	0.048	0.044
Mg	1.640	1.640	1.555	1.561	1.617
Ca	0.013	0.012	0.019	0.057	0.094
Cation Sum	8.031	8.037	8.029	8.038	8.049
Mg	54.3	54.4	52.2	52.9	54.1

1. Gt in Cd-Gt-Sill reaction rim (Cd Mg 91.7) between Sa and Qtz. (Sample 76283350).
2. Gt core in Cd-Gt-Sill-Qtz assemblage (Cd Mg 91.8) (Sample 76283368).
3. Gt rim in Cd Gt-Sill-Qtz assemblage (Cd Mg 91.2) (Sample 76283368).
4. Gt in Cd-Gt-Hy-Qtz assemblage (Cd Mg 92.8, Opx 78) (Sample 76283368).
5. Gt in Gt-Os-Sa-Qtz assemblage (Os Mg 91, Sa Mg 81.7) (Sample 76283358).
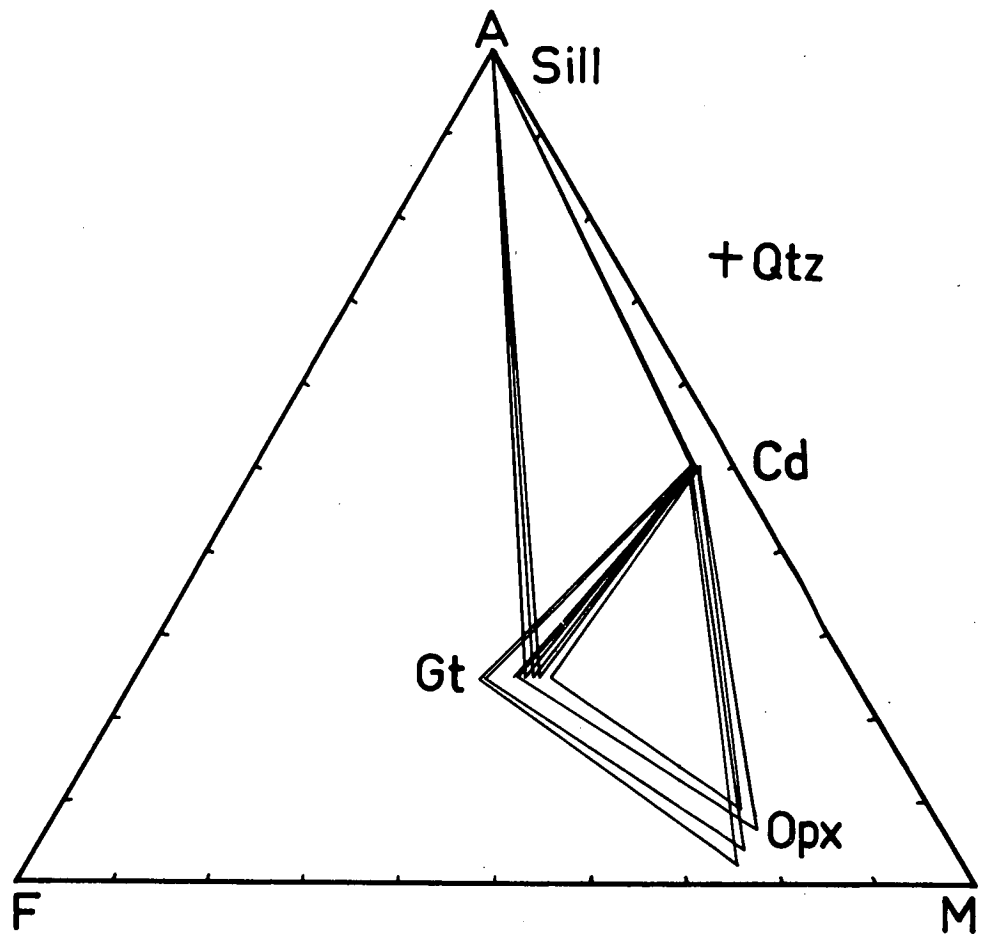
Fig. 4.9   AFM compositional variations in the assemblages
Gt-Cd-Sill-Qtz and Gt-Cd-Hy-Qtz.

A similar but slightly larger range in garnet compositions ($Mg_{48.1}$-$Mg_{53.6}$) is present in garnet from the assemblage Gt-Cd-Hy-Qtz, though with a slightly higher CaO content than that in the Gt-Cd-Sill assemblage ($\approx$ 0.8 and 0.2 wt. % CaO respectively). The garnet in association with osumilite and its Cd-Kfeld-Qtz-Hy breakdown products is slightly more Mg-rich than in the other assemblages (Mg_{53-56}), and also contains a small amount of CaO (0.7-1.2 wt. % CaO). Garnet coexisting with secondary biotite extends to even more iron-rich compositions (Mg_{56-40}).

6. SPINEL

The spinels are essentially unzoned spinel-hercynite solid solutions ($Mg_{46.9}$-$Mg_{60.5}$) and contain between 1 and 8 wt. % Cr_2O_3 (Table 4.8). The sum of the trivalent cations is very close to the ideal of twice the number of divalent cations, indicating the absence of appreciable ferric iron. Spinel in the assemblage Gt-Sp-Kfeld-Sill is in places associated with ilmenite (Table 4.8). Recalculations following the method of Carmichael (1967) indicate that the ilmenite has less than 3 percent of the total iron present as ferric iron. An analyzed grain of spinel in direct contact with quartz contained 6.56 wt. % Cr_2O_3.

7. FELDSPAR

Alkali feldspar is the main feldspar in the pelitic rocks, with plagioclase occurring commonly in perthite, but only rarely as a separate phase, and did not coexist with a separate alkali feldspar. Probe analyses of coexisting alkali and plagioclase feldspar exsolved from the perthites together with area scanned average analyses of the perthite are presented in Table 4.9. The rare separate grains of plagioclase are similar in composition (An_{28}) to that exsolved from the

Table 4.8

Chemical analyses of Spinels and Ilmenite

	1.	2.	3.	4.	5.	6.
TiO_2						52.08
Al_2O_3	61.14	55.53	60.82	58.78	63.69	0.15
Cr_2O_3	5.40	10.95	3.65	7.78	1.03	0.11
FeO	17.83	19.52	21.85	20.97	21.47	43.57
MnO						0.17
MgO	15.63	12.65	12.48	12.46	13.81	2.43

Cations on the basis of 4(O) for spinel, 3(O) for ilmenite

	1.	2.	3.	4.	5.	6.
Ti						0.987
Al	1.888	1.789	1.928	1.857	1.971	0.004
Cr	0.115	0.237	0.078	0.165	0.021	0.002
Fe^{2+}	0.394	0.446	0.491	0.470	0.47	0.918
Mn						0.002
Mg	0.604	0.515	0.500	0.498	0.540	0.091
Cation Sum		2.987	2.997	2.989	3.004	2.010
Mg	61.0	53.6	50.5	51.4	53.4	

1. Inclusion in Gt (Mg 55.4) (Sample 76280358)
2. In contact with Qtz (Sample 76283358)
3. Inclusion in Cd (Mg 89.1) (Sample 76283362)
4. Inclusion in Sa (Mg 83.4, 2.52 wt% Cr_2O_3) (Sample 76283355)
5. Coexisting with Gt (Mg 47.7) Kfeld, Ilmenite (Sample 76283265)
6. Ilmenite included in above spinel. Recalculates to 1.56 wt% Fe_2O_3 42.23 wt% FeO after the method of Carmichael (1967) (Sample 76283265)

Table 4.9

Chemical Analyses of Feldspars

	1.	2.	3.	4.	5.	6.
SiO_2	62.31	60.58	64.69	59.69	64.66	64.65
Al_2O_3	22.85	24.77	19.86	25.34	19.03	19.05
CaO	4.72	5.99	0.99	6.57	0.19	
Na_2O	6.24	8.05	2.70	8.08	1.62	1.44
K_2O	3.50	0.28	11.63	0.32	14.50	14.54

Cations on the basis of 8(O)

	1.	2.	3.	4.	5.	6.
Si	2.795	2.702	2.947	2.664	2.973	2.978
Al	1.208	1.302	1.067	1.333	1.031	1.035
Ca	0.227	0.286	0.048	0.314	0.010	
Na	0.543	0.696	0.239	0.699	0.145	0.129
K	0.200	0.016	0.676	0.018	0.850	0.855
Cation Sum	4.973	5.003	4.977	5.028	5.009	4.996

1. Area scan of original Kfeldspar (Sample 76283235)

2. Na-rich exsolutions in perthite from above grain

3. K-rich host of perthite from above grain

4. Na-rich exsolutions in perthite (sample 76283265)

5. K-rich host of perthite (Sample 76283265)

6. K-feldspar in Cd-Kf-Q-Hy intergrowth after osumilite (Sample 76280351)

perthite. A plagioclase in contact with hypersthene in one pelite sample is more anorthite rich (An_{58}) than the plagioclase in the other pelites.

The K-feldspars show a range in composition. That in the inter-growths formed by the breakdown of osumilite is distinct in composition from that in the other mineral assemblages. It has a negligible CaO content (<0.1 wt. % CaO).

Plagioclase in the analyzed mafic granulites is of two compositions (An_{52} and An_{83-85}) reflecting different rock compositions.

8. MICA

The micas in the metapelites are all Mg-rich ($Mg_{91.4-85.5}$) and can be termed phlogopites (Table 4.10). All are low in Al_2O_3, with no significant solid solution from the normal phlogopite formula $K_2R_6^{2+}Si_6Al_2O_{20}(OH)_4$ towards eastonite $K_2R_5^{2+}AlSi_5Al_3O_{20}(OH)_4$. They have moderate Ti contents (3.25-5.16 wt. % TiO_2) and the small range in concentration is probably related to the proximity of rutile during mica formation. Little chemical zoning was found in any of the phlogopites. Comparison of coexisting garnet- phlogopite pairs indicates that the more Fe-rich phlogopites coexist with the more Fe-rich garnets.

Table 4.10

Chemical Analyses of Phlogopites

	1.	2.
SiO_2	39.07	38.95
TiO_2	4.26	3.25
Al_2O_3	13.54	14.40
Cr_2O_3	0.36	
FeO	4.29	5.55
MnO		
MgO	21.21	21.19
CaO		0.21
K_2O	9.79	10.15
Total	92.52	93.29

Cations on the basis of 22(O)

	1.	2.
Si	5.716	5.695
Ti	0.469	0.358
Al	2.335	2.413
Cr	0.042	
Fe^{2+}	0.525	0.679
Mn		
Mg	4.625	4.618
Ca		0.032
K	1.828	1.893
Cation Sum	15.54	15.687
Mg	89.8	87.2

1. Phlogopite intergrown with Qtz next to Gt (Mg 53.1) (Sample 76283354)

2. Coexisting with Gt(rim Mg 40.2, core Mg 47.0) (Sample 76283361)

VII. <u>MINERAL ASSEMBLAGES AND REACTIONS</u>

In pelitic rocks described by the system K_2O-FeO-MgO-Al_2O_3-SiO_2 the interpretations of mineral reactions occurring at high temperatures above the breakdown of biotite and in the absence of a melt (refractory granulites) have commonly assumed that K_2O is present as an excess inert component, as K-feldspar (see Hensen and Green, 1971, 1972, 1973; Hess, 1969; Holdaway, 1976). As a result, the phase relations and mineral reactions had been quite well modelled on the subsystem FMAS. The occurrence of osumilite on a regional scale in the granulites of Enderby Land, as well as in two contact aureoles from Canada and Norway (Berg and Wheeler, 1976; Maijer et al., 1977) invalidates this assumption (see also Hensen, 1978). Most of the reactions in which osumilite-K feldspar do not participate are extremely rare in nature, but have been extensively studied by experiment. In addition most of the osumilite reactions and mineral assemblages have not previously been reported from other granulites nor predicted from theoretical and experimental studies.

The mineral assemblages and reactions observed in the Antarctic granulites can be divided into two groups - those in which neither K-feldspar nor osumilite participate in reactions and those in which they do. The mineral assemblages and reactions in these two groups can be explained in terms of the systems FMAS and KFMAS, respectively.* This is justified for the Antarctic granulites in view of the fact that the system KFMAS accounts for over 99% of the composition of these rocks.

---

* The mineral equilibria in these chemical systems can be studied by the methods developed by Schreinemakers (see Schreinemakers, 1965; Zen, 1966).

1. FMAS System Reactions and Mineral Associations

It is inferred on the basis of mineral textures that apart from quartz-free sapphirine-cordierite intergrowths, cordierite was not stable under the highest P-T conditions of metamorphism of these granulites. There have been numerous experimental studies defining the upper stability limit of cordierite due to terminal and non-terminal univariant reactions in the systems MAS and FMAS which are applicable to the Antarctic granulites (see introduction for references).

Reaction rims separating sapphirine and quartz suggest the reaction

$$Sa + Qtz \rightarrow Gt + Cd + Sill \qquad (10)$$
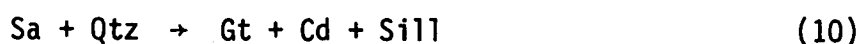
This reaction has been experimentally studied by Hensen and Green (1971, 1972, 1973). Reaction rims of cordierite with or without sillimanite between sapphirine and quartz are also observed. The fine grained nature of this texture, together with its widespread development elsewhere in Enderby Land suggests that garnet was not involved in this reaction. In the limiting pure Mg system MAS, the univariant reaction

$$Sa + Qtz \rightarrow Cd \qquad (11)$$

has been experimentally studied (Schreyer and Seifert, 1969; Newton, 1972). The presence of iron in the Antarctic samples, together with the fact that $X_{Mg}(Cd) > X_{Mg}(Sa)$ prohibits the above reaction from being a discontinuous reaction in the system FMAS. The observed texture has probably developed by a continuous (divariant) reaction (see terms of Thompson, 1976) in which the three phase triangle Sa-Cd-Sill-(Qtz) shifts to more Fe-rich compositions with decreasing temperature (Figure 4.10), together with a possible decrease in Al content of sapphirine due to the continuous reaction -
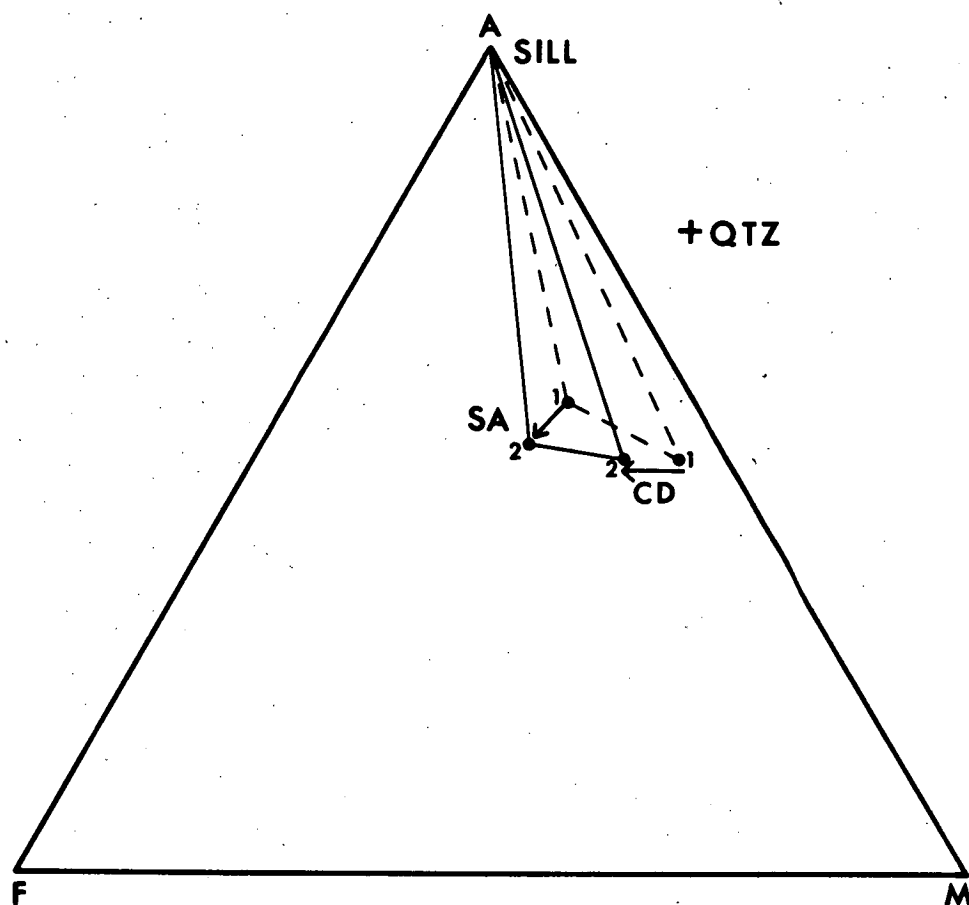
Fig. 4.10   Movement of the three phase triangle Sa-Cd-Sill
             to more Fe-rich compositions on an AFM diagram.
             Sapphirine 1 (+Qtz) reacts to sapphirine 2 +
             Cd + Sill with decreasing temperature.

$$m(Mg,Fe)_2Al_4SiO_{10}.n(Mg,Fe)Al_6O_{10} + 9SiO_2 \rightarrow$$
Complex Sa solid solution

$$m(Mg,Fe)_2Al_4SiO_{10}.(n-2)(Mg,Fe)Al_6O_{10} + 2(Mg,Fe)_2Al_4Si_5O_{18} + 4Al_2SiO_5 \qquad (12)$$
Cd
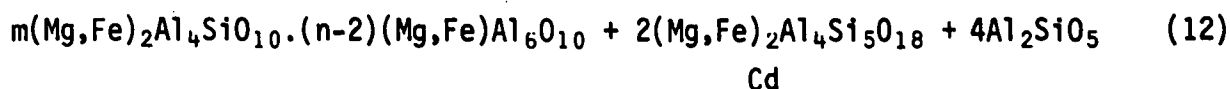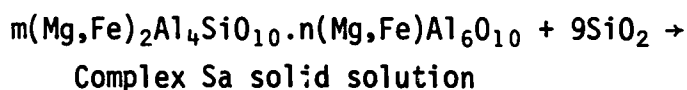
Note that the Al/(Fe+Mg) content of the natural sapphirines is greater than cordierite.

Some metapelites also contain the assemblage Hy-Sa-Qtz in which thin coronas of Cd and Sill commonly separate the sapphirine and quartz. Hypersthene and sapphirine remain in contact. This assemblage is consistent with the reaction -

$$Sa + Qtz \rightarrow Cd + Hy + Sill \qquad (13)$$

Both reaction (10) and (13) proceed from left to right with decreasing temperature but at different pressures using the experimental data of Hensen and Green (1973). It is difficult to reconcile the existence of both reactions at the one locality, implying that both the Cd-Gt and the Hy-Sill tie lines were stable under the same P-T conditions of metamorphism. The Sa and Cd are slightly more Fe-rich in reaction (13). The possible effect of small differences in CaO contents of garnet from the different assemblages may explain this feature (see mineral chemistry), and P-T conditions close to invariant point (Sp) (Figure 4.11) are suggested for this locality.

Rare grains of spinel are in contact with quartz, but spinel is usually enclosed in garnet, sapphirine and sillimanite. These observations can be explained by the reaction -

$$Sp + Qtz \rightarrow Gt + Sa + Sill \qquad (14)$$
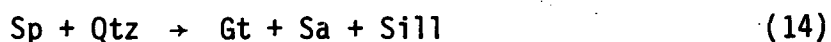
This reaction has been experimentally studied by Hensen and Green (1971, 1972, 1973). The chemographic relations consistent with the above assemblages and sequence of reactions are shown schematically in Figure 4.11.
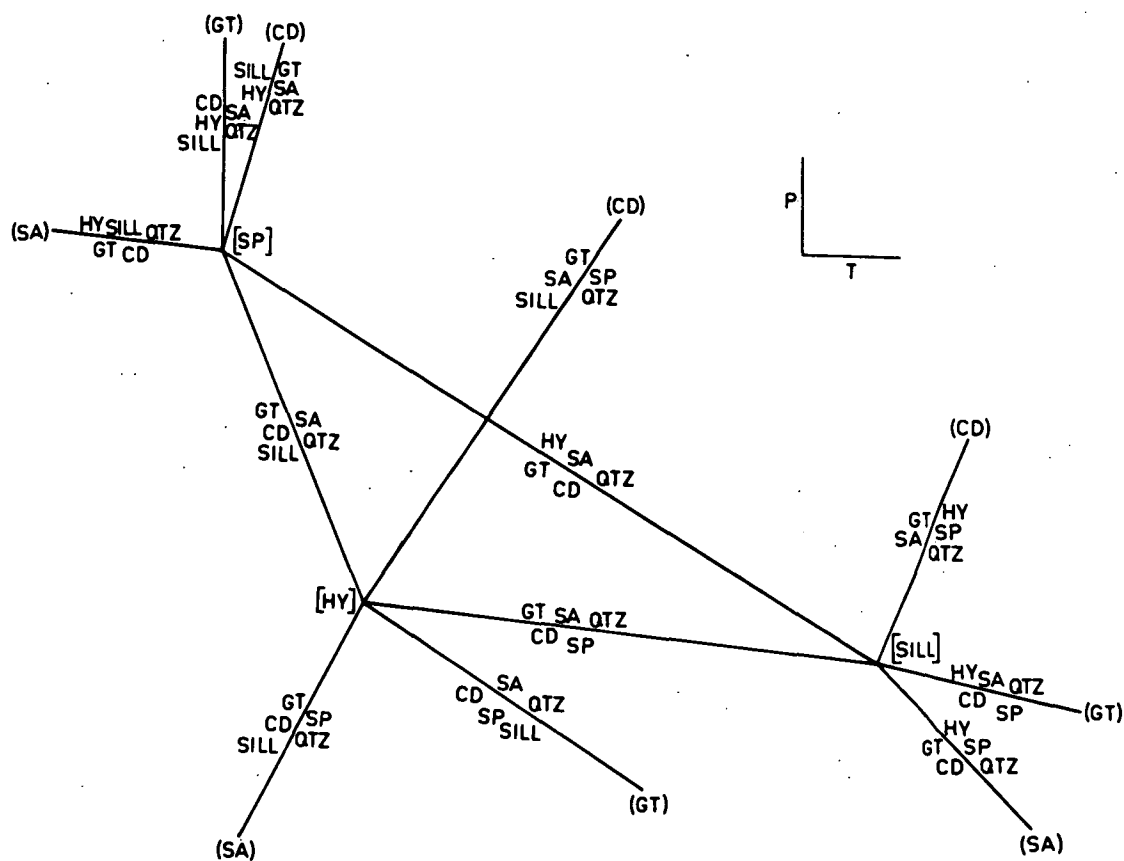
Fig. 4.11A Schreinemakers analysis of the inferred quartz-excess
stable univariant boundaries and invariant points
for the system FMAS, consistent with the mineral
assemblages in the Antarctic granulites (modified after
Hensen and Green, 1973, fig. 1). The invariant points
are labelled by the absent phase in square brackets.
The univariant reactions are labelled by additional
absent phase (curved brackets). The locations of the
metastable invariant points (Sa) and (Gt) can be
located at the intersections of the metastable
extensions of the relevant univariant lines.
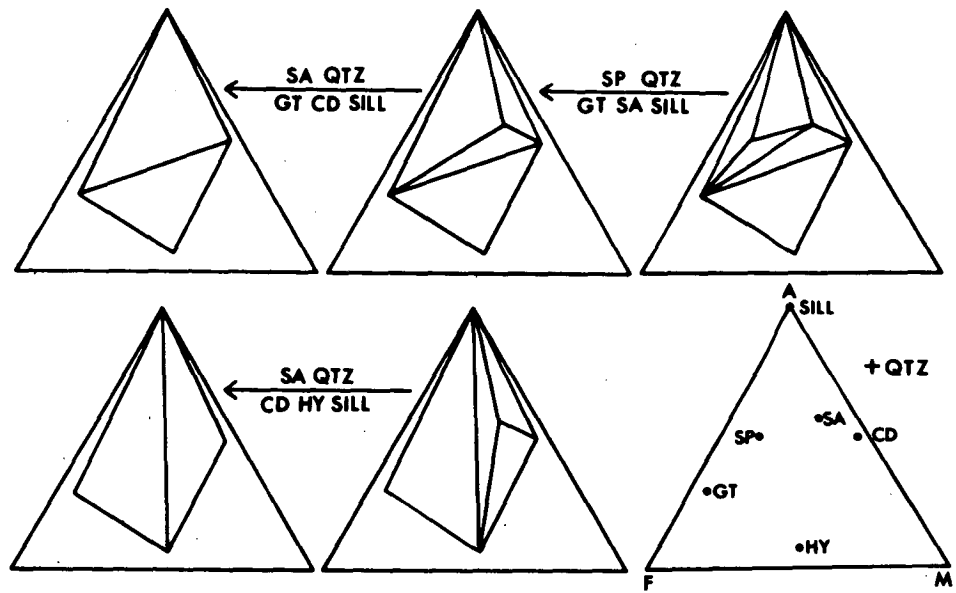
Fig. 4.11B   FMAS mineral reactions observed in the granulites
               from Spot Height 945.

The possibility that several of the spinel grains were also involved in oxidation reactions is suggested. The assemblage spinel-magnetite-corundum is extremely rare at Spot Height 945, but has been found elsewhere in Enderby Land (Sheraton et al., in press). The presence of fine grained corundum lamellae in the magnetite suggests the reaction -

$mMgAl_2O_4 \cdot nFeAl_2O_4 \quad + \quad \frac{1}{2}O_2 \rightarrow$
Spinel solid solution

$$mMgAl_2O_4 \cdot (n-3)FeAl_2O_4 + Fe_3O_4 + Al_2O_3 \qquad (15)$$
Spinel solid solution   Mt   Corundum
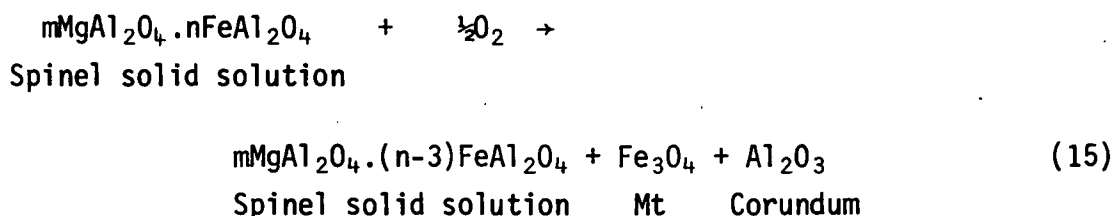
In the quartz-bearing rocks the assemblage spinel-magnetite-sillimanite is found, which may be due to a similar reaction -

$mMgAl_2O_4 \cdot nFeAl_2O_4 \quad + \quad \frac{1}{2}O_2 + 3SiO_2 \rightarrow$
Spinel solid solution   Quartz

$$mMgAl_2O_4 \cdot (n-3)FeAl_2O_4 + Fe_3O_4 + Al_2SiO_5 \qquad (16)$$
Spinel solid solution   Mt   Sill
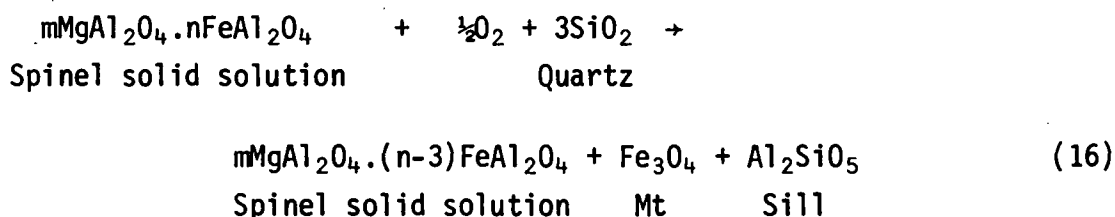
Turnock and Eugster (1969) note that below 900°C two spinel phases (hercynite- and magnetite-solid solution) should occur rather than one, because of a temperature dependent solvus.

2. KMAS and KFMAS System Reactions and Mineral Associations

This section considers the osumilite and K-feldspar mineral assemblages in the Enderby Land granulites and the reactions involving these minerals in the chemical systems KMAS and KFMAS. In their experimental study, Schreyer and Seifert (1967) concluded that synthetic osumilite is metastable, but it is now known that natural osumilite lies off the cordierite-K feldspar-quartz join with solid solution towards hypersthene (see also Berg and Wheeler, 1976). Following the discovery of osumilite in the Nain and Enderby Land granulites, Hensen (1977) reported an earlier synthesis of the assemblage osumilite-cordierite-hypersthene (± feldspar, quartz, glass) at 3.6-7.2 kb, 1000-1100°C,

similar to the assemblages reported by Berg and Wheeler (1976). However Hensen's (1978) predicted chemographic relations involving osumilite in the system KFMAS cannot explain the mineral assemblages and reactions in the Antarctic granulites. The minerals garnet, cordierite, sapphirine, hypersthene, spinel, sillimanite, quartz and K-feldspar are all in association with osumilite in different assemblages, but primary assemblages are commonly masked by subsequent mineral reactions. Evidence for the following reactions has been found -

$$Os \rightarrow Cd + Hy + Kf + Qtz \qquad (17)$$

$$Gt + Os \rightarrow Cd + Hy + Kf + Qtz \qquad (18)$$

$$Sa + Os + Qtz \rightarrow Cd + Gt + Kf \qquad (19)$$

$$Sill + Os \rightarrow Cd + Kf + Q \qquad (20)$$
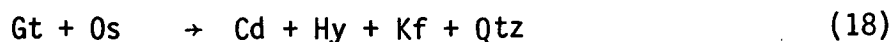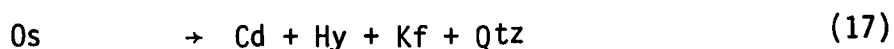
The relative X_{Mg} values of these minerals decreases in the order Os > Cd > Sa > Hy > Sp > Gt. Reaction (17) has previously been described by Berg and Wheeler (1976). Osumilite and K-feldspar have not been found to coexist in the highest temperature assemblages, due to inappropriate bulk rock compositions (Figure 4.12). The additional presence of appreciable Na_2O would of course stabilize coexisting feldspar and osumilite.

Reaction (18) is also consistent with the observed mineral compatabilities in the lower pressure Nain granulites in which the stability of coexisting cordierite-hypersthene-K feldspar prohibits the coexistence of garnet and osumilite. Thus at lower pressures ($\approx$ 5 kb) osumilite is restricted to rocks more Mg-rich than defined by the compositions of coexisting cordierite-hypersthene, whereas at higher pressure-temperature the range in compositions is extended due to the stability of coexisting garnet-osumilite.
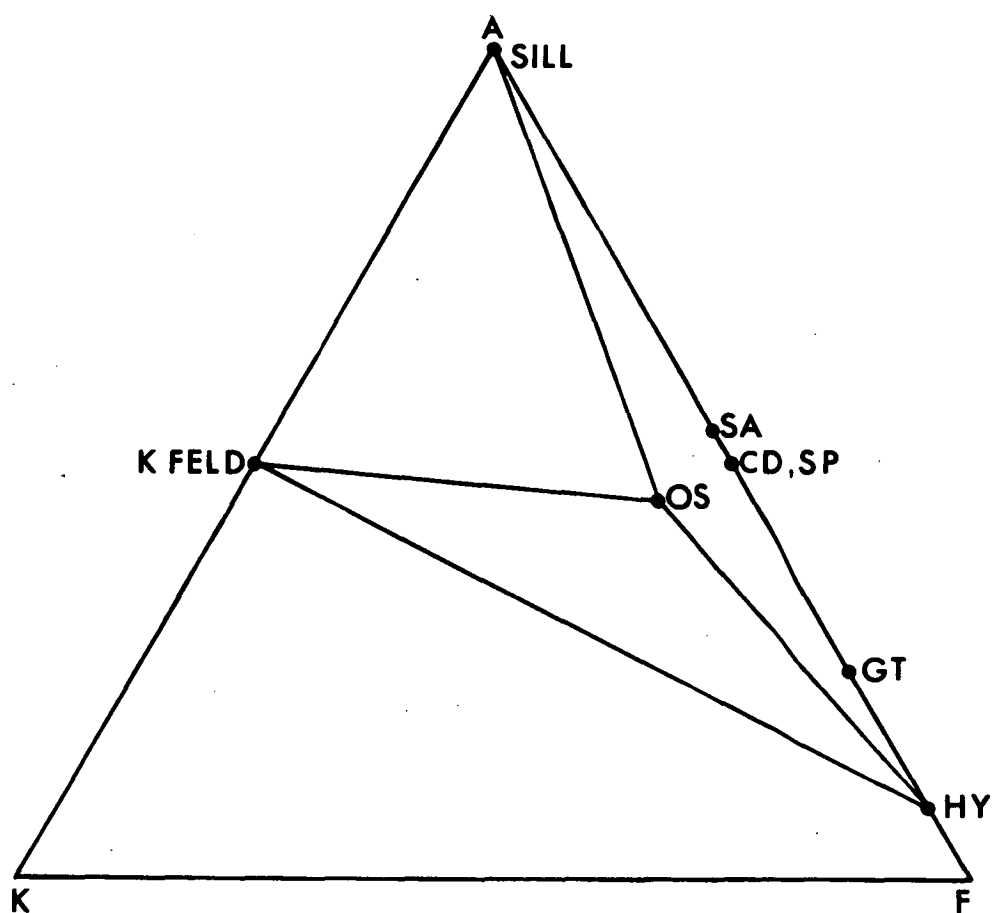
Fig. 4.12   AKF diagram which shows that rock compositions to
            the right of the stable tie line Os-Opx do not
            contain both osumilite and Kfeldspar with other
            ferromagnesium silicates, by virtue of the Os-Hy
            tie line being stable.

Spinel only coexists with osumilite as inclusions within the latter mineral. This may well be due to a prograde reaction in which spinel-K feldspar-quartz is unstable relative to osumilite. In several instances the textural evidence is ambiguous as to the reactions which have occurred. In particular the liberation of free quartz due to reaction (17) can result in the overstepping of higher temperature reactions to lower temperatures (e.g. reaction 14) because a mineral stable in a quartz-free assemblage is unstable in the presence of quartz. The presence of reaction rims of cordierite around spinel inclusions in the osumilite intergrowth may be due to this effect.

On the basis of the above reactions, mineral compatabilities and knowledge of the relative X_{Mg} values of the coexisting phases, it is useful to discuss in general terms the possible P-T stability fields and chemographic relations involving osumilite in model pelite systems. In particular, the previous discussion of mineral reactions in terms of the two systems FMAS and KFMAS can be combined to produce a generalized P-T diagram.

The maximum stability limit of pure Mg osumilite in the system KMAS is probably defined by melting reactions at high temperatures. The low temperature (900-1000°C) stability limit is inferred to be defined from low to high pressure by three terminal univariant reactions -

$$Os \rightarrow Cd-En-Kf-Qtz \tag{21}$$

$$Os \rightarrow Sa-En-Kf-Qtz \tag{22}$$

$$Os \rightarrow Sill-En-Kf-Qtz \tag{23}$$

Invariant point [Sa] (Figure 4.13 is inferred to be metastable because of the previous experimental work determining the stability of invariant point [Kf,Os]. Further experimental work needs to be undertaken. It can be seen from the chemographic relations for the KMAS system that many assemblages containing osumilite and other ferromagnesian silicates
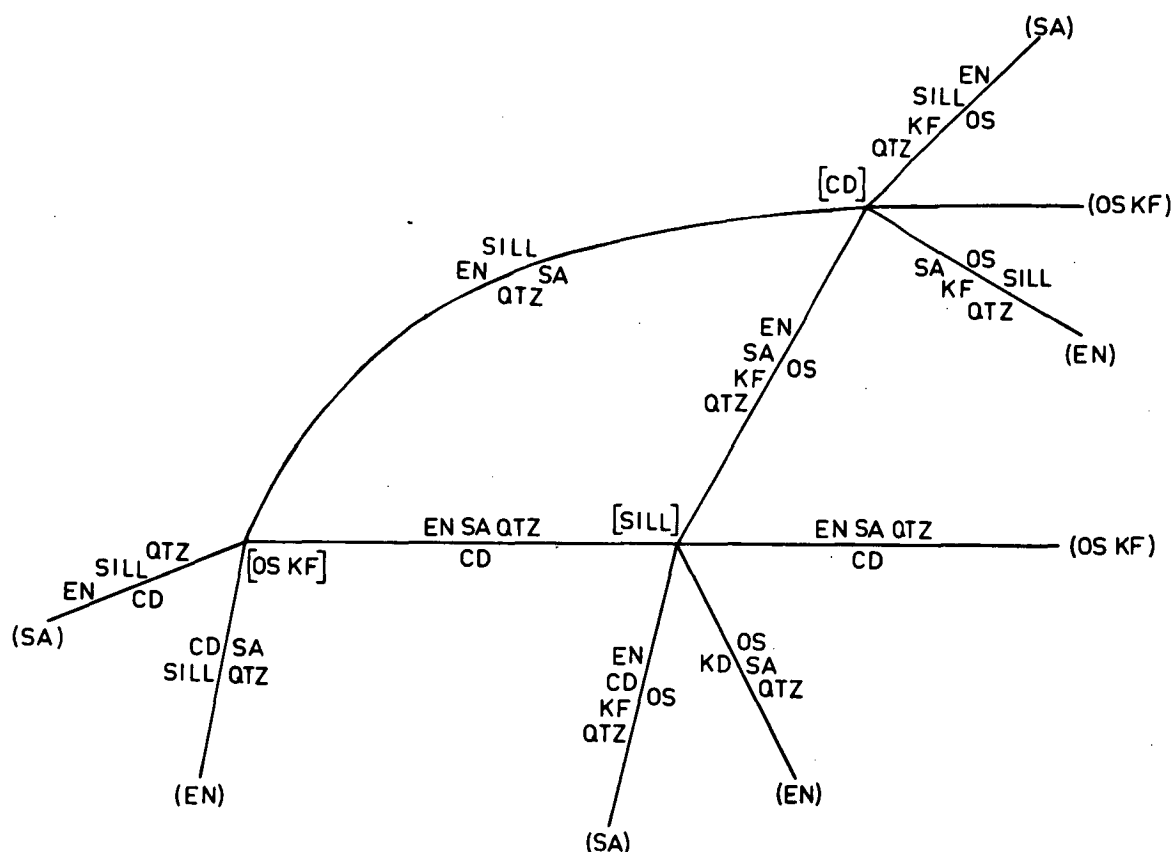
Fig. 4.13 Schreinemakers analysis of inferred quartz-excess stable
          univariant equilibria and invariant points involving pure-
          Mg osumilite in the system KMAS. Invariant points are
          labelled by the absent phase(s) in square brackets. The
          univariant reactions are labelled by the additional absent
          phase (curved brackets). At the invariant point (Os, Kf)
          potassium feldspar is the only potassic phase present.
          The locations of the metastable invariant points (Sa) and
          (En) can be located at the intersections of the metastable
          extensions of the relevant univariant lines. Curvature
          is likely to be present for many of these univariant lines,
          as has been experimentally demonstrated for the reaction
          (Os,Kf).

will not coexist with K-feldspar (Figure 4.12). Pyrope cannot be involved in these reactions due to the instability of pyrope-quartz relative to enstatite-sillimanite below 15 kb pressure (Hensen and Essene, 1971).

The univariant reaction

$$Os + Sill \rightarrow Cd + Kf + Qtz \tag{24}$$

is inferred to be metastable in the KMAS system. This reaction is observed in the Enderby Land granulites, and it is believed that the metastable Fe-free univariant reaction becomes a stable (divariant) assemblage with the addition of another component (FeO) in the system KFMAS.

Under anhydrous conditions the P-T location of invariant point [Kf,Os] would be at 8 kbar using the experimental data of Newton (1972). In the presence of a fluid phase ($p_{H_2O} \ll p_{Total}$) it would probably shift to higher pressures and temperatures (11 kbar, $1000^{\circ}C$) by comparison with the data of Newton (1972), Hensen and Green (1973). Many of these reactions would be metastable relative to a melt under moderate water pressures, as the assemblage Cd-Kf-Qtz melts at temperatures less than $\approx 750^{\circ}C$ at moderate water pressure - p_{H_2O} = 5-10 kbar (Seifert, 1976). Under anhydrous conditions coexisting sanidine-quartz does not melt till temperatures are in excess of $\approx 1150^{\circ}C$, P ≈ 10 kb (Luth, 1967).

It is not possible to predict with confidence the P-T slopes of these univariant boundaries. Reaction (17) has a very small ΔV with considerable uncertainty (Hensen, 1978). Solid solutions in enstatite and sapphirine ($R^{2+}Si \gtrless 2Al$) would cause marked curvature in some of the reaction boundaries.

A schematic P-T diagram showing the possible stability of osumilite in the KFMAS system, and which is consistent with the observed assemblages in the Enderby Land granulites and the Nain granulites (Berg and Wheeler,

1976) is shown in Figure 4.14. The osumilite absent invariant points [Sp, Kf, Os], [Hy, Kf,Os], [Sill, Kf, Os] are from Hensen and Green (1973), Hensen (1977a) and are slightly modified because of the fact that A/F+M of natural sapphirine is greater than 0.5 (Figure 4.11). The most important reaction limiting the stability field of osumilite for most common metapelites in the KFMAS system is -

$$Os + Gt \rightarrow Cd + Hy + Kf + Qtz \qquad (25)$$
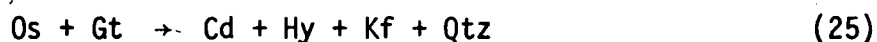
Note that the reaction -

$$Os + Sill + Sa \rightarrow Cd + Kf + Qtz \qquad (26)$$
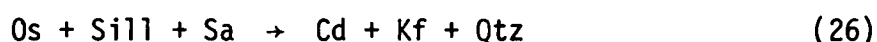
extends to the metastable invariant point [En] in the pure Mg system. In the absence of melting or biotite, coexisting osumilite-hypersthene is believed to be always stable within the stability field of osumilite. Under hydrous conditions the lower temperature stability of osumilite is most likely defined by reactions involving the dehydration of biotite (see Maijer et al., 1977).

3. The Development of Secondary Biotite

The assemblage Gt-Bi-Sill (-Qtz-Kf) is sporadically developed in these granulites due to introduction of a minor amount of water during cooling. Biotite is not present as a primary phase in the original mineral assemblages at Spot Height 945. The Cd-Hy-Kf-Qtz intergrowths formed by the breakdown of osumilite are in rare instances replaced by fine grained biotite-quartz intergrowths due to the reaction -

$$Cd + Hy + Kf + H_2O \rightarrow Bi + Qtz \qquad (27)$$
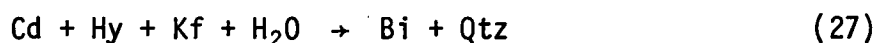
The assemblage Gt-Bi-Sill (-Qtz-Kf) has developed through the reaction -

$$Gt + Cd + Kf + H_2O \rightarrow Bi + Sill + Qtz \qquad (28)$$
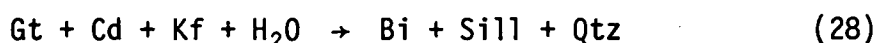
In some less aluminous rocks, Gt-Bi-Qtz has developed due to the reaction -

$$Hy + Kf + H_2O \rightarrow Gt + Bi + Qtz \qquad (29)$$

Fig. 4.14 Schreinemakers analysis of the inferred quartz-excess
stable univariant lines and invariant points involving
osumilite in the KFMAS system (labelled with capital letters).
Reactions marked with small letters define the terminal
univariant reactions for pure-Mg osumilite and cordierite
in the KMAS system (Figure 4.13). The dashed extension to
the univariant reaction Os+Sa+Sill+Qtz ⇌ Cd+Kf terminates
in the iron-free KMAS system at the metastable invariant
point (En) in Figure 4.13. The inferred stable invariant
points involving osumilite are based on the petrographic
data for Enderby Land. In a 5-component system involving
9-phases in which there is a degeneracy (Os-Kf) there are
15 possible quartz-excess invariant points. It is not
possible to tell how many of these could actually be stable.
The three Os-Kf absent invariant points are from
Figure 4.11A.

The univariant reaction (28) for the system KFMAS is metastable relative to melt under moderate water pressures (Holdaway and Lee, 1977). Under conditions of low p_{H_2O} this reaction shifts to lower temperatures, but is limited on its low temperature side by the reaction -

$$Kf + Sill + H_2O \rightarrow Musc + Qtz \qquad (30)$$
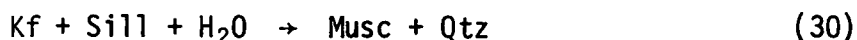
(Chatterjee and Johannes, 1974).

4. Mafic Rocks

The mafic rocks show little evidence of mineral reactions. The only textural adjustment has been the development of thin pyroxene exsolution lamellae. Garnet coronas separating plagioclase from hypersthene and opaque oxide are not present, although they are found elsewhere in Enderby Land (see Chapter 2; Sheraton et al., in prep.).

VIII. PRESSURES AND TEMPERATURES OF METAMORPHISM

The P-T conditions of metamorphism of granulite mineral assemblages can be estimated by comparison with experimentally determined stability fields of different mineral assemblages and appropriate mineral reaction boundaries and also by using experimentally calibrated cation exchange equilibria.

The upper P-T stability limit of coexisting garnet and cordierite is defined by reactions in which the assemblages sapphirine-quartz and hypersthene-sillimanite-quartz are produced. The experimental data of Hensen and Green (1971, 1972, 1973) implies metamorphism at 9-10 kb pressure, 1000-1050°C, but in the presence of additional components the reaction boundaries will shift to lower temperatures and pressures. In particular, published experimental data suggests that the upper pressure stability limit of Mg-cordierite is at lower pressures under anhydrous,

compared to hydrous conditions (≈ 8 and 11 kbar, respectively -
Newton, 1972; Newton et al., 1974; Hensen and Green, 1971, 1972, 1973;
Schreyer and Yoder, 1966, 1964).

1. Temperature Estimates

The extreme rarity in nature of the cordierite breakdown products
sapphirine-quartz and hypersthene-sillimanite-quartz may imply that the
Enderby Land granulites equilibrated under higher P-T and lower P_{H_2O}
conditions than inferred for most crustal granulites. If the Antarctic
granulites were to have formed under ordinary conditions of granulite
metamorphism ($700-800^\circ C$) then the scarcity of such assemblages elsewhere
in the world needs to be explained (see Hensen, 1977b).

The compositions of coexisting phases in the Enderby Land granulites
are more Mg-rich and the orthopyroxenes more aluminous than those of
other granulites. In the Enderby Land granulites, sapphirine-quartz and
hypersthene-sillimanite-quartz (-sapphirine) occur over a large area in
contrast to the rare occurrence of such assemblages elsewhere within
otherwise typical medium-high pressure granulite terrains (Morse and
Talley, 1971; Bondarenko, 1972; Hermans et al., 1976). In the latter
occurrences the presence of high Fe_2O_3 contents stabilizes these
assemblages (Sa-Qtz, Hy-Sill-Qtz) to much lower pressures and temperatures
than those deduced from the experimental data (see introduction). Although
Fe_2O_3 is not a significant component in the silicates from Spot Height 945,
the presence of Cr_2O_3 in the sapphirine and spinel would have a similar
effect to Fe_2O_3 in hypersthene on contracting the P-T stability field
of coexisting cordierite-garnet relative to spinel-quartz and sapphirine-
quartz compared to the experimental data of Hensen and Green (1973).
Hence the Enderby Land granulites probably developed these unusual
mineral assemblages at slightly lower temperatures than indicated by the
experimental data of Hensen and Green (1971, 1972, 1973).

Lower limits to the maximum temperature of metamorphism can be deduced from the absence of muscovite and primary biotite in the pelitic rocks and garnet in the basic rocks as defined by the reactions shown in Figure 4.15.

The compositions of coexisting minerals can be used to estimate P-T conditions of metamorphism where appropriate exchange reactions have been experimentally studied. The mutual solubility of enstatite and diopside in coexisting orthopyroxene and clinopyroxene is temperature dependent. At less than 15 kb the effect of pressure on the pyroxene miscibility gap is minimal for both the iron-free (Boyd and Schairer, 1964; Davis and Boyd, 1966; Mori and Green, 1975) and iron-bearing systems (Lindsley et al., 1974a, b; Simmons et al., 1974). Wood and Banno (1974) and Wood (1975) devised such a geothermometer which over-estimates temperatures of crustal granulites by about 50°C when compared to the 15 kb experimental data of Lindsley et al. (1974a, b) and compared to other geothermometers (Hewins, 1975; Chapter 2, this thesis). Temperatures of 880-920°C are obtained for the Antarctic mafic granulite pyroxenes with the greatest miscibility gap (cores, area analyses of Cpx and Opx exsolution lamellae) after correcting for this overestimate. Exsolution lamellae in the pyroxenes indicate temperatures of 750-820°C, though the accuracy of using the pyroxene miscibility gap decreases at low temperatures.

The pyroxene Fe^{2+}-Mg K_D ($Fe/Mg^{opx}/Fe/Mg^{cpx}$) can also be used as a geothermometer, but the small temperature dependence of K_D results in considerable uncertainty. The K_D increases with decreasing temperature for Mg-rich pyroxenes (Mori and Green, 1978) and decreases with increasing Fe content (Davidson, 1968) for orthopyroxenes less Mg-rich than Mg_{60}. The highest temperature Antarctic pyroxenes have K_D as low as 1.2 whereas the exsolution lamellae have K_D up to 2.05. The 15 kb, 820°C
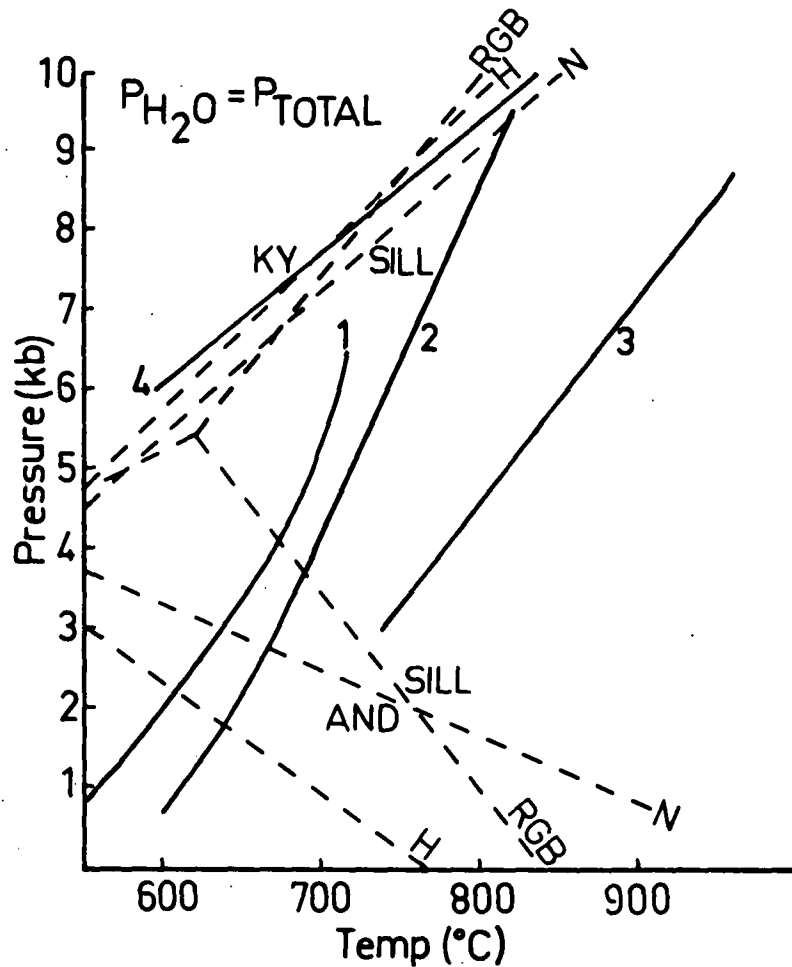
Fig. 4.15 P-T diagram showing mineral reactions which place lower temperature limits of the conditions of metamorphism of the Antarctic granulites. Ky-And-Sill boundaries are from Newton (1966), Richardson et al. (1969) and Holdaway (1971). Reaction 1. Musc + Qtz = Als + Kf + H_2O. 2. Musc = Kf + Corundum + H_2O (Chatterjee and Johannes, 1974). 3. Bi + Sill + Qtz = Cd + Gt + Kf + H_2O (Holdaway and Lee, 1977). 4. Extrapolated boundary for the appearance of garnet in a quartz-tholeiite (Green and Ringwood, 1967). Boundary most probably has slight curvature.

data of Lindsley et al. (1974)   has K_D = 1.3-1.5. Thus the lower K_D and more subcalcic nature of the Antarctic clinopyroxenes implies that the peak of metamorphism was in excess of 820^oC.

The compositions of coexisting plagioclase and alkali feldspar in the perthites indicate exsolution temperatures of $780-800^oC$ at 10 kb pressure using the data of Powell and Powell (1977). Thus the peak of metamorphism must have been greater than 800^oC.

The garnet-cordierite Fe-Mg exchange reaction -

$$\tfrac{1}{3} Mg_3Al_2Si_3O_{12} + \tfrac{1}{2} Fe_2Al_4Si_5O_{18} \rightarrow \tfrac{1}{3} Fe_3Al_2Si_3O_{12} + \tfrac{1}{2} Mg_2Al_4Si_5O_{18} \qquad (31)$$
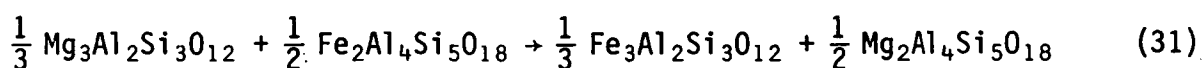
has received increasing attention in recent years (Hensen and Green, 1971, 1972, 1973; Currie, 1971; Thompson, 1976; Holdaway and Lee, 1977; Hensen, 1977). It can in theory provide an excellent geothermometer and geo-barometer for pelitic rocks, with K_D $(Fe/Mg^{Gt}/Fe/Mg^{Cd})$ decreasing with increasing temperature. The Antarctic garnet-cordierite pairs have K_D=9-12.6 (Table 4.11), which implies unrealistically low temperatures of metamorphism $(520-600^oC)$, well within the kyanite stability field using the data of Hensen and Green (1973) and Thompson (1976). Garnet and cordierite porphyroblasts from one sample have compositional profiles in which there is Mg-Fe zoning in opposite senses, with gradual changes in composition from cores to rims (Gt $Mg_{50-44.1}$, Cd $Mg_{86.7-90.9}$ from core to rim respectively). The cores could have equilibrated at 700^oC using the above data.

Garnet that coexists with secondary phlogopite $(Mg_{85.5-91.4})$ extends to more Fe-rich compositions $(Mg_{56-39.8})$ than in the above assemblages. The garnet rims are often more Fe-rich than cores, but unzoned grains are common, with K_D $(Fe/Mg^{Gt}/Fe/Mg^{Bi})$ ranging from 5.03-10.11. The K_D data of Thompson (1976) and Ferry and Spear (1978) implies

Table 4.11

Representative compositions and Fe-Mg K_D data

for garnet-bearing assemblages

Gt-Cd-Hy-Qtz assemblage				K_DGt-Cd	K_DGt-Hy	K_DGt-Bi
	X_{Mg}^{Gt}	X_{Mg}^{Cd}	X_{Mg}^{Hy}			
1.	52.9	92.8	78.2	11.47	3.19	
2.	53.6	92.4	79.5	10.52	3.35	
3.	48.2	90.7	76.3	10.48	3.45	
4.	48.1	90.9	75.6	10.78	3.34	
Gt-Cd-Sill-Qtz assemblage						
5.	54.3	91.7		9.30		
6.	55.9	91.4		8.38		
7.	56.6	92.3		9.19		
Gt-Cd assemblage						
8.	51.4	91.4		10.05		
9.	56.7	92.1	- core	8.90		
	56.3	92.1	- rim	9.05		
10.	50.0	86.7	- core	8.67		
	44.1	90.9	- rim	12.66		
Gt-Hy assemblage						
11.	49.9	75.1			3.03	
12.	55.6	74.9			2.38	
13.	54.5	75.6			2.59	
14.	55.2	77.0			2.72	
15.	50.7	73.8			2.74	
Gt-Bi assemblage						
16.	47.0	87.2	- core			7.68
17.	40.2	87.2	- rim			10.13
18.	39.8	86.5				9.69
19.	53.7	91.5				9.28
20.	49.5	89.7				8.88

temperatures of 380-600°C and 400-600°C respectively. Such temperatures are also well within the kyanite stability field, but sillimanite is common and kyanite never found in these rocks.

2. Pressure Estimates

Although the K_D values for all of the Gt-Cd assemblages give similar temperatures of metamorphism, pressure estimates based on the cordierite composition differ considerably for the two assemblages Cd-Gt-Sill-Qtz and Cd-Gt-Hy-Qtz using the data of Hensen and Green (1973). The virtual absence of compositional zoning and extremely limited range in composition of cordierites from the latter assemblage indicate pressures of 8.5 kb at 500-600°C using the data of Hensen and Green (1973), but this would imply increasing K_D and thus re-equilibration of garnet to more Fe-rich compositions with decreasing temperature. The lack of cordierite zoning and high K_D values are consistent with isobaric cooling. The cordierites from the former assemblage are of the same composition as those in the latter, but the data of Hensen and Green (1973) imply final equilibration of the Gt-Cd-Sill-Qtz assemblage at 11.5 kb pressure. In contrast, the plot of Thompson (1976) indicates pressures of 8 kb for this assemblage, but reversed experimental data of Hensen (1977) is inconsistent with this. Even if the pressure calibration of the experiments of Hensen and Green (1973) is incorrect, the experimental data for the two assemblages would still be internally consistent, and would require different pressures for the different Antarctic Gt-Cd assemblages from the one locality.

Two other methods can be used to estimate the pressures of metamorphism. The solubility of Al_2O_3 in orthopyroxene coexisting with garnet is a function of temperature and pressure, due to the reaction -

$$R_2^{2+}Si_2O_6 + R^{2+}Al_2SiO_6 \; \rightleftharpoons \; R_3^{2+}Al_2Si_3O_{12} \qquad (32)$$
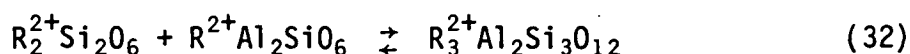
Application of the method of Wood (1974) gives entirely erroneous results, with negative pressures for some samples. Current interpretations of the effect of pressure upon this reaction depend critically upon the evaluation of the excess molar volume for the $R^{2+}Si \rightleftharpoons 2Al$ substitution in orthopyroxene, for which it has been assumed that R^{2+} = Mg in orthopyroxene. However it has been shown that the Al_2O_3 variations in the Antarctic orthopyroxenes can equally well be explained in terms of the presence of a $FeAl_2SiO_6$ substitution also, and not solely in terms of the arbitrary $MgAl_2SiO_6$ component. It is interesting to note that the 3 kb, 800°C experimental data of Holdaway (1976) shows a clear increase in Al_2O_3 with increase in FeO for orthopyroxenes coexisting with Cd-Qtz. If this data is accurate, then it is consistent with an $FeAl_2SiO_6$ rather than an $MgAl_2SiO_6$ substitution, as it is impossible for an <u>end member</u> component ($MgAl_2SiO_6$) to increase in concentration as the orthopyroxenes become more Fe-rich.

The solubility of Al_2O_3 in clinopyroxene coexisting with plagioclase and quartz in the mafic rocks provides an excellent geobarometer (Wood, 1976), because of the large ΔV of the exchange reaction -

$$CaAl_2SiO_6 \quad + \quad SiO_2 \quad \rightleftharpoons \quad CaAl_2Si_2O_8 \tag{33}$$

Ca Tschermaks   Quartz   Anorthite
Molecule
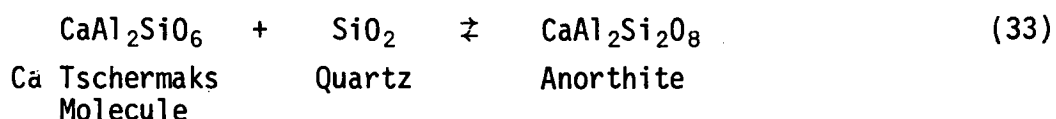
This reaction is discussed in Appendix 1, and indicates pressures of equilibration of the Enderby Land mafic granulites in the range 8-10 kb, consistent with pressure estimates deduced from cordierite compositions.

IX. <u>DISCUSSION</u>

It can be concluded from the previous section that the granulites from Spot Height 945 in Enderby Land were metamorphosed at 8-10 kb pressure under conditions of very low P_{H_2O}. Although the various geothermometers do not give coincident temperature estimates, the co-existing pyroxenes suggest equilibration at ≈ 900-920°C. It is not known whether the highest temperature assemblages (Sa-Q, Hy-Sill-Qtz) developed at this or slightly higher temperatures. The sequence of mineral reactions and very minor amount of zoning in the cordierite is consistent with cooling under isobaric conditions, during which the higher temperature assemblages Sp-Qtz, Sa-Qtz, Hy-Sa-Sill-Qtz and the osumilite-bearing assemblages became unstable relative to the assemblages Cd-Gt-Sill-Qtz, Cd-Gt-Hy-Qtz and Cd-Hy-Kf-Qtz.

There are numerous descriptions of amphibolite-granulite terrains for which coincident temperatures and pressures of metamorphism are obtained using geothermometers and geobarometers for different coexisting mineral assemblages (e.g. Berg, 1976). Also, Thompson (1976) has studied the variation in Gt-Cd and Gt-Bi Fe-Mg K_D data from various metamorphic rocks and found that the variation in K_D with temperature, when constrained by the P-T limitations defined by the various mineral assemblages was consistent with the experimental higher temperature Gt-Cd K_D data of Hensen and Green (1973).

The general applicability of such K_D data implies that for the Antarctic granulites, Gt-Cd Fe-Mg intercrystalline exchange has maintained chemical equilibrium throughout entire grains down to 500-600°C, in marked contrast to observations elsewhere (Thompson, 1976). Cordierite and garnet from the assemblages Cd-Gt-Sill-Qtz and Cd-Gt-Hy-Qtz show only limited ranges in composition (Mg_{88-92} and Mg_{48-56} respectively). The very small range in cordierite compositions in the assemblage Gt-Cd-Hy-Qtz

is consistent with isobaric cooling (Hensen and Green, 1973), but an increase in K_D with decreasing temperature would cause the garnet to become more Fe-rich. At an original temperature of $900^{o}C$, the garnet in equilibrium with cordierite Mg_{90} would have been $\approx Mg_{70}$ (K_D data of Hensen and Green, 1973; Thompson, 1976). None of the garnets in any of the rocks are more Mg-rich than Mg_{57}. On this basis homogeneous reequilibration would have continued with decreasing temperature until garnets of Mg_{57} ($T \approx 700^{o}C$) formed. The small amount of zoning in some garnets more Fe-rich than this would imply that it was only below this temperature that the sluggishness of reaction prohibited inter-crystalline diffusion from maintaining complete homogeneity in the garnets.

The homogeneity of many of the garnets and the absence of narrow rims abruptly different in composition from cores is in marked contrast to the retrogressive cation exchange profiles found in many other amphibolites and granulites (see Thompson, 1976; Berg, 1977; Hollister, 1977). At moderate grades of metamorphism garnet is typically zoned and appears to be a very unreactive mineral, whereas at higher grades of metamorphism (upper amphibolite facies or above), it loses these characteristics and homogeneous equilibrium is approached (Grant and Weiblen, 1971; Hollister, 1977).

In view of the wide range in temperatures of metamorphism obtained using different mineral equilibria, acceptance of the above interpretation implies that the cut off temperatures at which intercrystalline diffusion can no longer maintain chemical equilibrium differ considerably for the different mineral systems. Many cases can be cited from the literature where broadly coincident temperatures are obtained. It is often assumed though not conclusively shown that exchange reactions in different mineral systems record similar cut off temperatures below which intercrystalline diffusion becomes too sluggish to record further P-T variations.

The observations that many amphibolites-granulites do show coincident temperatures could reflect the fact that their prograde metamorphic paths did not exceed by much the cut-off temperatures of different mineral systems. In contrast, the Antarctic granulites reached a peak of metamorphism at over $900^\circ C$. The subsequent cooling path was such that a sufficiently large interval existed over which the reequilibration could cease due to different closure temperatures in the various mineral systems. Acceptance of this interpretation, in particular the equilibration of Gt-Cd pairs down to temperatures as low as $500^\circ C$, would require caution in the use of such geothermometers in estimating the P-T conditions of formation of an observed mineral assemblage.

Such an interpretation is not without some unanswered problems. Although the Cd-Gt K_D data from both of the assemblages Cd-Gt-Sill-Qtz and Cd-Gt-Hy-Qtz indicate reequilibration down to $500-600^\circ C$, the relative compositions of the phases in the different assemblages are entirely inconsistent with this interpretation. In the latter assemblage, coexisting Cd Mg_{90} and Gt Mg_{50} indicates reequilibration to low temperatures at constant pressure (8-9 kb) using the data of Hensen and Green (1973, Fig. 3). In contrast, reequilibration of the former assemblage under the same conditions should have resulted in much more Fe-rich phases (Cd $\approx Mg_{60}$, Gt $\approx Mg_{16}$) than are actually observed (Cd Mg_{90}, Gt Mg_{50}) (Hensen and Green, 1973, Fig. 2). The data of Thompson (1976) is in agreement with the general trends of Fe-enrichment with decreasing temperature for sillimanite-bearing assemblages shown by Hensen and Green (1973), but at lower pressures. In view of the careful experimental reversals of Hensen (1977) and the same experimental method used in all experiments by Hensen and Green (1973), the observed experimental relative shift in compositions with decreasing temperature is internally consistent.

The relative movement of the three phase triangles towards more Fe-rich compositions on an AFM diagram with decreasing temperature is illustrated in Figure 4.16. The two phase field Cd-Gt expands with decreasing temperature so that the compositions of the garnet and cordierite in the three phase triangles differ considerably. A broad two phase field of Cd-Gt is well illustrated by the granulites described by Berg (1977). In theory the width of a two phase field separating coexisting three phase fields should progressively shrink with increasing temperature because of continuous reactions and become a single tie line at the temperature of a discontinuous reaction (see e.g. Hensen, 1971, Fig. 7; Thompson, 1976). An excellent example of this feature is given by Blumel and Schreyer (1977) for which the two phase field Bi-Sill separating the three phase triangles Bi-Sill-Gt and Bi-Sill-Cd progressively contracts towards the temperature at which the reaction Bi + Sill + Qtz → Cd + Gt + Kfeld + H_2O occurred.

The experimental data of Hensen and Green (1973) shows that at 8-9 kb, garnet and cordierite in both assemblages are only similar in composition at high temperatures (Figure 4.16). Thus the similarity in compositions of the garnet and cordierite from the different Antarctic assemblages is consistent with the observed compositions having developed at the original high temperatures ($\approx 900^{o}C$) at which Sa-Q, Hy-Sill-Qtz etc. reacted to form garnet and cordierite. This would also imply that the high K_D values also reflect high temperatures, which disagrees with the experimental data of Hensen and Green (1973), Hensen (1977) and Holdaway (1976), and the data of Thompson (1976). In most amphibolite-granulite terrains the above K_D data gives reasonable temperature estimates when compared with other geothermometers (see Berg, 1977; Thompson, 1976). It should be noted that the experimental data of Currie (1971) in which K_D increases with increasing temperature has
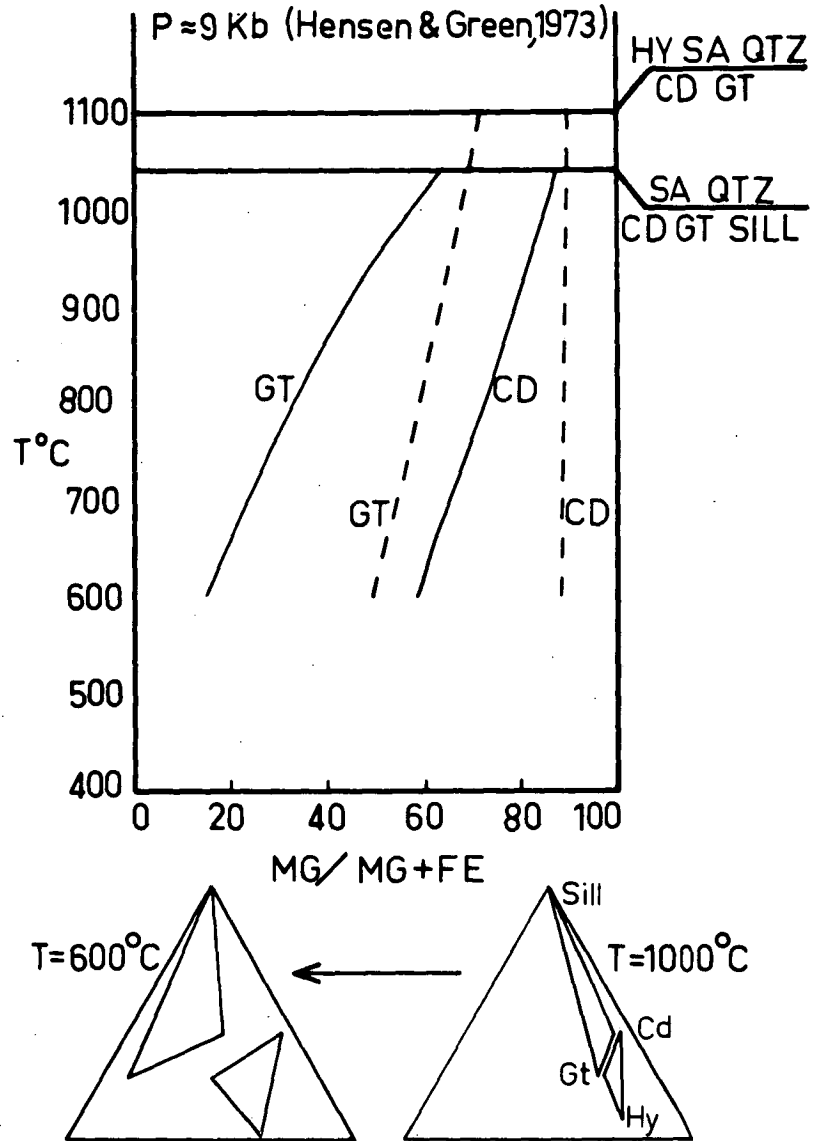
Fig. 4.16   Fe-Mg variations with temperature for coexisting garnet
and cordierite in the assemblages Gt-Cd-Sill-Qtz and
Gt-Cd-Hy-Qtz (from Hensen and Green, 1973, figs. 2,3).
Note the increasing width of the two phase field Gt-Cd
with decreasing temperature.

since been questioned experimentally (Holdaway, 1976; Hensen, 1977) and is inconsistent with the observed increase in K_D in retrogressed rims described from many localities, including Antarctica.

Equilibration down to 500-600°C is inconsistent with the presence of sillimanite and not kyanite in these rocks (Figure 4.15). Idiomorphic sillimanite has also developed due to the late stage introduction of water to form very rare traces of biotite (e.g. reaction 16). Similarly, at temperatures of 500°C, muscovite should have replaced coexisting Kfeld-Sill-Qtz. It is difficult to conceive how garnet could re-equilibrate in the pelitic rocks to such low temperatures, yet be entirely absent in reactions occurring in quartz-bearing mafic rocks at 700-800°C, 8-9 kb (see Figure 4.15). Elsewhere in Enderby Land, garnet in mafic rocks has equilibrated to different compositions in a variety of mineral systems at 600-800°C (Chapter 2).

Many of the above inconsistencies would be eliminated if it were assumed that the current interpretation of the temperature dependence of the Gt-Cd K_D was in error. The temperature dependence of Gt-Cd K_D, based on a study of natural mineral assemblages by Thompson (1976), was considered to be consistent with that determined experimentally by Hensen and Green (1973), even though there is considerable scatter in their experimental data (see Thompson, 1976, fig. 2). Reexamination of the 1000°C experimental data of Hensen and Green (1971, 1972) indicates that the K_D "scatter" shows an increase in K_D with increasing Mg-content of the cordierite (K_D 2.6 to 5.5). This was noted by Hensen and Green (1972) and in fact they state that K_D may also depend on composition and increase at high values of Mg/(Mg+Fe). Neglect of this effect results in temperature estimates ranging from 1200 to 770°C using the plot of Thompson (1976, fig. 2) for this 1000°C K_D data. On this basis it is perhaps not unreasonable to consider that the Antarctic samples with K_D of 9 could well correspond to a temperature of 900°C rather than 500-600°C.

It is not possible to decide on the actual cause of this variation in K_D (P_{H_2O}, P_{CO_2}, Mg-Fe non-ideality, Al-Si order-disorder). Wood (1973) suggested that the conflicting experimental results obtained by Hensen and Green (1973) and Currie (1971) may be due to the effect of water on K_D, with K_D decreasing temperature under conditions of high P_{H_2O}. The experimental data of Currie (1971) has since been questioned (see Thompson, 1976; Holdaway, 1976; Hensen, 1977). Although the hydrothermal experimental data of Holdaway (1976) are consistent with that of Hensen and Green (1973), this does not constitute proof of the independence of K_D with variations in P_{H_2O}-P_{CO_2}. Hensen and Green (1973, p.157) state "It is concluded that even though conditions of $P_{H_2O} < P_{Total}$ prevailed in the experiments (Hensen and Green, 1971) enough water was present to stabilize the cordierites to conditions identical or very close to the maximum stability limit under "wet" conditions ($P_{H_2O} = P_{Total}$)". Newton (1972) has shown that the upper pressure stability limit of pure Mg-cordierite is lower under anhydrous than hydrous conditions. If by analogy this also extends to Fe-Mg systems then Gt-Cd K_D would be dependent upon P_{H_2O} as the Gt-Cd Fe-Mg exchange reaction would also be a dehydration reaction. It only requires a displacement to about 1 kb lower pressure of the Mg$_{90}$ Cd isopleth relative to the garnet isopleths to have the high K_D values of the Antarctic granulites indicating temperatures of 800-900°C rather than 500-600°C (Figure 4.16). As yet, no experimental study of Gt-Cd Fe-Mg equilibria under completely anhydrous conditions has been undertaken. The effect of P_{H_2O} upon K_D would decrease with increasing Fe-content of the cordierite. It is interesting to note that the data used by Thompson (1976) were for moderately Fe-rich cordierites, and the results of his study confirmed the "hydrothermal" experimental results of Hensen and Green (1973). Also the data of Hensen and Green gave consistent results with other geothermometers and

geobarometers when used by Berg (1976) for the Nain granulites
(Cd Mg_{44-75}). In contrast, there are several other occurrences of
granulites with Mg-rich cordierites and garnets which, like the
Antarctic example indicate unrealistically low temperatures of meta-
morphism using Hensen and Green's (1973) or Thompson's (1976) K_D data
(Gable and Sims, 1969; Marakushev and Kudryavtsev, 1965; Hollister,
1977).

X. CONCLUSIONS

The work presented in this chapter has shown that osumilite is
an important mineral in granulite facies pelitic rocks. It coexists with
a number of different minerals and theoretical considerations indicate
that it can exist together with cordierite as well as beyond the P-T
stability field of cordierite. The maximum P-T conditions of metamorphism
cannot be obtained by direct comparison with the experimental data of
Hensen and Green (1973) for the stability of sapphirine-quartz, spinel-
quartz, hypersthene-sillimanite because of the presence of a small
amount of Cr_2O_3 in these rocks.

Cordierite has developed by reaction of these high temperature
assemblages at lower temperature conditions. The temperature of these
reactions can in theory be derived from the compositions of coexisting
garnet and cordierite. The calculated temperatures using the Gt-Cd
K_D suggest equilibration at very low temperatures (500-600°C) within the
kyanite stability field, yet sillimanite is the stable Al_2SiO_5.

Compositions of coexisting pyroxenes in the mafic granulites have
been equilibrated at 900-920°C. Arguments have been presented which
suggest that the Gt-Cd assemblages may also have formed at these high
temperatures. The assemblages sapphirine-quartz, spinel-quartz and
hypersthene-sillimanite must have initially formed at slightly higher

temperatures than the temperatures of development of the secondary cordierite (T $\geqslant$ 900-920°C).

These mineral assemblages have revealed inadequacies in the current understanding of Gt-Cd Fe-Mg exchange equilibria as a geothermometer. The possibility that this exchange reaction may be dependent upon P_{H_2O} as well as temperature is discussed, and this topic will be further considered in the next chapter.

Chapter 5

GARNET-CORDIERITE Fe-Mg EXCHANGE EQUILIBRIA -

THEORETICAL AND EXPERIMENTAL OBSERVATIONS.

Contents   page

I. INTRODUCTION

This chapter will consider the possible reasons for the inconsistencies in P-T estimates of the Enderby Land granulites based on published experimental and theoretical studies of garnet-cordierite Fe-Mg equilibria. Two points deserve attention -

1. Available garnet-cordierite Fe-Mg geothermometers imply unrealistically low temperatures of equilibration of the granulites described in the last chapter, but apparently provide reasonable temperature estimates for other granulites.

2. Estimated pressures of equilibration of the Enderby Land granulites based on Plag-Cpx-Qtz equilibria (last chapter) are consistent with those deduced from the cordierite isopleth diagrams of Hensen and Green (1973, Figs. 2,3). Pressure estimates based on the cordierite data of Newton, 1972; Thompson, 1976 and Holdaway and Lee, 1977 are several kilobars lower.

The temperature dependence to the garnet-cordierite K_D calculated by Thompson (1976) is shown in Figure 5.1. Also shown is the 1000°C experimental data of Hensen and Green (1971, 72, 73). The scatter in this data, particularly at 1000°C (Figure 5.2, Table 5.1) is due to a systematic increase in K_D with increase in pressure (and X_{Mg}^{Cd}) which was previously noted by Hensen and Green (1973). This variation cannot be accounted for by the predicted effect of pressure on K_D alone, assuming ideal solid solutions and no effect of water on K_D (Figure 5.2). If these experimentally determined values of K_D at 1000°C are correct, then the $\ln K_D \propto \frac{1}{T}$ plot of Thompson (1976) overestimates and underestimates the equilibration temperatures for the lowest and highest 1000°C K_D values of Hensen and Green (implied temperatures of 1200 and 770°C
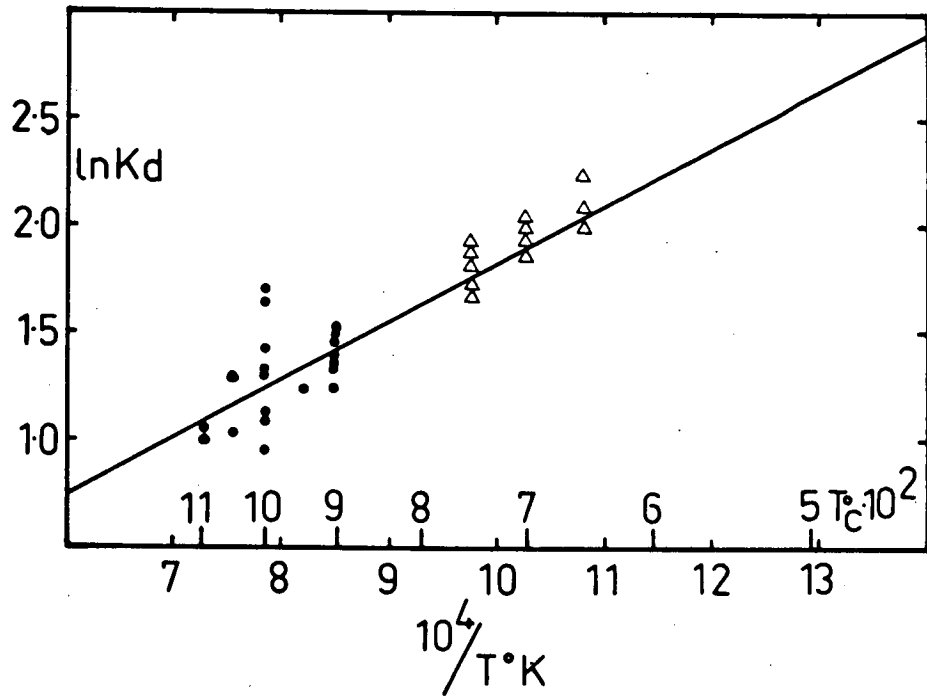
Fig. 5.1 Plot of ln K_D against $1/T_K$ for the (Fe-Mg) garnet-
cordierite exchange reaction. Diagram is from
Thompson (1976, fig. 1A). Open triangles are K_D
values from natural assemblages, solid circles are
the experimental results of Hensen and Green (1971,
1972).
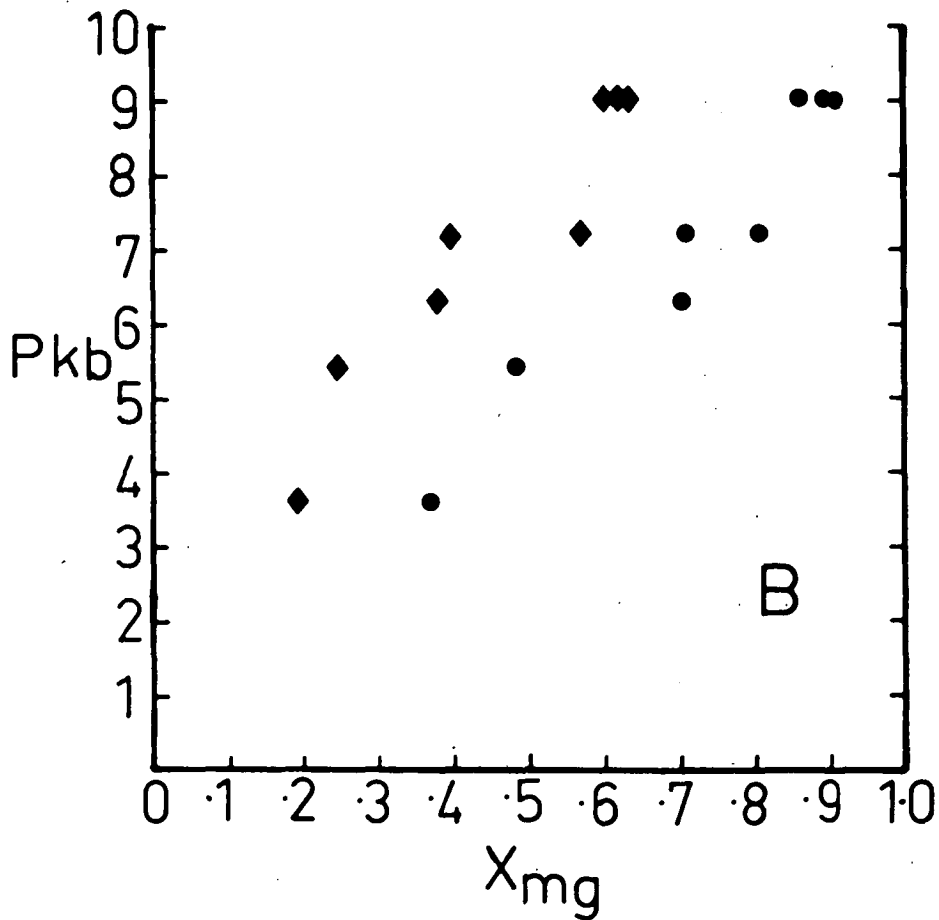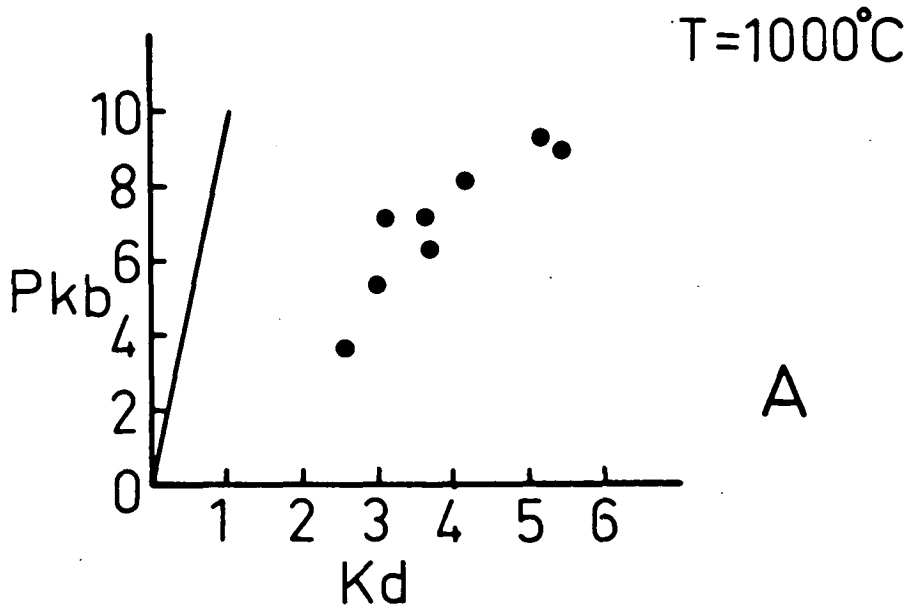
Fig. 5.2A Variation in the Gt-Cd Fe-Mg K_D with pressure at 1000^0C – experimental data of Hensen and Green (1971, 1972)(see Table 5.1). The straight line shows the predicted increase in K_D with pressure based on anhydrous molar volume data.

Fig. 5.2B Mg/Mg + Fe (= X_{Mg}) ratios of coexisting garnet and cordierite from the experimental data of Hensen and Green (1971, 1972).

TABLE 5.1

Experimental K_D data for garnet-cordierite from the
experimental studies of Hensen and Green (1971, 72, 73),
and Hensen (1977)

Run	P(Kb)	T°C	X_{Mg}^{Gt}	X_{Mg}^{Cd}	X_{Mg}^{Hy}	Gt-Cd K_D
		C70 Starting Mix (excess sillimanite)				
1884	8.1	1000	49	80		4.2±0.6
2395	9-9.5	1000	61(57-72)	89		5.2±1.1
2459	9	900	49	81		4.5±0.6
		C30 Starting Mix (excess sillimanite)				
1952	7.2	950	24	52-53		3.43
		B70 Starting Mix				
1694	7.2	1100	59	79-80	68-70	2.7±0.3
1664	9	1050	63	86		3.6
1573	7.2	1000	56	78-81	70-71	3.1
1560	9	1000	62	90-91		5.5
1586	6.3	900	49.5	77-78		3.5
1570	7.2	900	50	78-80	68	3.5
		B50 Starting Mix				
1781	6.3	1100	42	66-69	56	2.9±0.4
2731	6.3	1000	37	68-70		3.7±0.5
2722	7.2	1000	39	70		~3.7
2688	5.4	900		75-76	57-58	
2685	6.3	900	34	66-67		3.9±0.4
2665	6.3	900	43	74-76		4.0±0.5
		B30 Starting Mix				
2039	5.4	1100	28	51-54		2.9±0.2
1711	4.5	1050	24	45-49		2.8±0.2
1689	3.6	1000	18	34-38		2.6±0.2
1726	5.4	1000	23.5	44-50		3.0±0.2
D1, 2, 3	9	1000	60	85		3.7±0.8

respectively from Thompson's plot).

Both of these points will now be examined by consideration of the assumptions which have been necessary in the previously mentioned studies because of our incomplete knowledge of many aspects of crystalline solid solutions. There could be several possible causes for the variation in K_D with pressure (and X_{Mg}^{Cd}) in the Hensen and Green data at the one temperature -

a. the garnet-cordierite Fe-Mg exchange reaction is in fact a dehydration reaction (Wood, 1973).

b. Mg-Fe non-ideality in cordierite

c. Al-Si order-disorder in cordierite

d. a combination of each of the above.

Newton et al., (1974) have considered possible Al-Si ordering in cordierite. According to these authors, cordierite has tetrahedrally coordinated Al and Si and hence there is the possibility of framework order-disorder relations, as in feldspars. Some disordering among Al and Si atoms probably is associated with the observed polymorphic transition from orthorhombic to hexagonal symmetry (Gibbs, 1966), which involves quite minor variations in the positions and intensities of x-ray reflections of natural and synthetic specimens. However, evidence from solution calorimetry (Navrotsky and Kleppa, 1973) and from IR absorption spectroscopy (Langer and Schreyer, 1968) indicates that the distortional poly-morphism is not produced by a cation-site variation as profound as complete framework disordering. It therefore does not seem likely that this apparently minor effect could cause the wide range in K_D found by Hensen and Green at 1000°C.

II. THERMODYNAMIC CONSIDERATIONS

This section discusses the thermodynamic basis for three relevant garnet-cordierite reactions under anhydrous and hydrous conditions.

1. Anhydrous Equilibria

There are three reactions to consider in garnet-cordierite-sillimanite-quartz assemblages under anhydrous conditions -

$$3 \ Fe_2Al_4Si_5O_{18} \rightleftharpoons 2 \ Fe_3Al_2Si_3O_{12} + 4 \ Al_2SiO_5 + 5 \ SiO_2 \tag{1}$$

$$3 \ Mg_2Al_4Si_5O_{18} \rightleftharpoons 2 \ Mg_3Al_2Si_3O_{12} + 4 \ Al_2SiO_5 + 5 \ SiO_2 \tag{2}$$

$$\tfrac{1}{3}Mg_3Al_2Si_3O_{12} + \tfrac{1}{2} \ Fe_2Al_4Si_5O_{18} \rightleftharpoons \tfrac{1}{3}Fe_3Al_2Si_3O_{12} + \tfrac{1}{2} \ Mg_2Al_4Si_5O_{18} \tag{3}$$
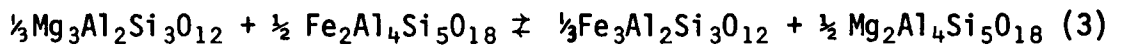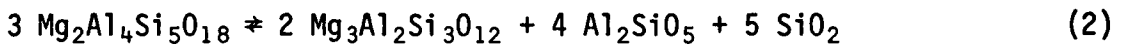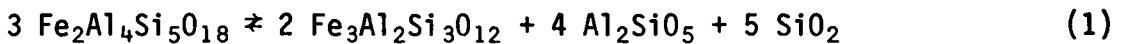
Reactions (1) and (2) define the upper pressure stability limit of the Fe- and Mg-Cd end-members respectively. Following the notation of Thompson (1976) we may write for the end member reactions (as _anhydrous_ reactions), that at equilibrium -

$$2\mu \ [Fe\text{-}Gt] + 4\mu \ [Sill] + 5\mu \ [Qtz] = 3\mu \ [Fe\text{-}Cd] \tag{4}$$

$$2\mu \ [Mg\text{-}Gt] + 4\mu \ [Sill] + 5\mu \ [Qtz] = 3\mu \ [Mg\text{-}Cd] \tag{5}$$
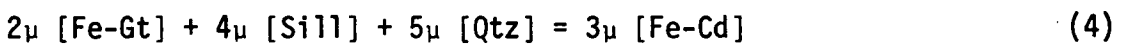
For each phase

$$\mu_i = \mu_i^o + RT\ln a_i \tag{6}$$

and thus the equilibrium conditions may be written in terms of standard chemical potentials and activities. Thus from (4) and (5) considering the cordierite + garnet + sillimanite + quartz assemblage at equilibrium, with pure sillimanite and quartz (unit activity), we can write

$$2\mu^o \ [Fe\text{-}Gt] + 4\mu^o \ [Sill] + 5\mu^o \ [Qtz] - 3\mu^o \ [Fe\text{-}Cd]$$

$$= - \ RT\ln \left[a_{Fe\text{-}Gt}^{Gt} \right]^2 \left[a_{Fe\text{-}Cd}^{Cd} \right]^{-3} \tag{7}$$

and

$$2\mu^{o}[\text{Mg-Gt}] + 4\mu^{o}[\text{Sill}] + 5\mu^{o}[\text{Qtz}] - 3\mu^{o}[\text{Mg-Cd}]$$
$$= -RT\ln \left[a_{\text{Mg-Gt}}^{\text{Gt}}\right]^{2} \left[a_{\text{Mg-Cd}}^{\text{Cd}}\right]^{-3} \tag{8}$$

For the case of pure end-member reactions (1) and (2) the right hand side (R.H.S.) of (7) and (8) would be zero, because for pure phases the activity is unity (a = 1).

Subtracting (8) from (7) we obtain,

$$2\left[\mu^{o}(\text{Fe-Gt}) - \mu^{o}(\text{Mg-Gt})\right] - 3\left[\mu^{o}(\text{Fe-Cd}) - \mu^{o}(\text{Mg-Cd})\right]$$
$$= -RT\ln \left[a_{\text{Fe-Gt}}^{\text{Gt}}\right]^{2} \left[a_{\text{Mg-Gt}}^{\text{Gt}}\right]^{-2} \left[a_{\text{Fe-Cd}}^{\text{Cd}}\right]^{-3} \left[a_{\text{Mg-Cd}}^{\text{Cd}}\right]^{3} \tag{9}$$

Assuming Fe-Mg garnet and cordierite crystalline solutions are ideal ($\gamma= 1$), then because there are three equivalent Fe-Mg sites in garnet and two in cordierite, $\left[a_{\text{Mg-Gt}}^{\text{Gt}}\right]$ and $\left[a_{\text{Mg-Cd}}^{\text{Cd}}\right]$ may be approximated by $\left[X_{\text{Mg}}^{\text{Gt}}\right]^{3}$ and $\left[X_{\text{Mg}}^{\text{Cd}}\right]^{2}$ respectively. With these substitutions (9) becomes

$$2\mu^{o}(\text{Fe-Gt}) + 3\mu^{o}(\text{Mg-Cd}) - 2\mu^{o}(\text{Mg-Gt}) - 3\mu^{o}(\text{Fe-Cd})$$

$$= -RT\ln\left[X_{\text{Fe}}^{\text{Gt}}\right]^{6} \left[X_{\text{Mg}}^{\text{Cd}}\right]^{6} \left[X_{\text{Mg}}^{\text{Gt}}\right]^{-6} \left[X_{\text{Fe}}^{\text{Cd}}\right]^{-6}$$

$$= -6RT\ln\left[\frac{X_{\text{Fe}}^{\text{Gt}}}{X_{\text{Mg}}^{\text{Gt}}}\right] \cdot \left[\frac{X_{\text{Mg}}^{\text{Cd}}}{X_{\text{Fe}}^{\text{Cd}}}\right]$$

$$= -6RT\ln K_{D} \tag{10}$$

where K_{D} is the distribution coefficient, and the quantity on the left hand side (L.H.S.) of (10) is the Fe-Mg exchange potential for the case of multicomponent ideal solutions.

From this it follows that if the P-T locations of both the Fe and Mg end member reactions (1) and (2) are known from experimental studies, then the temperature and pressure dependence of the Fe-Mg distribution coefficient (K_{D}) can be readily obtained. The pure-Fe

reaction (1) has been experimentally studied by Richardson (1968) and Wiesbrod (1973), but the pure-Mg reaction is metastable (see Hensen and Essene, 1971; Hensen and Green, 1971, 1972, 1973). Because the P-T location of reaction (2) cannot be determined directly, Thompson (1976) obtained values of exchange potentials from measured K_D values where equilibrium temperatures could be measured experimentally or estimated for natural assemblages (see Figure 5.1). Assuming that the above garnet-cordierite reactions are essentially anhydrous then for reactions (1) and (2) at equilibrium ($\Delta\mu^\circ = 0$) we have -

$$\Delta\mu^\circ_{Fe}/RT = -\ln(X^{Gt}_{Fe})^6 (X^{Cd}_{Fe})^{-6}$$

$$= \Delta H^\circ_{Fe}/RT - \Delta\overline{S}^\circ_{Fe}/R + P\,\Delta\overline{V}^\circ_{Fe}/RT \qquad (11)$$

and

$$\Delta\mu^\circ_{Mg}/RT = -\ln(X^{Gt}_{Mg})^6 (X^{Cd}_{Mg})^{-6}$$

$$= \Delta H^\circ_{Mg}/RT - \Delta\overline{S}^\circ_{Mg}/R + P\,\Delta\overline{V}^\circ_{Mg}/RT \qquad (12)$$

Similarly, the exchange potential may be defined by subtracting (12) from (11), compare (7) - (8) = (9) above, that is

$$\Delta\mu^\circ_{FeMg_{-1}}/RT = (\Delta\overline{H}^\circ_{Fe} - \Delta\overline{H}^\circ_{Mg})/RT - (\Delta\overline{S}^\circ_{Fe} - \Delta\overline{S}^\circ_{Mg})/R$$

$$+ P(\Delta\overline{V}^\circ_{Fe} - \Delta\overline{V}^\circ_{Mg})/RT$$

$$= -6\ln (X^{Gt}_{Fe}/X^{Gt}_{Mg})\cdot(X^{Cd}_{Mg}/X^{Cd}_{Fe})$$

$$= -6\ln K_D \qquad (13)$$

Because reaction (2) is metastable in the system M-A-S, the temperature dependence of K_D cannot be indirectly determined by the methods outlined above [(13)=(11)-(12)]. Thompson (1976) used an alternative approach. He obtained values of $\Delta\overline{H}^\circ$ and $\Delta\overline{S}^\circ$ for reaction (13)

from measured K_D values for coexisting minerals, where equilibrium
temperatures could be measured experimentally or estimated from natural
assemblages (Figure 5.1). Values of $\Delta \overline{H}^o$ and $\Delta \overline{S}^o$ for the Fe end member
reaction (1) can be obtained from the experimental studies of
Richardson (1968) and Weisbrod (1973a). Although these experiments
were carried out under hydrous conditions, as a first approximation
reaction (1) may be treated as anhydrous. The values obtained by
Thompson for reaction (1) and (3) are given in Table 5.2 together with
the relevant molar volume data. The molar volume, enthalpy and
entropy data derived by Thompson (1976) for reactions (1) and (3)
can be combined using the above principles to derive the relevant
constants for the pure Mg reaction (2) and thus the upper pressure
stability limit of Mg-cordierite under nominally anhydrous conditions
(Table 5.2). The calculated P-T locations of this boundary (Thompson,
1976; Holdaway and Lee, 1977) are shown in Figure 5.3.

As mentioned by Thompson (1976), the experimental reversals of
Hensen (1973) at 9 kb, 1000°C are difficult to reconcile with Thompson's
calculated lower pressure stability limit of Mg-cordierite. The experi-
mental reversals of Hensen (1973, 1977) imply that reaction (2) must
lie at higher pressure than 9 kb at 1000°C. Holdaway and Lee (1977)
suggested that the discrepancy between Hensen and Green's experimental
data and Thompson's and their own data on the P-T location of reaction
(2) (using a similar approach to that adopted by Thompson, 1976) may be
due to errors in the piston-cylinder apparatus. The pressure calibration
carried out by Hensen (1977) suggests that Hensen and Green's (1971, 1972,
1973) experimental data should be lowered in pressure by approximately
0.5 kb, but this still gives slightly higher pressures than calculated by
Thompson (1976) and Holdaway and Lee (1977).

TABLE 5.2

Thermodynamic data for reactions 1, 2, 3 from Thompson (1976) together with molar volumes of minerals. See text for description of reactions.

Reaction | Reference

(1) $\Delta\mu^\circ_{Fe}/RT = \dfrac{13394.579}{T} - 7.601 - \dfrac{1.9558\ P}{T} = -6\ \ln K$ | 1

(2) $\Delta\mu^\circ_{Mg}/RT = \dfrac{30344.27}{T} - 12.982 - \dfrac{1.909\ P}{T} = -6\ \ln K$ | 1

(3) $\Delta\mu^\circ_{FeMg}/RT = \dfrac{2724.948}{T} - 0.896 - \dfrac{0.0155\ P}{T} = \ln K$ | 1

<u>Molar Volume Data</u> | 2

Almandine	115.27 cm^3	
Pyrope	113.27 cm^3	
High Mg Cd^3	232.78 cm^3	
Low Mg Cd	233.22 cm^3	3
High Fe Cd^3	235.40 cm^3	
Sillimanite	49.899 cm^3	
Quartz	22.688 cm^3	

1. Thompson, 1976
2. Robie et al., 1967
3. See Thompson, 1976, p. 435
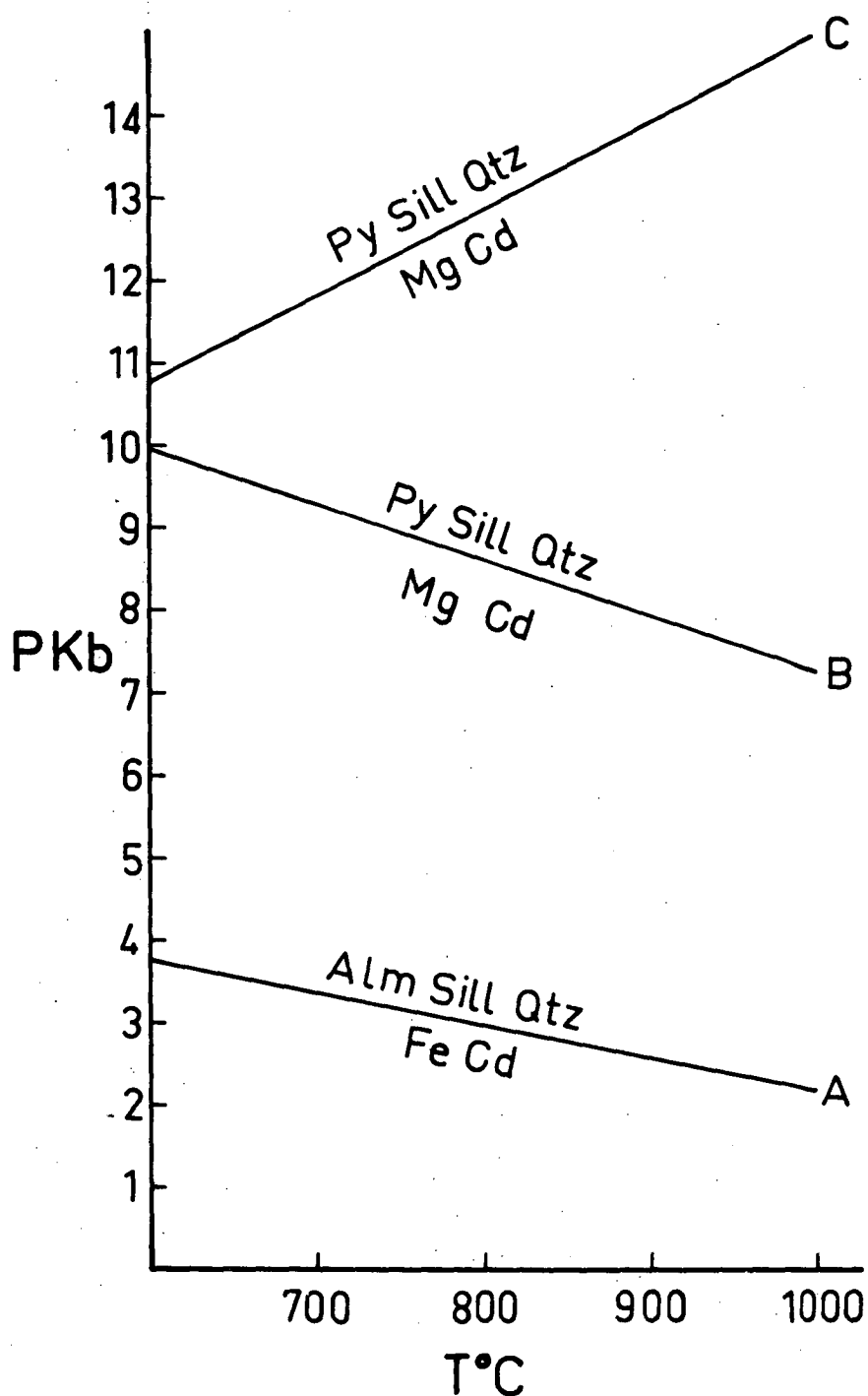
Fig. 5.3   P-T locations of the Fe- and Mg-end member reactions (1)
and (2). The reactions do not extend over the indicated
temperature range because of intersections with other
reactions. A, B - calculated position of boundary by
Thompson (1976), see Table 5.2. C - calculated position
of Mg reaction in this study, equation (14) in text.

Although reaction (2) is metastable in the M-A-S and M-A-S-H_2O
systems, it is also possible to calculate its P-T location directly
from the Gibbs free energy of formation data ($\Delta\overline{G}^\circ f$) of the pure
phases. These thermodynamic parameters can then be combined with
those for reaction (1) to derive an independent equation for the
temperature dependence to K_D. The relevant $\Delta\overline{G}^\circ f$ data for reaction (2)
are tabulated in Robie et al. (1978) and given in Table 5.3 for
the temperature range 298-1200°K. A linear least-squares fit to this
data of the form $\Delta G = a + bT$ provides an excellent fit to all data
sets (Table 5.3). This can be combined with molar volume data
(Table 5.2) to give a general equation of the form

$$\Delta G^\circ_f = \Delta H - T\Delta S + (P-1)\Delta V = -6RT \ln K \qquad (14)$$
$$= 6399.6 + 39.8256T - 3.826099P = -6RT \ln K$$

which describes the metastable upper pressure stability limit of
anhydrous Mg-cordierite reacting to pyrope-sillimanite-quartz
(Figure 5.3). The calculated position of reaction (2) using equation
(14) lies at higher pressure and has a positive dP/dT slope of 10 bar/
degree, in contrast to the calculations of Thompson (1976) or
Holdaway and Lee (1977).

If one accepts for the moment that (14) is the correct equation
for reaction (2) under anhydrous conditions, then $\Delta\overline{G}^\circ f$ for the Fe-Mg
exchange reaction (3) can be derived by the methods already outlined
$[\Delta\overline{G}^\circ f(3) = \Delta\overline{G}^\circ f(1) - \Delta\overline{G}^\circ f(2)]$ using the data given in Table 5.2 and
equation (14). The calculated equation for the P-T dependence of K_D
under anhydrous conditions, assuming ideal solid solutions is -

$$\Delta\overline{G}^\circ f_{Fe-Mg} = 21410 - 54.9256T - 0.0604P = 6RT \ln K_D \qquad (15)$$

Equation (15) shows that K_D increases with increasing temperature,
which is the reverse to the experimental data of Hensen and Green (1973)

TABLE 5.3

Gibbs free energy of formation data for reaction (2)

from Robie et al. (1978) at 1 bar pressure

T°K	Mg-Cd (orthorhombic) KJ/mol	Pyrope KJ/mol	Sill KJ/mol	Qtz[1] KJ/mol	$\Delta G^{\circ}{}_f$ reaction (2) Kcal/mol
298.15	-8651.112	-5920.856	-2438.988	-856.288	17.742
400	-8476.171	-5796.306	-2388.660	-837.660	22.218
500	-8304.353	-5674.184	-2339.238	-819.395	26.473
600	-8133.000	-5552.526	-2289.948	-801.219	30.607
700	-7962.358	-5431.461	-2240.847	-783.176	34.628
800	-7792.357	-5310.872	-2191.922	-765.287	38.528
900	-7622.957	-5190.645	-2143.153	-747.572	42.33
1000	-7449.584	-5066.933	-2092.987	-729.982	46.135
1100	-7274.828	-4942.050	-2042.207	-712.474	49.997
1200	-7100.620	-4817.323	-1991.593	-695.017	53.957

Least squares fit to this data -

$\Delta G^{\circ}{}_{f\ 1\ bar} = 6.3996 + 0.0398256\ T°K \qquad r^2 = 0.99$

[1] α quartz up to 800°K, β quartz 900-1200°K.

and the calculations of Thompson(1976) and Holdaway and Lee (1977) (Currie, (1971) considered K_D to increase with increasing temperature, but this experimental data is questionable - see later section). Of critical importance to these calculations is the dP/dT slopes of the end member reactions (1) and (2), which determine whether K_D will increase or decrease with increasing temperature. In theory it is possible for the K_D in an exchange reaction to either decrease or increase with increasing temperature (see Currie, 1973).

An independent check on the calculated positive dP/dT slope of the Mg reaction (2) can be obtained by using the solution calorimetry data tabulated by Kleppa and Newton (1975). This data (Table 5.4) indicates that at 973°K reaction (2) has a standard enthalpy change (ΔH^{o}_{973}) of -0.96 kcal/gfw. No significant additional error should be present if we assume ΔH^{o} to be constant over a temperature range of several hundred degrees. The volume change of this reaction is -3.5956 cal/bar (Table 5.2). The previous calculations (14) indicate that at 973°K reaction (2) is located at 11.8 kb pressure. Neglecting the slight dependence of ΔV on pressure, we accordingly have for this anhydrous reaction at 973°K -

$$\Delta G^{o}_{(973)} \cong -V^{o}(P-1) = 42.428 \text{ kcal} \tag{16}$$

Now $\Delta G^{o}_{(973)} = \Delta H - T\Delta S$ (17)

Hence $\Delta S^{o}_{(973)} = (\Delta H^{o} - \Delta G^{o})/T = -44.592 \text{ cal/deg}$ (18)

Hence $dP/dT \simeq \Delta S^{o}/\Delta V^{o} = -44.592/-3.5956 = 12.40 \text{ bar/deg.}$ (19)

This positive dP/dT slope compares very well with that estimated from the Gibbs free energy of formation data for reaction (2) derived from the tables of Robie et al. (1978) (+10.4 bar/degree) and hence confirms the large ΔS^{o} of the pure Mg reaction.

TABLE 5.4

Enthalpies of solution of minerals in $2PbO \cdot B_2O_3$ melts at about 700°C. (as tabulated in Kleppa and Newton 1975).

Mineral	$\Delta \overline{H}_{solution}$ (kcal/gfw)	Reference
Mg-Cordierite-DRY $Mg_2Al_4Si_5O_{18}$	28.3 ± 0.3	1, 2
Pyrope $Mg_3Al_2Si_3O_{12}$	30.65 ± 1.64	3
Sillimanite Al_2SiO_5	6.96 ± 0.15	4, 5
Quartz SiO_2	-1.04 ± 0.07	6

1. Newton, Charlu and Kleppa (1974) C.M.P. 44, 295-312.

2. Navrotsky and Kleppa (1973) J. Am. Cer. Soc. 56, 198-199.

3. J.A. Shearer, unpubl. reference (1973). Tabulated in Kleppa and Newton, 1975. Fortschritte der Mineralogie, Spec. Issue to Vol. 52. Papers and Proceedings of the Ninth General Meeting of the International Mineralogical Association. pp. 3-20.

4. Anderson and Kleppa (1969) Am. J. Sci., 267, 285-289.

5. Navrotsky, Newton and Kleppa (1973) Geochim. Cosmochim. Acta 37, 2497-2508.

6. Shearer and Kleppa (1973) J. Inorg. Nucl. Chem. 35, 1073-1078.

An independent check of the P-T location and slope of this reaction (2) can be ascertained from Schreinemaker's principles (see also Hutcheon et al., 1974). The position of this metastable reaction can be constrained by the P-T location of the relevant stable invariant points and slopes of the univariant reactions in the simple system M-A-S.

The dP/dT slope of reaction (2) must lie between that of the two reactions

$$En + Sill + Qtz = Cd \tag{20}$$

$$and \; Py + Qtz = En + Sill \tag{21}$$

Newton et al. (1974) calculated the dP/dT slope of reaction (20) as +8 bar/degree and Hensen and Essene (1976) and Hensen (1973) suggest an average slope of +15 bar/degree for reaction (21).

If the calculated positive slope for reaction (2) is correct, then the temperature dependence and the sense of change of $K_D(3)$ with temperature depends critically upon the position and slope of reaction (1) as well. Even though the experimental data on reaction (1) were determined under hydrothermal conditions (Richardson, 1968; Weisbrod, 1973) this data has been treated as anhydrous in the previous investigations (e.g. Thompson, 1976). The possible effects of water on garnet-cordierite equilibria will now be examined.

2. Hydrous Equilibria

In a qualitative sense the high K_D values for (3) in the Antarctic granulites would be consistent with equilibration at high temperatures using the above arguments. However the calculated positive dP/dT slope for reaction (2), in contrast to its predicted negative slope by Thompson (1976) and Holdaway and Lee (1977), deserves further comment.

Thompson (1976) treated the experimental data for reaction (1)
(Richardson, 1968; Weisbrod, 1973) and the Fe-Mg K_D data for
reaction (3) derived from natural rocks, both as anhydrous. The
experimental studies on (1) were under hydrothermal conditions and
the natural rocks used by Thompson (1976) contained micas. Under
hydrous conditions, reactions (1) and (2) become dehydration reactions
because cordierite can contain variable amounts of water in its
structure -

$$3Fe_2Al_4Si_5O_{18}.xH_2O \rightleftharpoons 2Fe_3Al_2Si_3O_{12} + 4Al_2SiO_5 + 5SiO_2 + 3xH_2O \qquad (22)$$

$$3Mg_2Al_4Si_5O_{18}.yH_2O \rightleftharpoons 2Mg_3Al_2Si_3O_{12} + 4Al_2SiO_5 + 5SiO_2 + 3yH_2O \qquad (23)$$
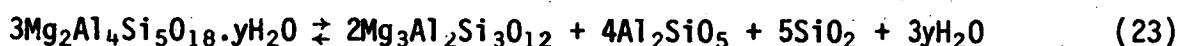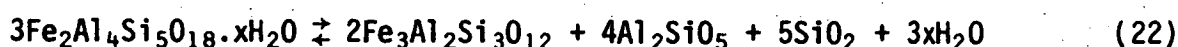
The Fe-Mg exchange reaction is accordingly -

$$\tfrac{1}{3}Mg_3Al_2Si_3O_{12} + \tfrac{1}{2}Fe_2Al_4Si_5O_{18}.xH_2O \rightleftharpoons \tfrac{1}{3}Fe_3Al_2Si_3O_{12}$$
$$+ \tfrac{1}{2}Mg_2Al_4Si_5O_{18}.yH_2O \qquad (24)$$
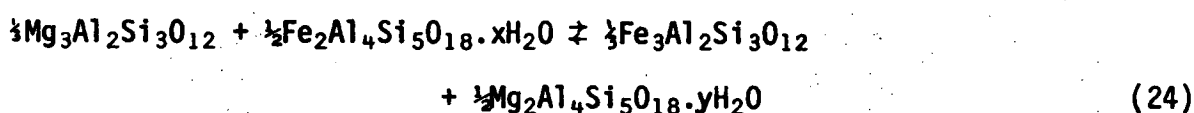
Equation (24) is strictly applicable for the case where
$xH_2O = yH_2O$, and has been assumed to be so by Weisbrod (1973) and
Holdaway and Lee (1977). In this case K_D is independent of P_{H_2O}.
If $xH_2O \neq yH_2O$ then reaction (24) would also be a dehydration reaction
and hence K_D will also depend upon P_{H_2O} (see also Wood, 1973).

In a dehydration reaction such as (22) or (23), water must
normally be on the high entropy and hence the high temperature side of
a reaction boundary. To achieve this the positive dP/dT slope
calculated for reaction (2) must become a negative dP/dT slope in
reaction (23) as shown diagrammatically in Figure 5.4. Thus the
presence of water would have a considerable effect on the enthalpy,
entropy and volume change of the end member reactions compared to the
anhydrous equivalents. There is no reason to doubt that this will
not also apply to the pure Fe system (1, 22). Although the experimental
data of Richardson (1968) and Weisbrod (1973) have been treated as
anhydrous by Thompson (1976), these experiments were carried out under
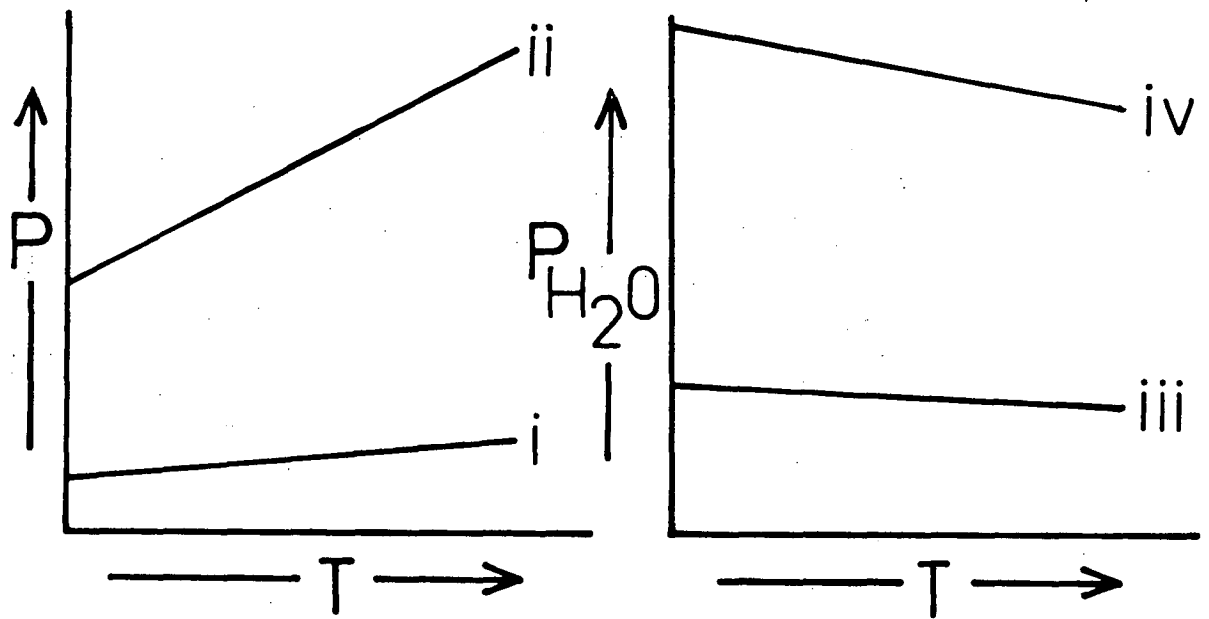
Fig. 5.4   Schematic representation of the effect of water on the
slope of the pure Fe and Mg reactions -
(i)   Fe Cd = Alm + Sill + Qtz
(ii)   Mg Cd = Py + Sill + Qtz
(iii) Fe Cd.OH = Alm + Sill + Qtz + H_2O
(iv)   Mg Cd.OH = Py + Sill + Qtz + H_2O
Cordierite is on the low pressure side in all cases and
for anhydrous reactions is on the high temperature side,
but is on the low temperature side for hydrous reactions.

hydrous conditions. Weisbrod (1973) calculated that reaction (22) has a negative slope of -3 bars/degree. It is possible for the above reasons that under anhydrous conditions reaction (1) will also have a positive dP/dT slope. If this were the case then under anhydrous conditions K_D would decrease with increasing temperature, i.e. the opposite to that of (15) which was calculated treating the available experimental data for Fe-cordierite as anhydrous (1) rather than hydrous (22).

Unfortunately, our present state of knowledge is insufficient to quantify these various possibilities. There has been no experimental study of the pure Fe reaction (1) under anhydrous conditions and it is not known whether Fe-cordierite contains the same amount of water as Mg-cordierite - a point of critical importance as to whether K_D depends upon P_{H_2O}.

The importance of water on the upper pressure stability limit of Mg-cordierite has been demonstrated by Newton (1972), who found that the breakdown of Mg-cordierite to sapphirine and quartz is reduced in pressure under anhydrous conditions, which also implies that the meta-stable reaction (2) is at lower pressures than the equivalent hydrous reaction (23). This is confirmed by the calculations of Chernosky (1974), on the breakdown of clinochlore. Chernosky calculated that the free energy of Mg-cordierite decreases with increasing water content and hence the stability of Mg-cordierite increases as the degree of hydration increases. However, Chernosky stressed that the calculated free energy data "are my 'best estimates' (guesses) and should be treated accordingly."

Wood (1973) first suggested that the Gt-Cd K_D may be dependent upon P_{H_2O} as well as temperature, and attempted to reconcile the different experimental results of Currie (1971) and Hensen and Green (1971, 1972, 1973). He proposed that if Mg- and Fe-cordierite under

the same P_{H_2O}-T conditions contained markedly different water contents, then water must have been involved in the reaction studied by Currie (1971). He proposed that Fe-Cd contained more water than Mg-Cd, and hence reaction (24) above was a dehydration exchange reaction with free water being present on the R.H.S. of (24).

Wood's calculations suggested that at a given temperature, K_D would therefore increase with increasing P_{H_2O}. Several points can be raised in objection to the proposition of Wood (1973). Firstly, the experimental results of Hensen and Green, do not (as assumed by Wood) represent anhydrous equilibria. Hensen and Green (1973) state that even though conditions of $P_{H_2O} < P_{Total}$ prevailed in their experiments, enough water was present to stabilize the cordierites to conditions identical or very close to the maximum stability limit under "wet" conditions ($P_{H_2O} = P_{Total}$). Secondly, acceptance of the interpretation of Wood (1973) implies that the Antarctic granulites described in the previous chapter must have equilibrated at conditions near $P_{H_2O} = P_{Total}$. This is inconsistent with the petrologic evidence presented in the last chapter, which indicates equilibration under conditions of $P_{H_2O} << P_{Total}$.

Petrologic evidence for high K_D values under very low P_{H_2O} conditions[*] suggests that the Gt-Cd K_D is dependent on P_{H_2O}, but in an opposite sense to that proposed by Wood (1973). It is therefore suggested that at the same P_{H_2O}-T conditions, the water content of Mg-cordierite is greater than Fe-cordierite, and hence the exchange reaction (24) becomes a dehydration reaction -

$\frac{1}{3}Mg_3Al_2Si_3O_{12} + \frac{1}{2}Fe_2Al_4Si_5O_{18}.yH_2O + \frac{1}{2}(x-y)H_2O$

$$\rightleftharpoons \frac{1}{3}Fe_3Al_2Si_3O_{12} + \frac{1}{2}Mg_2Al_4Si_5O_{18}.xH_2O \qquad (25)$$

---
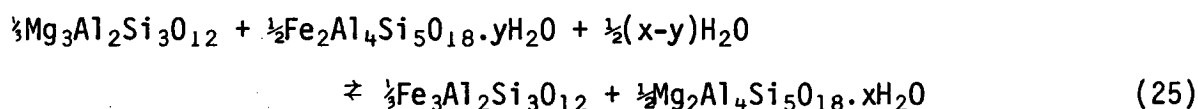
[*] Gable and Sim (1969) have shown that K_D increases on passage from non-migmatic to migmatic rocks in Colorado. This may possibly reflect a lower P_{H_2O} in the migmatic rocks due to solubility of a fluid phase in the melt.

None of the previous experimental studies of this exchange reaction have been carried out under completely anhydrous conditions to test this possibility. Furthermore, it is not yet known whether Fe- and Mg-cordierite do contain the same water contents, even though it is commonly assumed that this is so (Weisbrod, 1973; Holdaway and Lee, 1977). Schreyer and Yoder (1964) investigated the hydration state of Mg-cordierite and constructed an "isofract" diagram relating the degree of hydration to P_{H_2O} and T. No such data is available for Fe-cordierite.

At this stage it is appropriate to discuss the experimental data of Currie (1971) who found that K_D increased with increasing temperature. In Currie's experiments cordierite and garnet compositions were determined by optical and X-ray techniques. It is difficult to accept that experiments at such low temperatures (600-800°C) with short run durations (less than 48 hours) could have reached equilibrium, and furthermore display no compositional zoning in the minerals (see the comments of Holdaway and Lee, 1977; Hensen, 1977, on this point). Garnet-cordierite experiments carried out in this study (see next section) show considerable zoning and lack of reproducibility at 1000°C with run times of up to 200 hours.

The above discussion and calculations can only be considered qualitative at this stage, because of the many assumptions which have to be made because of incomplete knowledge. There are several different approaches which can be undertaken to test experimentally if K_D depends upon P_{H_2O} (or Mg-Fe non-ideality etc.). These are:

1. An experimental study of the anhydrous reaction

$$3 \text{ Fe Cd } = 2 \text{ Alm } + 4 \text{ Sill } + 5 \text{ Qtz}$$

In particular, the study should ascertain if it has a positive dP/dT slope compared to the well documented negative dP/dT slope for this reaction in the presence of water.

2. The water contents of cordierites with various Mg/(Mg + Fe) contents could be studied to ascertain whether the assumption of water content of cordierite is in fact independent of its composition.

3. An experimental study of garnet-cordierite equilibria in the system F-M-A-S can be undertaken for both hydrous and anhydrous conditions at the one P and T to determine if K_D is dependent upon the water content.

The remainder of this chapter deals with an experimental study pertaining to point 3. The pure Fe reaction (1) under anhydrous conditions can only be accurately studied under controlled fO_2 conditions for long duration experiments. It has not been attempted in the piston-cylinder apparatus at the University of Tasmania.

III. EXPERIMENTAL STUDY OF GARNET-CORDIERITE EQUILIBRIA UNDER ANHYDROUS AND HYDROUS CONDITIONS

1. The Stability of Mg-cordierite in the System M-A-S under Anhydrous Conditions

Before commencing experiments on garnet-cordierite equilibria in the system F-M-A-S, it was decided to repeat the experiments of Newton (1972) on the stability of Mg-cordierite under anhydrous conditions. Newton found that water had a marked effect on the upper pressure stability limit of pure Mg-cordierite, with the maximum pressure stability limit being 8.2 kb and 11.2 kb under anhydrous and hydrous conditions respectively. He attributed this to the stabilization of molecular water in the cordierite structure (see also Chernosky, 1974).

Water in cordierite is located in the structural channels which run parallel to the c-axis (Smith and Schreyer, 1960). The approximate

P-T stability of Mg-cordierite under conditions of $P_{H_2O} = P_{Total}$
had previously been determined by Schreyer and Yoder (1964) and
Schreyer (1968). This water is loosely bound and can be driven
off by heating to a few hundred degrees at one atmosphere without
affecting the cordierite structurally (Schreyer and Yoder, 1964),
and without measurable change in the unit-cell parameter (Newton,
1966; Holdaway and Lee, 1977).

Newton's (1972) deduced P-T stability field of Mg-cordierite
is shown in Figure 5.5. Of particular importance is the reaction

$$Mg\ Cd \rightleftharpoons Sa + Qtz \qquad\qquad (26)$$

which Newton (1972) deduced to be independent of temperature below
the solidus. This was later confirmed by solution calorimetry (Newton,
Charlu and Kleppa, 1974).

It was decided to repeat Newton's (1972) experiments for the
following reasons -

1. To assess whether we could achieve anhydrous conditions in the
M-A-S system before proceeding to the system F-M-A-S.

2. To ascertain if the upper pressure stability limit of anhydrous
cordierite using apparatus at the University of Tasmania would closely
duplicate the results obtained by Newton (1972).

3. Determine whether or not enstatite is a reaction product together
with sapphirine and quartz in reaction (26) above. This is of
importance as the calculated pressures for the anhydrous metastable
reaction (2) are several kilobars higher when calculated using Gibbs
energy of formation data (see 14) compared to the very low pressures
for reaction (2) deduced from the experimental data of Newton (1972)
using Schreinemakers' principles. For reasons given later on, it is
believed that the upper pressure stability of anhydrous Mg-cordierite
(Figure 5.5) determined by Newton (1972) is in fact a metastable reaction
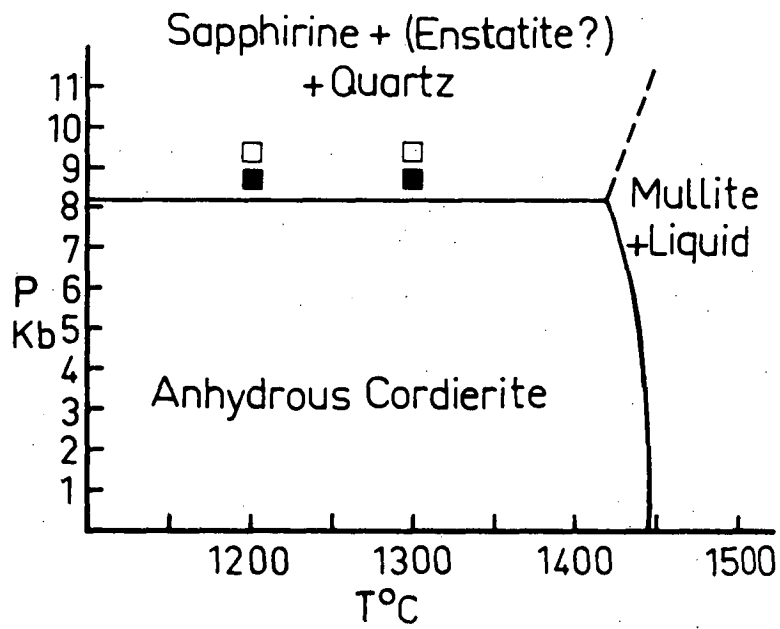
Fig. 5.5   P-T stability of Mg-cordierite under anhydrous conditions
           - from Newton (1972). The experimentally determined
           position of the upper pressure stability limit of Mg-
           cordierite from this thesis is shown by squares - filled
           squares, cordierite grew; open squares, sapphirine plus
           quartz grew.

boundary lying at lower pressure than the true stability limit of anhydrous Mg-cordierite.

Experimental Methods

The experimental method used in the present study was almost identical to that employed by Newton (1972). Mg-cordierite was dried at $1400^\circ C$, 1 atmosphere for 24 hours, and then mixed with equal weight proportions of its breakdown products (sapphirine + quartz). This mixture was then dried at $850^\circ C$ for between 1 hour and 4 days before rapidly welding shut in a Pt capsule. The complete pressure assembly was then dried at $350^\circ C$ for approximately 24 hours before commencing each experiment.

Experimental results are given in Table 5.5. Run products were examined optically and by X-ray techniques. The direction of reaction was determined by the relative heights of the most intense X-ray peaks of both the high and low pressure assemblages before and after each run. The upper pressure stability limit of anhydrous Mg-cordierite was located at 9-9.25 kb pressure, $1200^\circ C$ (Figure 5.5) which is 1 kb higher than that determined by Newton (1972). This is still at a lower pressure than under .hydrous conditions (references op. cit.)

Similar to the experimental results of Newton (1972), enstatite was not found in the breakdown products of anhydrous Mg-cordierite. Thus the observed reaction can be written as -

$$\text{Cordierite} \rightleftarrows \text{Sapphirine} + \text{Quartz} \qquad (27)$$

$$Mg_2Al_4Si_5O_{18} \rightleftarrows Mg_2Al_4SiO_{10} \quad 4SiO_2$$
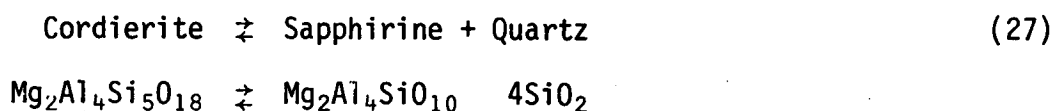
The extent to which this reaction reflects mineral compositions in natural granulites is of importance in deciding whether it is in fact a stable reaction. Natural sapphirines (see last chapter and references

TABLE 5.5

Experimental data for the breakdown of anhydrous
Mg cordierite to sapphirine and quartz

Run Number	P(kb)	T(°C)	Time (hours)	Capsule	Starting Mix	Results
T-315	12	1250	5	Pt	1	100% Sa + Qtz
T-316	8.5	1200	23	Pt	2	Cd grew
T-318	12	1250	5	Pt	1	Cd + Sa + Qtz
T-319	9	1200	25	Pt	2	Cd grew
T-320	9-8.5	1200	23	Pt	2	Cd grew
T-323	9	1200	22	Pt	2	No change in mineral abundances
T-329	9.5-9.25	1200	25	Pt	2	Sa + Qtz grew
T-330	10	1200	25	Pt	3	Corundum + glass
T-333	9	1300	10	Pt	2	Cd grew
T-334	9.5	1300	9	Pt	2	Sa + Qtz Grew
T-336	12	1250	23	Pt	1	Sa + Qtz
T-337	10	1300	15	Pt	1	Sa + Qtz grew

1. Mg Cordierite starting material

2. 50% Mg cordierite, 50% sapphirine-quartz (Run T-315 or T-318)

3. Mix 2 plus 3 wt.% H_2O.

therein) contain considerable MgSi ⇄ 2Al substitution, which prohibits colinearity of Cd-Sa-Qtz, and hence the more likely reaction in nature is -

Mg-cordierite ⇄ Sapphirine + Aluminous Enstatite + Quartz   (28)

Probe analyses of experimental sapphirines, even in iron-bearing systems do not deviate from the ideal formula $R_2^{2+}Al_4SiO_{10}$. It therefore appears quite possible that reaction (27) defining the upper pressure stability limit of anhydrous Mg-cordierite is metastable with respect to reaction (28) which so far has not been realized experimentally. Because of the general relation that a metastable phase or assemblage will have a greater P-T stability field than the stable assemblage, it is considered quite likely that the low pressures for the breakdown of anhydrous Mg-cordierite determined by Newton (1972) and above give too low a pressure for the stability field of Mg-cordierite in nature.

2. Garnet-Cordierite Equilibria in the system F-M-A-S under wet and dry conditions

This experimental study was designed to test the following -

1. Whether the garnet-cordierite Fe-Mg exchange reaction (3) was dependent upon P_{H_2O}.

2. To see whether the marked increase in K_D with pressure at 1000°C apparent in the data of Hensen and Green could be duplicated (see Figure 5.2 and Table 5.1).

3. If the Fe-Mg exchange reaction proved to be independent of P_{H_2O}, then to test whether 2. above could be due to Mg-Fe or Al-Si non ideality in the cordierite solid solutions.

Experimental Methods

Experiments were carried out using large diameter multibore spec-pure Fe capsules sealed inside Au or Pt capsules. Metallic iron capsules proved entirely satisfactory in preventing iron-loss or gain to the sample during experiments. Electron probe area scan analyses of cross sections of the charges revealed them to be homogeneous in composition and texture. Starting materials for the majority of runs consisted of fine grained (<5μ) end member minerals mixed in the appropriate amounts to produce two quartz excess bulk rock compositions - one with excess sillimanite and one with excess hypersthene (A/AFM = 52 and 30 respectively). In several runs these mineral mixes were melted at 10 kb, 1400°C and then quenched. To these glasses were added 10 wt. % of the original mineral mixes as seeds. Mineral mixes rather than glass plus seeds were initially used in an attempt to get unambiguous reversals.

In the experiments carried out under anhydrous conditions, Mg-cordierite was dried at 1400°C for 1 hour in a one atmosphere furnace before adding to the other minerals. The mineral mixes were then further dried at 120°C for up to 24 hours before rapidly welding shut the enclosing Au or Pt capsule. Hydrous experiments were carried out by the addition of hydrated cordierite formed by running coarse grained Mg-Cd with water at 750°C 8 kb for 5 minutes. The work of Scheyer and Yoder (1964) indicates that the cordierite contains $\approx$ 1 wt.% H_2O (RI = 1.30). In runs with no cordierite present, free water (1-2%) was added to the starting mixes.

Experimental Results

Experimental results are given in Table 5.6, and compositional phase relations presented in Figures 5.6 - 5.9. It was found that at 1000°C,

TABLE 5.6

Garnet-cordierite experimental data obtained in this study

Run No	P(kb)	T(°C)	Time (hours)	Starting Mix	X_{Mg}^{Gt}	X_{Mg}^{Cd}	X_{Mg}^{Opx}	Opx wt.% Al_2O_3	K_D Gt-Cd	K_D Gt-Opx	K_D Cd-Hy
T-339	9	1000	195	Alm-MgCd-En-Fs-Qtz Mg$_{70}$ A/AFM=30	(45-)48	81-82	77	6.59-8.22	4.6	3.62	1.27
Dry				Alm-MgCd-En-Fs-Qtz Mg$_{70}$ A/AFM=30	54	82-86			3.88		
				Alm-MgCd-Sill-Qtz Mg$_{70}$ A/AFM=50	47	82			5.1		
T-354	9	1000	198	Alm-MgCd (OH)-En-Fs-Qtz	44(-51)	84	73(-75)	10.01(-7.05)	6.68(-5.04)	3.44(-2.88)	1.94
				Alm-MgCd (OH)-Sill-Qtz	42	83			6.74		
T-368	9.5	1000	138	Alm-MgCd (OH)-Sill-Qtz	63	87-88			3.93-4.3		
				Alm-MgCd (OH)-Fs-Qtz	61.6	87	79	13.23	4.1	2.34	1.78
T-382	9.5	1000	162	Py-Sill-Fs-Qtz Mg$_{70}$ A/AFM=52	54						
Dry				Py-Sill-En-Fs-Qtz Mg$_{70}$ A/AFM=30	51	79*	74-82	11.9-4.2	3.6	2.73	1.32
T-383	4	1000	161	Alm-MgCd-En-Fs-Qtz Mg$_{35}$ A/AFM=30	28.6	44.1	30.4	6.8	1.97	1.09	1.806
Dry				Py$_{50}$-Alm$_{50}$-En-Fs-Sill-Qtz Mg$_{35}$ A/AFM=30	29.1	45.8	34-35	12-8.8	2.05	1.26	1.64
T-394	9.5	1000	168	0.9 Glass 0.1 Seeds Alm-MgCd-Sill-Qtz Mg$_{70}$ A/AFM=52	61.7	83.8			3.21		
+2%H$_2$O				0.9 Glass+0.1 Seeds Alm-MgCd-En-Fs-Qtz Mg$_{70}$ A/AFM=30		79	70.2	14.55			1.597
				0.9 Glass+0.1 Seeds Py-Fs Mg$_{70}$ A/AFM=30	56	81.3	70.8	9.88	3.35	1.9	1.79
T-396	9.5	1000	191	0.9 Glass+0.1 Seeds Alm-MgCd-En-Fs-Qtz Mg$_{70}$ A/AFM=30	59.07	83.9	73.8	12.5	3.61	1.957	1.85
				0.9 Glass+0.1 Seeds Py-Fs Mg$_{70}$ A/AFM=30	65.7	83.6	75.6	14.5	2.66	1.62	1.64

* One analysis only of cordierite obtained.

K_D ranged from 1.95 to 6.74, but unfortunately the results are too ambiguous to establish whether K_D is dependent upon P_{H_2O}.

Those runs in which starting compositions consisted entirely of mineral mixes, displayed considerable zoning in garnet and hypersthene compositions. Cordierite generally equilibrated to a more homogeneous composition. Mg-Fe zoning in garnet showed a complete range from the original seed end member composition onwards (Figure 5.6). Such zoning in fine grained run products has two consequences. Firstly, true equilibrium was not achieved and secondly taking the most extreme rim composition possibly does not necessarily mean that it was in equilibrium with the rim compositions of the other phases. The analysis of rim compositions is also hindered by contamination from either hypersthene or cordierite (Figure 5.6).

The experimental determination of K_D cannot be considered accurate unless there is a quite tight cluster in the compositions of each phase in the run products. A cordierite Mg_{90} coexisting with a garnet Mg_{60} has a K_D of 6. If there is a 16% error in the garnet composition, then a garnet of Mg_{50} together with cordierite Mg_{90} has a K_D of 9, which is a 50% difference in K_D. Such an error in K_D can well mask any true variations due to a compositional effect.

9kb, 1000°C Results

The results of experiments at 9kb, 1000°C under wet and dry conditions are given in Table 5.6 and summarized in Figure 5.7. Rim compositions have been used to calculate K_D values. Several features are apparent from this data. Firstly, the Gt-Cd K_D is higher in the hydrous runs than in the anhydrous runs (5.04 - 6.74 and 3.88 - 5.1 respectively). This is mainly due to the almandine reacting to a more Mg-rich run product in the anhydrous runs. Secondly the presence of
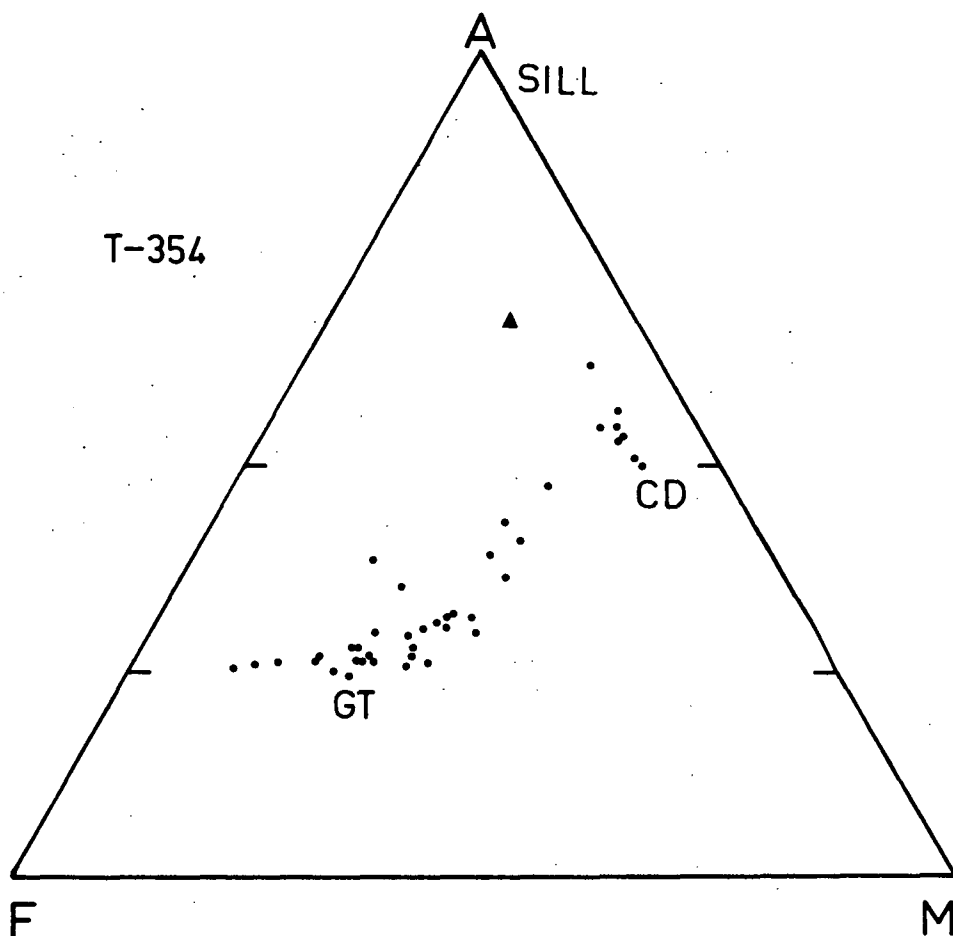
Fig. 5.6   AFM plot showing probe data results (solid dots) for
           experiment T-354, 9 kb, 1000°C - Table 5.6. Triangle -
           starting mix compositions. Run products - Gt,Cd,Sill,
           Qtz; Gt, Cd, Hy, Qtz. Note the zoning present in
           garnet (almandine in starting mix) and hypersthene
           (enstatite+ferrosilite in starting mix). Note also the
           compositional trends between Gt-Cd, Gt-Opx, Cd-Opx and
           Cd-Sill where analyses of rim compositions were
           attempted.

           (Figure continued over page.)
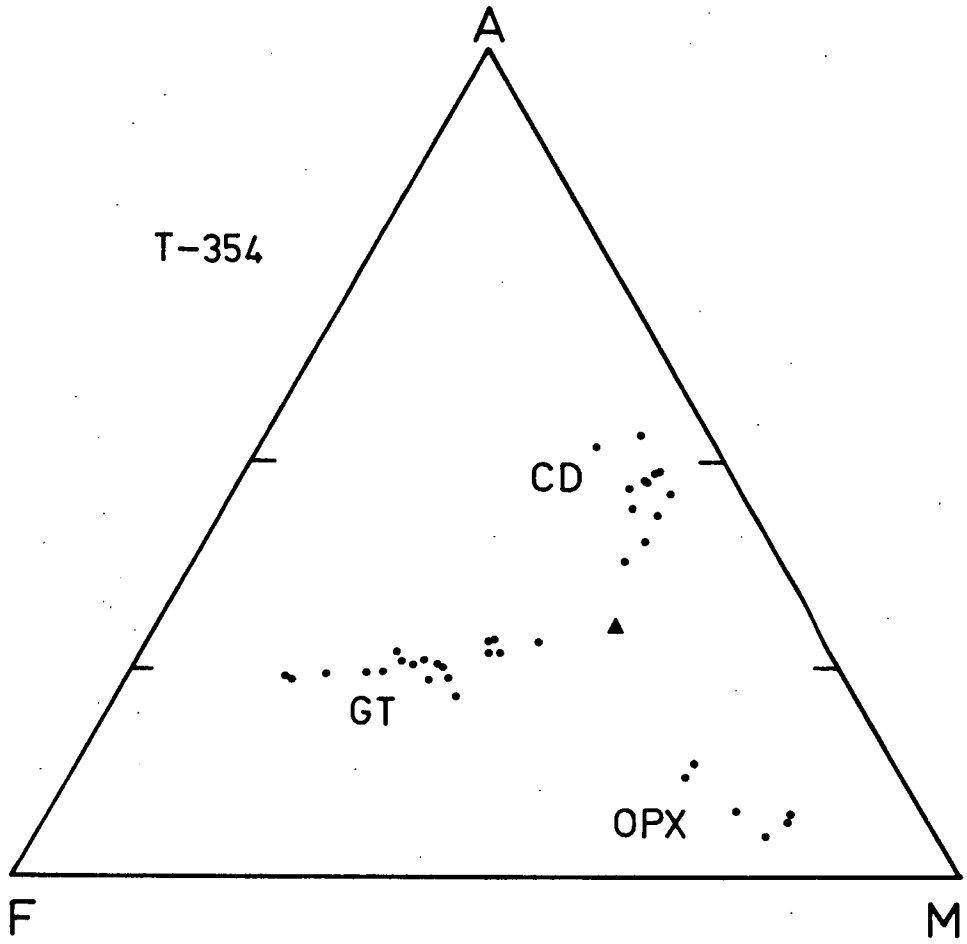
Fig. 5.6 cont.
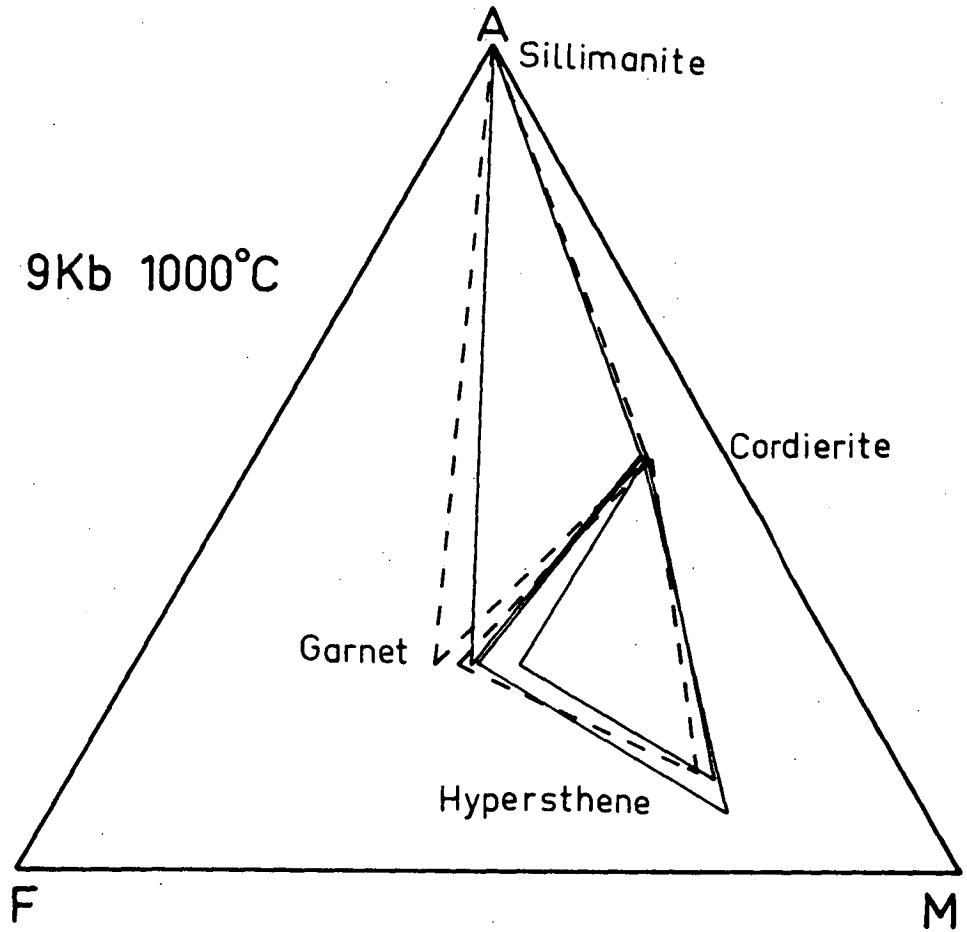
Fig. 5.7 9 kb, 1000°C experimental data (Table 5.6) showing rim
compositions only. Dashed lines connect compositions of
coexisting phases from hydrous experiments, solid lines -
anhydrous experiments. Almandine and Mg-cordierite
in starting mixes.

cordierite in both dry and wet runs confirms the stability of cordierite at higher pressures than predicted by Thompson (1976) and Holdaway and Lee (1977). The relative positions of the three phase triangles on an AFM diagram indicate the presence of only a very narrow two phase field of Gt-Cd, which is similar to the phase relations observed in the Antarctic granulites. This data by itself would suggest that K_D is higher under hydrous than anhydrous conditions. These K_D values are considerably higher than implied by the data of Thompson (1976), Holdaway and Lee (1977) or the accepted "average" K_D value of Hensen (1977).

9.5kb, 1000°C Results

Experiments were also carried out at 9.5kb, 1000°C in an attempt to more closely duplicate the phase relations in the Antarctic granulites (cordierite Mg_{90} rather than Mg_{82}). Two things are apparent from this data (Table 5.6, Figure 5.8). Firstly, the K_D values are considerably lower than in the 9kb results and secondly, the anhydrous experiments have _higher_ K_D values than the hydrous experiments. This is the reverse of what was observed in the 9kb results. In fact in the 9.5kb results the K_D values would indicate higher temperatures than implied by the data of Hensen (1977), Thompson (1976), and Holdaway and Lee (1977).

Compared to the 9kb results, at 9.5kb the garnets are more Mg-rich, but the cordierites are similar in Mg-value. Furthermore, many of the hypersthenes at 9.5kb are more Fe-rich than those at 9kb. Clearly there is no internal consistency in these results. Reversals were attempted at 9.5kb using pyrope seeds instead of almandine, with no cordierite present at all (Table 5.7, Run T-382). Compared to run T-382, rather than bracketing the Mg value of the garnet and cordierite, the garnet is more _Fe_-rich in the run products using pyrope seeds than it is when
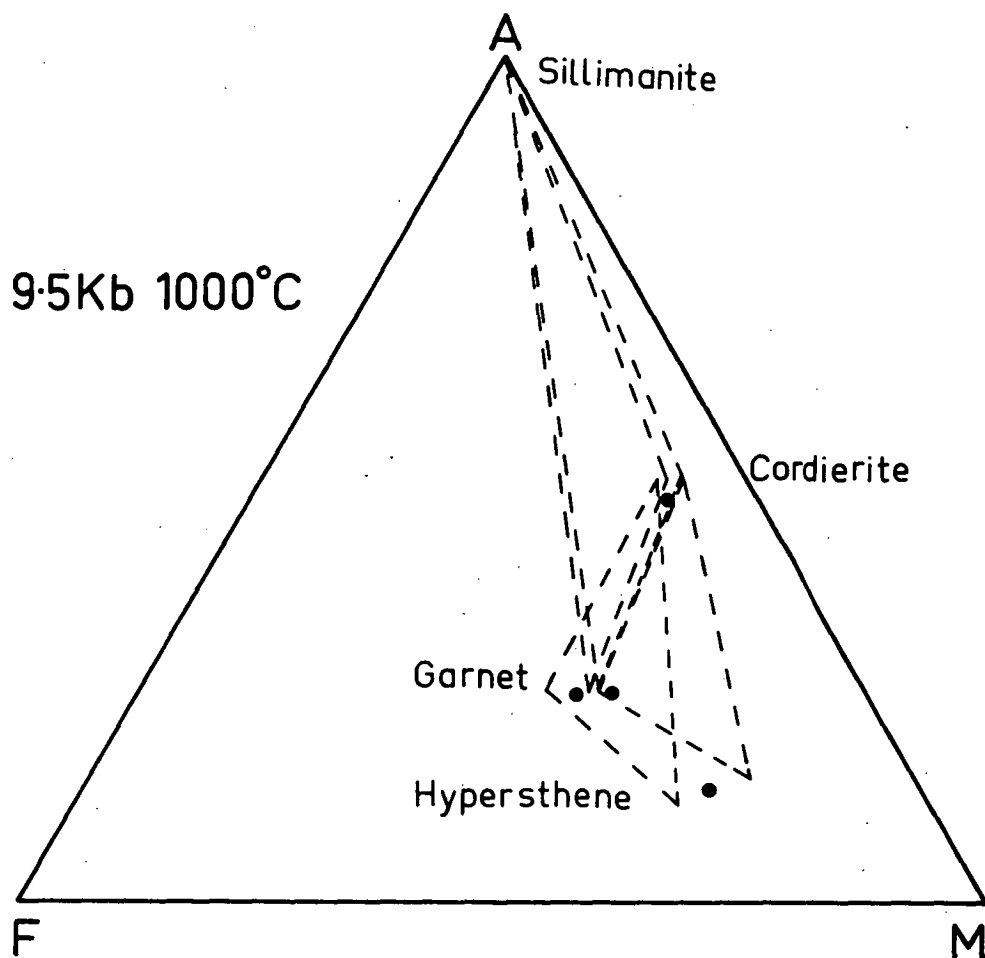
Fig. 5.8   9.5 kb, 1000°C experimental data (Table 5.6) showing
           rim compositions only. Solid dots show compositions
           of phases in which an inferred metastable cordierite
           formed - note the lower A/AFM content compared to the
           stoichiometric cordierite from other runs - see Table
           5.7.

almandine seeds were used. However, the formation of a stoichiometric cordierite from a mineral mix of garnet-orthopyroxene-sillimanite-quartz at 9.5kb, 1000°C tends to rule out the possibility that the cordierite present at these pressures in the experiments of Hensen and Green (1971, 72, 73) is due to the metastable persistence of cordierite seeds.

Part of this problem in attainment of compositional equilibrium lies in the nature of the cordierites at 9.5kb. Although stoichiometric cordierite was definitely present in some runs, in others, the "cordierite" analyses were too rich in SiO_2 and low in Al_2O_3 to be stoichiometric cordierites (Table 5.7). The A-F-M ratios consistently plotted below the A/AFM = 0.5 line, indicating that this cannot be due to the presence of quartz inclusions. In these cases the possibility of a metastable cordierite cannot be ruled out, even though cordierite was identified by x-ray methods. If such were the case, then the true cordierite composition could well be more Mg-rich, and the garnets in equilibrium with cordierite could be more Fe-rich than the analyzed garnet rims.

4kb, 1000°C Results

Experimental results for the 4kb, 1000°C run are shown in Table 5.6 and Figure 5.9. An excellent reversal was obtained in this experiment, with both the cordierite and garnet clustering tightly in run product compositions. The calculated K_D values (1.95 and 2.05) are much lower than would be expected on the basis of the $\ln K_D = \frac{1}{T}$ plot of Thompson (1976) or the average 1000°C K_D value (K_D = 3.7) of Hensen (1977). This value is much lower than expected simply from the effect of pressure on K_D compared to the 9-9.5 kb data. This tight reversal may indicate that the low K_D values ($K_D \geq 2.6$) obtained by Hensen and Green (1971, 72, 73) are

TABLE 5.7

Probe analysis of "cordierite" present in Run T-396, 9.5 kb, 1000°C.
Cordierite identified by x-ray diffraction, but not of stoichiometric
composition from probe analysis.   Scanning electron microscope
pictures revealed analyzed "cordierites" to be patches up to
approximately 40 micron width and free of inclusions.

SiO_2	55.32
Al_2O_3	29.00
FeO	4.94
MgO	10.76
Si	5.470
Al	3.380
Fe	0.409
Mg	1.586
Cation Sum	10.845
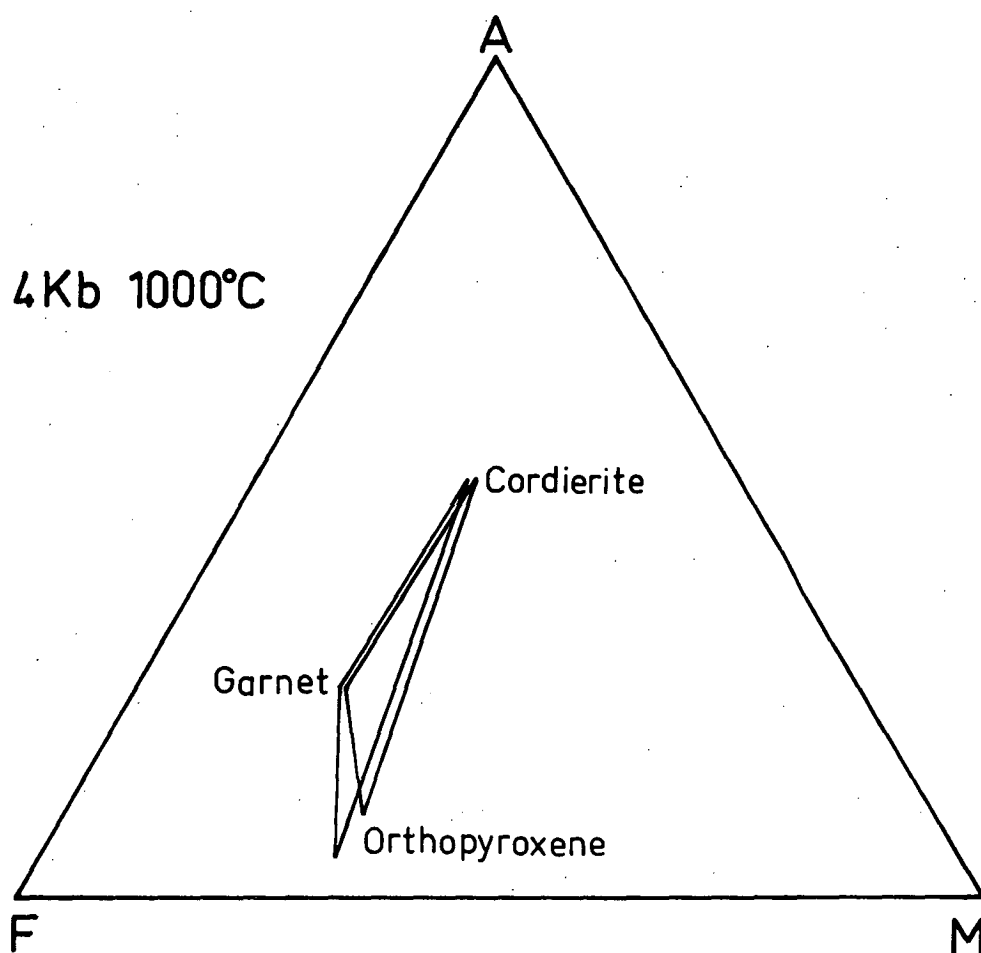
Fig. 5.9   4 kb, 1000°C experimental data (Table 5.6) showing run
product compositions of Gt, Cd and Hy (+ Qtz). Garnet
and cordierite displayed little compositional zoning.
Almandine and pyrope were present in each starting mix
respectively.

also correct.   If we accept that the 9-9.5kb, 1000°C K_D does lie within the range found in this experimental study, then the low K_D values bracketed by reversals at 4 kb would be evidence for a compositional (or water) dependence to K_D, even though this is not quantitative at present.

Many of the problems encountered in this experimental study lie in the failure of the mineral mixes to react to homogeneous reaction product compositions.   Mineral mixes rather than glass plus seeds were used in an attempt to obtain unambiguous reversals.   This approach has proved unsuccessful at 1000°C.   In contrast, experiments using glass plus seeds of the mineral mixes resulted in a tighter clustering of run product compositions, but insufficient data is available, and in some cases an apparently non-stoichiometric cordierite formed.

If we accept that at 9kb, 1000°C the garnet-cordierite K_D is approximately 5, then it is not unreasonable to consider that if K_D increases with decreasing temperature then at 900°C the K_D could be approximately 9.   This is the lower value for the garnet-cordierite pairs described in chapter 4, for which independent geothermometers suggest metamorphism at 900°C.

. Experiments were not attempted at 900°C because of the failure to obtain equilibrium at 1000°C.   Two avenues of further experimental work are suggested.   The tighter clustering in run product compositions using the glass plus seed technique compared to mineral mix technique indicates that less ambiguous results may be obtained through further experimentation using glass plus seeds.   Secondly, the reaction of Fe-cordierite to almandine-sillimanite-quartz can be studied under anhydrous conditions in order to see if the reaction

boundary has a positive dP/dT slope compared to the negative slope under hydrous conditions.

In conclusion, this experimental study has not been able to prove in a quantitative sense, whether the garnet-cordierite K_D is dependent on P_{H_2O}. The low K_D values obtained by reversals at 4kb, 1000°C are considerably lower than the values obtained at 9-9.5 kb pressure, even though there is a range in K_D at the higher pressures. The 4kb K_D data is much lower than the average 1000°C K_D value of Hensen (1977) or that deduced from the ln K_D - $\frac{1}{T}$ plots of Thompson (1976) and Holdaway and Lee (1977). The similarity of the 4kb K_D to the low pressure K_D values of Hensen and Green (see Table 5.1) and the fact that the high K_D values of these authors at higher pressures is within the range found in this experimental study suggests that the systematic increase in K_D with increasing X_{Mg}^{Cd} at 1000°C apparent from the data of Hensen and Green (Figure 5.2) using the glass plus seeds technique is valid. Further experiments using the glass plus seeds technique rather than mineral mixes are warranted before garnet-cordierite equilibria can be accurately used as a geothermometer and geobarometer.

Chapter 6

DISCUSSION

Contents   page

I. INTRODUCTION

In this chapter the broader implications of the work presented in this thesis will be discussed. This thesis has dealt with the pressures and temperatures of equilibration of the mineral assemblages and mineral reactions in granulite facies mafic and pelitic rocks. Rocks from two localities in Enderby Land, Antarctica, were metamorphosed at c. 10 kb pressure followed by isobaric cooling from high temperatures. The highest temperature mineral assemblages readjusted on cooling by the development of reaction coronas and the unmixing of aluminous clinopyroxenes. Temperatures at least as high as $900^{o}C$ are indicated for some of these rocks.

II. STAGGERED CLOSURE TEMPERATURES FOR DIFFERENT GEOTHERMOMETERS

It has often been assumed, though not conclusively shown, in metamorphic petrology that in different mineral systems, geothermometers and geobarometers should give coincident temperatures and pressures of metamorphism. In contrast to this assumption, evidence has been presented to show that there are staggered closure temperatures in different mineral systems which can provide valuable information on the P-T path of a particular metamorphic terrain. In Chapters 2 and 4 it was argued that equilibria between and within minerals of the Enderby Land granulites have closed at different stages of the thermal history (irrespective of the problems associated with temperature deductions from garnet cordierite equilibria).

This is particularly evident in the mafic granulites described in Chapter 2. In these rocks, coexisting pyroxenes equilibrated at

temperatures of c. 800°C, whereas garnet-clinopyroxene rims and garnet exsolution lamellae in clinopyroxene indicate temperatures of c. 700°C. It is significant that coincident temperature estimates using the above two geothermometers are only obtained at the one grain level (100μ), where both garnet and orthopyroxene have exsolved from the same clinopyroxene. This is particularly evident in the metamorphosed basaltic dyke, in which coexisting pyroxenes equilibrated at temperatures of c. 800°C and garnet-clinopyroxene in reaction coronas between plagioclase and orthopyroxene equilibrated at c. 600°C. Recognition of staggered closure temperatures enables calculation of P-T paths of evolution of specific parts of a metamorphic terrain.

The reason for staggered closure temperatures is related to the different activation energies and diffusion rates of different elements in minerals, a topic which is beyond the scope of this thesis. Deformation may also be important in such processes. Thus the intrusive garnet peridotite-garnet pyroxenite mass at Mt. Higasi-Akaisi, Japan (Mori and Banno, 1973) has apparently equilibrated both orthopyroxene-clinopyroxene and garnet-clinopyroxene to similar temperatures of c. 600-650°C (Table 6.1). There is excellent agreement in the estimated temperatures of equilibration using both the garnet-clinopyroxene and orthopyroxene-clinopyroxene geothermometers. The influence of deformation on diffusion processes in this intrusive massif is unknown. It would be of interest to know whether this metamorphism was part of the associated Sanbagawa metamorphism, the rocks of which contain kyanite eclogites and glaucophane.

Table 6.1

Temperature estimates for the garnet-peridotite
(sample GO-103) and garnet pyroxenite (sample
(GO-61) samples from Mt. Higasi-Akaisi, Japan
(Mori and Banno, 1973).

Sample	Temperature Estimate (^{O}C at 10 kb pressure)		
	1.	2.	3.[*]
GO-103	659	612	657
GO-61	631	636	603

[*] 1. Opx-Cpx geothermometer of Wood and Banno, 1973; Wood (1975) – see Chapter 2 for this method.

2. Opx-Cpx geothermometer of Mori and Green (1978).

3. Gt-Cpx geothermometer – this thesis, Chapter 3.

III. <u>THE BASALT-ECLOGITE TRANSITION</u>

The complete reequilibration of the Mt. Higasi-Akaisi intrusive mass prohibits any information being obtained on its higher temperature history. In contrast, the staggered closure temperatures in the mafic granulites of Enderby Land (Chapter 2) enables some discussion of the P-T path of evolution of these rocks. In particular, the appearance of garnet in the quartz tholeiite dyke at a temperature of c. $600^{o}C$ is much lower than would be expected for the appearance of garnet through linear extrapolation of the high temperature-pressure experimental data of Green and Ringwood (1967) to lower temperatures. At temperatures of c. $500^{o}C$ the proposed pressures required to form garnet in a quartz tholeiite composition (c. Mg_{60}) range from 6 kb to more than 15 kb depending upon whether the gabbro-garnet granulite-eclogite transitions at lower temperatures can be based on a linear extrapolation of the high temperature experimental data of Green and Ringwood (1967) or the curved boundary proposed by O'Hara <u>et al</u>. (1971) and Herzberg (1978). The appearance of garnet at c. $600^{o}C$ in the Enderby Land mafic granulite (Chapter 2) would be in agreement with a curvature to the gabbro-garnet granulite-eclogite transitions.

This is supported by petrologic evidence from other amphibolite-granulite terrains, as kyanite is the only aluminosilicate found in eclogites, and there are many kyanite-bearing terrains in which basic rocks are not in the eclogite facies (O'Hara, 1977). These facts suggest that the stability of eclogite-facies rocks must be restricted to pressures substantially greater than the lower pressure stability limit of kyanite for amphibolite-granulite facies terrains (consistent with the high temperature experimental data of Green and Ringwood, 1967).

In contrast there are examples of glaucophane schist terrains containing basaltic eclogites in which basaltic pillow structures, realtively undeformed fossils and even euhedral lawsonite crystals growing into quartz pods (Black, 1977) are found. Such features would more likely have formed at considerably less than 10 kb pressure, contrary to the evidence from amphibolite-granulite facies terrains on the lower pressure stability limit of eclogite. One of the best studied glaucophane schist terrains is that of New Caledonia, for which Black (1977) calculated that the total lithostatic pressure could not have exceeded 6 kb in these rocks, which is considerably less than that necessary to form eclogite if the basalt-eclogite transition is very strongly curved with decreasing temperature. However unlike amphibolites-granulites in which the assumption that $P_{Total} \approx P_{Lithostatic}$ seems reasonable, this need not necessarily be correct in glaucophane schist regions. Brothers (1974) and Black (1977) give evidence to show that P_{Total} probably exceeded 9 kb in the highest grade rocks of New Caledonia, and Black (1977) proposed that P_{fluid} was high and exceeded $P_{Lithostatic}$. These conditions would be consistent with the possible curvature to the gabbro-eclogite transition and the restriction of basaltic eclogite to above c. 9-10 kb pressure. Clearly further experimental work is needed on the position of this boundary at lower temperatures than have so far been investigated experimentally.

The temperatures and pressures of metamorphism of these low temperature (including glaucophane schist type) eclogites have been determined by Raheim and Green (1975) and Ryburn et al. (1975). They considered that the compositions of zoned cores and rims of minerals in eclogites provide a record of the P-T path of subduction. These garnets are slightly zoned in grossular contents (maximum 6 mol. %), but this range is insufficient to necessitate significant revision in the

temperature differences between cores and rims using the Gt-Cpx geothermometer presented in Chapter 3, compared to that of Raheim and Green (1974). However any significance which can be accorded to such temperature differences (40-270°C) must be tempered by the fact that in such low temperature, low-Fe clinopyroxenes, uncertainty in Fe_2O_3 content is a significant problem in the application of the Gt-Cpx geothermometer.

IV. GEOTHERMAL GRADIENTS DURING METAMORPHISM

Strong curvature to the gabbro-eclogite boundary at low temperatures would not permit the shallow formation of basaltic eclogites. Under higher temperature conditions the relative steepness of a geotherm in relation to the position of the gabbro-eclogite transition is of importance for considering tectonic processes in the Archaean compared to the models of subduction style tectonics operating now. An Archaean steady state geotherm which is any steeper than c. 20°C/km would not allow eclogitization and hence subduction of basaltic oceanic crust into the upper mantle (assuming the high temperature position of the boundary of Green and Ringwood, 1967).

This sort of geotherm is much less than the perturbed geotherm which must have been present during the peak of metamorphism of the Enderby Land granulites (Chapter 4). On the basis of liquidus temperatures of Archaean komatiitic magmas, Green (1975) has argued for steeper Archaean geotherms which would not enable eclogite subduction to occur. One of the key questions for such a proposal is the nature and role of the steady state Archaean geotherm, as both the Enderby Land metamorphism and komatiitic magmatism are a consequence of the disturbance of the steady state geotherm.

Indeed, most metamorphic rocks cannot be considered the result of erosion exposing deeper buried rocks heated along a normal geotherm. Turner and Verhoogen (1960) consider that in a sinking sedimentary pile, when temperatures reach the metamorphic range, reactions start which will most generally be endothermic, heat is absorbed in the reaction and the temperature cannot rise beyond the equilibrium point until the reaction is completed. The general effect is that as long as reactions proceed, the temperature at any depth will be less than the "normal" geotherm. This is an appreciable effect, and suggests that the geothermal gradient during metamorphism is appreciably higher than its "normal" value (Turner and Verhoogen, 1960).

The question arises as to the cause of these "abnormal" geothermal gradients and whether the distinctive mineralogy of the Enderby Land pelitic granulites can be explained by higher temperatures during metamorphism compared to other granulite terrains, or whether their exposure at the Earth's surface is due to a more effective tectonic method of uplift of deep seated rocks without subsequent metamorphism, deformation and hydration.

Although the Archaean geotherm is believed to have been steeper than that at the present day (e.g. Clark and Ringwood, 1964; Brooks and Hart, 1974), metamorphism at c. 10 kb, $900^{o}C$ would require an even steeper geothermal gradient than these estimates. Such metamorphism must be the result of a more localized temperature increase combined with an inflection in the slope of the geotherm with depth. Extrapolation of a steady state geotherm through 10 kb, $900^{o}C$ would create a physically impossible situation in the mantle (Figure 6.1). Such a geotherm would pass through the 30% melting curve for model pyrolite mantle with 0.1% water at ≈ 70 km depth. As pointed out by Green (1975) this would be an
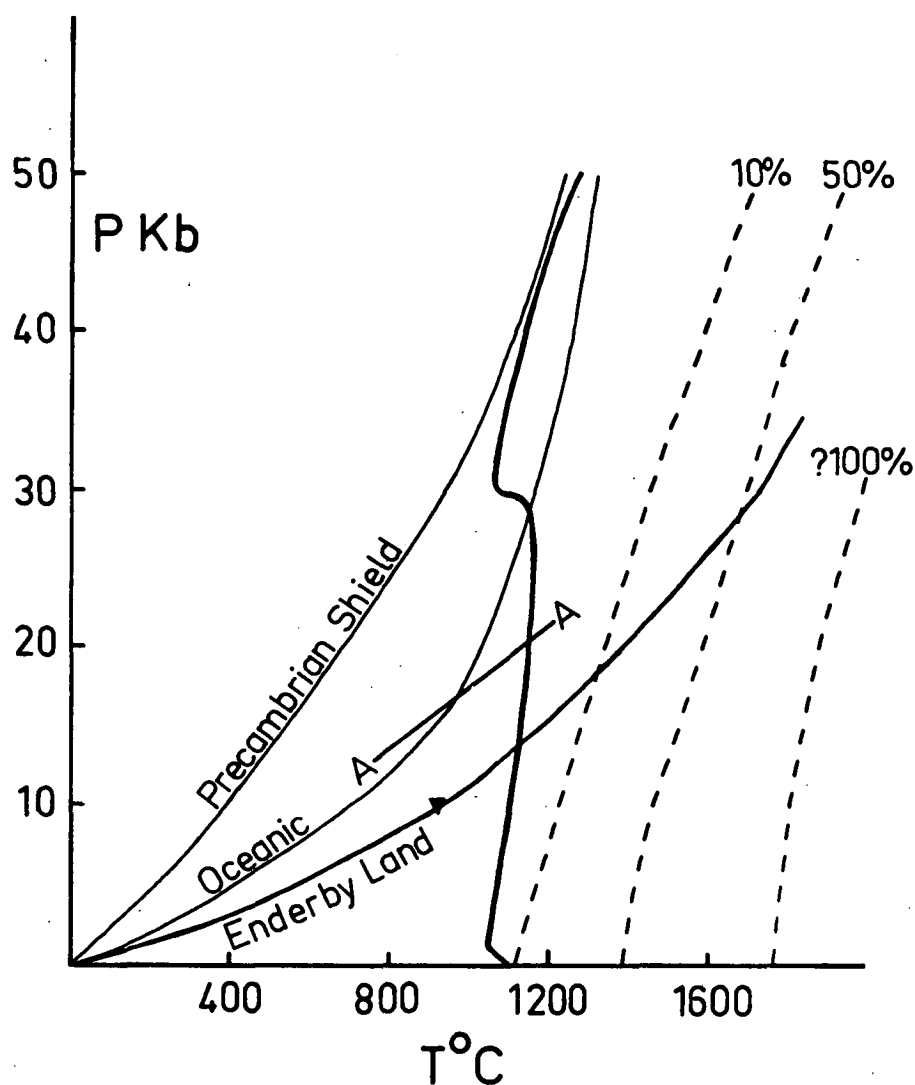
Fig. 6.1   Comparison of model geothermal gradients with the solidus
            for the model mantle composition (pyrolite) with 0.1%
            water (Green, 1973). The Precambrian Shield and modern
            oceanic geotherms are those illustrated by Ringwood (1966).
            Dashed lines present 10%, 50% and 100%(?) contours for the
            degree of partial melting of pyrolite with 0.1 % water
            (from Green, 1975, fig.2). The line A-A is the position of
            the garnet granulite-eclogite transition for basaltic rocks
            at high temperatures (Green and Ringwood, 1972). The
            triangle represents the P-T conditions of metamorphism of the
            sapphirine-quartz granulites discussed in Chapter 4.
            Continuation of a model geotherm for this point to upper
            mantle pressures would necessitate ≈50% melting of the
            mantle at depths of ≈ 100 km.

impossible situation because, for greater than c. 30% melting (and probably for lower degrees of melting) dynamic processes of segregation of magma from crystals must occur rapidly in the Earth's gravitational field. Hence this situation could not be a normal Archaean geotherm, but could possibly be a short lived geotherm caused by mantle peridotite diapirism.

Gravity data for Enderby Land is consistent with there being a thinner continental crust where the inferred highest temperature-pressure rocks are now exposed. This data indicates that the crust and ice load in Enderby Land is isostatically compensated at the base of the crust (Wellman and Tingey, 1977). Modified free-air anomalies range from +90 to -30 mGal and an isolated outcrop of high anomaly (maximum +90 mGal) occurs over the Napier Mountains and is surrounded by low anomalies (Figure 6.2). Wellman and Tingey (1977) interpret this high as an area of relatively high density upper crust with regional isostatic compensation, even though there is no surface expression of this. The maxima in the modified free-air anomaly patterns over Enderby Land correlate quite well with the delineated changes in the granulite facies mineral assemblages (Figure 4.1). These gravity differences are not likely to be caused by differences in the density of the exposed crust as all of the rocks are granulites. The positive anomaly over the Napier Mountains was also recognized by Koriakine et al. (1970) who explained it as being caused by a lack of crustal thickening under the mountains.

The proximity of denser rock closer to the surface under exposed areas of highest grade metamorphic rocks could be due to the presence of a zone of basic rocks (a source of heat as magmas ?) or possibly the presence of locally uplifted mantle. Such features would cause a marked inflection to the "abnormal" geotherm.
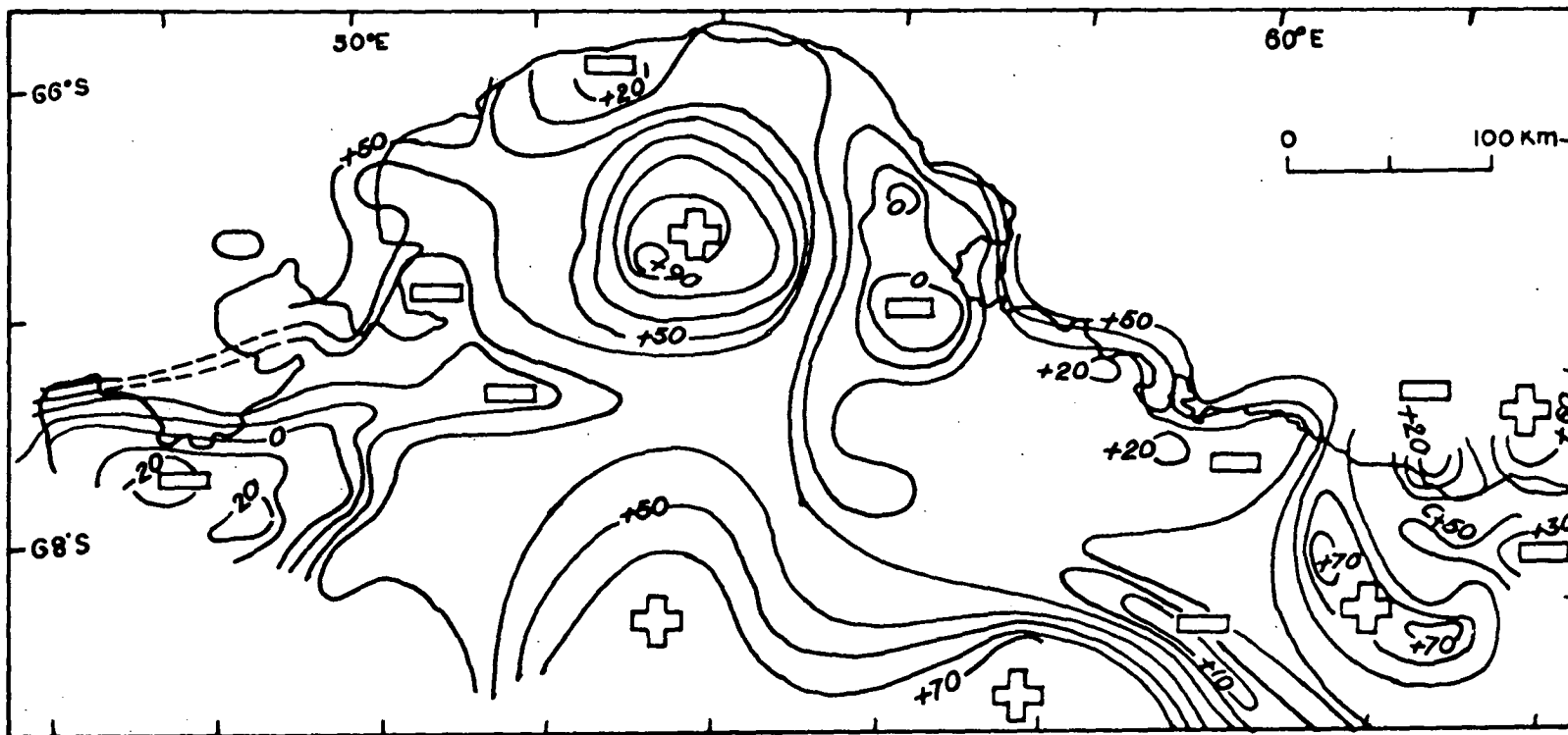
Fig. 6.2   Map of modified free-air Bouguer anomalies for Enderby
Land and Kemp Land, Antarctica.   Contour interval
10 mGal.   (Reproduced from Wellman and Tingey, 1977,
fig. 3).

The style of tectonic uplift and exposure of the Enderby Land granulites apparently differs from the P-T evolution of granulite terrains such as the Scottish and Norwegian Caledonides. The amphibolite-granulite terrains of Scotland and Norway show petrographic evidence for a rapid drop in pressure at relatively high temperatures (e.g. Griffin, 1971; O'Hara, 1977), as evidenced for example by the prograde breakdown of garnet to a symplectite of orthopyroxene, plagioclase, spinel (± clinopyroxene) in the mafic rocks. Griffin (1971) suggests that this decompression is probably related to the formation of the Jotun Nappes in Norway.

This contrast with the Enderby Land granulites which appear to have cooled to temperatures below $\approx 600^{\circ}C$ (Chapter 2) before uplift to the surface occurred. These granulites are characterized by the presence of retrograde reaction coronas and unmixing textures. Such cooling must have taken a considerable period of time and tectonic uplift would not have been synchronous with granulite facies metamorphism as was apparently the case in Norway.

England and Richardson (1977) have studied the influence of erosion upon the mineral facies of rocks from different metamorphic environments and discussed several different (though not mutually exclusive) styles of metamorphism. They consider that metamorphism of tectonically thickened crust or subducted sediment wedges is likely to take place in a thermal regime where temperature increases by conductive relaxation whilst concurrently pressure decreases by erosion of the rock pile. In this model, the metamorphic geotherm will generally be concave towards the temperature axis. In contrast, crust thickened by addition of hot magma is likely to yield a metamorphic geotherm convex towards the temperature axis, and conductive relaxation is towards lower temperatures.

England and Richardson (1977) consider that in the former style of crustal thickening and metamorphism, it will be more likely that prograde reaction products of the highest temperature assemblages would be common, such as might be expected to form on an almost iso-thermal segment of the cooling path (e.g. Norwegian and Scottish Caledonides ?). In the latter case, conductive relaxation is towards lower temperatures. If erosion were very rapid, a rock deep within the pile would reach shallow depths essentially along an isotherm, crossing as it did so reactions with positive dP/dT slopes. If on the other hand, erosion were very slow, the possibility of prograde reaction during return to the surface would be minimized. Thus the identification of conditions extreme in both pressure and temperature is to be expected from this type of metamorphic terrain (England and Richardson, 1977). Isobaric retrograde reactions are characteristic of the granulites from Enderby Land, and have also been reported in the sapphirine granulites near Wilson Lake, Central Labrador, Canada (Morse and Talley, 1971).

It is not possible to establish the cause of the high geothermal gradients during metamorphism of the Enderby Land granulites, but the ultimate cause (magmatism, mantle diapirism ?) is probably connected with deep seated (convective ?) disturbances in the mantle. The dis-tinctive nature of the Enderby Land granulites may not be the high temperatures and pressures achieved during metamorphism, but rather the slow isobaric cooling and post metamorphic uplift to the surface, which allowed preservation of these granulite assemblages without subsequent deformation, hydration and lower temperature-pressure recrystallization. There is no reason to believe that such granulites are restricted to the Archaean. Exceptional thicknesses of continental

crust (up to ≈70 km) are found at present day sites of continent-continent collisions (e.g. the Himalayas) and at active plate margins (e.g. New Zealand). Also, temperatures of present crustal melting of c. 900°C are indicated by the eruption of salic volcanic melts in New Zealand with liquidus temperatures of c. 900°C and isotopic ratios indicative of crustal melting (Ewart and Stipp, 1968; Ewart et al., 1975).

Clearly further work needs to be undertaken to elucidate the P-T paths of equilibration of rocks from elsewhere in Enderby Land before the models such as those of England and Richardson (1977) can be tested in a more rigorous fashion.

V. KIMBERLITE PETROGENESIS

Finally I wish to consider the application of the garnet-clinopyroxene geothermometer to some problems in upper mantle petrology. In Chapter 3 it was shown that on the basis of both orthopyroxene-clinopyroxene and garnet-clinopyroxene geothermometry, some garnet peridotite and eclogite xenoliths in kimberlites had equilibrated at temperatures as high as 1500-1600°C and at up to 60 kb pressure. Such temperature and pressure estimates for upper mantle xenoliths are inconsistent with our current understanding of undersaturated basalt petrogenesis.

The spectrum in compositions of basaltic magmas erupted at the Earth's surface are believed to be caused by the adiabatic ascent of peridotite diapirs in the mantle which intersect the peridotite solidus, and cause melting. The type of magma produced depends upon the amount of partial melting and the depth at which melting takes place. This is controlled to a large extent by the initial temperature of the

upwelling diapir (e.g. Green, 1970). If this model is correct, then peridotite xenoliths and high pressure cumulates in basalts must have equilibrated at temperatures equal to or less than the liquidus temperature of the enclosing magma at the depth of partial melting. There are many examples in the literature (especially alkali basalt-olivine nephelinite basalts) where the xenoliths within magmas are consistent with such models. Furthermore in several instances the experimental duplication of natural cognate mineral assemblages at temperatures on or below the liquidus of specific basalt types have been well demonstrated (see e.g. Green and Hibberson, 1970). Current models of olivine melilitite-kimberlite petrogenesis argue for the derivation of such magmas by equilibrium partial melting (<5%) of upper mantle peridotite at c. 30 kb, 1150-1200°C with a minor amount of H_2O and CO_2 present in the source region (e.g. Brey and Green, 1975). The occurrence of mantle xenoliths equilibrated at temperatures as high as 1600°C and at up to 60 kb pressure is inconsistent with the concepts of strongly silica-undersaturated basalt petrogenesis. In fact on the above models of adiabatic mantle diapirism and partial melting a diapir at 1500-1600°C would result in peridotitic komatiite melts rather than olivine melilitite melts (see e.g. Green, 1975). One of the distinctive features of kimberlite magmatism is the importance of volatiles (H_2O, CO_2) as evidenced by the explosive nature of the volcanism. It may be possible that adiabatic P-T paths (Birch, 1952) for such volatile rich melts and mantle diapirs need reappraisal.

Appendix 1

PLAGIOCLASE-CLINOPYROXENE-QUARTZ EQUILIBRIA

For the assemblage plagioclase-clinopyroxene-quartz, the following exchange reaction may be written -

$$\text{Anorthite} \rightleftharpoons \text{Ca Tschermaks Molecule} + \text{Quartz} \tag{1}$$
$$\begin{array}{ccc} CaAl_2Si_2O_8 & CaAl_2SiO_6 & SiO_2 \end{array}$$
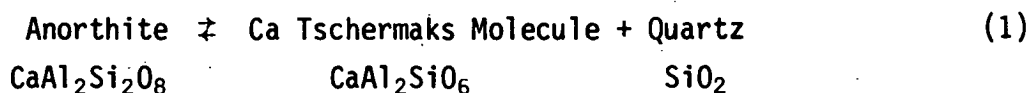
Because of the large ΔV and small ΔS of this reaction it provides a potentially useful geobarometer, particularly for crustal mafic granulites.

The condition of equilibrium for this reaction in the $CaO-Al_2O_3-SiO_2$ system may be written as -

$$G^o_{P,T} = \Delta H - T\Delta S + (P-1)\Delta V = -RT \ln K \tag{2}$$

$$\text{where } K = \frac{a^{Cpx}_{CaTs} \cdot a^{Qtz}_{SiO_2}}{a^{Plag}_{An}} \tag{3}$$

and a^j_i represents the activity of component i in phase j etc. Because a_{SiO_2} may be assumed to be unity, (3) reduces to

$$K = \frac{a^{Cpx}_{CaTs}}{a^{Plag}_{An}} .$$

The data of Robie and Waldbaum (1968) is used to estimate ΔG^o for this reaction (Table 1). An excellent least squares fit of the form

$$\Delta G^o = aT + b \tag{4}$$

has been obtained for the data:

$$\Delta G^o_{\substack{cal \\ 1\ bar,T}} = 5359.8 + 2.9876T \qquad (r^2 = 0.977) \tag{5}$$

where ΔG^o is the standard Gibbs free energy change of reaction (1) at temperature T (^oK) and 1 bar pressure. The effect of pressure on this

Table 1

Gibbs free energy data for the reaction An $\rightleftharpoons$ CaTs + Qtz at 1 bar, using the data of Robie and Waldbaum (1968). Data for βqtz used from 700-1100°K, β tridymite from 1200-1700°K.

Temp (°K)	ΔG CaTs	ΔG Qtz	ΔG An	ΔG° Kcals
700	-688.787	-187.176	-883.317	7.354
800	-674.905	-182.905	-865.506	7.696
900	-661.052	-178.680	-847.733	8.001
1000	-646.440	-174.494	-829.650	8.716
1100	-632.554	-170.325	-811.459	8.580
1200	-618.137	-166.198	-793.184	8.849
1300	-603.710	-162.107	-774.930	9.113
1400	-589.045	-158.032	-756.783	9.706
1500	-575.045	-153.974	-738.733	9.714
1600	-560.774	-149.928	-720.770	10.068
1700	-546.445	-145.775	-702.699	10.749

$$\Delta V = \overline{V}_{CaTs} + \overline{V}_{\beta qtz} - \overline{V}_{An} = 0.349 \text{ cal/bar.}$$

equilibrium is given by the more general relationship -

$$\Delta G^o_{P,T} = \Delta H - T\Delta S + (P-1)\Delta V = -RT \ln K.$$

The molar volume data given in Robie and Waldbaum (1968) indicate $\Delta V = -0.349$ cal/bar.

Thus

$$-RT \ln K = 5359.8 + 2.9876T(^oK) - 0.349P(bars) \tag{6}$$

This equation (6) reproduces to within 1 kb the experimental data of Hariya and Kennedy (1968) on the pressures of breakdown of anorthite to CaTs and quartz (Figure 1).

The application of equation (6) to mafic granulites also requires consideration of the activity-composition relations for clinopyroxene and feldspar solid solutions, as both solid solutions are known to be non-ideal (a $\neq$ x).

Clinopyroxene Activity-Composition Relations

Ca Tschermaks solid solutions in clinopyroxenes have been considered in both high pressure experimental studies (Wood, 1976) and solution calorimetry studies (Newton et al., 1977). The activity-composition relations for Di-CaTs solid solutions are critically dependent upon the possible substitution models (Table 2). The work of Wood (1975) suggested that in Di-CaTs substitutions, a^{Cpx}_{CaTs} is very nearly equal to its mole fraction. This would be true of an ideal solution of Di and CaTs end members (Newton, 1977) where Al and Si are ordered on the tetrahedral sites and Mg and Al are ordered on the corresponding M1 sites. However, as Wood (1975) pointed out, the X-ray crystallographic data of Okamura et al. (1974) showed that synthetic CaTs pyroxene has a high degree of (SiAl) tetrahedral disorder. The ideal model activity in the case of complete cation randomness on M1 and T sites would be -
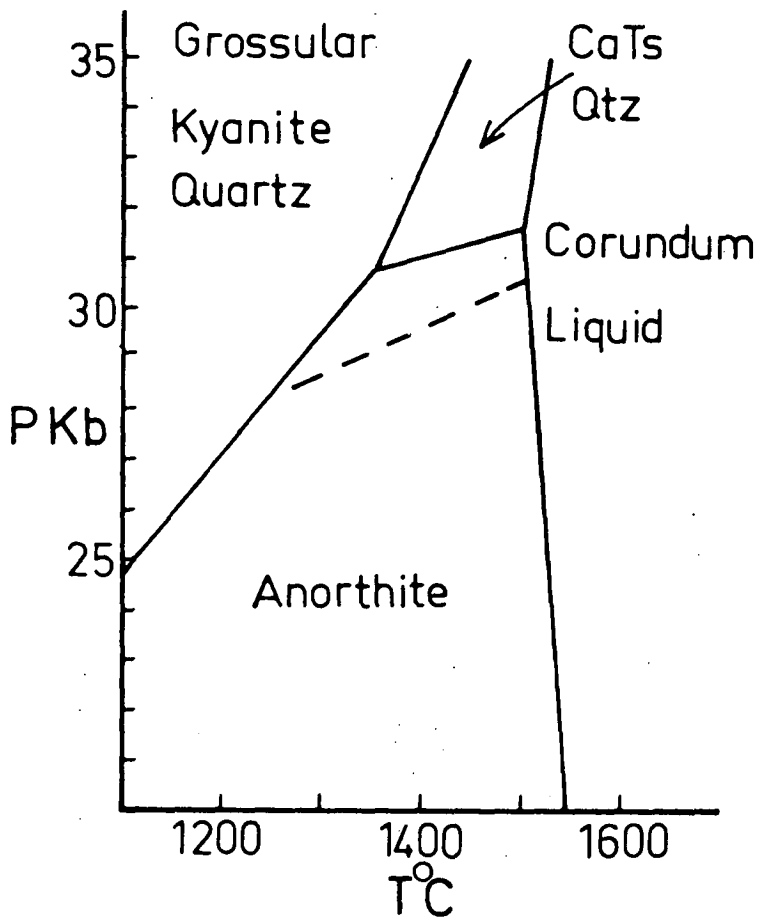
Fig. 1   P-T stability field of anorthite relative to
         grossular-kyanite-quartz, Ca Tschermaks molecule-
         quartz and corundum-liquid (after Hariya and
         Kennedy, 1968). The dashed line represents the
         calculated position of the reaction An → CaTs + Qtz
         using equation (6) - see text.

Table 2

Clinopyroxene activity-composition models.
(after Wood, 1975; Herzberg, 1978).

Four models can be devised for Di-CaTs substitutions.

1. CaTs in Cpx is completely ordered

$$a_{CaTs}^{Cpx} = X_{CaTs}^{Cpx} \gamma_{CaTs}^{Cpx} \cdot$$

2. CaTs in Cpx is completely disordered

　　Ca-Mg randomly mix on the M2 site.
　　Al-Mg randomly mix on the M1 site.
　　Al-Si randomly mix on the T site.

$$a_{CaTs}^{Cpx} = 4(X_{Ca}^{M2})(X_{Al}^{M1})(X_{Al}^{T})(X_{Si}^{T}) \cdot \gamma_{CaTs}^{Cpx}$$

$$a_{CaTs}^{Cpx} = X_{CaTs}(2 - X_{CaTs})\gamma_{CaTs}^{Cpx} \cdot$$

3. Local charge balance model A.

　　Al-Mg mix randomly on M1 site.

　　Al in T is coupled to its nearest neighbour in M1 in order to preserve local charge balance. In this model there is no configurational entropy contribution due to mixing of Al and Si on T site.

$$a_{CaTs}^{Cpx} = (X_{Ca}^{M2})(X_{Al}^{M1})\gamma_{CaTs}^{Cpx} \cdot$$

4. Local charge balance model B.

　　Al in M1 is coupled to its nearest neighbour Al in T in order to preserve local charge balance.

$$a_{CaTs}^{Cpx} = 4(X_{Ca}^{M2})(X_{Al}^{T})(X_{Si}^{T}) \cdot \gamma_{CaTs}^{Cpx}$$

$$a_{CaTs}^{Ideal} = X_{CaTs}^2 (2 - X_{CaTs}) \qquad (7)$$

(Wood, 1975; Newton, 1977) and X_{CaTs} would be considerably larger than a_{CaTs} for an ideal solution (enthalpy of mixing = 0). Thus the finding of activity nearly equal to its mole fraction implies a significant positive excess enthalpy of mixing. Various other activity-composition models are also possible, differing essentially in the presence or absence of ordering on the M1 and T sites (Table 2).

Newton et al. (1977) realized the possibility of discriminating amongst the various proposed order-disorder models by making calorimetric measurements of the enthalpy of mixing of Di-CaTs solid solutions. They found that the heat of solution data are in best agreement for the completely disordered model for pyroxenes in the Di-rich range ($\leqslant$ 0.35 CaTs). However as the clinopyroxenes become more Al-rich they considered that the structure becomes unable to tolerate increasing amounts of charge imbalance, so that the ordering state approaches that of the local charge balance configuration of Wood (1976). Thus at high CaTs contents the local charge balance model more closely describes the excess enthalpy of mixing.

The Di-CaTs excess enthalpy of solution (ΔH^{ex}) data of Newton et al. (1977) can be fitted very well to a symmetric regular solution model using Maclaurian type expansions for Di-rich clinopyroxenes (< 0.35 CaTs) -

$$\Delta H_{cal}^{ex} = 12864 \ X_{CaTs}(1-X_{CaTs}) - 26885 \ [X_{CaTs}(1-X_{CaTs})]^2 \qquad (8)$$

This does not adequately represent the ΔH^{ex} variations at high CaTs contents, but fortunately crustal granulite clinopyroxenes contain less than 0.35 CaTs. Equation (8) can probably be assumed to be also applicable to Fe-bearing clinopyroxenes, as Wood (1976) found Di-CaTs and Di-Hd-CaTs substitutions to be very similar.

Furthermore this excess Gibbs free energy of mixing can be assumed to be independent of temperature, and it is expected that this assumption will hold for real solutions over temperature ranges of a few hundred degrees (Newton, 1977). The solution calorimetry data of Newton et al. (1977) was determined at $970^{O}K$, a temperature that is directly applicable to metamorphic conditions within the crust. Equations (6) and (8) can thus be combined to take account of pyroxene non-ideality -

$$P_{bar} = \frac{5360 + T(2.9876 + 1.9872 \ln K) + 12864 \, X_{CaTs}(1-X_{CaTs})}{0.349}$$

$$\frac{- 26885 \, [(X_{CaTs}(1-X_{CaTs}))]^2}{0.349} \tag{9}$$

Plagioclase Feldspar Activity-Composition Relations

Na-Ca substitutions in plagioclase feldspars are also non-ideal. Windom and Boettcher (1976) found that $a_{An}^{Plag} \approx X_{An}^{Plag}$ in the range An_{80}-An_{100}, but for more sodic compositions, $\gamma_{An}^{Plag} \approx 1.2$ (where γ_{An}^{Plag} is the activity coefficient for the anorthite fraction of plagioclase). Saxena and Ribbe (1972) presented a thermodynamic interpretation of the experimental data of Orville (1972) and Seck (1971) and found that the excess free energy of mixing for the binary Na-Ca plagioclase substitution using Orville's data can be expressed as a polynomial -

$$\Delta G_{cal/mole}^{ex} = X_{Ab} \, X_{An}[967 + 715(X_{Ab}-X_{An})] \tag{10}$$

This expression can be considered in the same way as that for clino-pyroxene, that is according to the simplest kinds of non-ideal mixing theory ΔG^{ex} is independent of temperature and it is expected that this

will approximately hold for real solutions over temperature ranges of a few hundred degrees. The experiments of Orville (1972) were carried out at 700°C, which is directly appropriate to many crustal metamorphic rocks.

The above ΔG^{ex} term (10) can be combined with equation (9) to give a general equation for deriving the pressures of formation of crustal granulites (< 0.35 CaTs) -

$$P = \frac{5360 + T(2.9876 + 1.9872 \ln K) + 12864\ X_{CaTs}(1-X_{CaTs}) -}{0.349}$$

$$\frac{26885\left[X_{CaTs}(1-X_{CaTs})\right]^2 - X_{Ab}X_{An}\left[967 + 715(X_{Ab}-X_{An})\right]}{0.349} \tag{11}$$

where P is in bars, T $^\circ$K.

It is found that substituting the complete cation disorder model for CaTs $\left[X_{CaTs}(2 - X_{CaTs})\right]$ in K above gives entirely erroneous and in some cases negative pressures. Using instead $K = X_{CaTs}^{Cpx}/X_{An}^{Plag}$ reproduces reasonably well (Figure 2) the experimental data of Wood (1976) for pyroxenes with less than 0.35 CaTs.

Also shown in Figure 2 for comparison, are the pressure estimates obtained if the pyroxene and feldspar non-idealities are neglected, when the estimated equilibrium pressures are lowered by 1-2 kb. Application of this geobarometer to the mafic granulites described in Chapter 2 indicates that the plagioclase-quartz-opaque oxide exsolution lamellae in clinopyroxene in the sheared basaltic gneiss (mineral analyses given in Table 2.5) could have equilibrated at 10.4 to 11.0 kb at 600°C (using equations 6 and 9 respectively). Thus in this example, neglecting the effect of pyroxene and feldspar non-idealities lowers the pressure estimate by only 0.6 kb.
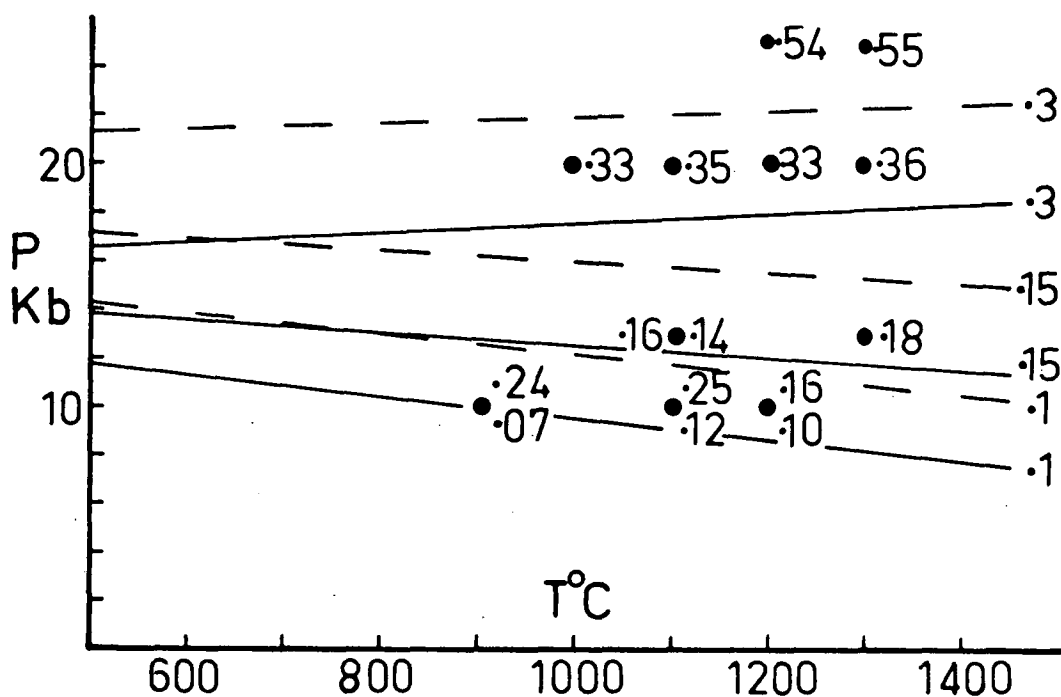
Fig. 2   P-T plot of experimentally determined CaTs contents of
diopside in equilibrium with anorthite and quartz
(Wood, 1976). The dashed and solid lines represent
calculated P-T location of diopsides with various CaTs
contents, with and without taking account of pyroxene
and feldspar non-idealities respectively (see equations
5 and 11 in text).

Appendix 2

AN ANALYSIS OF THE GARNET-CLINOPYROXENE EXPERIMENTAL DATA
IN TERMS OF INTERACTION (MARGULES) PARAMETERS

Contents   page

I. INTRODUCTION

Two of the main aims of deriving quantitative thermodynamic information on the mixing properties of various mineral solid solutions is to be able to extrapolate on thermodynamic grounds the conditions of equilibration of a particular mineral reaction to P-T conditions outside of those investigated experimentally, and secondly to be able to apply the derived information to other mineral systems. An alternative approach to that adopted here is the determination of activity-composition relations for specific binary solid solutions through either high pressure experimental studies or solution calorimetry studies (see Wood, 1975, 1977; Hensen et al., 1975; Newton et al., 1977; Newton, 1977). The application of such parameters determined from binary systems to multicomponent cation exchange equilbria often requires assumptions about the mixing models of other solid solutions involved in the equilibria. In theory it is also possible to derive interaction parameters for specific binary solid solutions from a thermodynamic treatment of data sets derived from multicomponent equilibria (see Ganguly and Kennedy, 1974). It must always be stressed that the assumptions involved in such an analysis often render the derived parameters as having little thermodynamic significance other than being mathematical expressions defining the variations in mineral compositions with P-T and compositional variations.

It has already been mentioned (Chapter 3) that the observed independence of the Ca-effect on K_D with varying Mg/(Mg + Fe) cannot solely be explained in terms of a Ca-Mg non-ideality in the garnet solid solution, but rather a combination of Ca-Mg interactions in both garnet and clinopyroxene. The net effect on the garnet-clinopyroxene Fe-Mg exchange reaction is believed to be such that the excess Gibbs free

energy of mixing (ΔG^{XS}) at a given P,T remains approximately constant with changing Mg/(Mg + Fe), <u>within the error of the experimental techniques</u>.

The following treatment of our data in terms of ternary and quaternary regular solution models provides a partial confirmation of the importance of Ca-Mg interactions in both garnet and clino-pyroxene.

II. THERMODYNAMIC CONSIDERATIONS

For the garnet-clinopyroxene Fe-Mg exchange reaction -

$$1/3\ Mg_3Al_2Si_3O_{12} + CaFeSi_2O_6 \rightleftarrows 1/3\ Fe_3Al_2Si_3O_{12} + CaMgSi_2O_6 \tag{1}$$

the equilibrium constant K for this reaction may be defined as -

$$K = \frac{(a_{Fe}^{Gt})^{\frac{1}{3}}}{(a_{Mg}^{Gt})^{\frac{1}{3}}} \cdot \frac{(a_{Mg}^{Cpx})}{(a_{Fe}^{Cpx})} \tag{2}$$

where a_i^j is the activity of component i in phase j. At equilibrium

$$\Delta G_{P,T}^0 = \Delta H - T\Delta S + (P-1)\Delta V = -RT\ \ln\ K \tag{3}$$

If the minerals are ideal solid solutions (a = x) then -

$$K = \frac{(x_{Fe}^{Gt})}{(x_{Mg}^{Gt})} \cdot \frac{(x_{Mg}^{Cpx})}{(x_{Fe}^{Cpx})} = K_D \tag{4}$$

where K_D is the distribution coefficient, x_{Fe}^{Gt} is the mole fraction of Fe in the three equivalent divalent sites in the garnet structure and x_{Fe}^{Cpx} is the mole fraction of Fe in the clinopyroxene etc.

If the minerals are not ideal then a $\neq$ x but a = xγ where γ is defined as the activity coefficient. Thus -

$$K = \left[\frac{x_{Fe}^{Gt}}{x_{Mg}^{Gt}} \cdot \frac{x_{Mg}^{Cpx}}{x_{Fe}^{Cpx}}\right] \cdot \left[\frac{\gamma_{Fe}^{Gt}}{\gamma_{Mg}^{Gt}} \cdot \frac{\gamma_{Mg}^{Cpx}}{\gamma_{Fe}^{Cpx}}\right] = K_D \cdot K_\gamma \tag{5}$$

To a first approximation the activity terms in (5) can be derived by treating the Ca-Mg-Fe garnets and Ca-Mg-Fe-Al clinopyroxenes as ternary and quaternary (symmetric) regular solutions respectively (see Thompson, 1967).

In a ternary regular solution model (garnet) -

$$RT \ln \gamma_{Fe}^{Gt} = X_{Mg}^2 W_{FeMg} + X_{Ca}^2 W_{FeCa} + X_{Mg} X_{Ca} (W_{FeMg} + W_{FeCa} - W_{MgCa}) \qquad (6)$$

and

$$RT \ln \gamma_{Mg}^{Gt} = X_{Fe}^2 W_{FeMg} + X_{Ca}^2 W_{MgCa} + X_{Fe} X_{Ca} (W_{FeMg} + W_{MgCa} - W_{FeCa}) \qquad (7)$$

where W_{FeMg} is the Fe-Mg interaction or Margules parameter. For a quaternary regular solution (clinopyroxene) -

$$RT \ln \gamma_{Fe}^{Cpx} = X_{Mg}^2 W_{FeMg} + X_{Ca}^2 W_{FeCa} + X_{Al}^2 W_{FeAl} + X_{Mg} X_{Ca} (W_{FeMg} + W_{FeCa} - W_{MgCa})$$
$$+ X_{Mg} X_{Al} (W_{FeMg} + W_{FeAl} - W_{MgAl}) + X_{Ca} X_{Al} (W_{FeCa} + W_{FeAl} - W_{CaAl}) \qquad (8)$$

and

$$RT \ln \gamma_{Mg}^{Cpx} = X_{Fe}^2 W_{FeMg} + X_{Ca}^2 W_{MgCa} + X_{Al}^2 W_{MgAl} + X_{Fe} X_{Ca} (W_{FeMg} + W_{MgCa} - W_{FeCa})$$
$$+ X_{Fe} X_{Al} (W_{FeMg} + W_{MgAl} - W_{FeAl}) + X_{Ca} X_{Al} (W_{MgCa} + W_{MgAl} - W_{CaAl}) \qquad (9)$$

At the one P,T condition the equilibrium constant K should remain constant with changes in the chemical system and the Fe-Mg distribution coefficient K_D will vary as a function of the bulk rock composition for non-ideal solid solutions. Thus a linear regression analysis of our 30 kb, 1200°C experimental data can solve for the unknowns in the above equations because, at a given pressure -

$$RT \ln K = RT \ln K_D + RT \ln K_\gamma \qquad (10)$$

Substituting (6)-(9) in (10), rearranging and noting that

$(X_{Fe} + X_{Mg} + X_{Ca})^{Gt} = 1$ and $(X_{Fe} + X_{Mg} + X_{Ca} + X_{Al})^{Cpx} = 1$ gives -

$$RT \ln K = RT \ln K_D + W^{Gt}_{FeMg}\left[X^{Gt}_{Mg}(X^{Gt}_{Mg}+X^{Gt}_{Ca}) - X^{Gt}_{Fe}(X^{Gt}_{Fe}+X^{Gt}_{Ca})\right]$$

$$+ X^{Gt}_{Ca}(W^{Gt}_{FeCa}-W^{Gt}_{MgCa}) + W^{Cpx}_{FeMg}\left[X^{Cpx}_{Fe}(X^{Cpx}_{Fe}+X^{Cpx}_{Ca}+X^{Cpx}_{Al})\right.$$

$$\left. - X^{Cpx}_{Mg}(X^{Cpx}_{Mg}+X^{Cpx}_{Ca}+X^{Cpx}_{Al})\right] - X^{Cpx}_{Ca}(W^{Cpx}_{FeCa}-W^{Cpx}_{MgCa})$$

$$- X^{Cpx}_{Al}(W^{Cpx}_{FeAl}-W^{Cpx}_{MgAl}) \qquad (11)$$

Note that a linear regression analysis of the data for equation (11) cannot discriminate W^{Gt}_{FeCa} from W^{Gt}_{MgCa} etc.

The methods of calculating the garnet and clinopyroxene end members are given in Table 1, and the reduced data used in the calculations are summarized in Table 2. Two methods have been used to calculate clinopyroxene end members. Model 1 end members (Table 1) represent "actual pyroxene molecules" whereas Model 2 represent the usual convention in classification of the various pyroxene end members. Values for X^{Cpx}_{Ca} and X^{Cpx}_{Mg} differ considerably in the two methods. Although Model 1 calculations more closely describe the various pyroxene types, it does not adequately define Fe-rich clinopyroxenes, for which a deficiency in X^{Ca}_{Mg} exists (Table 2).

III. RESULTS

Results of the linear regression analysis are summarized in Table 3, using both models for data reduction. Interaction parameters for both models assuming that all Fe-Mg solid solutions are ideal (W_{FeMg} = 0) are also presented.

The first point which is apparent from Table 3 is that, as suggested in Chapter 3, Ca-substitution in garnet is not the sole factor causing a compositional dependence to K_D. In particular, making the assumption that Fe-Mg substitution in both garnet and clinopyroxene

TABLE   1

Methods of calculating garnet and clinopyroxene end-members.

Garnet End-Members

$$X_{Ca}^{Gt} \quad = \quad Ca_3Al_2Si_3O_{12} \quad = \quad Ca/Ca + Mg + Fe$$

$$X_{Mg}^{Gt} \quad = \quad Mg_3Al_2Si_3O_{12} \quad = \quad Mg/Ca + Mg + Fe$$

$$X_{Fe}^{Gt} \quad = \quad Fe_3Al_2Si_3O_{12} \quad = \quad Fe/Ca + Mg + Fe$$

Clinopyroxene End-Members

MODEL 1.

$$X_{Al}^{Cpx} \quad = \quad CaAl_2SiO_6$$

$$X_{Ca}^{Cpx} \quad = \quad CaMgSi_2O_6$$

$$X_{Mg}^{Cpx} \quad = \quad Mg_2Si_2O_6$$

$$X_{Fe}^{Cpx} \quad = \quad Fe_2Si_2O_6$$

MODEL 2.

$$X_{Al}^{Cpx} \quad = \quad CaAl_2SiO_6$$

$$X_{Ca}^{Cpx} \quad = \quad Ca_2Si_2O_6$$

$$X_{Mg}^{Cpx} \quad = \quad Mg_2Si_2O_6$$

$$X_{Fe}^{Cpx} \quad = \quad Fe_2Si_2O_6$$

TABLE 2

End-member components used in linear regression analysis of
30kb, 1200°C experimental data.

Experimental Run	X_{Al}^{Cpx}	X_{Ca}^{Cpx}	X_{Mg}^{Cpx}	X_{Fe}^{Cpx}	X_{Ca}^{Gt}	X_{Mg}^{Gt}	X_{Fe}^{Gt}
	MODEL 1 PYROXENE END MEMBERS						
T-26	.3032	.6060	.0326	.0582	.437	.344	.218
	.1180	.7490	.0514	.0816	.308	.437	.254
	.1242	.5364	.1206	.2187	.189	.492	.319
	.0691	.5894	.2189	.1226	.158	.574	.268
T-47	.0620	.7218	.0848	.1313	.207	.479	.313
	.1217	.6287	.1107	.1389	.227	.440	.332
	.0831	.6382	.1201	.1586	.207	.452	.341
T-52	.0719	.6710	-.0550	.3121	.245	.195	.560
	.0989	.7522	-.1008	.2497	.385	.149	.469
	.1704	.7380	-.0759	.1675	.454	.176	.370
	.0769	.6618	.1419	.1194	.113	.616	.270
T-53	.1420	.7716	-.0355	.1219	.301	.350	.349
	.1051	.7139	.0137	.1673	.208	.415	.377
	.0624	.6764	.0421	.2190	.207	.313	.481
	.0833	.6957	.9042	.1268	.175	.486	.388
	MODEL 2 PYROXENE END MEMBERS						
T-26	.303	.303	.336	.058	.437	.344	.218
	.118	.374	.426	.081	.308	.437	.254
	.139	.301	.436	.123	.189	.492	.319
	.069	.295	.513	.123	.158	.574	.268
T-47	.062	.361	.446	.131	.207	.479	.313
	.122	.314	.425	.139	.227	.440	.332
	.083	.319	.439	.159	.207	.452	.341
T-52	.072	.336	.280	.312	.245	.195	.560
	.099	.376	.275	.250	.385	.149	.469
	.170	.369	.293	.167	.454	.176	.370
	.152	.279	.454	.115	.113	.616	.270
T-53	.143	.385	.350	.122	.301	.350	.349
	.214	.279	.349	.158	.208	.415	.377
	.062	.338	.380	.219	.207	.313	.481
	.083	.348	.442	.127	.175	.486	.338

TABLE 3

Interaction parameters determined for the 30kb, 1200°C experimental data using models for mineral end members listed in Tables 1 and 2.

	$RTlnK$	W^{Gt}_{FeMg}	$\left(W^{Gt}_{FeCa}-W^{Gt}_{MgCa}\right)$	W^{Cpx}_{FeMg}	$\left(W^{Cpx}_{FeCa}-W^{Cpx}_{MgCa}\right)$	$\left(W^{Cpx}_{FeAl}-W^{Cpx}_{MgAl}\right)$
1.	1754	1319	6432	866	656	464
2.	-978	3422	3728	4959	4349	2270
3.	992	0	6647	0	208	861
4.	-295	0	5375	0	4911	192

1. Calculations based on Model 1 (Table 1).
2. Calculations based on Model 2 (Table 1).
3. Calculations based on Model 1, but assuming Fe-Mg solid solutions in garnet and clinopyroxene are ideal ($W_{FeMg} = 0$).
4. Calculations based on Model 2, but assuming Fe-Mg solid solutions in garnet and clinopyroxene are ideal ($W_{FeMg} = 0$).

is ideal reveals the importance of Ca substitution in clinopyroxene on K_D was well (Table 3, data sets 3 and 4). In data set 3 (Model 1 pyroxene end members) grossular substitution in garnet and Ca Tschermak substitution in clinopyroxene are both important, whereas using Model 2 pyroxene end members (Table 3, data set 4) grossular in garnet and $Ca_2Si_2O_6$ in clinopyroxene are important. In the latter case the neglect of Ca Tschermak substitution has little effect on K_D.

The interaction parameters in Table 3 (data set 2) give reasonable temperature estimates for all of the 30 kb, $1200^{\circ}C$ data. The equilibrium constant K is less than unity in these calculations. Values for the equilibrium constant K can be obtained at other temperatures using the 30 kb data and making the assumption that the interaction parameters do not vary with temperature (strictly regular solution model). It is found that K decreases with decreasing temperature, which is the opposite to K_D variations with temperature. This may indicate that the interaction parameters are temperature dependent.

Comparison with other data.

One of the unfortunate aspects of the present treatment is that the interaction parameters vary by up to a factor of five depending upon the method of clinopyroxene end member calculations. It is possible to choose a best set by comparison with solution calorimetric and high pressure experimental studies of specific binary solid solutions. These problems are not necessarily important in the derivation of mathematical expressions describing mineral solid solutions for practical geothermometers (as in Chapter 3), but they are of critical importance when one assigns to them a thermodynamic significance as excess enthalpies of mixing. This is especially so when specific interaction parameters for a particular binary solid solution (e.g. Ca-Mg in garnet) are

dependent upon the arbitrary method of calculating other solid solutions (Cpx) in a linear regression program for multicomponent solid solution equilibria.

Excess enthalpies of mixing (ΔH^{ex}) of Ca-Mg binary garnet solid solutions have been determined by solution calorimetry (Newton et al., 1977) and by high pressure experimental studies (Hensen et al., 1975). Their results, at 0.2 grossular are given in Table 4. Hensen et al. (1975) found a significant temperature dependence to the Ca-Mg interaction parameter. Newton (1977) cautioned that the lack of agreement between these two studies meant that the results could not be considered quantitative at present. The excess enthalpies determined in the present study are also presented in Table 1, assuming $W_{FeCa}^{Gt} = 0$. This data indicates that ΔH^{ex} for 0.2 grossular ranges from 771-2172 cal/g fw (at 1 bar) depending upon the method of pyroxene end member calculation. Although it is certainly encouraging that this range is comparable to the values obtained by the latter two investigations, the very large range in values depending upon the method of pyroxene end member calculations necessitates that caution must be exercised in attaching any thermodynamic significance to these parameters. Because the excess enthalpies determined for binary solution studies (Hensen et al., 1977; Newton et al., 1977) differ by a factor of two which brackets the range predicted from our data, it is not possible to use these two studies to make a "best choice" amongst our methods of calculation.

There is also a range in the Ca-Mg and Ca-Fe interaction parameters for clinopyroxene depending upon the method of calculation (Table 3). The existence of a miscibility gap between coexisting calcic and magnesian pyroxenes supports the high values calculated for these interaction parameters. A problem exists in comparison of the values calculated using our data with those from even the Ca-Mg binary system in pyroxenes.

TABLE 4

Excess Enthalpies of Mixing of Binary Ca-Mg Garnet Solid
Solutions at 1200°C, 1bar.

ΔH^{ex} (cal/gfw)

Solution Calorimetry (Newton et al. 1977)	1659	
High Pressure Experiment (Hensen et al. 1975)	3149	

This study (Table 3)

	1bar	30kb
Data Set 1.	2069	3081
Data Set 2.	771	1789
Data Set 3.	2172	3190
Data Set 4.	1562	2580

1bar excess enthalpies calculated from the relationship

$$\Delta H_{P,T} = \Delta H_{1bar} + (P-1) \Delta V$$

For a binary regular solution model $\Delta H^{ex}_{1bar} = n\, X_A\, X_B\, W^{ex}_{1bar}$

Phase equilibrium data on the Di-En join cannot be used to evaluate activity-composition relations by means of strictly regular solution models (as in binary garnet solid solutions) because of the different crystal structures (diopside C_{bca}, monoclinic; orthoenstatite P_{bca}, orthorhombic). Strictly speaking the pyroxene solvus is a miscibility gap. Because of these different crystal structures, clinopyroxene and orthopyroxene do not obey the same equation of state, hence -

$$\mu_{Mg}^{0~Opx} \neq \mu_{Mg}^{0~Cpx}$$

and

$$\mu_{Ca}^{0~Opx} \neq \mu_{Ca}^{0~Cpx}$$

It is not possible to directly obtain information on the thermodynamic mixing properties of Ca-Mg clinopyroxenes from an analysis of two phase experimental data on the Di-En system using Margules type solution models. The two phase data can still be used to derive analytic expressions for the miscibility gap (see Warner and Luth, 1974; Saxena and Nehru, 1975).

The miscibility gap may be considered as the summation of parts of two solvii, one with orthorhombic and one with monoclinic structure. The free energy of mixing (G_m) can be considered a minimum at the two points on the miscibility gap with two structurally different pyroxene types (Saxena and Nehru, 1975). Saxena and Nehru derived Ca-Mg interaction parameters for Di and En by making the assumption that for the two reactions -

$$Mg_2Si_2O_{6Opx} = Mg_2Si_2O_{6Cpx}$$

and

$$CaMgSi_2O_{6Opx} = CaMgSi_2O_{6Cpx}$$
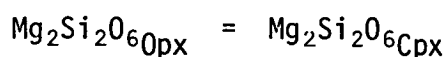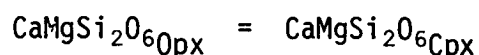
the standard free energy changes are 500 and 1000-3000 cal/mol. respectively.

They determined $W_{Ca-Mg}^{Cpx} \approx 7000$ cal/mol. This is somewhat higher than the range of values determined from our data (Table 3) but not unreasonable considering that the present analysis determined a net value $(W_{FeCa}^{Cpx} - W_{MgCa}^{Cpx})$.

Recent work has also shown that the intracrystalline partitioning of Mg and Fe^{2+} between the M1 and M2 sites in clinopyroxene $[K_D = (FeM1/MgM1) \cdot (MgM2/FeM2)]$ increases with increasing temperature and decreases with increasing $CaSiO_3$ content in the clinopyroxene (Saxena et al., 1973; McAllister et al., 1976). This implies that Ca selectively replaces Mg in the clinopyroxene M2 site, which would have the effect of decreasing the Gt-Cpx K_D with increasing Ca-content of the clinopyroxene. Ca-Fe substitution in clinopyroxene should be more ideal than Ca-Mg substitution. This would be consistent with the increase in miscibility between Ca- and Mg-pyroxenes with increasing iron content.

As both garnet and clinopyroxene show similar variations in Ca-contents with changing rock compositions, then the Ca-Mg non ideality of both would tend to cancel. On this basis the effect of Ca upon K_D in both garnet and clinopyroxene would diminish with increasing iron content, whereas the net effect, as given by equation (8) in Chapter 3, would be approximately independent of Mg/(Mg + Fe).

Although our data shows that within experimental error the effect of Ca upon K_D is approximately independent of iron content $[(Mg/(Mg + Fe) \geq 0.24]$, several of the very iron-rich experimental data points of Raheim and Green (1974a) do show a slightly decreasing effect of Ca upon K_D with increasing iron (Runs 4256, 4258, Gt Mg/(Mg+Fe) = 0.099 and 0.035). Calculations based on this data still do not extrapolate back to no Ca effect at Mg/(Mg + Fe) = 0, consistent with our earlier discussion. The relationship derived from this data, in which the effect of Ca decreases with decreasing Mg/(Mg + Fe) is -

$$T^{o}K = \frac{(1782 \; Mg^{Gt} + 2121)X^{Gt}_{Ca} + 2837 + 17.08P}{(\ln K_D + 1.9034)} \tag{11}$$

where $Mg^{Gt} = Mg/(Mg + Fe)$ in the garnet.

The above relation (11) gives temperature overestimates and underestimates of $\approx 30^{o}C$ for garnet peridotite and extremely iron-rich eclogites respectively in comparison with our general equation (8). Such differences are still within the error limits placed on our data and interpretation ($\pm 5\%$). Significant differences in temperature estimates only appear between the two equations for extremely Ca- and Fe-rich eclogites (e.g. $\approx Py_5Alm_{45}Gross_{50}$) at very low pressures and temperatures. Such rocks would be extremely rare in nature.

IV. CONCLUSIONS

It can be concluded from the above study, that the variation of K_D with mineral compositions is a function of non-ideal substitutions in both the garnet and clinopyroxene. Because of the lack of unambiguous data on the specific mixing properties of these binary solid solutions, and the inevitable assumptions which are needed for their derivation from multicomponent experimental data, the derived constants cannot be considered as valid thermodynamic parameters describing the various solid solutions. Rather, the Margules representation in this study only gives a mathematical expression for the variation in K_D with changing mineral compositions. For this reason, the simple mathematical expression derived in Chapter 3 (equation 8) which more accurately describes the variation in K_D with P,T and mineral composition than the above Margules parameters is preferred as a practical geothermometer at this stage of our knowledge.

Appendix   3

MINERAL DATA FOR GARNET-CLINOPYROXENE EXPERIMENTS

Run T-26   30 kb, 1200°C

	1	1	2	2	3	3	4	4*
	Cpx	Gt	Cpx	Gt	Cpx	Gt	Cpx	Gt
SiO_2	49.54	40.9	52.37	41.8	50.93	44.02	54.74	41.67
Al_2O_3	13.23	22.83	5.35	22.01	6.39	21.2	3.08	22.5
FeO	3.58	10.39	5.21	12.3	7.92	14.83	7.71	13.33
MgO	11.57	9.22	15.26	11.89	15.8	12.8	18.11	16.0
CaO	21.81	16.29	21.6	11.67	18.69	6.86	16.15	6.14
Si	1.786	3.023	1.908	3.070	1.867	3.207	1.979	3.027
Al	0.562	1.988	0.230	1.906	0.276	1.820	0.131	1.927
Fe	0.108	0.642	0.159	0.755	0.243	0.904	0.233	0.810
Mg	0.622	1.016	0.828	1.302	0.863	1.394	0.976	1.733
Ca	0.843	1.289	0.843	0.918	0.734	0.535	0.626	0.478
Total	3.928	7.986	3.974	7.971	3.992	7.874	3.946	7.996
Ca	53.6	43.7	46.0	30.8	39.9	18.9	34.1	15.8
Mg	39.5	34.4	45.2	43.7	46.9	49.2	53.2	57.4
Fe	6.8	21.8	8.7	25.4	13.2	31.9	12.7	26.8
A	26.3	40.3	11.1	39.0	13.0	39.1	6.7	38.9
C	39.5	26.1	40.9	18.8	34.7	11.5	31.8	9.7
F	34.2	33.6	47.9	42.1	52.3	49.4	61.5	51.4
K_D	3.64		3.03		2.31		1.96	

* 1.   0.7 Ec Mg70 + 0.3 CaTs
  2.   0.88 Ec Mg70 + 0.12 CaTs
  3.   1.0 Ec Mg70
  4.   0.63 Ec Mg70 + 0.37 Opx 2539

Run T-27   30 kb, 1300°C

	1	1	2	2	3	3	4	4	4*
	Cpx	Gt	Cpx	Gt	Cpx	Gt	Cpx	Gt	Opx
SiO_2	48.56	42.48	51.47	42.36	52.71	43.83	52.95	41.89	54.85
Al_2O_3	16.17	22.24	7.44	22.05	4.42	21.47	5.4	21.52	2.04
FeO	3.56	9.96	6.29	12.53	8.54	14.74	7.06	13.43	1.85
MgO	9.8	8.36	13.85	11.18	15.5	11.54	18.22	15.62	28.79
CaO	21.62	16.45	20.69	11.42	18.62	8.13	16.09	7.37	12.29
Si	1.747	3.125	1.878	3.109	1.932	3.203	1.913	3.056	1.951
Al	0.686	1.928	0.320	1.908	0.191	1.849	0.230	1.851	0.085
Fe	0.107	0.613	0.192	0.769	0.262	0.901	0.213	0.576	0.070
Mg	0.526	0.916	0.753	1.223	0.847	1.257	0.981	1.699	1.526
Ca	0.833	1.297	0.809	0.898	0.731	0.637	0.623	0.819	0.365
Total	3.899	7.879	3.959	7.943	3.970	7.865	3.968	8.012	4.003
Ca	56.8	45.9	46.1	31.1	39.7	22.8	34.3	18.6	3.6
Mg	35.8	32.4	42.9	42.3	46.0	45.0	54.0	54.9	77.8
Fe	7.3	21.7	10.9	26.6	14.2	32.2	11.7	26.5	18.6
A	31.9	40.6	15.4	39.8	9.4	39.8	11.2	37.4	4.2
C	35.8	27.3	39.0	18.7	36.0	13.7	30.4	11.6	3.4
F	7.3	32.1	45.6	41.5	54.6	46.4	58.3	50.9	92.4
K_D	3.29			2.45	2.32			2.22	

* 1.   0.7 Ec Mg70 + 0.3 CaTs
  2.   0.88 Ec Mg70 + 0.12 CaTs
  3.   1.0 Ec Mg70
  4.   0.63 Ec Mg70 + 0.37 Opx 2539.

Run T-28   24 kb, 1200°C

	1	1	2	2	3	3	4	4	4*
	Cpx	Gt	Cpx	Gt	Cpx	Gt	Cpx	Gt	Opx
SiO_2	48.15	40.58	50.4	42.06	51.51	41.44	52.5	41.99	55.62
Al_2O_3	15.46	22.41	8.03	22.22	6.5	22.5	4.88	22.83	2.14
FeO	3.69	10.65	5.57	11.76	6.1	11.6	8.09	11.12	2.48
MgO	10.76	10.35	14.43	13.7	16.47	17.01	19.9	18.54	29.13
CaO	21.59	15.8	21.28	9.96	19.11	7.26	14.24	5.21	10.43
Si	1.737	3.001	1.840	3.064	1.873	3.000	1.899	3.013	1.962
Al	0.657	1.953	0.346	1.908	0.279	1.921	0.208	1.930	0.089
Fe	0.111	0.659	0.170	0.716	0.185	0.703	0.245	0.667	0.094
Mg	0.579	1.140	0.785	1.488	0.892	1.836	1.073	1.982	1.532
Ca	0.835	1.251	0.833	0.779	0.745	0.563	0.552	0.400	0.308
Total	3.929	8.018	3.984	7.972	3.983	8.034	3.989	8.01	3.99
Ca	54.7	41.0	46.6	26.1	40.9	18.2	29.5	13.1	4.8
Mg	38.0	37.4	43.9	49.9	49.0	59.2	57.4	65.0	79.2
Fe	7.3	21.6	9.5	24.0	10.2	22.6	13.1	21.9	15.9
A	30.1	39.0	16.2	39.0	13.3	38.2	10.0	38.8	4.4
C	38.2	25.0	39.0	15.9	35.4	11.2	26.6	8.0	4.6
F	31.6	36.0	44.8	45.1	51.3	50.5	63.4	53.2	91.0
K_D		3.0		2.22		1.84		1.47	

*   1.   0.7 Ec Mg70 + 0.3 CaTs
    2.   0.88 Ec Mg70 + 0.12 CaTs
    3.   1.0 Ec Mg70
    4.   0.63 Ec Mg70 + 0.37 Opx 2539.

Run T-36   24 kb, 1300°C

	1	1	1	1	3	3	3*
	Cpx	Gt	Cpx	Gt	Cpx	Gt	Gt
SiO_2	47.45	41.22	45.27	40.84	50.78	41.33	41.56
Al_2O_3	16.00	22.81	18.76	22.39	9.05	23.71	22.96
FeO	4.04	9.73	4.58	12.02	5.38	9.85	11.57
MgO	11.41	12.85	10.36	11.62	15.57	17.59	15.95
CaO	20.83	13.15	20.64	12.84	18.93	7.32	7.77
Si	1.713	3.008	1.641	3.011	1.837	2.968	3.009
Al	0.681	1.962	0.802	1.946	0.386	2.007	1.959
Fe	0.122	0.594	0.139	0.741	0.163	0.592	0.700
Mg	0.614	1.398	0.560	1.278	0.839	1.883	1.722
Ca	0.806	1.028	0.802	1.015	0.774	0.563	0.603
Total	3.936	7.990	3.944	7.991	3.999	8.013	7.993
Ca	52.3	34.1	53.4	33.5	42.3	18.5	21.6
Mg	39.8	46.3	37.3	42.1	48.4	62.0	53.8
Fe	7.9	19.7	9.3	24.4	9.4	19.5	24.5
A	30.6	39.4	34.8	39.1	18.2	39.8	38.4
C	36.3	20.6	34.8	20.4	34.6	11.2	13.3
F	33.1	40.0	30.4	40.5	47.2	49.1	48.3
K_D		2.13		2.33		1.62	2.10

* 1.   0.7 Ec Mg70 + 0.3 CaTs

  3.   1.0 Ec Mg70

<u>Run T-47   30 kb, 1200°C</u>

	3	3	5	5	6	6*
	Cpx	Gt	Cpx	Gt	Cpx	Gt
SiO_2	53.52	44.47	53.57	41.44	53.91	40.92
Al_2O_3	2.78	20.37	7.29	21.96	10.37	21.79
FeO	8.28	14.69	7.71	15.98	7.05	16.58
MgO	15.75	12.6	13.25	11.87	10.96	12.34
CaO	19.28	7.58	16.29	8.52	12.51	7.86
Na_2O			1.51		4.7	
Si	1.964	3.244	1.941	3.066	1.937	3.037
Al	0.120	1.751	0.311	1.915	0.439	1.906
Fe	0.254	0.896	0.234	0.989	0.212	1.029
Mg	0.862	1.371	0.716	1.310	0.587	1.365
Ca	0.758	0.593	0.632	0.676	0.482	0.625
Na			0.106		0.328	
Total	3.958	7.855	3.940	7.955	3.985	7.962
Ca	40.5	20.7	40.0	22.7	37.6	20.7
Mg	46.0	47.9	45.3	44.0	45.8	45.2
Fe	13.6	31.3	14.8	33.2	16.5	34.1
A	6.0	38.0	16.5	39.2	25.5	38.7
C	38.0	12.9	33.4	13.8	28.0	12.7
F	56.0	49.2	50.1	47.0	46.5	48.6
K_D		2.21		2.3		2.09

```
*  3.   1.0 Ec Mg70
   5.   0.945 Ec Mg70 + 0.055 Jd
   6.   0.833 Ec Mg70 + 0.167 Jd
```

Run T-52   30 kb, 1200°C   Graphite

	7	7	8	8	9	9	6	6*
	Cpx	Gt	Cpx	Gt	Cpx	Gt	Cpx	Gt
SiO_2	49.84	42.04	51.17	41.76	50.81	43.21	54.08	40.64
Al_2O_3	5.1	20.14	4.23	20.97	9.24	21.37	8.41	23.62
FeO	17.84	23.99	15.03	20.25	9.3	15.84	6.01	13.62
MgO	9.0	4.68	9.29	3.65	9.14	4.23	13.32	17.43
CaO	16.59	8.2	19.98	13.08	19.71	15.15	14.48	4.45
Na	1.33				1.54		3.48	
Si	1.912	3.224	1.943	3.185	1.878	3.236	1.942	2.948
Al	0.231	1.821	0.189	1.886	0.403	1.886	0.358	2.019
Fe	0.573	1.539	0.477	1.292	0.288	0.992	0.180	0.826
Mg	0.515	0.535	0.526	0.415	0.504	0.472	0.713	1.884
Ca	0.682	0.674	0.813	1.069	0.781	1.216	0.557	0.346
Na	0.099				0.110		0.242	
Total	4.012	7.793	3.948	7.847	3.964	7.802	3.992	8.023
Ca	38.5	24.5	44.8	38.5	49.7	45.4	38.4	11.3
Mg	29.1	19.5	28.9	14.9	32.0	17.6	49.1	61.6
Fe	32.4	56.0	26.3	46.9	18.3	37.0	12.4	27.0
A	11.5	39.9	9.4	40.5	20.4	41.3	19.7	39.8
C	34.1	14.7	40.5	22.9	39.5	26.6	30.9	6.8
F	54.4	45.4	50.0	36.6	40.1	32.1	49.4	53.4
K_D		2.59	3.43			3.7		1.73

* 7.   1.0 Ec Mg30
  8.   0.88 Ec Mg30 + 0.12 CaTs
  9.   0.7 Ec Mg30 + 0.3 CaTs
  6.   0.833 Ec Mg70 + 0.167 Jd

Run T-53   30 kb, 1200°C

	10	10	11	11	12	12	3	3*
	Cpx	Gt	Cpx	Gt	Cpx	Gt	Cpx	Gt
SiO_2	51.92	40.82	52.09	41.44	51.73	39.06	52.6	40.69
Al_2O_3	7.94	22.3	6.69	22.5	3.38	22.39	4.76	23.07
FeO	6.96	16.33	9.52	17.52	17.66	22.46	7.8	16.34
MgO	11.21	9.19	11.81	10.81	13.07	8.19	15.26	13.17
CaO	20.33	11.01	18.16	7.53	13.42	7.53	18.71	6.6
Na_2O	1.33		1.48		0.42		0.62	
Si	1.901	3.048	1.920	3.075	1.941	2.981	1.927	3.001
Al	0.245	1.963	0.290	1.968	0.150	2.014	0.201	2.006
Fe	0.213	1.020	0.293	1.087	0.421	1.434	0.239	1.008
Mg	0.612	1.023	0.649	1.196	0.731	0.932	0.833	1.448
Ca	0.798	0.881	0.717	0.598	0.710	0.616	0.734	0.522
Na	0.095		0.106		0.030		0.044	
Total	3.964	7.935	3.975	7.924	3.983	7.977	4.068	7.985
Ca	49.2	30.1	43.2	20.8	38.1	20.7	40.7	17.5
Mg	37.7	35.0	39.1	41.5	39.3	31.3	46.1	48.6
Fe	13.1	34.9	17.7	37.7	22.6	48.1	13.2	33.8
A	17.4	40.2	14.9	40.6	7.4	40.3	10.2	40.3
C	40.6	18.0	36.8	12.3	35.3	12.3	36.5	10.5
F	42.0	41.8	48.3	47.1	57.3	47.4	53.3	49.3
K_D	3.0		2.01		2.67		2.43	

* 10. 0.7 Ec Mg50 + 0.3 CaTs
   11. 0.88 Ec Mg50 + 0.12 CaTs
   12. 1.0 Ec Mg50
    3. 1.0 Ec Mg70

Run T-72   30 kb, 900°C

	7	7	7	8	8	8*
	Cpx	Gt	Gt	Cpx	Gt	Gt
SiO_2	51.3	36.86	37.33	51.3	37.46	38.91
Al_2O_3	0.42	20.84	20.71	0.94	21.93	20.16
FeO	17.47	31.45	28.46	15.53	28.24	26.08
MgO	9.9	3.52	3.48	10.58	3.63	3.96
CaO	20.72	7.18	9.64	21.03	9.12	10.69
Si	1.984	2.949	2.965	1.979	2.963	3.054
Al	0.019	1.966	1.939	0.043	1.994	1.865
Fe	0.565	2.105	1.890	0.501	1.868	1.712
Mg	0.571	0.419	0.412	0.608	0.428	0.464
Ca	0.859	0.615	0.820	0.869	0.773	0.899
Total	3.998	8.054	8.026	4.000	8.026	7.994
Ca	43.1	19.6	26.3	43.9	25.2	29.2
Mg	28.6	13.4	13.2	30.7	14.0	15.1
Fe	28.3	67.0	60.5	25.3	60.8	55.7
A	0.9	38.5	38.3	2.1	39.4	37.8
C	42.6	13.4	16.2	43.0	15.3	18.2
F	56.4	67.0	45.5	54.9	45.3	44.0
K_D		5.07	4.63		5.30	4.48

*   7.   1.0 Ec Mg30
    8.   0.88 Ec Mg30 + 0.12 CaTs

Run T-77   15 kb, 900°C

	8	8	7	7	9	9	9*
	Cpx	Gt	Cpx	Gt	Cpx	Gt	Gt
SiO_2	51.17	37.82	50.76	37.67	52.37	38.66	39.45
Al_2O_3	2.0	21.01	1.06	20.35	4.27	21.24	20.52
FeO	15.24	25.45	18.35	30.09	10.59	23.53	21.93
MgO	10.11	4.06	8.95	3.17	10.76	3.17	4.13
CaO	21.25	11.26	20.57	8.35	21.74	13.1	13.75
Si	1.962	2.972	1.976	3.001	1.954	3.019	3.061
Al	0.090	1.946	0.049	1.911	0.187	1.955	1.877
Fe	0.489	1.672	0.597	2.005	0.330	1.537	1.423
Mg	0.578	0.476	0.519	0.376	0.599	0.369	0.478
Ca	0.873	0.948	0.858	0.713	0.869	1.096	1.143
Total	3.992	8.014	4.000	8.006	3.939	7.976	7.982
Ca	45.0	30.6	43.4	23.0	48.3	36.5	37.6
Mg	29.8	15.4	26.3	12.2	33.3	12.3	15.7
Fe	25.2	54.0	30.2	64.8	18.4	51.2	46.7
A	4.5	38.6	2.4	38.2	9.5	39.4	38.1
C	43.0	18.8	42.4	14.2	43.8	22.1	23.2
F	52.5	42.6	55.2	47.6	46.8	38.4	38.6
K_D		4.16		4.63		7.55	5.4

* 8.   0.88 Ec Mg30 + 0.12 CaTs
  7.   1.0 Ec Mg30
  9.   0.7 Ec Mg30 + 0.3 CaTs

Run T-81   30 kb, 750°C

	9	9	9	9*
	Cpx	Gt	Cpx	Gt
SiO_2	51.66	38.1	53.09	37.39
Al_2O_3	1.15	21.09	0.23	21.2
FeO	11.24	25.87	9.92	26.26
MgO	12.17	2.93	13.22	2.47
CaO	23.21	11.63	23.21	12.41
Si	1.965	2.999	1.998	2.961
Al	0.052	1.957	0.010	1.979
Fe	0.358	1.703	0.312	1.739
Mg	0.690	0.344	0.741	0.292
Ca	0.946	0.981	0.936	1.053
Total	4.009	7.984	3.997	8.024
Ca	47.5	32.4	47.0	34.2
Mg	34.6	11.4	37.3	9.4
Fe	17.9	56.2	15.7	56.4
A	2.5	39.3	0.5	39.1
C	46.3	19.7	46.8	20.8
F	51.2	41.1	52.7	40.1
K_D		9.54		14.15

* 9.   0.7 Ec Mg30 + 0.3 CaTs

Run T-88   30 kb, 900°C

	13	13	13	13	13*
	Cpx	Gt	Cpx	Gt	Opx
SiO_2	52.24	38.23	51.85	38.06	50.81
TiO_2	0.38		0.20		0.18
Al_2O_3	0.40	19.67	1.02	19.44	0.70
Cr_2O_3	0.45	1.26	0.44	1.29	0.34
FeO	13.47	26.46	12.94	26.84	26.62
MgO	13.41	6.53	13.68	6.28	20.06
CaO	19.67	6.83	19.85	7.25	1.32
Si	1.976	3.020	1.959	3.013	1.941
Ti	0.011	0.000	0.006		0.005
Al	0.018	1.832	0.045	1.814	0.031
Cr	0.014	0.079	0.013	0.081	0.010
Fe	0.426	1.748	0.409	1.777	0.850
Mg	0.757	0.769	0.770	0.741	1.143
Ca	0.797	0.578	0.804	0.615	0.054
Total	3.999	8.025	4.001	8.040	4.034
Ca	40.3	18.7	40.5	19.6	2.6
Mg	38.2	24.8	38.9	23.7	55.8
Fe	21.5	56.5	20.6	56.7	41.6
A	0.9	37.2	2.2	36.7	1.5
C	39.9	11.7	39.6	12.4	2.6
F	59.2	51.1	58.1	50.9	95.9
K_D		4.03		4.51	

*   13. Lunar sample 12009

Run T-96   30 kb, 900°C

	14	14	14	12	12*
	Cpx	Gt	Zoisite	Cpx	Gt
SiO_2	52.47	39.53	42.81	53.89	44.5
TiO_2	0.7		0.45		
Al_2O_3	9.92	21.88	30.33	1.57	18.91
Cr_2O_3	0.47	0.37	0.39		
FeO	3.46	15.75	2.08	12.62	22.78
MgO	11.46	9.15	1.89	13.23	5.57
CaO	18.96	12.22	22.07	17.95	7.85
Na_2O	2.22				
Si	1.890	3.001	5.840	2.020	
Ti	0.019	0.000	0.046	0.000	
Al	0.421	1.958	4.878	0.069	
Cr	0.013	0.022	0.042	0.000	
Fe	0.104	1.000	0.237	0.396	
Mg	0.615	1.035	0.384	0.739	
Ca	0.732	0.994	3.226	0.721	
Na	0.155				
Total	3.951	8.009	14.654	3.945	
Ca	50.4	32.8	83.8	38.9	23.51
Mg	42.4	34.2	10.0	39.8	23.2
Fe	7.2	33.0	8.2	21.3	53.3
A	22.5	39.3	55.9	3.6	38.4
C	39.1	19.9	37.0	37.5	14.5
F	38.4	40.8	7.1	58.9	47.1
K_D		5.69			4.29

* 14. Lunar sample 14310
   12. 1.0 Ec Mg50

Run T-110   30 kb, 750°C   Run T-126   30 kb, 750°C

	13	13	13*	14	14	14*
	Cpx	Gt	Opx	Cpx	Gt	Gt
SiO_2	52.52	37.41	52.88	54.38	40.52	38.74
TiO_2	0.17			0.18	0.55	0.90
Al_2O_3	1.17	19.31	1.21	6.75	21.77	21.81
Cr_2O_3	0.38	0.94	0.18	0.57	0.44	0.39
FeO	11.4	27.14	23.0	3.32	17.03	21.69
MnO				0.00	0.00	0.00
MgO	13.61	4.68	21.08	12.55	7.74	5.59
CaO	20.76	7.81	1.67	19.13	11.95	10.24
Na_2O				3.13	0.00	0.00
Si	1.971	3.031	1.976	1.958	3.049	2.983
Ti	0.005	0.000	0.000	0.005	0.031	0.052
Al	0.052	1.844	0.053	0.286	1.931	1.979
Cr	0.011	0.060	0.005	0.016	0.026	0.024
Fe	0.358	1.839	0.719	0.100	1.072	1.397
Mn				0.000	0.000	0.043
Mg	0.762	0.565	1.174	0.674	0.869	0.642
Ca	0.835	0.678	0.067	0.738	0.964	0.845
Na				0.218	0.000	0.000
Total	3.994	8.017	3.994			
Ca	42.7	22.0	3.4	48.8	33.2	29.3
Mg	39.0	18.3	59.9	44.6	29.9	22.3
Fe	18.3	59.7	36.7	6.6	36.9	48.4
A	3.1	38.2	2.9	15.9	39.9	40.7
C	41.4	13.6	3.3	41.0	19.9	17.4
F	55.4	48.2	93.8	43.0	40.1	41.9
K_D		6.93			8.32	14.67

* 13. Lunar sample 12009
  14. Lunar sample 14310

Appendix 4

MINERAL ANALYSIS DATA FOR GRANULITES DESCRIBED IN CHAPTER 4.

Appendix 4

	1	2	3	4	5	6	7
	Gt	Gt	Bi	Cd	Opx	Sa	Cd
SiO_2	38.07	38.74	38.73	49.89	52.38	13.49	50.24
TiO_2	0.10		4.64				
Al_2O_3	22.28	22.67	12.67	34.81	5.47	61.09	34.89
Cr_2O_3	0.15					0.36	
FeO	27.75	24.96	5.67	2.25	15.05	8.33	2.07
MnO	0.17	0.19					
MgO	10.29	12.34	20.41	12.66	27.09	16.47	12.80
CaO	1.04	0.92					
Na_2O				0.31			
K_2O			10.32				
Si	2.933	2.940	5.736	4.923	1.877	0.807	4.943
Ti	0.006		0.516				
Al	2.023	2.027	2.210	4.048	0.231	4.307	4.045
Cr	0.009					0.017	
Fe^{2+}	1.788	1.584	0.702	0.186	0.451	0.417	0.170
Mn	0.011	0.012					
Mg	1.182	1.396	4.504	1.863	1.447	1.468	1.877
Ca	0.086	0.075					
Na				0.060			
K			1.949				
O atoms	8	8	22	18	6	10	18
Mg/Mg+Fe	0.40	0.47	0.87	0.91	0.76	0.79	0.92

1. Gt rim against Bi. Sample 76283335. Gt-Bi-Sill-Qtz assemblage.
2. Gt core. Sample 76283335.
3. Bi rim against Gt. Sample 76283335. Bi core Mg.86
4. Cordierite. Intergrown with Opx-Qtz. Sample 76283350.
5. Opx intergrown with Cd-Qtz. Sample 76283350.
6. Sapphirine with reaction corona of Gt-Cd-Sill separating it from quartz. Sample 76283350.
7. Cd in reaction corona around above Sa.

Appendix 4 cont.

	8	9	10	11	12	13	14
	Gt	Gt	Bi	Sp	Cd	Kf	Cd
SiO_2	39.56	39.74	38.48		50.10	64.65	50.11
TiO_2		5.01					
Al_2O_3	23.24	22.95	13.74	62.60	35.06	19.05	34.78
Cr_2O_3				2.14			
FeO	22.11	23.31	5.66	22.10	2.40		2.62
MnO	0.18	0.19					
MgO	14.76	13.72	20.14	13.16	12.44		12.49
CaO	0.16	0.10					
Na_2O						1.44	
K_2O			10.24			14.54	
Si	2.948	2.976	5.641		4.935	2.970	4.942
Ti			0.552				
Al	2.041	2.025	2.374	1.951	4.071	1.031	4.043
Cr				0.045			
Fe^{2+}	1.378	1.460	0.694	0.489	0.198		0.216
Mn	0.011	0.012					
Mg	1.640	1.531	4.400	0.518	1.826		1.836
Ca	0.013	0.008					
Na							
K			1.915			0.852	
O atoms	12	12	22	4	18	8	
Mg/Mg+Fe	0.54	0.51	0.86	0.52	0.90		0.90

8. Gt in reaction corona around above Sa.
9. Gt rim against Bi (Gt core Mg0.53). Sample 76283351.
10. Bi next to above Gt.
11. Spinel with reaction corona of Cd next to quartz. Sample 76283351.
12. Cd reaction corona around above Sp.
13. K feldspar in intergrowth after osumilite. Sample 76283351.
14. Cd in intergrowth after osumilite. Sample 76283351.

Appendix 4 cont.

	15 Opx	16 Sa	17 Opx	18 Sa	19 Opx	20 Opx	21 Cd
SiO_2	53.15	13.31	49.62	13.01	47.91	49.00	51.11
TiO_2			0.21		0.11		
Al_2O_3	5.78	62.25	8.27	62.95	10.71	8.97	34.31
Cr_2O_3	0.53			0.28		0.11	
FeO	15.51	7.47	17.61	6.57	17.78	18.27	2.84
MnO					0.17		
MgO	25.48	16.44	24.30	17.19	23.34	23.65	11.49
CaO							
Na_2O							
K_2O							
Si	1.904	0.792	1.803	0.771	1.745	1.787	5.038
Ti			0.006		0.003		
Al	0.244	4.366	0.354	4.396	0.460	0.385	3.987
Cr		0.025		0.013		0.003	
Fe^{2+}	0.465	0.372	0.535	0.325	0.542	0.557	0.234
Mn					0.005		
Mg	1.360	1.458	1.316	1.518	1.267	1.286	1.688
Ca							
Na							
K							
O atoms	6	10	6	10	6	6	18
Mg/Mg+Fe	0.75	0.80	0.71	0.82	0.70	0.70	0.88

15. Opx in intergrowth after osumilite. Sample 76283351.
16. Sapphirine with corona of sillimanite separating it from Opx. Sample 76283352.
17. Opx from above assemblage (+ Qtz).
18. Sapphirine 2 in assemblage Sa-Sill-Opx. Sample 76283353.
19. Opx core in above assemblage.
20. Opx rim next to Sa in above assemblage.
21. Cd corona separating Sa 2 and Qtz.

Appendix 4 cont.

	22	23	24	25	26	27	28
	Sa	Sa	Sa	Gt	Bi	Opx	Opx
SiO_2	14.29	14.53	16.64	39.68	38.96	50.48	49.07
TiO_2		0.25			4.21		
Al_2O_3	62.07	60.69	57.71	23.24	13.51	8.37	9.91
Cr_2O_3	0.72	0.66	0.67	0.28	0.60	0.38	0.49
FeO	6.64	7.32	7.69	20.70	4.06	14.11	15.11
MnO				0.59			0.15
MgO	15.69	16.00	17.29	14.80	22.03	26.67	25.27
CaO				0.71			
Na_2O					0.16		
K_2O					9.88		
Si	0.847	0.864	0.988	2.950	5.656	1.806	1.767
Ti		0.011			0.459		
Al	4.337	4.257	4.041	2.036	2.312	0.353	0.420
Cr	0.033	0.030	0.031	0.016	0.069	0.011	0.014
Fe^{2+}	0.329	0.364	0.382	1.287	0.492	0.422	0.455
Mn				0.037			0.005
Mg	1.386	1.419	1.531	1.640	4.767	1.422	1.356
Ca				0.057			
Na					0.045		
K					1.829		
O atoms	10	10	10	12	22	6	6
Mg/Mg+Fe	0.81	0.80	0.80	0.56	0.91	0.77	0.75

22. Sapphirine 2 with above Cd corona. Rim against Cd.
23. Above Sa2 further from rim.
24. Core of above Sa 2.
25. Gt 1 core near Bi inclusion. Gt-Bi-Opx-Qtz. Sample 76283354.
26. Bi 1 inclusion in Gt 1.
27. Opx 1 rim against Gt 1.
28. Opx 1 core.

Appendix 4 cont.

	29	30	31	32	33	34	35
	Gt	Bi	Opx	Gt	Gt	Opx	Cd
SiO_2	39.49	39.07	48.94	39.55	39.81	52.58	50.78
TiO_2		4.26					
Al_2O_3	22.91	13.54	10.39	23.34	23.17	6.35	34.69
Cr_2O_3	0.25	0.36	0.58	0.50	0.34	0.32	
FeO	21.93	4.29	14.61	21.23	20.84	12.83	1.83
MnO	0.67			0.72	0.70		
MgO	13.90	21.21	25.31	13.56	14.31	27.94	12.70
CaO	0.85				0.84		
Na_2O							
K_2O		9.79					
Si	2.956	5.716	1.758	2.952	2.963	1.865	4.985
Ti		0.469					
Al	2.021	2.335	0.440	2.053	2.032	0.265	4.014
Cr	0.015	0.042	0.016	0.029	0.019	0.008	
Fe^{2+}	1.373	0.525	0.439	1.325	1.297	0.380	0.149
Mn	0.042			0.045	0.043		
Mg	1.551	4.625	1.355	1.509	1.587	1.477	1.858
Ca	0.068			0.086	0.066		
Na							
K		1.828					
O atoms	12	22	6	12	12	6	18
Mg/Mg+Fe	0.53	0.90	0.75	0.53	0.55	0.80	0.93

29. Gt 2. Recrystallized Gt intergrown with Bi-Qtz (+Opx). Sample 76283354.
30. Bi 2 from above assemblage.
31. Opx 2 from above assemblage.
32. Gt 3. Rim next to Cd-Hy intergrowth (after Gt-Qtz). Sample 76283354.
33. Gt 3 core.
34. Opx 3 in Cd-Opx intergrowth to Gt 3.
35. Cd in above intergrowth.

Appendix 4 cont.

	36	37	38	39	40	41	42
	Gt	Bi	Gt	Opx	Opx	Cd	Gt
SiO_2	39.29	38.77	39.15	50.82	48.17	49.90	40.06
TiO_2		3.68					
Al_2O_3	22.91	14.01	22.91	8.72	11.34	34.85	23.18
Cr_2O_3	0.26	0.37	0.18	0.40	0.43		
FeO	21.77	3.67	22.10	13.28	14.71	1.82	20.13
MnO	0.54		0.76		0.13		0.65
MgO	14.17	22.03	13.94	26.78	25.22	13.12	14.87
CaO	0.78		0.71				0.84
Na_2O							
K_2O		10.44					
Si	2.942	5.654	2.938	1.809	1.732	4.914	2.971
Ti		0.404					
Al	2.022	2.408	2.026	0.366	0.481		2.026
Cr	0.016	0.043	0.011	0.011	0.012		
Fe^{2+}	1.363	0.448	1.387	0.395	0.442	0.150	1.248
Mn	0.034		0.048		0.004		0.041
Mg	1.581	4.789	1.560	1.421	1.351	1.925	1.643
Ca	0.063		0.057				0.067
Na						0.059	
K		1.942					
O atoms	8	22	8	6	6	18	12
Mg/Mg+Fe	0.54	0.91	0.53	0.78	0.75	0.93	0.57

36. Gt. Sample 76283355.
37. Bi in above Gt. Gt-Bi assemblage.
38. Gt rim against Opx. Sample 76283355.
39. Opx rim against Cd and above Gt.
40. Opx core.
41. Cd rim between above Gt and Opx.
42. Gt. Gt-Os assemblage (now separated by osumilite intergrowth).
    Sample 76283358.

Appendix 4 cont.

	43	44	45	46	47	48	49
	Os	Os	Opx	Cpx	Opx	Cpx	Gt
SiO_2	61.51	61.54	51.14	50.81	50.23	48.77	39.18
TiO_2			0.44	0.67		0.78	
Al_2O_3	23.57	23.60	1.56	3.85	2.01	5.59	22.58
Cr_2O_3			0.29	0.73	0.18	0.45	0.15
FeO	1.35	1.34	23.45	8.81	25.83	12.43	24.70
MnO			0.40		0.49	0.28	0.24
MgO	8.61	8.67	21.62	13.86	18.93	12.15	12.28
CaO			1.10	21.27	2.02	19.52	0.86
Na_2O	0.60	0.45			0.30		
K_2O	4.35	4.40					
Si	10.138	10.139	1.925	1.891	1.921	1.842	2.965
Ti			0.013	0.018		0.022	
Al	4.579	4.583	0.069	0.169	0.091	0.248	2.014
Cr			0.009	0.021	0.005	0.013	0.009
Fe^{2+}	0.186	0.185	0.738	0.274	0.826	0.392	1.564
Mn			0.013		0.016	0.009	0.016
Mg	2.116	2.128	1.213	0.769	1.079	0.684	1.385
Ca			0.045	0.848	0.083	0.790	0.070
Na	0.191	0.143			0.022		
K	0.915	0.924					
O atoms	30	30	6	6	6	6	8
Mg/Mg+Fe	0.92	0.92	0.62	0.74	0.57	0.64	0.47

43. Os 1 with above Gt.
44. Os 2 in quartz, surrounded by osumilite intergrowth.
45. Opx core. Qtz-bearing mafic granulite. Sample 76283259.
46. Cpx core. Sample 76283259. Coexisting Plag An89.
47. Opx core. Sample 76283261. Cpx-Opx-Plag-Mt-Hbld.
48. Cpx core. Sample 76283261.
49. Gt core. Sample 76283361. Gt-Bi-Sill-Qtz assemblage.

Appendix 4 cont.

	50	51	52	53	54	55	56
	Gt	Bi	Kf	Gt	Sp	Cd	Opx
SiO_2	38.49	38.95	65.43	39.96		50.13	50.20
TiO_2		3.25					0.11
Al_2O_3	22.44	14.00	19.02	23.32	60.82	34.48	8.21
Cr_2O_3	0.15			0.15	3.65		0.26
FeO	26.99	5.55		20.92	21.85	2.66	15.01
MnO	0.33			0.36			
MgO	10.18	21.19		14.31	12.48	12.21	26.13
CaO	1.16	0.21	0.91	0.68			0.07
Na_2O			1.71				
K_2O		10.15	12.94				
Si	2.955	5.695	2.985	2.970		4.957	1.804
Ti		0.358					0.003
Al	2.030	2.413	1.022	2.042	1.913	4.018	0.348
Cr	0.092			0.009	0.077		0.007
Fe^{2+}	1.733	0.679		1.300	0.488	0.220	0.451
Mn	0.022			0.023			
Mg	1.164	4.618		1.585	0.496	1.800	1.400
Ca	0.095	0.032	0.044	0.054			0.003
Na			0.151				
K		1.893	0.753				
O atoms	8	22	8	12	4	18	6
Mg/Mg+Fe	0.40	0.87		0.55	0.50	0.89	0.76

50. Gt rim next to Bi. Sample 76283361.
51. Bi rim next to Gt. Bi core Mg .86. Sample 76283361.
52. K feldspar. Gt-Kf-Sp-Sill (+ secondary Cd). Sample 76283262.
53. Gt from above assemblage.
54. Sp from above assemblage.
55. Cd rim with Kf around above Sp.
56. Opx core. Gt-Opx pair. Sample 76283364.

Appendix 4 cont.

	57	58	59	60	61	62	63
	Opx	Gt	Gt	Plag	Kf	Kf	Plag
SiO_2	50.91	39.46	39.36	54.26	64.04	64.66	59.69
TiO_2							
Al_2O_3	7.50	23.21	23.02	29.20	19.18	19.03	25.34
Cr_2O_3	0.21	0.17	0.20				
FeO	14.38	20.81	21.10				
MnO		0.47	0.52				
MgO	27.01	14.39	14.17				
CaO		1.48	1.54	10.84	0.18	0.19	6.57
Na_2O				5.35	1.08	1.62	8.08
K_2O				0.25	15.37	14.50	0.32
Si	1.823	2.941	2.941	2.449	2.957	2.973	2.664
Ti							
Al	0.316	2.031	2.027	1.553	1.044	1.031	1.333
Cr	0.006	0.010	0.012				
Fe^{2+}	0.431	1.297	1.319				
Mn		0.030	0.033				
Mg	1.441	1.598	1.578				
Ca		0.118	0.123	0.524	0.009	0.010	0.314
Na				0.468	0.097	0.145	0.699
K				0.014	0.905	0.850	0.018
O atoms	6	12	12	8	8	8	8
Mg/Mg+Fe	0.77	0.55	0.55				

57. Opx rim at Gt.
58. Gt rim in above assemblage.
59. Gt core.
60. Plagioclase. Sample 76283364.
61. K feldspar, not in contact with above plag.
62. K feldspar host with exsolved plagioclase. Gt=Kf-Plag-Sp-Ilm
    assemblage. Sample 76283265.
63. Plag exsolved from above Kf.

Appendix 4 cont.

	64	65	66	67	68	69	70
	Plag	Kf	Sp	Ilm	Sa	Cd	Gt
SiO_2	59.93	64.80			13.02	50.00	39.42
TiO_2				52.08			
Al_2O_3	25.44	18.95	63.69	0.15	63.41	35.24	23.63
Cr_2O_3			1.03	0.11	0.33		0.13
FeO			21.47	43.57	6.21	2.12	20.83
MnO				0.17			0.31
MgO			13.81	2.43	17.03	12.65	14.84
CaO	6.39	0.00					0.84
Na_2O	7.96	0.84					
K_2O	0.29	15.42					
Si	2.670	2.984			0.770	4.920	2.929
Ti				0.987			
Al	1.336	1.028	1.971	0.004	4.419	4.087	2.070
Cr			0.021	0.002	0.016		0.008
Fe^{2+}			0.471	0.918	0.307	0.174	1.294
Mn				0.004			0.019
Mg			0.540	0.091	1.501	1.855	1.644
Ca	0.305						0.067
Na	0.687	0.075					
K	0.016	0.906					
O atoms	8	8	4	3	10	18	12
Mg/Mg+Fe					0.83	0.91	0.56

64. Recrystallized, separate plagioclase.
65. Recrystallized, separate K feldspar.
66. Spinel.
67. Ilmenite intergrown with above spinel.
68. Sapphirine with reaction rim of Cd where surrounded by osumilite intergrowth (after osumilite). Sample 76283365.
69. Cd corona around above Sa.
70. Gt surrounded by osumilite intergrowth.

Appendix 4 cont.

	71	72	73	74	75	76	77
	Opx	Opx	Opx	Opx	Sa	Sa	Gt
SiO_2	48.50	53.19	50.89	50.51	12.81	14.82	39.38
TiO_2	0.11						
Al_2O_3	11.04	4.77	6.52	7.86	63.39	60.48	23.30
Cr_2O_3	0.33				0.96	0.72	
FeO	14.71	14.94	18.24	17.75	7.46	7.85	23.30
MnO							0.68
MgO	24.98	27.10	24.36	23.88	14.69	15.47	13.05
CaO							0.28
Na_2O							
K_2O							
Si	1.743	1.903	1.852	1.832	0.763	0.884	2.957
Ti	0.003						
Al	0.468	0.201	0.279	0.336	4.457	4.253	2.062
Cr	0.009					0.033	
Fe^{2+}	0.442	0.447	0.555	0.538	0.372	0.391	1.463
Mn							0.043
Mg	1.338	1.445	1.321	1.291	1.305	1.375	1.460
Ca							0.022
Na							
K							
O atoms	6	6	6	6	10	10	12
Mg/Mg+Fe	0.75	0.76	0.70	0.71	0.78	0.78	0.50

71. Large primary Opx sitting in osumilite intergrowth,
72. Fine grained Opx forming part of Cd-Kf-Qtz-Opx intergrowth surrounding above Opx.
73. Opx rim. Opx-Sa association with thin corona of Cd-Sill between the two. Sample 76283367.
74. Opx core.
75. Sa rim.
76. Sa core. There is a gradual change in composition from core to rim.
77. Large Gt 1 core. Sample 76283368.

Appendix 4 cont.

	78	79	80	81	82	83	84
	Gt	Cd	Cd	Sa	Gt	Cd	Cd
SiO_2	38.63	50.76	50.51	13.20	39.34	50.02	49.89
TiO_2							
Al_2O_3	22.66	34.67	34.43	62.14	23.05	34.93	34.79
Cr_2O_3				0.18			
FeO	26.01	2.17	3.29	7.42	23.34	2.17	2.67
MnO	0.80				0.30		
MgO	11.51	12.12	11.51	17.06	13.86	12.89	12.21
CaO	0.39				0.10		
Na_2O							
K_2O							
Si	2.946	4.996	4.996	0.785	2.951	4.925	4.931
Ti							
Al	2.036	4.022	4.014	4.357	2.038	4.053	4.052
Cr							
Fe^{2+}	1.659	0.178	0.272	0.369	1.464	0.178	0.221
Mn	0.051				0.019		
Mg	1.308	1.778	1.696	1.513	1.549	1.891	1.799
Ca	0.031				0.008		
Na							
K							
O atoms	12	18	18	10	12	18	18
Mg/Mg+Fe	0.44	0.91	0.86	0.80	0.51	0.91	0.89

78. Above Gt 1, rim next to large Cd.
79. Cd 1 rim at above Gt.
80. Cd 1 core for above Cd.
81. Sapphirine with Gt-Cd-Sill reaction corona separating Sa from Qtz.
82. Gt 2 in reaction corona around Sa.
83. Cd 2 in reaction corona around Sa.
84. Cd 3 in Cd-Kf-Qtz-Opx intergrowth after osumilite.

Appendix 4 cont.

	85 Opx	86 Gt	87 Gt	88 Cd	89 Cd	90 Opx
SiO_2	51.31	39.61	39.66	50.24	50.64	51.26
TiO_2						
Al_2O_3	5.94	23.28	23.31	34.92	34.97	7.52
Cr_2O_3			0.13			0.12
FeO	17.52	20.44	20.39	1.95	2.40	16.36
MnO		0.38	0.46			
MgO	25.22	15.03	14.77	12.77	11.82	24.75
CaO		1.25	1.19			
Na_2O						
K_2O						
Si	1.862	2.942	2.947	4.943	4.986	1.847
Ti						
Al	0.254	2.038	2.047	4.049	4.057	0.319
Cr			0.008			
Fe^{2+}	0.532	1.270	1.267	0.161	0.197	0.493
Mn		0.024	0.029			
Mg	1.364	1.664	1.636	1.872	1.734	1.329
Ca		0.100	0.094			
Na						
K						
O atoms	6	12	12	18	18	6
Mg/Mg+Fe	0.72	0.57	0.56	0.92	0.90	0.73

85. Opx in above intergrowth.
86. Large Gt core. Sample 76283370.
87. Above Gt rim against Cd.
88. Cd 1 next to above Gt.
89. Cd 2 part of Cd-Kf-Qtz-Opx intergrowth after osumilite.
90. Opx part of above intergrowth.

REFERENCES

Akella, J., 1976. Garnet-pyroxene equilibria in the system

$CaSiO_3$-$MgSiO_3$-Al_2O_3 and in a natural mineral mixture.

Am. Mineral., 61, pp. 589-598.

Arima, M., 1978. Phase Equilibria in the System $MgSiO_3$-Al_2O_3-Fe_2O_3

at high temperatures and pressures, with special reference

to the solubility of Al_2O_3 and Fe_2O_3 in enstatite.

J. Fac. Sci. Hokkaido Univ., Ser. IV, 18, pp. 305-338.

Banno, S., 1970. Classification of eclogites in terms of their

physical conditions of origin. *Phys. Earth Planet. Int.*,

3, pp. 405-421.

_____ and Green, D.H., 1968. Experimental studies on eclogites:

The roles of magnetite and acmite in eclogitic assemblages.

Chem. Geol., 3, pp. 21-32.

_____ and Matsui, Y., 1965. Eclogite types and partition of

Mg, Fe and Mn between clinopyroxene and garnet. *Proc. Jap.*

Acad., 41, pp. 716-721.

Barrow, G., 1893. On an intrusion of muscovite-biotite gneiss

in the southeastern Highlands of Scotland. *Geol. Soc. Lond.*,

Quart. J., 49, pp. 330-358.

_____ 1912. On the geology of lower Deeside and the

southern Highland border. *Geol. Ass. Lond., Proc.*, 23,

pp. 268-284.

Battey, M.H., and Davidson, W., 1977. Exsolution of plagioclase

from clinopyroxene in a pyroxenite from Jotunheimen, Norway.

Min. Mag., 41, pp. 513-518.

Berg, J.H., 1977. Dry Granulite Mineral Assemblages in the

Contact Aureoles of the Nain Complex, Labrador. *Contrib.*

Mineral. Petrol., 64, pp. 33-52.

Berg, J.H., 1977. Regional geobarometry in the contact aureoles of the Anorthositic Nain Complex, Labrador. *J. Petrol.*, 18, pp. 399-430.

_____ and Wheeler, E.P., II, 1976. Osumilite of deep-seated origin in the contact aureole of the Anorthositic Nain Complex, Labrador. *Am. Miner.* 61, pp. 29-37.

Birch, F., 1952. Elasticity and constitution of the earth's interior. *J. Geophys. Res.*, 57, pp. 227-286.

Black, P.M., 1974. Mineralogy of New Caledonian metamorphic rocks. III. Pyroxenes and major element partitioning between coexisting pyroxenes, amphiboles and garnets from the Ouéga district. *Contrib. Mineral. Petrol.*, 45, pp. 281-288.

_____ 1977. Regional high-pressure metamorphism in New Caledonia: Phase equilibria in the Ouéga district. *Tectonophysics*, 43, pp. 89-107.

Blümel, P., Schreyer, W., 1977. Phase relations in pelitic and psammitic gneisses of the sillimanite-potash feldspar and cordierite-potash feldspar zones in the Moldanubicum of the Lam-Bodenmais Area, Bavaria. *J. Petrol.*, 18, 431-459.

Boyd, F.R., 1973. A pyroxene geotherm. *Geochim. et Cosmochim. Acta*, 37, pp. 2533-2546.

_____ and Schairer, J.F., 1964. The system $MgSiO_3-CaMgSi_2O_6$. *J. Petrol.*, 5, 275-309.

Brey, G., and Green, D.H., 1975. The role of CO_2 in the genesis of olivine melilitite. *Contrib. Mineral. Petrol.*, 49, pp. 93-103.

Brothers, R.N., 1974. High-pressure schists in northern New Caledonia. *Contrib. Mineral. Petrol.*, 46, pp. 109-127.

Brown, G.E., and Gibbs, G.V., 1969. Refinement of the crystal
structure of osumilite. *Am. Mineral.*, 54, pp. 101-116.

Carmichael, I.S.E., 1967. The iron-titanium oxides of salic
volcanic rocks and their associated ferromagnesium silicates.
Contr. Mineral. Petrol., 14, pp. 36-64.

Cawthorn, R.G. and Collerson, K.D., 1974. The recalculation of
pyroxene end-member parameters and the estimation of ferrous
and ferric iron content from electron microprobe analyses.
Am. Mineral., 59, pp. 1203-1208.

Chatterjee, N.D., and Schreyer, W., 1972. The reaction enstatite+
sillimanite=sapphirine+quartz in the system $MgO-Al_2O_3-SiO_2$. *Contrib.*
Mineral. Petrol., 36, pp. 49-62.

_____ and Johannes, W., 1974. Thermal stability and
standard thermodynamic properties of synthetic $2M_1$- muscovite,
$KAl_2[AlSi_3O_{10}(OH)_2]$. *Contrib. Mineral. Petrol.*, 48, pp. 89-114.

Chernosky, Jr., J.V., 1974. The upper stability of chlinochlore
and the free energy of formation of Mg-cordierite. *Am. Mineral.*,
59, pp. 496-507.

Chinner, G.A., and Dixon, P.D., 1973. Irish osumilite.
Mineral. Mag., 39, pp. 189-192.

Church, W.R., 1967. Eclogites. In: Basalts. H.H.Hess (Ed.).
Wiley-Interscience.

Clarke, J.R., and Papike, J.J., 1968. Crystal-chemical
characterization of omphacites. *Am. Mineral.*, 53, pp. 840-868.

Coleman, R.G., Lee, D.E., Beatty, L.B., and Brannock, W.W., 1965.
Eclogites and eclogites: their differences and similarities.
Geol. Soc. Am. Bull., 76, pp. 483-508.

Conquéré, F., 1977. Petrologie des pyroxénites litées dans les complexes ultramafiques de l'Ariège (France) et autre gisements de lherzolite à spinelle. I. Compositions mineralogiques et chimiques, évolution des conditions d'équilibre des pyroxénites. *Bull. Soc. fr. Minéral Cristallogr.*, 100, pp. 42-80.

Crohn, P.W., 1959. A contribution to the geology and glaciology of the western part of Australian Antarctic Territory. *Bur. Miner. Resour. Aust. Bull.*, 52.

Currie, K.L., 1971. The reaction 3 cordierite = 2 garnet + 4 sillimanite + 5 quartz as a geological thermometer in the Opinicon Lake region, Ontario. *Contrib. Mineral. Petrol.*, 33, pp. 215-266.

_____ 1974. A note on the calibration of the garnet-cordierite geothermometer and geobarometer. *Contrib. Mineral. Petrol.*, 44, pp. 35-44.

Dallwitz, W.B., 1968. Co-existing sapphirine and quartz in granulite from Enderby Land, Antarctica. *Nature*, 219, pp. 476-477.

Davidson, L.R., 1968. Variation in ferrous iron-magnesium distribution coefficients of metamorphic pyroxenes from Quairading, Western Australia. *Contrib. Mineral. Petrol.*, 19, pp. 239-259.

Davis, B.T.C., and Boyd, F.R., 1966. The join $Mg_2Si_2O_6$-$CaMgSi_2O_6$ at 30 kilobars pressure and its application to pyroxenes from kimberlites. *J. Geophys. Res.*, 71, pp. 3567-3576.

Deer, W.A., Howie, R.A., Zussman, J., 1962. Rock-forming minerals. Longmans, London.

England, P.C., and Richardson, S.W., 1977. The influence of erosion upon the mineral facies of rocks from different metamorphic environments. *J. Geol. Soc. Lond.*, 134, pp. 201-213.

Eskola, P., 1920. The mineral facies of rocks. *Norsk. Geol. Tiddskr.*, 6, pp. 143-194.

_____ 1939. Die metamorphen Gesteine, pp. 263-407. In: Barth, T.F.W., Correns, C.W., and Eskola, P., Die Ertstehung der Gesteine, 442p., Berlin: Springer.

Ewart, A., and Stipp, J.J., 1968. Petrogenesis of the volcanic rocks of the central North Island, New Zealand, as indicated by a study of Sr^{87}/Sr^{86} ratios, and Sr, Rb, K, U and Th abundances. *Geochim. Cosmochim. Acta*, 32, pp. 699-735.

_____ Hildreth, W., and Carmichael, I.S.E., 1975. Quaternary acid magma in New Zealand. *Contrib. Mineral. Petrol.*, 51, pp. 1-27.

Ferry, J.M., and Spear, F.S., 1978. Experimental calibration of the partitioning of Fe and Mg between biotite and garnet. *Contrib. Mineral. Petrol.*, 66, pp. 113-117.

Gable, D.J., and Sims, P.K., 1969. Geology and regional metamorphism of some high-grade cordierite gneisses, Front Range, Colorado. *Geol. Soc. Am. Spec. Pap.* 128.

Ganguly, J., 1973. Activity-composition relation of jadeite in omphacite pyroxene: Theoretical deductions. *Earth Planet. Sci. Letters*, 19, pp. 145-153.

_____ 1976. The energetics of natural garnet solid solution. II. Mixing of the calcium-silicate end members. *Contrib. Mineral. Petrol.*, 55, pp. 81-90.

Ganguly, J., and Kennedy, G.C., 1974. The energetics of natural
garnet solid solution. I. Mixing of the alumino-silicate
end-members. *Contrib. Mineral. Petrol.*, 48, pp. 137-148.

Gibbs, G.V., 1966. The polymorphism of cordierite I: The
crystal structure of low cordierite. *Am. Mineral.*, 51,
pp. 1068-1087.

Gjelsvik, T., 1952. Metamorphosed dolerites in the gneiss area
of Sunmore on the west coast of southern Norway. *Norsk
geologisk tidsskrift*, 30, pp. 33-134.

Goldman, D.S., and Rossman, G.R., 1978. The site distribution of
iron and anomalous biaxiality in osumilite. *Am. Miner.* 63,
pp. 490-498.

Goldschmidt, V.M., 1911. Die Kontaktmetamorphose in Kristiania-
gebiet. *Kristiania Videnk, Skr., I, Math-Naturv., Kl.,* 11.

Grant, J.A., and Weiblen, P.W., 1971. Retrograde zoning in garnet
near the second sillimanite isograd. *Am. J. Sci.,* 270,
pp. 281-296.

Green, D.H., 1966. The origin of the "eclogites" from Salt Lake
Crater, Hawaii. *Earth Plan. Sci. Letters.,* 1, pp. 414-420.

_____ 1969. Mineralogy of two Norwegian eclogites. In:
Contributions to physico-chemical petrology, vol. 1, pp.
37-44. Korzhinskii volume (in Russian).

_____ 1970. The origin of basaltic and nephelinitic magmas.
Trans. Leicester Lit. Phil. Soc., 64, pp. 28-54.

_____ 1973. Experimental melting studies on a model upper
mantle composition at high pressure under water-saturated and
water-undersaturated conditions. *Earth Planet. Sci. Letters,*
19, pp. 37-53.

Green, D.H., 1975. Genesis of Archaean peridotitic magmas and constraints on Archaean geothermal gradients and tectonics. *Geology*, January, pp. 15-18.

_____ and Hibberson, W., 1970. Experimental duplication of conditions of precipitation of high-pressure phenocrysts in a basaltic magma. *Phys. Earth Planet. Interiors*, 3, pp. 247-254.

_____ and Ringwood, A.E., 1967. The genesis of basaltic magmas. *Contrib. Mineral. Petrol.*, 15, pp. 103-190.

_____ 1967. An experimental investigation of the gabbro to eclogite transformation and its petrological applications. *Geochim. et Cosmochim. Acta*, 31, pp. 767-833.

_____, Ware, N.G., and Hibberson, W.O., 1972. Experimental petrology and petrogenesis of Apollo 14 basalts. *Proc. Third Lunar Sci. Conf. (Suppl. 3, Geochim. et Cosmochim. Acta)* 1, pp. 197-206.

_____, Ware, N.G., Hibberson, W.O., and Major, A., 1971. Experimental petrology of Apollo 12 Basalts: Part 1, Sample 12009. *Earth Planet. Sci. Letters*, 13, pp. 85-96.

Green, T.H., 1967. An experimental investigation of sub-solidus assemblages formed at high pressure in high-alumina basalt, kyanite eclogite and grospydite compositions. *Contrib. Mineral. Petrol.*, 16, pp. 84-114.

_____, Ringwood, A.E., and Major, A., 1966. Friction effects and pressure calibration in a piston-cylinder apparatus at high pressure and temperature. *J. Geophys. Res.*, 71, pp. 3589-3594.

Grew, E.S., 1978. Precambrian basement at Molodezhnaya station, East Antarctica. *Geol. Soc. Am. Bull.*, 89, pp. 801-813.

Griffin, W.L., 1971. Genesis of coronas in anorthosites of the Upper Jotun Nappe, Indre Sogn, Norway. *J. Petrol.*, 12, pp. 219-243.

Hariya, Y., and Kennedy, G.C., 1968. Equilibrium study of anorthite under high pressure and high temperature. *Am. J. Sci.*, 266, pp. 193-203.

Hearn, B.C., Jr., and Boyd, F.R., 1975. Garnet peridotite xenoliths in a Montana, U.S.A., kimberlite. *Phys. and Chem. of the Earth*, 9, pp. 247-255.

Hensen, B.J., 1971. Theoretical phase relations involving cordierite and garnet in the system $MgO-FeO-Al_2O_3-SiO_2$. *Contrib. Mineral. Petrol.*, 33, pp. 191-214.

_____ 1973. Pyroxenes and garnets as geothermometers and barometers. *Ann. Rep. Dir. Carnegie Inst. Wash. Year Book*, 72, pp. 527-534.

_____ 1977. Cordierite-garnet bearing assemblages as geothermometers and barometers in granulite facies terranes. *Tectonophysics*, 43, 73-88.

_____ 1977. The stability of osumilite in high grade metamorphic rocks. *Contr. Mineral. Petrol.*, 64, pp. 197-204.

_____ and Essene, E.J., 1971. Stability of pyrope-quartz in the system $MgO-Al_2O_3-SiO_2$. *Contrib. Mineral. Petrol.*, 30, pp. 72-83.

_____ and Green, D.H., 1971. Experimental study of cordierite and garnet in pelitic compositions at high pressures and temperatures. I. Compositions with excess aluminosilicate. *Contrib. Mineral. Petrol.*, 33, pp. 309-330.

Hensen, B.J., and Green, D.H., 1972. Experimental study of cordierite and garnet in pelitic compositions at high pressures and temperatures. II. Compositions without excess aluminosilicate. *Contrib. Mineral. Petrol.*, 35, pp. 331-354.

_____ 1973. Experimental study of the stability of cordierite and garnet in pelitic compositions at high pressures and temperatures. III. Synthesis of experimental data and geological applications. *Contrib. Mineral. Petrol.*, 38, pp. 151-166.

_____, Schmid, R., and Wood, B.J., 1975. Activity-Composition relationships for pyrope-grossular garnet. *Contrib. Mineral. Petrol.*, 51, pp. 161-166.

Hermans, G.A.E.M., Hakstege, A.L., Jansen, J.B.H., and Poorter, R.P.E., 1976. Sapphirine occurrence near Vikeso in Rogaland, Southwestern Norway. *Norsk. Geologisk Tidsskrift*, 56, pp. 397-412.

Herzberg, C.T., 1978a. Pyroxene geothermometry and geobarometry: experimental and thermodynamic evaluation of some subsolidus phase relations involving pyroxenes in the system $CaO-MgO-Al_2O_3-SiO_2$. *Geochim. et Cosmochim. Acta*, 42, pp. 945-957.

_____1978b. The bearing of phase equilibria in simple and complex systems on the origin and evolution of some well-documented garnet-websterites. *Contrib. Mineral. Petrol.*, 66, pp. 375-382.

Hess, P.C., 1969. The metamorphic paragenesis of cordierite in pelitic rocks. *Contrib. Mineral. Petrol.*, 24, pp. 191-207.

Hewins, R.G., 1975. Pyroxene geothermometry of some granulite facies rocks. *Contrib. Mineral. Petrol.*, 50, pp. 205-209.

Holdaway, M.J., 1976. Mutual compatibility relations of the Fe^{+2}-Mg-Al silicates at $800^{\circ}C$ and 3 kb. *Am. J. Sci.*, 276, pp. 285-308.

_____, Lee, S.M., 1977. Fe-Mg cordierite stability in high-grade pelitic rocks based on experimental, theoretical, and natural observations. *Contrib. Mineral. Petrol.*, 63, pp. 175-198.

Hollister, L.S., 1977. The reaction forming cordierite from garnet, the Khtada Lake metamorphic complex, British Columbia. *Can. Mineral.*, 15, pp. 217-229.

Hutcheon, I., Froese, E., and Gordon, T.M., 1974. The assemblage quartz-sillimanite-garnet-cordierite as an indicator of metamorphic conditions in the Daly Bay Complex, N.W.T. *Contrib. Mineral. Petrol.*, 44, pp. 29-34.

Irving, A.J., 1974. Geochemical and high pressure experimental studies of garnet pyroxenite and pyroxene granulite xenoliths from the Delegate Basaltic Pipes, Australia. *J. Petrol.*, 15, pp. 1-40.

Ito, K., and Kennedy, G.C., 1968. Melting and phase relations in the plane tholeiite-lherzolite-nepheline basanite to 40 kilobars with geological implications. *Contrib. Mineral. Petrol.*, 19, pp. 177-211.

Kamenev, E.N., 1972. Geological structure of Enderby Land. In: R.J. Adie (Ed.). Antarctic Geology and Geophysics. Universitetsforlaget, Oslo, pp. 579-583.

_____ 1975. The geology of Enderby Land (in Russian). Acad. Sci. USSR, Comm. on Ant. Res. Rep. 14.

Khan, A.A., Baur, W.H., and Forbes, W.C., 1972. Synthetic magnesium merrihueite, dipotassium pentamagnesium dodecasilicate: A tetrahedral magnesiosilicate framework crystal structure. *Acta Crystallogr.*, B28, pp. 267-272.

Kleppa, O.J., and Newton, R.C., 1975. The role of solution calorimetry in the study of mineral equilibria. *Fortschr. Miner. Spec. Issue.* IMA-Papers 9th melting, Berlin, Regensburg, pp. 3-20.

Koriakine, E.D., Stroiev, P.A., and Frolov, A.I., 1970. Results of gravity measurements in Enderby Land, East Antarctica. In: Fedinskii, V.V., ed. Gravity measurements at sea - Collection of Articles No. 5, Moscow, University of Moscow, pp. 83-95 (In Russian).

Kushiro, I., 1962. Clinopyroxene solid solutions Pt. 1. The $CaAl_2SiO_6$ component. *Jap. J. Geol. Geog.*, 33, pp. 213-220.

_____ 1969. Clinopyroxene solid solutions formed by reactions between diopside and plagioclase at high pressures. *Mineral. Soc. Am. Spec. Pap.* 2, pp. 179-191.

_____, Shimizu, N., and Nakamura, Y., 1972. Compositions of coexisting liquid and solid phases formed upon melting of natural garnet and spinel lherzolites at high pressures: a preliminary report. *Earth Planet. Sci. Letters,* 14, pp. 19-25.

_____, Syono, Y., and Akimoto, S., 1967. Effect of pressure on garnet-pyroxene equilibrium in the system $MgSiO_3$-$CaSiO_3$-Al_2O_3. *Earth Planet. Sci. Letters,* 2, pp. 460-464.

_____ and Yoder, Jr., H.S., 1966. Anorthite-forsterite and anorthite-enstatite reactions and their bearing on the basalt-eclogite transformation. *J. Petrol.,* 7, pp. 337-362.

Langer, K., and Schreyer, W., 1969. Infrared and powder X-ray diffraction studies of the polymorphism of cordierite, $Mg_2Al_4Si_5O_{18}$. *Am. Mineral.*, 54, pp. 1442-1459.

Lindsley, D.H., King, H.E. Jr., Turnock, A.C., 1974a. Compositions of synthetic augite and hypersthene coexisting at 810^oC : Application to pyroxenes from lunar highland rocks. *Geophys. Res. Lett.*, 1, pp. 134-136.

_____ 1974b. Phase relations in the pyroxene quadrilateral at 980^oC and 15 kb. *Geol. Soc. Am. Abstracts with Programs*, 6, p. 846.

Lovering, J.F., and White, A.J.R., 1969. Granulitic and eclogitic inclusions in basic pipes at Delegate, Australia. *J. Petrol.*, 21, pp. 9-52.

Luth, W.C., 1969. The systems $NaAlSi_3O_8$-SiO_2 and $KAlSi_3O_8$-SiO_2 to 20 kb and the relationship between H O content, P_{H_2O} and P_T in granitic magmas. *Am. J. Sci., Schairer Vol.* 267-A, pp. 325-341.

Maijer, C., Jansen, J.B.H., Wevers, J., and Poorter, R.P.E., 1977. Osumilite, a mineral new to Norway. Contribution to the Mineralogy of Norway, No. 63. *Norsk Geologisk Tidsskrift*, 57, pp. 187-188.

Marakushev, A.A., and Kudryavtsev, V.A., 1965. Hypersthene-sillimanite paragenesis and its petrological implications. *Dokl. Akad. Nauk. SSSR.* 164, pp. 145-148.

McCallister, R.H., Finger, L.W., and Ohashi, Y., 1976. Intra-crystalline Fe^{2+}-Mg equilibria in three natural Ca-rich clinopyroxenes. *Am. Mineral.*, 61, pp. 671-676.

McLelland, J.M., and Whitney, P.R., 1977. The origin of garnet
in the anorthosite-charnockite suite of the Adirondacks.
Contrib. Mineral. Petrol., 60, pp. 161-181.

McLeod, I.R., 1959. Report on geological and glaciological work
by the 1958 Australian National Antarctic Research Expedition.
Bur. Miner. Resour. Aust. Rec. 1959/131 (unpubl.).

_____ 1964. An outline of the geology of the sector from
longitude 45° to 80°E, Antarctica, in R.J. Adie (Ed.),
Antarctic Geology. North Holland, Amsterdam, pp. 237-247.

_____, Trail, D.S., Cook, P.J., and Wallis, G.R., 1966.
Geological work in Antarctica, January to March, 1965.
Bur. Miner. Resour. Aust. Rec. 1966/9 (unpubl.).

Mercy, E.L.P., and O'Hara, M.J., 1968. Nepheline normative
eclogite from Loch Duich, Ross-shire. *Scot. J. Geol.*, 4,
pp. 1-9.

Meyer, H.O.A., and Boyd, F.R., 1972. Composition and origin of
crystalline inclusions in natural diamond. *Geochim et
Cosmochim. Acta*, 36, pp. 1255-1273.

Miyashiro, A., 1956. Osumilite, a new silicate mineral and
its crystal structure. *Am. Mineral.* 41, pp. 104-116.

Moore, P.B., 1969. The crystal structure of sapphirine.
Am. Mineral. 54, pp. 31-49.

Mori, T., 1977. Geothermometry of spinel lherzolites.
Contrib. Mineral. Petrol., 59, pp. 261-279.

_____ and Banno, S., 1973. Petrology of peridotite and
garnet clinopyroxenite of the Mt. Higasi-Akaisi Mass,
Central Sikoku, Japan - subsolidus relations of anhydrous
phases. *Contrib. Mineral. Petrol.*, 41, pp. 301-323.

Mori, T., and Green, D.H., 1975. Pyroxenes in the system $Mg_2Si_2O_6$-$CaMgSi_2O_6$ at high pressure. *Earth Planet. Sci. Lett.*, 26, pp. 277-286.

_____1978. Laboratory duplication of phase equilibria observed in natural garnet lherzolites. *J. Geol.*, 86, pp. 83-97.

Morse, S.A., and Talley, J.H., 1971. Sapphirine reactions in deep seated granulites near Wilson Lake, Central Labrador, Canada. *Earth Planet. Sci. Letters*, 10, pp. 325-328.

Mysen, B., and Heier, K.S., 1972. Petrogenesis of eclogites in high grade metamorphic gneisses exemplified by the Hareidland Eclogite, Western Norway. *Contrib. Mineral. Petrol.*, 36, pp. 73-94.

Navrotsky, A., and Kleppa, O.J., 1973. Estimate of enthalpies of fusion and formation of cordierite. *J. Am. Ceram. Soc.*, 56, pp. 198-199.

Newton, R.C., 1966. Kyanite-andalusite equilibrium from 700°C to 800°C. *Science*, 153, pp. 170-172.

_____ 1972. An experimental determination of the high-pressure stability limits of magnesian cordierite under wet and dry conditions. *Jour. Geol.*, 80, pp. 398-420.

_____ 1977. Thermochemistry of garnets and aluminous pyroxenes in the CMAS system. In: Thermodynamics in Geology, pp. 29-55, D.G. Fraser (Ed.). 410p. D. Reidel Publ. Co.

_____, Charlu, T.V., and Kleppa, O., 1974. A calorimetric investigation of the stability of anhydrous magnesium cordierite with application to granulite facies metamorphism. *Contrib. Mineral. Petrol.*, 44, pp. 295-311.

Newton, R.C., Charlu, T.V., and Kleppa, O.J., 1977. Thermo-
chemistry of high pressure garnets and clinopyroxenes in
the system $CaO-MgO-Al_2O_3-SiO_2$. *Geochim. et Cosmochim. Acta,*
41, pp. 369-377.

Nixon, P.H., and Boyd, F.R., 1973. Petrogenesis of the granular
and sheared ultrabasic nodule suite in kimberlites. In:
Lesotho Kimberlites. P.H. Nixon (Ed.). Cape and Transvaal
Printers Ltd., Cape Town, pp. 48-56.

Novak, G.A., and Gibbs, G.V., 1971. The crystal chemistry of
the silicate garnets. *Am. Mineral.,* 56, pp. 791-825.

O'Hara, M.J., 1960. A garnet-hornblende-pyroxene rock from
Glenelg, Inverness-shire. *Geol. Mag.,* 97, pp. 145-156.

_____ 1977. Thermal history of excavation of Archaean
gneisses from the base of the continental crust. *J. Geol.*
Soc. Lond., 134, pp. 185-200.

Okamura, F.P., Ghose, S., and Ohashi, H., 1974. Structure and
crystal chemistry of calcium Tschermak's pyroxene,
$CaAl_2SiO_6$. *Am. Mineral.,* 59, pp. 549-557.

Olsen, E., and Bunch, T.E., 1970. Compositions of natural
osumilites. *Am. Mineral.,* 55, pp. 875-879.

Orville, P.M., 1972. Plagioclase cation-exchange equilibria with
aqueous chloride solution : results at $700^\circ C$ and 2000 bars
in the presence of quartz. *Am. J. Sci.,* 272, pp. 234-272.

Pieters, P.E., and Wyborn, D., 1977. Geological work in
Antarctica - 1974/75. *Bur. Miner. Res. Aust. Rec.* 1977/16.

Ponomarenko, A.I., Sobolev, N.V., Pokhilenko, N.P., Laurent'yev,
Yu. G., and Sobolev, V.S., 1977. Diamond-bearing grospidite
and diamond-bearing kyanite-eclogite from the Udachnaya
kimberlite pipe, Yakutia. *Dokl. Akad. Nauk, SSSR,* 226, pp.158-161.

Powell, M., and Powell, R, 1977. Plagioclase-alkali-feldspar geothermometry revisited. *Min. Mag.*, 41, pp.253-256.

Raheim, A., and Green, D.H., 1974a. Experimental determination of the temperature and pressure dependence of the Fe-Mg partition coefficient for coexisting clinopyroxene and garnet. *Contrib. Mineral. Petrol.*, 48, pp.179-203.

_____ 1974b. Experimental petrology of Lunar Highland Basalt Composition and applications to models for the Lunar interior. *Jour. Geol.*, 82, pp.607-622.

_____ 1975. P, T paths of natural eclogites during metamorphism - a record of subduction. *Lithos*, 8, pp.317-328.

Reed, S.J.B., 1975. *Electron Microprobe Analysis*. Cambridge University Press.

_____, and Ware, N.G., 1975. Quantitative electron micro-probe analysis of silicates using energy dispersive X-ray spectrometry. *J. Petrol.*, 16, pp.499-519.

Richardson, S.W., 1968. Staurolite stability in a part of the system Fe-Al-Si-O-H. *J. Petrol.*, 9, pp.467-488.

_____ , Gilbert, M.C., and Bell, P.M., 1969. Experimental determination of kyanite-andalusite and andalusite-sillimanite equilibria; the aluminium silicate triple point. *Am. J. Sci.*, 267, pp.259-272.

Ringwood, A.E., 1966. Mineralogy of the mantle. In: Hurley, P.M., (Ed.), Advances in Earth Science. Cambridge, Mass., M.I.T. Press, pp.357-417.

Robie, R.A., Bethke, P.M., and Beardsley, K.M., 1967. Selected X-ray crystallographic data, molar volumes, and densities of minerals and related substances. *U.S. Geol. Surv. Bull.*, 1248, 87p.

Robie, R.A., and Waldbaum, D.R., 1968. Thermodynamic properties of minerals and related substances at 298.15^{O}K (25.0^{O}C) and one atmosphere (1.013 bars) pressure and at higher temperatures. *U.S. Geol. Surv. Bull.*, 1259.

_____, Hemingway, B.S., and Fisher, J.R., 1978. Thermodynamic properties of minerals and related substances at 298.15^{O}K and 1 bar (10^5 pascals) pressure and at higher temperatures. *U.S. Geol. Surv. Bull.*, 1452.

Rossi, G., 1963. Ritrovamento della osumilite in uno riolite de Monte Arci. *Rend. Soc. Mineral. Ital.*, 19, pp.187-193.

Ruker, R.A., 1964. Geological reconnaissance in Enderby Land and Southern Prince Charles Mountains, Antarctica. *Bur. Miner. Resour. Aust. Rec.* 1963/154 (unpubl.).

Rutstein, M.S., and Yund, R.A., 1969. Unit-cell parameters of synthetic diopside-hedenbergite solid solutions. *Am. Mineral.*, 54, pp. 238-245.

Ryabchikov, I.D., Green, D.H., and Brey, G., (in prep.). The oxidation state of carbon in the environment of the low velocity zone.

Ryburn, R.J., Raheim, A., and Green, D.H., 1975. Determination of the P, T paths of natural eclogites during metamorphism - record of subduction. *Lithos*, 9, pp.161-164.

Saxena, S.K., 1973. Thermodynamics of rock-forming crystalline solutions. Minerals and Rocks, vol.8, Springer-Verlag, Heidelberg.

_____, and Ghose, S., 1971. Mg^{2+}-Fe^{2+} order-disorder and thermodynamics of the orthopyroxene crystalline solution. *Am. Mineral.*, 56, pp.532-559.

Saxena, S.K., Ghose, S., and Turnock, A.C., 1974. Cation distribution in low-calcium pyroxenes: dependence on temperature and calcium content and the thermal history of lunar and terrestrial pigeonites. *Earth Planet. Sci. Letters*, 21, pp.194-200.

_____, and Ribbe, P.H., 1972. Activity-composition relations in feldspars. *Contrib. Mineral. Petrol.*, 37, pp.131-138.

_____, and Nehru, C.E., 1975. Enstatite-diopside solvus and geothermometry. *Contrib. Mineral. Petrol.*, 49, pp. 259-267.

Schreinemakers, F.A.H., 1965. In-, mono-, and divariant equilibria. *Penn. State Univ. Publ.*, 2, 322p.

Schreyer, W., 1968. Upper pressure stability limit of Mg-cordierite. *Carnegie Inst. Washington Year Book*, 66, pp.387-388.

_____, and Abraham, K., 1975. Peraluminous sapphirine as a metastable reaction product in kyanite-gedrite-talc schist from Sar e Sang, Afghanistan. *Mineral. Mag.*, 40, pp.171-180.

_____, and Abraham, K., 1976. Natural boron-free kornerupine and its breakdown products in a sapphirine rock of the Limpopo Belt, Southern Africa. *Contrib. Mineral. Petrol.*, 54, pp.109-126.

_____, and Seifert, F., 1967. Metastability of an osumilite and member in the system $K_2O-MgO-Al_2O_3-SiO_2-H_2O$ and its possible bearing on the rarity of natural osumilite. *Contr. Mineral. Petrol.*, 14, pp.343-358.

_____, and Seifert, F., 1969. Compatibility relations of the aluminium silicates in the system $MgO-Al_2O_3-SiO_2-H_2O$ and $K_2O-MgO-Al_2O_3-SiO_2-H_2O$ at high pressures. *Am. J. Sci.*, 267, pp.371-388.

_____, and Yoder, H.S., 1960. Hydrous Mg-cordierite. *Carnegie Inst. Washington Year Book*, 59, pp.91-94.

Schreyer, W., and Yoder, H.S., 1964. The system Mg-cordierite-H_2O

and related rocks. *Neues Jb. Miner. Abh.*, 101, pp.271-342.

Seifert, F., 1970. Low-temperature compatibility relations of

cordierite in the haplopelites of the system K_2O-MgO-Al_2O_3-

SiO_2-H_2O. *J. Petrol.*, 11, pp.73-99.

_____ , 1976. Stability of the assemblage cordierite+

Kfeldspar+quartz. *Contr. Mineral. Petrol.*, 57, pp.179-185.

_____ , and Schreyer, W., 1970. Lower temperature stability

limit of Mg cordierite in the range 1-7 kb water pressure:

a redetermination. *Contrib. Mineral. Petrol.*, 27, pp.225-238.

Sheraton, J.W., and Offe, L.A., 1977. Geological work in Antarctica -

1976. *Bur. Minera. Resour. Aust. Rec.*, 1977/60.

_____ , Offe, L.A., Tingney, R.J., and Ellis, D.J.

The geology of Enderby Land, Antarctica. Submitted to Geol.

Soc. Aust.

Simmons, E.C., Lindsley, D.H., and Papike, J.J., 1974. Phase

relations and crystallization sequence in a contact-metamorphosed

rock from the Gunflint iron formation, Minnesota. *J. Petrol.*,

15, pp.539-565.

Smith, J.V., and Schreyer, W., 1960. Location of argon and water in

cordierite. *Mineralog. Mag.*, 33, pp.226-236.

Smyth, J.R., and Hatton, C.J., 1977. A coesite-sanidine grospydite

from the Roberts Victor Kimberlite. *Earth Planet. Sci. Letters*,

34, pp.284-290.

Sobolev, N.V., Kuznetsova, I.K., and Zyuzin, N.I., 1968. The petrology

of grospydite xenoliths from the Zagadochnaya kimberlite pipes

in Yakutia. *J. Petrol.*, 9, pp.253-280.

Sobolev, N.V., Zyuzin, N.I., and Kuznetsova, I.K., 1966. The continuous series of pyrope-grossular garnets in grospidite. *Dokl. Akad. Nauk, S.S.S.R.*, 167, pp.126-129.

Sobotovich, E.V., Kamenev, E.N., Komaristyy, A.A., and Rudnik, V.A., 1976. The oldest rocks of Antarctica (Enderby Land). *Int. Geol. Rev.*, 18, pp.371-388.

Stormer, Jr., J.C., 1975. A practical two feldspar geothermometer. *Am. Mineral.*, 60, pp.667-674.

Takahashi, T., and Liu, L.G., 1970. Compression of ferromagnesian garnets and the effect of solid solutions on the bulk shear modulus. *J. Geophys. Res.*, 71, pp.5757-5766.

Thompson, A.B., 1976. Mineral reactions in pelitic rocks: II. Calculations of some P-T-X(Fe-Mg) phase relations. *Am. J. Sci.*, 276, pp.425-454.

Thompson, J.B., Jr., 1967. Thermodynamic properties of simple solutions. In: Researches in Geochemistry. P.H. Abelson (Ed.), vol.2, pp.340-361. Wiley, New York.

Tingey, R.J., in prep. The geology and geological evolution of the Prince Charles Mountains, Antarctica. In: C.Craddock (Ed.), Antarctic Geoscience. Proceedings of the third symposium on Antarctic geology and geophysics, Madison, 1977. Univ. Wisconsin Press.

Turner, F.J., and Verhoogen, J., 1960. Igneous and metamorphic petrology. Second ed. McGraw-Hill Book Company, New York. 694 p.

Virgo, D., and Hafner, S.S., 1969. Fe^{2+}, Mg order-disorder in heated orthopyroxenes. *Mineral. Soc. Am. Spec. Paper*, 2, pp.67-81.

De Waard, D., 1965. The occurrence of garnet in the granulite facies terrane of the Adirondack Highlands. *J. Petrol.*, 6, pp.165-191.

Warner, R.D., and Luth, W.C., 1974. The diopside-orthoenstatite two phase region in the system $CaMgSi_2O_6$-$Mg_2Si_2O_6$. *Am. Mineral.*, 59, pp.98-109.

Weisbrod, A., 1973. Cordierite-garnet equilibrium in the system Fe-Mn-Al-Si-O-H. *Carnegie Inst. Washington Year Book*, 72, pp.515-518.

_____ , 1973. Refinements of the equilibrium conditions of the reaction Fe cordierite → almandine + quartz + sillimanite (+ H_2O). *Carngeie Inst. Washington Year Book*, 72, pp.518-521.

Wellman, P., and Tingey, R.J., 1977. A gravity survey of Enderby and Kemp Lands. Third symposium on Antarctic Geology and Geophysics. Madison, U.S.A.

White, A.J.R., 1964. Clinopyroxenes from eclogites and basic granulites. *Am. Mineral.*, 49, pp.883-888.

Wilkinson, J.F.G., 1974. Garnet clinopyroxenite inclusions from diatremes in the Gloucester area, New South Wales, Australia. *Contrib. Mineral. Petrol.*, 46, pp.275-299.

Windom, K.E., and Boettcher, A.L., 1976. The effect of reduced activity of anorthite on the reaction grossular + quartz = anorthite + wollastonite: a model for plagioclase in the earth's lower crust and upper mantle. *Am. Mineral.*, 61, pp.889-896.

Wood, B.J., 1973. Fe^{2+}-Mg^{2+} partition between coexisting cordierite and garnet - a discussion of the experimental data. *Contrib. Mineral. Petrol.*, 40, pp.253-258.

_____ , 1974. The solubility of alumina in orthopyroxene coexisting with garnet. *Contr. Mineral. Petrol.*, 46, pp.1-15.

_____ , 1975. The influence of pressure, temperature and bulk composition on the appearance of garnet in ortho-gneisses - an example from South Harris, Scotland. *Earth Planet. Sci. Letters*, 26, pp.299-311.

Wood, B.J., 1975. Mixing properties of Tschermakitic clinopyroxenes and their application to geobarometry. Int . Conf. on Geotherm. and Geobarom., Penn. State Univ., Oct.5-10.

_____ , 1976. The partitioning of iron and magnesium between coexisting garnet and clinopyroxene. *Ann. Rep. Dir. Carnegie Inst. Washington Year Book,* 75, pp.571-574.

_____ , 1976. Mixing properties of Tschermakitic clinopyroxenes. *Am. Miner .,*61, pp.599-602.

_____ , 1977. Experimental determination of the mixing properties of solid solutions with particular reference to garnet and clinopyroxene solutions. In: Thermodynamics in Geology. D.G. Fraser (Ed.). NATO Advanced Study, Institute Series. D. Reidel Publ. Co.

_____ , 1977. The activities of components in clinopyroxene and garnet solid solutions and their application to rocks. *Phil. Trans. Roy. Soc. Lond. A,* 286, pp.331-342.

_____ , and Banno, S., 1973. Garnet-orthopyroxene and ortho-pyroxene-clinopyroxene relationships in simple and complex systems. *Contrib. Mineral. Petrol.,* 42, pp.109-124.

_____ , and Fraser, D.G., 1976. Elementary Thermodynamics for Geologists. Oxford Univ. Press.

Yoder, H.S., and Tilley, C.E., 1962. Origin of basalt magmas: an experimental study of natural and synthetic rock systems. *J. Petrol.,* 3, pp.342-532.

Zen, E-An., 1966. Construction of pressure-temperature diagrams for multicomponent systems after the method of Schreinemakers - A geometric approach. *U.S. Geol. Surv. Bull.,* 1225, 56 p.